

City Research Online

City St George's, University of London

Citation: Rajroop, P. J. (1995). Fast pulse interactions on a transmission system - (A novel EMP measuring technique using new designed loop probes). (Unpublished Doctoral thesis, City, University of London)

This is the accepted version of the paper.

This version of the publication may differ from the final published version. To cite this item please consult the publisher's version.

Permanent repository link: https://openaccess.city.ac.uk/id/eprint/29599/

Copyright and Reuse: Copyright and Moral Rights remain with the author(s) and/or copyright holders. Copies of full items can be used for personal research or study, educational, or not-for-profit purposes without prior permission or charge, unless otherwise indicated, provided that the authors, title and full bibliographic details are credited, a hyperlink and/or URL is given for the original metadata page and the content is not changed in any way. For full details of reuse please refer to City Research Online policy.

City Research Online: http://openaccess.city.ac.uk/ publications@citystgeorges.ac.uk

FAST PULSE INTERACTIONS ON A TRANSMISSION SYSTEM

(A novel EMP measuring technique using new designed loop probes)

by

Peter J. Rajroop

This thesis is presented for the

Degree of Doctor of Philosophy

at

City University

Department of Electrical, Electronic & Information Engineering

September, 1995

.....

Title of the Thesis

Table of Contents

Table of Contents....i
List of Tables....ix
Acknowledgements....x
Declaration....xii
Abstract....xiii
Symbols, Units and Abbreviations....xiv

CHAPTER 1....1
1-1 INTRODUCTION....1
1-2 General....1
1-3 Standards for electromagnetic-field measurements....6
1-4 The arrangement of the thesis....7
1-5 Sequence of investigation and original contributions....9
1-5.1 Construction and testing of the devices and apparatus....9
1-5.2 Directional properties of the loop probe....9
1-5.3 Equal electric- and magnetic-field coupling....10
1-5.4 Loop antenna design....10
1-5.4.1 Simultaneous electric- and magnetic-field measurements....10
1-5.5 Development of new antenna equations....11
1-6 Novel Applications of the Measurement system....12
1-6.1 A Simple Fault Detector/Locator....12
1-6.2 EMP/EMC Measurements....12
1-6.3 High Voltage Divider....12
1-6.4 Impulse Voltage Measurement....13
1-6.5 Interface Devices....13
1-7 Published Report and Papers....13

CHAPTER 2 THEORY AND REVIEW 15
Introduction 15
2-1 The transmission line concepts 15
2-1.1 Wave characteristics on an infinite transmission line 19
2-1.2 Lossy transmission line basics 20
2-2 Theory of operation of the directional coupler 23
2-3 Maxwell's equations 25
2-3.1 Integral form of Maxwell's equations 25
2-3.2 Gaussian representation of Maxwell's equations 27
2-4 Properties of antennas 29
2-4.1 Introduction and review 29
2-4.2 Radiation patterns 31
2-4.3 Characteristics of simple patterns 33
2-4.3.1 Radiation from electric-current elements 33
2-4.3.2 Radiation from magnetic-current elements 35
2-4.4 Polarisation 36
2-4.5 Directivity 38
2-4.6 Gain 38
2-4.7 Impedance 39
2-4.8 Bandwidth 41
2-5 Time-domain antenna characterisation 42
2-5.1 Introduction 42
2-5.2 Transient response of an antenna 43
2-5.3 Antenna characterisation 43
2-6 The loop antenna 44
2-6.1 Solving for the inductance and capacitance of the loop antenna 47
2-6.2 Electric and magnetic responses of the loop antenna 49
2-6.3 Modification of these equations to allow for unbalanced loads 51
2-6.4 Performance of electric-field transfer standards 54
2-6.5 Performance for magnetic-field transfer standards 55
2-7 Photonic probes 56

CHAPTER 3 A MATHEMATICAL LINK BETWEEN THE CONCEPTS OF CIRCUIT AND FIELD-THEORY 59

3-1 Introduction 59

3-2 The electromagnetic of circuits 60

3-3 Idealisations in classical circuit theory 62

3-4 Kirchhoff's voltage law 62

3-4.1 Resistance element 66

3-4.2 Inductance element 65

3-4.3 Capacitive element 66

3-5 Relation of field and circuit analysis for transmission lines 67

3-6 Analogy of wave characteristics on line and waves in lossy medium 70

3-7 Resistance calculations 72

3-8 Conclusions 74

CHAPTER 4 DEVICES AND APPARATUS 75

Systems Description and Testing 75

Introduction 75

4-1 The transmission line 76

4-2 The directional coupler 80

4-2.1 Introduction 80

4-2.2 descriptions 80

4-3 The 1 kv mercury pulser 83

4-3.1 Introduction 83

4-3.2 Initial development 84

4-3.3 Description 85

4-3.4 Testing of the mercury pulser 86

4-4 Impulse voltage measurement 93

4-4.1 Introduction 93

4-4.1.1 Precision impulse measurement 93

4-4.2 The SF_6 spark-gap pulser as a simulator for impulse voltages 94

4-4.3 Voltage breakdown in SF_6 96

4-4.4 Lightning impulses....100
4-4.5 Construction of the SF_6 pulser....100

CHAPTER 5 INSTRUMENTATION AND MEASUREMENT TECHNIQUE....103
5-1 Introduction....103
5-2 Instrumentation....103
5-2.1 The measuring oscilloscope....107
5-2.1.1 Features of the 7S12 TDR/Sampler....109
5-2.2 The C-5C camera....112
5-2.2.1 Specifications....113
5-2.3 The digital voltmeter....114
5-2.3.1 Self test....115
5-3 Test methods....117
5-3.1 Signal acquisition method....118
5-3.2 Time domain reflectometry (TDR) measurements....119
5-3.2.1 Experimental - Distance measurement of the line using TDR....122
5-3.3 Voltage reflection coefficient....124
5-3.4 Time or distance measurement procedure....125
5-3.4.1 The on-screen method....125
5-3.5 TDR measurements using the line pulser....126
5-3.5.1 Preview....126
5-3.5.2 Connections of the measurement system....127
5-3.6 Initial testing....128
5-4 The Bewley lattice (*reflection*) diagram....132

CHAPTER 6 TEST SEQUENCE ON THE TRANSMISSION LINE AND EXPERIMENTAL RESULTS....134
6-1 Introduction....134
6-1.1 Transients on transmission lines....134
6-1.2 Pulse excitation....139
6-2 Experimental - testing with open circuit termination....140
6-2.1 Electric (D) coupling....140

6-2.2 Maximum (B+ D) coupling 144
6-2.3 Results with brief remarks 147
6-2.4 Maximum coupling (270° position) 149
6-2.5 Cancelling effects of electric-field coupling 150
6-2.5.1 Reflections from the termination 150
6-2.5.2 Reflections from source 151
6-3 Line terminated into its characteristic impedance 152
6-3.1 The line matching resistor 153
6-3.2 Transmission line impedance matching 154
6-3.2.1 Quarter wavelength matching 155
6-3.2.2 Tapered line 155
6-3.2.3 Stub matching 156
6-3.2.4 Single stub matching 157
6-3.2.5 Double-stub matching 159
6-4 Testing with short-circuited termination 162
6-4.1 Electric-field coupling 162
6-4.2 Maximum electromagnetic coupling at 90° position 163
6-4.3 Maximum electromagnetic coupling at 270° position 164
6-5 Mismatched condition at source with open-circuit termination 165
6-6 Analysis of the results on cancellation 167
6-6.1 Effects from pulses reflected from termination 167
6-7 Conclusions 168
6-8 Reflections from curvature of the transmission system 169
6-8.1 Possible EMC application 171
6-9 Electromagnetic properties of materials 171
6-9.1 Introduction 172
6-9.2 Diamagnetic and paramagnetic responses 173
6-9.3 Ferrite magnetic material 174
6-10 Pulse sharpening phenomena 175
6-11 The SF_6 pulser as a high-voltage simulator used in conjunction with a loop probe as a voltage divider 179
6-11.1 Experimental - high voltage divider 180

6-11.2 The test procedure 180
6-12 Impulse voltage measurement 184
6-13 Conclusions 185

CHAPTER 7 FURTHER INVESTIGATIONS AND APPLICATIONS USING THE NEW DEVELOPED PROBING MEASUREMENT SYSTEM 186

7-1 The directional coupler as an accurate fault locator
7-1.1 Introduction 186
7-1.2 Review 186
7-1.3 Testing on the transmission line 188
7-1.4 Open-circuit fault condition 188
7-1.5 Calculation of distance to fault 188
7-1.6 Short-circuit fault condition 190
7-1.7 Detection of an impedance fault 191
7-1.8 Low impedance fault 191
7-1.9 High impedance fault 191
7-1.10 Intermediate impedance fault 192
7-1.11 Discussions 193
7-1.12 Conclusions 194
7-2 New loop-probe design for equal **B**-dot/**D**-dot coupling 194
7-2.1 Introduction 194
7-2.2 Experimental procedure 195
7-2.3 Loop termination with identical loads 196
7-2.4 Termination with one resistor in loop circuit 196
7-2.5 Loop without a load termination 197
7-2.6 Equality condition obtained by altering the loop geometry 197
7-2.7 Calculation of loop inductance and capacitance 199
7-2.8 Discussions 201
7-3 Probes for electromagnetic pulse (EMP) measurements 202
7-3.1 Introduction 202
7-3.2 Loop analysis 203
7-3.3 Application of the double-loaded matched probe 205

7-3.4 Experimental 207
7-3.5 Summary 210
7-4 Loop probes in EMP/EMC measurements 211
7-4.1 Introduction - the EMC problem 211
7-4-2 Computational modelling techniques 212
7-4.3 The nature of EMI 215
7-4.4 EMC measurements 215
7-4.5 Shielding performance 216
7-4.6 Shielding effectiveness 217
7-4.7 Experimental 218
7-4.8 Discussions on Near-field and Far-Field in EMC Testing 222
CHAPTER 8 SIGNAL INTERFACE METHODS 223
8-1 General purpose interface bus (*GPIB*) 223
8-1.1 Introduction 223
8-1.2 GPIB interface messages 225
8-1.2 GPIB theory 226
8-1.2.1 Signal lines 226
8-1.2.2 The handshake 227
8-1.3 The test procedure 229
8-1.4 Summary 230
8-2 Optically coupled (*OC*) interface 231
8-2.1 Introduction and review 231
8-2.2 Features of optical communications 232
8-2.3 Optical fibres - review 232
8-2.4 Planar dielectric - total internal reflection 234
8-2.5 Propagation modes 236
8-2.5.1 Transverse modes 237
8-2.6 Dispersion 238
8-2.7 Step index fibres 240
8-2.8 Graded index fibres 242
8-2.9 Light insertion 243
8-2.10 Transmission losses 244

8-2.10.1 Material absorption....244
8-2.10.2 Material scattering....244
8-2.10.3 Mechanical effects....245
8-3 Fibre optics communication - a proposed application....247
8-3.1 Optical test procedure....247
8-3.2 Summary....250

CHAPTER 9 DISCUSSIONS AND CONCLUSIONS....251
9-1 Discussions....251
9-2 Conclusions....253
9-3 Suggestions for further work....255

REFERENCES:....258

APPENDICES:....268
1-0 Stress calculations....269
2-0 Appendix....271
2-1 Line matching network calculations....271
2-2 Calculations of the characteristic impedance of the line....274
2-2.1 Capacitance between parallel conductors....274
2-3 Computer analysis of *C* and *L* for the line....277
2-4 Computer analysis for the capacitance and inductance of the line....278
3-0 Sampling decision tree for repetitive signals....279
4-0 E and H field Sensors....280

List of Tables

Table No.	Table Title	Page No.
Table 2-1:	Photonic **E**-field Measurement System	58
Table 4-1:	Specifications for Mercury -wetted Reed-Switch	92
Table 4-2:	Values for E_S for SF_6 (Mattingly and Ryan, 1973)	98
Table 5-1:	Electrical Characteristics - Performance Requirements	110
Table 5-2:	Electrical Characteristics - Systems Performance with S-6 and S-52	111
Table 5-3:	Optical Characteristics of Camera	113
Table 5-4:	Electrical Characteristics of Camera	113
Table 8-1:	Index of Refraction of Solids for different Wavelengths in the visible	239

Acknowledgements

The author wishes to express his gratitude to Professor A. T. Johns who initiated the first part of the research and for his role as the original official supervisor. The day-to-day supervision was carried out by Dr. W. Daum, who also gave valuable advice in the designing of the transmission line structure and other measuring devices. On the resignation of Dr. Daum, Professor H. House was responsible for the supervision, which he conducted very well. Prof. House helped in the presentation of my first international paper in which he was a co-author. The author sincerely acknowledged the contributions made by these supervisors.

The work reported in the thesis would not have been materialised without the support and encouragement from Professor K.T.V. Grattan, who was also instrumental in getting the registration through the appropriate board and committees, and to Dr. L. L. Lai for his expert supervision throughout the last four years of the research. I am greatly indebted to Prof. Grattan and Dr. Lai and wish to extend my sincere thanks and gratitude. Dr. Lai's constant review of the research, his critical comments and encouragement was invaluable for the completion of the work. He was primarily responsible for further paper generation and gave full support in the research activities as a co-author.

In recognition of my research activities, Professor R. Franklin, CBE, FEng. (Vice Chancellor of the City University), had made it possible, by way of grants, for the author to present papers at international conferences in Japan and Europe. I sincerely wish to thank him for his consideration in this manner. It was a tremendous boost to my research activities for support from such high authority.

Professor T. E. Allibone, CBE, Hon FIEE, FEng. FRS, has always been a source of inspiration and motivation. I sincerely wish to thank him for his advice, discussions and encouragement which he gave so willingly. It was particularly rewarding for me, knowing that Professor Allibone recognised my work which he supported at all times.

Although in different lands, Professor Dr. A. Braunstein (Tel-Aviv University) and in particular, Dr. W. Daum (General Electric Research Laboratory, N.Y., USA) were of tremendous help throughout the project, with numerous correspondences mainly through the electronic-mail link. I wish to thank them for their advice and for the extent in interest shown in my work.

Mr. R. Hughes from the National Physical Laboratory, and Dr. A. C. Lynch and the late Mr. P. Clifford (Retired Senior Visiting Fellows of the City University) were extremely helpful on their advice on measurement techniques and calibration. The author wishes to thank them all. Further discussions with Mr Hughes has led to the development of a new measurement technique for impulse voltage.

The author appreciates the advice and comments on *the application of the directional coupler as a fault locator*, from Professor O. Farish and Dr. B. F. Hampton from the Centre of Electrical Power Engineering, University of Strathclyde. Advice and suggestions from members of staff from the National Grid Company, the National Physical Laboratory, Culham Laboratory, Sowerby Research Centre - British Aerospace, Lucas Aerospace and BICC, is acknowledged. The author wishes to thank all those responsible for their valuable discussions.

Internally, within the Department of Electrical, Electronic and Information Engineering, I wish to acknowledge the support from Mr. B. R. Orrin (Departmental Superintendent), Mr. F. Carthy and Mr. B. Burns (Technical Staff) for discussions and to Dr. J. T. Ma, Mr. F. Ndeh-che and Mr. H. Braun (Energy Systems Group) for help and advise on computational matters. The advice from the Computer Unit on computational matters and the Central Workshop, in particular, Mr. G. Rudlands, for machining various components used in the construction of the devices and for pressure testing the SF_6 pulser, are also duly acknowledged.

The author is indebted to City University and the Department of Electrical, Electronic and Information Engineering for giving him the opportunity to conduct the research and for use of the laboratory equipment and facilities.

Once again, I wish to thank Professor Grattan for support in the continuation of research within the Department and for assistance in financial matters.

Last, but not least, I wish to thank my wife Marilyn and children Rosemary Belinda and Gavin Anthony for their patience and understanding, and for their encouragement during the period of study, but especially, during the writing up of the thesis.

"THIS THESIS IS DEDICATED TO THE LOVE AND CHERISHED MEMORIES OF MY DEAR DEPARTED PARENTS"

Declaration

The author hereby grant powers of discretion to the City University Librarian to allow this thesis to be copied in whole or in part without further reference to the author. This permission covers only single copies made for study purposes, subject to normal conditions of acknowledgement.

Abstract

Ideally, a pulsed signal guided through its intended transmission medium, should be subjected to a small attenuation and negligible degradation to its wave shape. In practice, this condition is difficult to achieve, since all transmission mediums will impose some form of interference or distortion on a travelling pulse. Also no practical transmission medium is completely loss-free. The amount of attenuation/distortion imposed on a travelling pulse is a sensitive measure of the transmission performance of the medium.

This thesis reports a novel attempt to investigate the effects of the transient electromagnetic (EM) fields produced by the pulse propagation pattern, and its interactions with single element antenna probes. Also to characterise and measure this distortion accurately, as a pulse travels through an open conductor-plane transmission system. In order to carry out the investigations, new loop probes which act as magnetic- and/or electric-field sensors, were analysed and designed for this purpose. The measurement technique consists of a pulser, purposely built in a coaxial arrangement which was used to generate fast (sub-nanosecond) risetime pulses for injection into the test line. An SF_6 insulated hemispherical-electrode pulser was also used as a simulator for an impulse voltage generator. Detection of the pulses as they travelled along the line was by directional couplers employing these **B**-dot/**D**-dot loop probes, the directional couplers being placed at strategic points in the earthplane.

Simultaneous electric- and magnetic-field measurements using a single loop antenna element is useful for the near-field electromagnetic measurements where the magnitude and phase of the wave impedance are not known. This type of loop probe, described, is not only useful to measure the polarisation ellipses of the electric- and magnetic-field vectors in the near-field region, but also measurements of the time-dependent Poynting vector so as to describe the energy flow.

By altering the geometry of the loop (as opposed to adding resistors in the loop circuit as reported previously), it was found that the loop exhibited a unique coupling characteristic such that it responded equally to the components of the time derivative electric- and magnetic-fields. This important practical feature is explained.

In addition to electromagnetic pulse (EMP) applications, the versatility of the coupling loop readily lends itself for use in electromagnetic compatibility (EMC) measurements and as a tool for fault detection and location on power systems network. These applications were investigated.

A theoretical concept for pulse propagation on a transmission line, using circuit and field theories, is presented. An attempt is made to link the circuit theory with the field theory, with a view to describe the experimental results. Full mathematical theory of the loop is reviewed in which new equations were developed to satisfy the general loading condition of the loop.

Descriptions and design specifications of the devices used in the experimental studies are given and their performances in transient field measurements have been verified in a number of unique applications. This demonstrates the integrity of the measurement system and the sensitivity characteristics of the directional coupler. With suitable angular adjustments, it was shown that the loop can be made to couple only to a pulse travelling in one direction.

Symbols, Units and Abbreviations

Derived Quantities

Quantity	Symbol	Unit	Abbreviation
Admittance	Y	siemens	S
Angular frequency	ω	radian/second	rad/s
Attenuation constant	α	neper/metre	Np/m
Capacitance	C	farad	F
Charge	Q,q	coulomb	C
Charge density (surface)	ρ_s	coulomb/metre^2	C/m^2
Charge density (volume)	ρ	coulomb/metre^3	C/m^3
Conductance	G	siemens	S
Conductivity	σ	siemens/metre	S/m
Current density (surface)	$\mathbf{J}_s$	ampere/metre	A/m
Current density (volume)	$\mathbf{J}$	ampere/metre^2	A/m^2
Dielectric constant (relative permittivity)	ε_r	(dimensionless)	—
Directivity	D	(dimensionless)	—
Electric displacement (Electric flux density)	$\mathbf{D}$	coulomb/metre^2	C/m^2
Electric field intensity	$\mathbf{E}$	volt/metre	V/m
Electric potential	V	volt	V
Frequency	f	hertz	Hz
Gain	G	(dimensionless)	—
Impedance	Z	ohm	Ω
Inductance	L	henry	H
Intrinsic wave impedance	η	ohm	Ω

Derived quantities cont'd.

Quantity	Symbol	Unit	Abbreviation
Magnetic field intensity	**H**	ampere/metre	A/m
Magnetic flux	Φ	weber	Wb
Magnetic flux density	**B**	tesla	T
Permeability	μ, μ_0	henry/metre	H/m
Permittivity	$\varepsilon, \varepsilon_0$	farad/metre	F/m
Phase	ϕ	radian	rad
Phase constant	β	radian/metre	rad/m
Propagation constant	γ	metre^{-1}	m^{-1}
Reactance	X	ohm	Ω
Reflection coefficient	Γ	(dimensionless)	—
Relative permeability	μ_r	(dimensionless)	—
Relative permittivity (dielectric constant)	ε_r	(dimensionless)	—
Resistance	R	ohm	Ω
Susceptance	B	siemens	S
Velocity	u	metre/s	m/s
Voltage	V	volt	V
Wavelength	λ	metre	m

Chapter 1

1-1 Introduction

1-2 GENERAL

A significant increase in interest in the production and measurements of fast electro-magnetic pulses (EMPs), and in electromagnetic compatibility (EMC) studies have taken place in the last decade or so ago. Most of the EMP/EMC measurements involve some kind of probe sensor as a detector, consequently there is a growing need to develop a more suitable sensor, in terms of size, bandwidth and sensitivity. Antennas are generally bulky and very often demands are such that they have to be integrated within the measurement system.

Transmission-line theory, using both circuit and field-theories, is a powerful tool for predicting the response of transmission lines when excited by an external electromagnetic field, such as lightning (LEMP) or nuclear electromagnetic pulse (NEMP), or from an internal EMP source, such as an impulse generator. In this experimental work, the pulses were injected into the transmission line and allowed to propagate throughout its length. Extensive studies were carried out on their interactions with the loop probes which were placed at suitable points along the line.

The first model describing transmission lines excited by an external electromagnetic source was presented by Taylor *et al.* (1965), for the case of a two-wire system in free space. In this model, the forcing functions in coupling equations are in terms of vertical-electric and transverse-magnetic excitation fields. Paul (1976), presented the excitation of this model to the case of a multiconductor line. Agrawal *et al.* (1980), derived a new formulation of coupling equations completely equivalent, but in which the forcing functions are expressed only in terms of electric-field excitation.

Such are the complexities of antenna design that there is continuing advancement in numerical techniques in antenna research. Engineers and researchers in this field have been active in developing (Burke and Poggio 1980) and utilising numerical electro-magnetic code (NEC) modelling techniques, for analysing and evaluating antenna design configurations.

Extensive work on the modelling and applications of small loop antennas and near-field probe sensors for detection purposes, especially in fast transients, are continuing with research progressing rapidly in this area, (Randa *et al.* 1995). Porti and Morente (1994) described an analysis of a wire antenna loaded with varistor-composite materials, which are non-linear transients elements with subnanosecond risetime response.

Upton and Marvin (1994) showed a theoretical analysis of a small resistively loaded loop using Numerical Electromagnetic Codes. Laroussi and Costache (1994), also presented a method based on numerical simulation to derive far-field data needed for antenna in EMC testing, from near-field measurements.

A directional coupler, using a half-turn loop, was reported since in the late forties for use in connecting test equipment to radio-frequency (RF) transmission lines, (Allan and Curling, 1949), and to study the mis-match between a transmitter and its load, (Boff 1951). Due to the inherent capacitive coupling which is always associated with the inductive coupling, little improvement was made in other areas, until recent years. Work also is now being done to characterise integrated circuit electromagnetic interference (EMI) emission, using loop probes and transverse electromagnetic (TEM) devices,

(Dischinger and Feser, 1991). More recently, a directional coupler with a 20 dB attenuator was used to connect a pulse generator to its load antenna, (Parkes and Smith 1987). Cerri *et al.* (1993) used a microstrip rectangular loop to investigate the radiated emission prediction in printed circuited board (PCB) circuits.

The application of field sensors, (Middlekoop,1991) and $\dot{B}/\dot{D}$ coupling loop probes, (Rajroop and Lai, 1993b) are continuing to progress in areas of EMP/EMC measurements and applications. In transient EMP measurements, the signal from a probe, such as the *King Surface Probe*, can be optically coupled to the sampling head of a suitable measuring oscilloscope, (Ryder and Holbrook, 1986). The King Probe and slotted line technique are suitable detectors for specific applications. However, they are not calibrated and versatile measuring devices as the directional coupler, employing new designed loop probes, as reported in this thesis.

Commercial probes now available, generally measure either the electric-field or the magnetic-field and can operate successfully at frequencies of only a few hundred Mega-Hertz, although the bandwidth can be made to increase with suitable loading of the probe antennas. The probes are very expensive and require equally expensive and sophisticated measuring equipment. The limited bandwidth is imposed mainly because of the large inductance and stray capacitance, on account of the large physical size of the coupling loop, sometimes with multi-turns, so as to increase its sensitivity.
The small loop sensor reported in this thesis, can operate at extended frequency ranges of over 2.5 GHz and can be modified to perform simultaneous $\dot{B}/\dot{D}$ measurements, as is verified in the experimental results.

For electric-field measurements, electrically short dipole antennas with a high input impedance load, such as a field-effect transistor (FET) and a high frequency (HF) diode detector may be employed. Since the input impedance of an electrically short dipole is predominantly a capacitive reactance, very broadband frequency response can be achieved with a high impedance capacitive load. However, because conventional dipole antennas support a standing wave current distribution, the useful frequency range of this kind of a dipole is usually limited by its natural resonant frequency. In order to suppress

this resonance a resistively loaded dipole has been developed and was used in this experimental study. The same dipole antenna, or loop probe, can be used for the magnetic-field measurements with the same loading. Although this arrangement gave a fast risetime response under pulse application, the sensitivity suffered on account of losses in the loading resistors.

Photonic probes can provide the wide bandwidth and low dispersion necessary to maintain the fidelity of time-domain signals. Since they consist of electro-optic modulators and optical fibres, they are free from electromagnetic interference (EMI).

Of all known switching transients, the electrostatic discharge (ED) of a metallic object combines the shortest risetimes, i.e. very steep fronts, resulting in very high discharges. Frequency response of probe sensors for frequencies of up to 1 GHz is necessary in order to model successfully, the coupling of fast electromagnetic transients such as electrostatic discharges through power cable into electronic equipment. Pommerenke and Kalkner, (1993) described a measurement system for transient fields caused by electrostatic discharges. Their technique involves an electric-field sensor, a magnetic-field sensor and a directional field sensor, whereas the same measurement could be made using a single sensor as described in the thesis.

The theory of a single loop sensor to perform simultaneous electric- and magnetic near-field measurements has been reported by Kanda (1984), and more recently by a different approach proposed by Rajroop and Lai (1995). Kanda's method was by terminating the loop with two identical loads at diametrically opposite points. The rigorous mathematical theory was based on the fact the two terminating resistors are identical. In practice it may be difficult and often inconvenient to precisely match these resistors to terminate the loop, especially when the loop sensor is to be used over a wide frequency band. Therefore the original theory is developed to take into account of the general case of unmatched loading of the loop. Hence some modified equations, based on the original theory, were developed to fully describe the loop.

The theory further indicated that it is possible to adjust the electric-dipole and magnetic-loop responses of the loop so as to obtain equal coupling. The method described in the

detection of an equal response due to these coupling effects was by changing the loop impedance. This was done by adding resistors to the loop circuit. In this way the magnetic field response was reduced and made equal to the electric-field response. The experimental results obtained from this research are in good agreement with the theory proposed by this author.

Although this simple arrangement is useful in many practical applications, it was not found to be very suitable for the fast (sub-nanosecond) front wave-matched measuring system used in the present experimental work.

The technique presented in this thesis does not depend on the addition of resistors in the loop circuit. The approach is based on the change of loop geometry which was kept to a minimum size, thereby giving an added advantage of reducing the loop inductance. It is shown that this approach also increased the sensitivity of the loop developed, and enables the directional coupler in its original form to be used, (Rajroop, 1990). The small size of the loop also minimise any possible perturbation of the electromagnetic-field when the loop is immersed into such field.

In the region near a transmitting antenna or scatterer, the electric- and magnetic-field vectors are not necessarily orthogonal or in phase. For time-harmonic fields, the end points of the field vectors trace out polarisation ellipses and the Poynton vector lies on the surface of a cone, with its end points on an ellipse. In these cases the electric- and magnetic-fields may be measured separately, or simultaneously, using the single loop antenna element described.

For standards EMC immunity testing, the open transmission line, (de Jong and Groenveld 1977) and the closed transverse electromagnetic (TEM) cell, (Crawford and Workman 1979), were proposed by Burbridge *et al.* (1987). The measurements are described using a three axis rectified dipole probe in the two cells, with and without an equipment under test (EUT). The field magnitude plots showed a distinctly different character for each cell. Kanda (1994), also gave a report on standards antenna for electromagnetic interference measurements and proposed a method to calibrate them.

Short risetime output from a pulse generator based on a ferrite pulse sharpener has been reported, (Seddon and Thornton 1988). The transmission system used in these experimental studies, gave rise to an unintentional pulse sharpening phenomena which was found to be linear over the range of working voltage. A report is given on this condition.

1-3 STANDARDS FOR ELECTROMAGNETIC-FIELD MEASUREMENTS

Establishing standards for electromagnetic-field measurements is a multi-faceted task which requires measurements made in:

1. Anechoic chambers, 2. Open sites and 3., Within guided wave structures.

The underlining principles of these standard measurements and transfer standards fall into one of two categories:

1. Measurements, and 2. Theoretical modelling and calculations.

Attempts reported in the thesis are focused on the former - *measurement techniques*.

One of the main objectives of this research was to design and evaluate a passive transmission line probing system. The measurement techniques observed the absolute magnitudes and directions, and accurately distinguish between the effects of the electric ($\dot{D}$) and magnetic ($\dot{B}$) coupling of the induced signals. It was also possible to observe the behaviour of one of the components with respect to the other, as the directional coupler was rotated at various angular positions in the electromagnetic-field. Applications are given to show the feasibility of the new designed loop for specific applications. Attention is focused on EMC studies since the new loop plays an integral part in such measurements. Various mathematical concepts, analysis and calculations were used throughout the experimental studies when designing the devices and apparatus and for making comparative studies with measured parameters. Only typical examples of these could be shown.

As a result of the experimental studies and extended investigations, five papers were published at international conferences, all of which were presented by the author. Three further papers were published in related areas, in which the author of this thesis is a co-author. These papers are listed in Section **1-7**. An *Internal Report* was also published.

1-4 THE ARRANGEMENT OF THE THESIS

In the presentation of the material, a great deal of emphasis was made on lucidity and for smooth and logical flow of ideas. Many examples are included to illustrate techniques in measurements, to demonstrate fundamental concepts and to illustrate methods of solving typical problems.

Considerable thought was given to including computer analysis for the solution of some problems, but it was finally decided against. Diverting attention and effort to numerical methods and computer software, would distract concentration on the main theme of work. Where appropriate, the dependence of important results on the value of a parameter is stressed by graphs. However, a review of numerical methods, together with several references, are given.

***Chapter* 1** - presents a general introduction to and review of the research. From literature surveys, a summary was made of past developments and applications, and of current activities in the area of the topic. This first chapter also outlines the arrangement of the thesis.

Theories on the directional coupler, transmission line, antenna and fields in particular, which are relevant to the research, are discussed in - ***Chapter* 2**. Since these are directly related to Maxwell's equations, a review of the fundamental equations in their simple form is given. Mathematical analysis is given to well known equations and theorems, so as to prove the validity of the devices used and their measurement accuracies. Calculations of relevant parameters are included where appropriate, whilst others are shown in the Appendix.

New equations, derived from the concept of mathematical theory, were developed to be applied to a general practical loop-matching situation. Therefore, the theory is defined first and then modified to present new equations. Well known equations, developed by the original theory, were used in the calculations of various circuit parameters.

***Chapter* 3** - discusses the concepts of circuit-theory and field-theory which are built on ideal models. Mathematical relationships based on these models are used to link the circuit and field theory concepts. The emphasis is on the two-wire transmission-line circuit parameters, since this network can support both circuit and field analogies.

The design, description and constructional details of the devices and apparatus used in the experimental work are presented in - ***Chapter* 4**. Relevant theories and analyses are given where appropriate, followed by the testing procedures and summaries as applicable

***Chapter* 5** - deals with the general measurement techniques and test methods. Preview of the main instrumentation and apparatus, setting-up and experimental procedures are given. Some theories, calculations, testing and results are also included.

***Chapter* 6** - is devoted to the test sequence of the transmission system with many results obtained from various testing, using different loop orientations and modes of operation. These are explained in detail and verified and/or compared as appropriate.

***Chapter* 7** is an extension to the scheduled programme of research and deals with some novel applications. It shows how the new designed loop sensor is unique in some very useful and practical measurements, such as in:

- The detection and location of a fault in a network.
- An equality condition in electric and magnetic-field coupling, and in
- EMC applications.

***Chapter* 8** - is also an extension study and is based on further work that is continuing. It describes two signal interfacing methods, namely:

1. Optically coupled (*OC*) and
2. General Purpose Interface Bus (*GPIB*), also known as the IEEE-488 interface (1978 standard).

These interfacing methods (which were used in the experimental work) are included due to their significant practical applications in today's ever increasing demands for more

accurate measurements, data acquisition and processing, over a wide range of technologies. These are specialised areas of study, but the interface was built as part of the measurement system. A preview of these interface methods are given.

***Chapter* 9** - is the concluding chapter and a general discussion is given. It also includes suggestions for further work. The list is fairly long and some of work has been progressing for quite some time now. Some collaboration in certain aspect of the work is continuing with other universities and industries, both nationally and internationally.
An appendix is included.

1-5 SEQUENCE OF INVESTIGATION AND ORIGINAL CONTRIBUTIONS

1-5.1 Construction and Testing of the Devices and Apparatus

The work commenced with the layout of the transmission system, designing and constructing all the devices such as the directional couplers, loop probes, a 1 kV coaxial mercury pulser and an 80 kV SF_6 pulser for use in the experimental investigation. These were built purposely to original design specifications. (A fast mercury pulser was reported, but not in a coaxial form). Apart from the machining of some components for the directional coupler and high voltage pulser, all the work were accomplished by the author. Each device was individually tested to meet the required specifications. A lot of skill and effort were required to embody these devices within the transmission system, so as to form a unique measurement platform. A considerable amount of time was spent to build and assemble the line structure. Each device was tested independently and in conjunction with the transmission system, as appropriate. A coaxial line pulser with sub-nanosecond risetime response, was developed for practical applications.

1-5.2 Directional Properties of the Loop Probe

The first test was to detect and measure an induced voltage caused by the impinging electromagnetic field (created by the travelling pulse) interacting with the loop probe. This was achieved with the directional coupler first placed at the angle for maximum

electromagnetic-field coupling, and then for only the components of the electric-field coupling. By deduction of the measured induced voltages, a means was obtain to distinguish between the component of the electric- and magnetic-field coupling. Angular adjustment of the directional coupler was then made such that a cancelling effect occurred and the loop probe coupled only to a pulse travelling in one direction. This demonstrated the directional property of the loop probe which is of significant practical importance, (Rajroop and House 1991).

1-5.3 Equal Electric- and Magnetic-Field Coupling

An equality condition, that is, a coupling loop responding equally to the electric- and magnetic-field change is of significant interest. Methods reported in literatures are by complex configuration in loop design and by adding resistors in the loop circuit. It is demonstrated that this same condition of equality can be achieved by altering the geometry of the loop (Rajroop and Lai 1995).

1-5.4 Loop Antenna Design

A wide-band, high sensitivity loop antenna, capable for operation in the Giga-hertz region, was designed. It is small in size, so that it will cause very little perturbation of the fields and could be integrated within a measurement system. Moreover, the design is simple and cost-effective.

1-5.4.1 Simultaneous Electric- and Magnetic-Field Measurements

A mathematical theory was proposed for an electromagnetic near-field sensor for simultaneous electric- and magnetic-field measurements. This theory was tested and verified experimentally, first with the suggested loop design and then with a different design. The results were consistent, but it should be pointed out that the new designed loop and measuring technique has several advantages over the previous reported loop sensor. These are discussed.

1-5.5 Development of New Antenna Equations

The loading of the designed antenna plays an important part in its sensitivity and performance. Formulations which are based on balanced loading, were given. In practice, it is not always easy or possible to precisely match the loading, therefore a pair of new equations (based on the original formulation) were developed to satisfy the general load condition.

1-5.6 Pulse Sharpening Condition

It was discovered experimentally that the line system exhibited a pulse sharpening condition, whereby the pulse risetime progressively decreased as it travelled along the line (Rajroop *et al.* 1992). As a result the induced voltages increased correspondingly in a linear relationship. This is reported and work is continuing into the significance of this phenomena.

1-5.7 Mathematical Link between the Concepts of Circuit and Field-Theory

Both circuit- and field-theories, using analytical and numerical techniques based on differential and Maxwell's equations respectively, have been well documented in numerous texts and literatures. Each theory is powerful in its own right, although there are limitations in the concept of circuit-theory in certain applications.
It is thought that it is of importance to establish a relationship between these two concepts, showing how circuit parameters can be characterised in terms of either voltages and currents, or electric- and magnetic-fields.

In transmission lines, the analysis is based on the circuit parameters being distributed over the entire line. This method of circuit analysis is not suitable for high frequency lines when the physical length of the line is short compared with the wavelength of the alternating currents and voltages which they handle. In these situations, the concept of field-theory has to be employed, with the analysis now being carried out using computational numerical techniques.

An attempt is made to establish a relationship between the concept of circuit- and field-theory, since such relationship, although relevant to this work, does not appear to be documented in literatures.

1-6 NOVEL APPLICATIONS OF THE MEASUREMENT SYSTEM

1-6.1 A Simple Fault Detector/Locator

From the investigations carried out in this area, a simple, yet accurate method of fault location is presented. It made use of the pulse injection principle, but instead of a travelling wave, a very fast risetime pulse was injected into the faulty section of the line. Any response from the line due to a fault impedance, (between zero impedance and infinity) will result in a backward travelling reflected pulse. The distance to the fault is a matter of simply applying Time-Domain Reflectometry (*TDR*) measurement technique.

1-6.2 EMP/EMC Measurements

Due to the versatility and sensitivity characteristics of the loop probe, it readily finds application in EMP/EMC measurements. This can be extended to detect flaws in seams or aperture on shielding and enclosures. These applications are described.

1-6.3 High Voltage Divider

Resistive and capacitive voltage dividers have long since come to maturity, and are truly accepted in high voltage engineering measurement applications. These resistive and capacitive elements are subjected to certain inherent technical problems, which in turn, are beginning to impose a limitation on their use. Being in a high voltage environment for many years, it became evident that a new technique should be developed. The method proposed is to employ a loop probe, which, when immersed into a high voltage electro-magnetic field, behaves as an **E**-Field sensor.

1-6.4 Impulse Voltage Measurement

The technique (in conjunction with **[1-6.3]**) is simply to connect the output from the loop probe (optically if necessary) to a suitable measuring oscilloscope, placed in a less hostile electromagnetic environment. The displayed waveform can then be taken photographically or through an interface device to a computer. With proper calibration, an accurate peak impulse voltage can be determined.

1-6.5 Interface Devices

Although not original, two interfacing methods, namely, the General Purpose Interface Bus (*GPIB*), also known as the IEEE-488 interface, and an Optically Coupled (*OC*) interface, were developed under design specifications. They were tested and evaluated, and were used to enhance the measuring technique in terms of accuracy, efficiency, convenience and economy.

It is clearly beyond the scope of the thesis to fully investigate all of the above mentioned applications. However, the underlying principles are portrayed.

Work is continuing in some of these areas.

1-7 PUBLISHED REPORT AND PAPERS

1. Rajroop, P.J. (1990). "An EMP coupling and measuring techique in testing the performance of a transmission system," *Internal Report*, City University, London.

2. Rajroop, P.J. and House, H. (1991). "EMP coupling and measuring techniques in testing the performance of transmission lines," Proceedings of the 7th International Symposium on High Voltage Engineering, Dresden, Germany, Paper No. 83.02, pp. 103-106.

3. Rajroop, P.J., House, H. and Lai, L.L. (1992). "A novel EMP and measuring technique illustrated by testing the performance of fast pulse on transmission lines," Proceedings of the 8th International Conference on Electromagnetic Compatibility, IEE, UK, pp. 80-84.

4. Rajroop, P.J. and Lai, L.L. (1993a). "Application of the directional coupler as an accurate fault locator on a transmission line," Proceedings of the 8th International Symposium on High Voltage Engineering, Yokohama, Japan, Paper No.56.05, pp. 475-478.

5. Rajroop, P.J. and Lai, L.L. (1993b) "EMC using loop probes," Proceedings of the 8th International Symposium on High Voltage Engineering, Yokohama, Japan, Paper No. 79.02, pp. 449-452.

6. Rajroop, P.J. and Lai, L.L. (1995). "Equal response measurements of a modified $\dot{B}/\dot{D}$ near field probe sensor," Proceedings of the 9th International Symposium on High Voltage Engineering, Graz, Austria, Vol. S8, Paper No. 8385, pp. 1 - 4.

7. Lai, L.L., Ndeh-Che, F., Chu, K.H., Rajroop, P.J., and Wang, X.F. (1993). "Design Neural Networks with Genetic Algorithms for Fault Section Estimination," 29th UPEC.

8. Lai, L.L., Ndeh-Che, F., Chari, T., Rajroop, P.J. and Chandrasekharaiah, H.S. (1993)."HVDC Systems Fault Diagnosis with Neural Networks," Proc. 5th European Conference on Power Electronics and Applications, The European Power Electronics Association, Vol. 8, pp. 145-150.

9. Lai, L.L., Ma, J.T. Almonacid, K. and Rajroop, P.J. (1995). "On-Line Pattern Recognition with Fuzzy Logic Rules for Multi-Machine Power System Stability Assessment," International Conference on Advances in Power System Control, Operation and Management, ASCOM-95, IEE. (*To be presented in November 1995*)

Chapter 2

Theory and Review

Introduction

Some of the general theories that are relevant to the investigations are included in the text. Mathematical expressions are used throughout in the design aspects of the work, while equations listed were used in the calculations in support of the experimental results. New equations were derived from standard equations to take into account the more complex analyses in the design specifications of a coupling loop probe. Emphasis is made on the transmission-line theory and on the electric-dipole/magnetic-loop antenna analyses, since these form the basis of the experimental studies.

Since most of the mathematical expressions are direct derivative from Maxwell's Equations and Fourier series/transformations, these are previewed in their simple form. Other important and relevant calculations are included in the Appendix.

2-1 THE TRANSMISSION LINE CONCEPTS

A transmission line is more than a set of long parallel conductors. To the Electrical Power Engineer it is a distributed-parameter physical system, one in which voltages and currents, whether conveying communication signals or supplying bulk power, must be

regarded as continuous functions of distance along the given line. For efficient point-to-point transmission of power and information, the source energy must be directed or guided. In this experimental study, transverse electromagnetic (TEM) waves were guided by a transmission line model, capable of supporting such a mode of propagation. The TEM mode of guided waves is one in which the **E**-field and **H**-field are perpendicular to each other and both are transverse to the direction of propagation along the guiding line. More specifically, the magnetic-fields that change with time, induce electric-fields (as explained by Faraday's law), and the time-varying electric-fields induce magnetic-fields (as explained by the generalised Ampere's law). This interelationship also occurs along conducting or dielectric boundaries, and can give rise to waves that are guided by such boundaries. These waves are of paramount importance in guiding electromagnetic energy from a source to a device or system in which it is to be used.

The three most common types of guiding structures that support TEM waves are:

1. ***Parallel-plate transmission line***: This type of transmission system consists of two parallel conducting plates separated by a dielectric slab of uniform thickness. At microwave frequencies, parallel-plate transmission lines can be fabricated inexpensively on a dielectric substrate using printed-circuit technology. They are often called *striplines*.

2. ***Two-wire transmission line***: This transmission line consists of a pair of parallel conducting wires separated by a uniform distance. The most common examples are the overhead power and telephone lines. The transmission model used in the experimental study, falls into this category.

3. ***Coaxial transmission line***: This consists of an inner conductor and a coaxial outer conducting sheath separated by a dielectric medium. This structure has the important advantage of confining the electric- and magnetic-fields entirely within the dielectric region. No stray fields are radiated by a coaxial transmission cable, and very little external interference is coupled into the line. A typical example is the connections to high frequency measuring instruments and devices.

It should be noted that other wave modes, more complicated than TEM mode, can propagate on all three of these transmission systems, when the separation between the conductors is greater then certain *fractions* of the operating wavelength.

Dielectric guides, hollow-pipe waveguides and surface guides, are all important for such transmission purposes, but one of the simplest systems to understand - and one very important in its own right - is the parallel two-conductor transmission line. This is a typical and important example of a transmission system that supports TEM mode of propagation.

In any transverse plane, the electric-field lines pass from one conductor to the other, defining a voltage between conductors for that plane. Magnetic-field lines surround the conductors, corresponding to current flow in one conductor, and an equal, but opposite directed current flow in the other. Both voltage and current (and the fields from which they are derived) are functions of distance along the line.

The concepts of energy propagation, reflections at discontinuities, standing waves versus travelling waves and the resonance properties of standing waves, phase and group velocities, and the effects of losses upon wave properties, are extended easily from these transmission-line results to the more general classes of guiding structures.

The inductance and capacitance of the line can be calculated by solving the electro-magnetic field equations. Numerical methods such as the boundary element or finite element method have made this easy to do on a personal computer, due to suitable packages now available, (Rajroop, 1990), (Leuchmann and Bobholt ,1993), (Paul 1994).

It is common to express the characteristics of a transmission line in terms of its distributed parameters, as illustrated in Fig. 2-1.

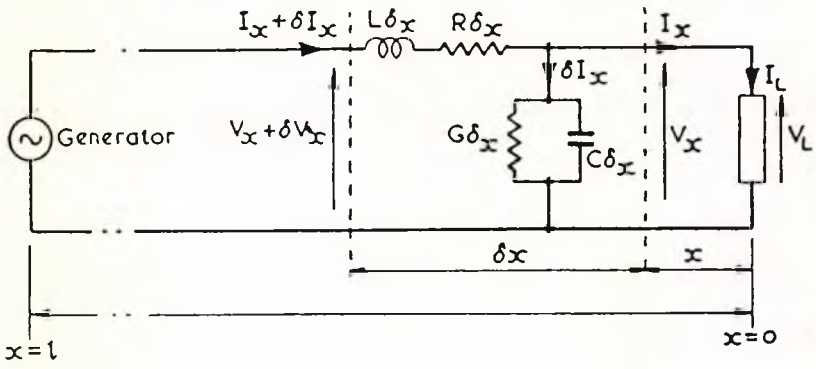


Fig. 2-1 The transmission line model.

This model includes the distributed series impedance of $(R + j\omega L)$ ohms per unit length, a distributed shunt admittance $(G + j\omega C)$ mho per unit length. The length δx, is small enough so that the parameters may be considered to be lumped. This gives a series impedance over the section of $(R + j\omega L)\delta x$ and a shunt admittance of $(G + j\omega C)\delta x$.

From the diagram in Fig. 2-1, it can be seen that:

$$\delta V_x = (R + j\omega L)\delta x(I_x + \delta I_x) \cong (R + j\omega L) I_x \delta x \tag{2-1}$$

assuming that $\delta I_x << I_x$

$$\delta I_x = (G + j\omega C)\delta x V_x \tag{2-2}$$

In the limit as $\delta x \to 0$ these equations become

$$\frac{\partial V_x}{\partial x} = (R + j\omega L) I_x \tag{2-3}$$

and

$$\frac{\delta I_x}{\partial x} = (G + j\omega C) V_x \tag{2-4}$$

Partial derivatives are used in order to indicate that only the variations with distance are being considered.

Equations (2-3) and (2-4) are known as the *time-harmonic transmission-line equations.*

2-1.1 Wave Characteristics on an Infinite Transmission Line

The coupled time-harmonic transmission-line equations, [Eqs. (2-3) and (2-4)], can be combined to solve for V_x and I_x .

Differentiating equation (2-4) with respect to x and substituting for $\frac{\partial V_x}{\partial x}$ from equation (2-3), gives:

$$\frac{\partial^2 I_x}{\partial x^2} = (R + j\omega L)(G + j\omega C)I_x = \gamma^2 I_x \tag{2-5}$$

Similarly,

$$\frac{\partial^2 V_x}{\partial x^2} = (R + j\omega L)(G + j\omega C) = \gamma^2 V_x \tag{2-6}$$

$$\text{Where } \gamma = \sqrt{[(R + j\omega L)(G + j\omega C)]} = \alpha + j\beta \tag{2-7}$$

For a given line γ - *the propagation coefficient*, will be constant. The real part α , is the *attenuation constant* (Np/m) and the imaginary part β , is the *phase constant* (rad/m) of the line.

These quantities are not really constants, because in general, they depend on the angular frequency ω , in a rather complicated way. Solving equations (2-5) and (2-6) gives:

$$I_x = Ce^{\gamma x} + De^{-\gamma x} \tag{2-8}$$

and

$$V_x = Ae^{\gamma x} + Be^{-\beta\gamma x} \tag{2-9}$$

Where C, D, A and B are complex constants which must be determined from known boundary conditions. Substituting V_x [(2-9)] in (2-3)], the following expression is obtained for I_x:

$$I_x = \frac{\gamma}{(R + j\omega L)} Ae^{\gamma x} - \frac{\gamma}{(R + j\omega L)} Be^{-\gamma x}$$

$$= \frac{A}{Z_0} e^{\gamma x} - \frac{B}{Z_0} e^{-\gamma x} \qquad (2,10)$$

where,

$$Z_0 = \frac{R + j\omega L}{\gamma} = \frac{\gamma}{G + j\omega C} = \frac{R + j\omega L}{G + j\omega C} \qquad (2\text{-}11)$$

The ratio of the voltage and current at any distance x, for an infinitely long line is independent of x and is called the *characteristics impedance* (Z_0) of the line.

2-1.2 Lossy transmission line basics

The quest to increase the speed of computing devices has made it necessary to change the way how engineers approach the problem in designing state-of-the-art computers. Many design decisions are made solely on the basis of achieving the highest performance in a design. All aspects of design from architecture to circuits and packaging must be scrutinised so that maximum performance can be achieved.

Faster circuit risetimes means that the packaging will have to be treated as if every inter-connect is a transmission line. The interconnects have proven to be a limiting factor in how fast a computer can operate. These factors forced the designer to treat transmission lines in a different manner, that is, to include frequency dependent losses in the transmission line analysis.

As the signal speeds increase, this simple model is not adequate to fully describe the transmission line. At higher frequencies a phenomena known as *skin effect* occurs. At low frequencies, the signal is carried uniformly across the cross section of the conductor. As the frequency increases the signal begins to be carried on only the outer surface of the conductor. The exact depth of penetration is determined by the skin depth of the conductor material. The net result is that the parameters of the line must take this into account. The resistance seen by the signal at higher frequencies is higher than that at lower frequencies. Every frequency has a different level of penetration into the conductor and thus sees a different resistance.

How this affects square waves is quite complex. Using the *Fourier* transform theory, it can be shown that a square wave can be represented as a summation of sine waves. This is expressed in the following relationship:

$$f(t) = \frac{V}{2} + \sum_{n=1}^{\infty} C_n \sin(\omega n t) \qquad (2\text{-}12)$$

Where V = amplitude

t = period

ω = frequency

n = 1,3,5 (odd harmonics)

C_n = coefficient of the n^{th} harmonic

This means that a square wave is actually made up of a number of sine waves that are of a frequency equal to the odd multiples of the fundamental frequency which is calculated by taking the reciprocal of the period. Combining this with the skin effect phenomena, it is interesting to see that a square wave travelling down a transmission line, really can be represented as many sine waves travelling down the line at the same time. Each of these sine waves experiences different transmission line properties as it penetrates the conductor at a different depth.

This led to the realisation that the transmission-line equations for propagation delay and impedance [shown in Eqs. (2-7) and (2-11)] are different for every frequency. Thus the impedance and propagation delay are dependent upon the frequency of the signal. In the case of a square wave, (which is comprised of sine waves of different frequencies), each frequency component sees a different impedance and travels at a different speed, resulting in the distortion of the pulse as it travels. The phenomena that different frequency components travel at different speeds is known as *dispersion*.

The following plots were taken which demonstrate these effects as a function of frequency. Fig. 2-2(a) shows the transmission line propagation delay (*pd*) versus frequency and Fig. 2-2(b) shows the transmission line attenuation versus frequency.

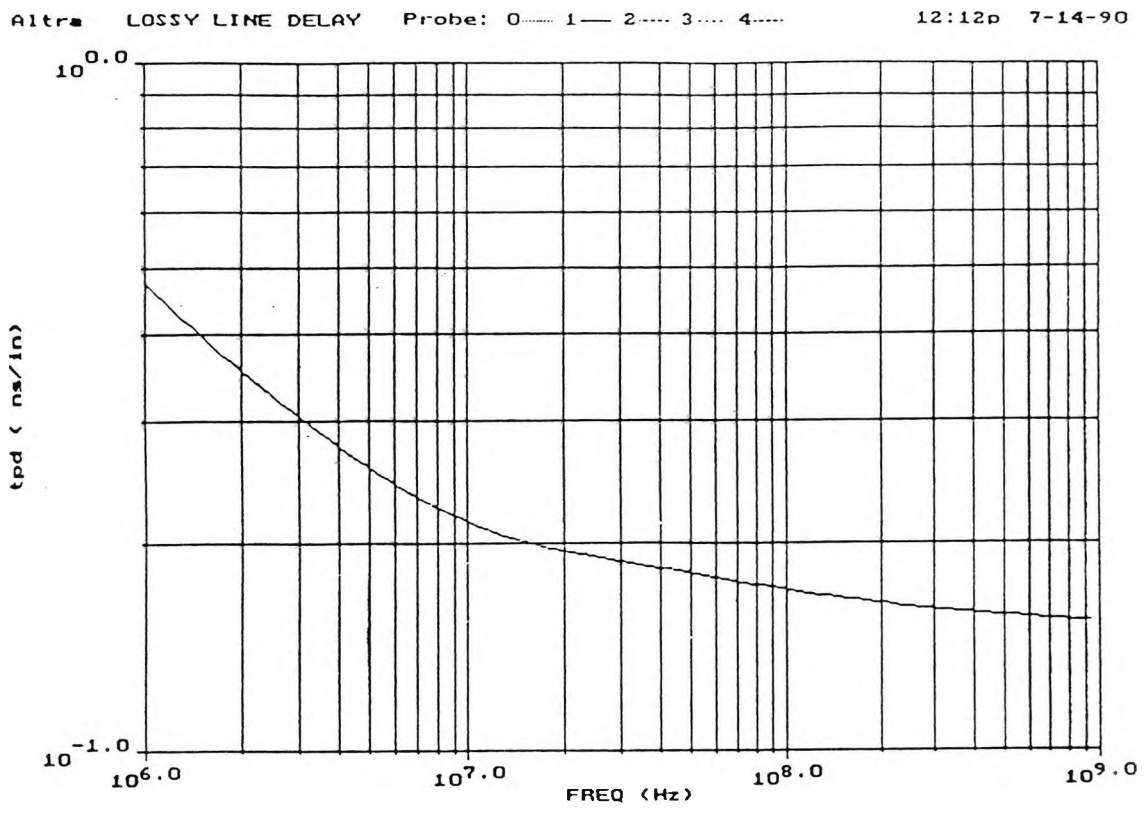


Fig. 2-2(a) Propagation delay versus frequency.

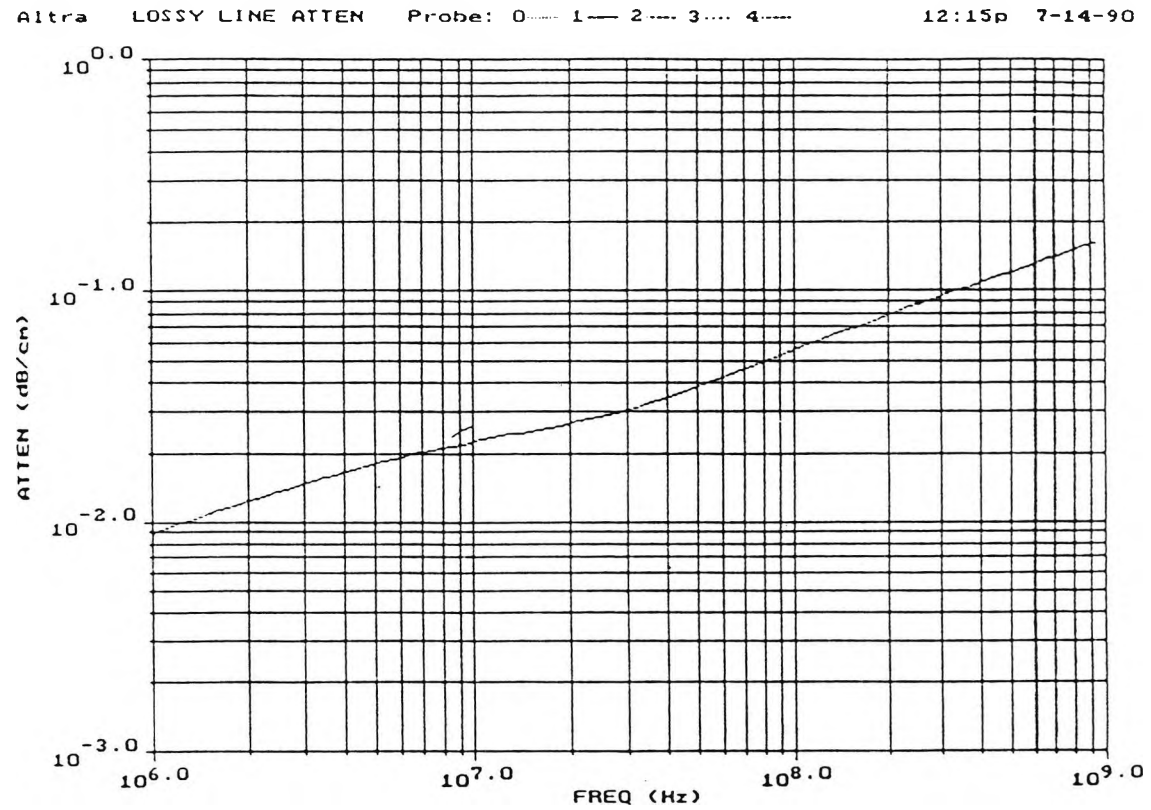


Fig. 2-2(b) Attenuation versus frequency.

2-1.3 Pulse Application

Although many equations and analysis used in this study are based on a sinusoidal wave-form, it is important to realise the Fourier transform representation in Eq. (2-12).
This is worth mentioning because the component that was injected into the test line was not an ultra high frequency *(UHF)* signal, as the line was operated under pulse condition. The fast risetime pulse is related by:

$$f = 1/t \tag{2-13}$$

Where f is the frequency in hertz and t, the time in second.

Few of the phenomena associated with high voltage transmission systems are linear, one most obvious example being electrical breakdown. This emphasises the need for diagnostic measurements. Since most phenomena involved are transients, the concept of pulse rise time is critical. It is rare that a black-box approach is possible with diagnostics, and therefore a knowledge of the significance of risetime is a minimum essential. A need to understand the interaction of the measuring equipment with the circuits under test is another almost unavoidable requirement, even at DC, but one which becomes more and more critical as the frequency increases (decreasing risetimes) .

2-2 THEORY OF OPERATION OF THE DIRECTIONAL COUPLER

Consider a small current-sampling probe, in the form of a tiny loop, (shown in Fig. 2-3), with one arm connected to a measuring oscilloscope and the other matched to the impedance of the oscilloscope. The relative phase for the electric and magnetic-fields due to the travelling pulse, depends upon the direction of propagation, and the coupling with these fields can be arranged to cancel in one direction of propagation. This method of measurement has not been used in this context to any great extent, mainly because of the inherent coupling of the electric-field which will always accompany the coupling of the magnetic-field. There will always exist this small but finite value of capacitance between the loop and the line conductor.

The loop is attached to a directional coupler which is mounted on the earth-plane of a single conductor/plane transmission line system and matched to the characteristic impedance of the line. When a travelling pulse front impinged on the loop, the electric field-created causes a current I_{fe} (fe - *forward electric*) to flow in the loop. Since the field distribution should be symmetrical around the loop, which is matched to the impedance of the oscilloscope, this current will be divided equally between the two branches. In practice, these I_{fe} components build up from zero at A to I_{fe} /2 at B and C respectively.

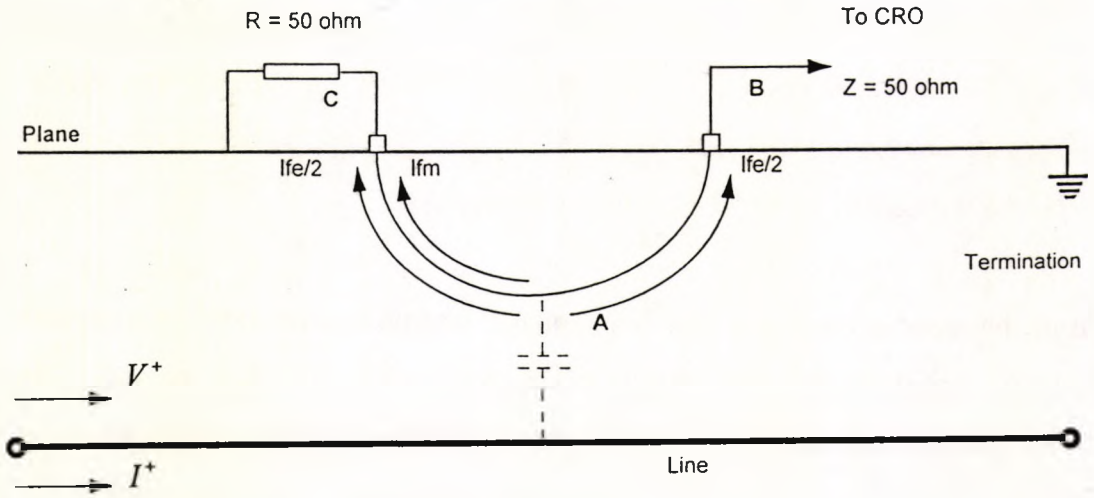


Fig. 2-3 Theory of operation of the directional coupler.

An induced current I_{fm} (fm - *forward magnetic*) due to the component of the magnetic-field change of the travelling pulse, also flows in the loop in a clockwise direction. It will add to the capacitive current in the left hand branch and subtract from the right hand branch.

The dimensions and angular position of the loop may be chosen so as to cause complete cancellation in one branch and summation in the other. These induced currents flowing in the loop will cause a voltage to be developed across its matching load resistor and the measuring oscilloscope input impedance. The loop may be adjusted so as to vary the magnetic-field coupling, but the electric-field coupling remains virtually constant. The induced component due to the electric-field coupling is proportional to the surface area of the loop conductor and is independent of any angular position. The induced component due to the magnetic-field coupling is proportional to the loop area projected normal to the magnetic-field and therefore varies as the cosine of the angle.

2-2.1 The following setting positions may be distinguished:

- When the loop is set at the angular position of 0/180 degree, and therefore without the influence of any magnetic-field, the directional coupler detects only the component of the electric-field.

- When the loop is set for maximum magnetic-field coupling (90/270 degree position) the directional coupler detects both the inherent electric-field component as well as the component of the magnetic-field due to the travelling pulse. These two components are in time-phase and they add together for a forward travelling pulse, but subtract for a reflected, or backward travelling pulse.

- When the angular position of the loop was adjusted so that both $(\dot{B} / \dot{D})$ components are equal, then they will add to give an induced voltage of twice the amplitude for the forward travelling pulse, but will cancel for a backward travelling pulse. In this mode the loop is described as a directional coupler in that it couples to a pulse travelling only in one direction. In general, for a given pulse, the electric-field component is always constant and is independent of the angular position of the loop.

2-3 MAXWELL'S EQUATIONS

The well known Maxwell's equations, the basis of all electromagnetic theory, are the relationship between the charge density ρ, electric-field **E,** electric displacement **D**, magnetic-field intensity **H** and magnetic-flux density **B**.

Maxwell's equations are important in this work since their solution for a certain set of conditions leads to the mathematical description of a plane wave - the sinusoidal variation in time and position of **E** and **H**, with the amplitude of each being constant in plane normal to the direction of propagation. These equations are used extensively in the characterisation of the transmission line, in antenna theory and in the mathematical relation between the concepts of field and circuit-theory.

It is easy to verify that $\partial \mathbf{D}/\partial t$ has the dimension of current density (A/m^2). The term $\partial \mathbf{D}/\partial t$ is called the displacement current density, and its introduction in the $\nabla \times \mathbf{H}$ equation was one of the major contribution of James Clerk Maxwell (1831-1879).

The fundamental of Maxwell's electromagnetic equations and the continuity equation are summarised in their differential form:

$$\nabla \times \mathbf{E} = -\partial \mathbf{B}/\partial t \tag{2-14}$$

$$\nabla \times \mathbf{H} = \mathbf{J} + \partial \mathbf{D}/\partial t \tag{2-15}$$

$$\nabla \cdot \mathbf{D} = \rho \tag{2-16}$$

$$\nabla \cdot \mathbf{B} = 0 \tag{2-17}$$

Note that ρ is the volume density of *free charges* (or charge density) and **J**, the current density of *free currents*, which may comprise both convection current ($\rho \mathbf{v}$) and conduction current ($\sigma \mathbf{E}$).

2-3.1 Integral form of Maxwell's Equations

The four Maxwell's equations shown in their differential form above are valid at every point in space. In explaining electromagnetic phenomena in a physical environment, it is necessary to deal with finite objects of specified shapes and boundaries. It is therefore convenient to convert these differential equations into their large-scale, or integral form equivalents.

By taking the surface integral of both sides of the curl equations (2-14) and (2-15) over an open surface S with a contour C and applying Stoke's theorem, the following equations are obtained:

$$\oint \mathbf{E} \cdot d\ell = -\int_S \partial \mathbf{B}/\partial t \cdot ds \tag{2-18}$$

$$\oint \mathbf{H} \cdot d\ell = \int_S (\mathbf{J} + \partial \mathbf{D}/\partial t) \cdot ds \tag{2-19}$$

Taking the volume of both sides of the divergence equations (2-16) and (2-17) over a volume V with a *closed* surface S, and using the divergence theorem, the following equations are obtained:

$$\oint \mathbf{D} \cdot ds = \int \rho \, dv \tag{2-20}$$

and

$$\oint \mathbf{B} \cdot ds = 0 \tag{2-21}$$

2-3.2 Gaussian Representation of Maxwell's Equations

These equations in their integral form can be illustrated by using lines of force as shown in Fig. 2-4(a-d). The illustration in Fig. 2-4(a) shows that the integral around the loop of the component of **E** tangent to the line, is equal to the negative of the change with time of the component of **B** normal to the area enclosed by the loop. Thus if the normal component of **B** directed out from the plane of the paper is decreasing with time, then the integral is positive. This is the Faraday's law of induction.

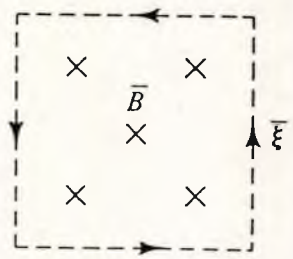


Fig. 2-4(a) Representation of Maxwell's equation - $\oint \mathbf{E} \cdot d\ell = -\int_S \partial \mathbf{B}/\partial t \cdot ds$

Equation (2-19) is the generalised Ampere's law including Maxwell's displacement current term. It states that the line integral of magnetic-field about a closed path

(magneto-motive force *mmf*) is equal to the total current (conduction, convection and displacement) flowing through the path. This is illustrated in Fig. 2-4(b).

There are two sources of **H,** namely, the current density **J,** and the displacement current density $\partial\ \mathbf{D}/\partial t$. The product of the normal components of these two current densities and the area is equal to the line integral of **H** around the loop enclosing the area.

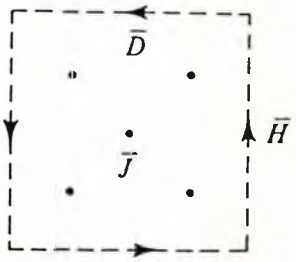


Fig. 2-4(b) Representation of Maxwell's equation - $\oint_c \mathbf{H} \cdot d\ell = \int_S (\mathbf{J} + \partial\, \mathbf{D}/\partial t) \cdot ds$

Equation (2-20) is the familiar form of Guass's law. In Fig. 2-4(c), it can be seen lines of **D** originate on a positive electrical charge and terminate on a negative one. Thus the integral of the product of the component of **D** parallel to the unit normal to the surface is equal to the total net electrical charge in the volume enclosed by the surface at that instant.

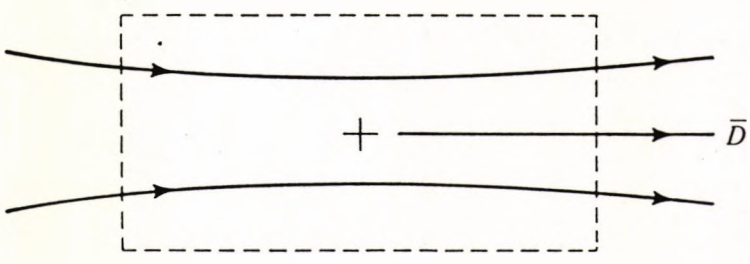


Fig. 2-4(c) Representation of Maxwell's equation - $\oint_s \mathbf{D} \cdot ds = \int \rho\ dv$

Equation (2-21) states that the surface integral of the magnetic-field or total magnetic flux flowing out of a closed surface is zero for all values of time, expressing the fact that such charges may never be found in nature. Since there are no isolated magnetic

monopole, the lines of **B** have no point from which to originate or terminate. Thus, the number of lines of **B** going into a volume element must equal to the number coming out.

This is illustrated in Fig. 2-4(d).

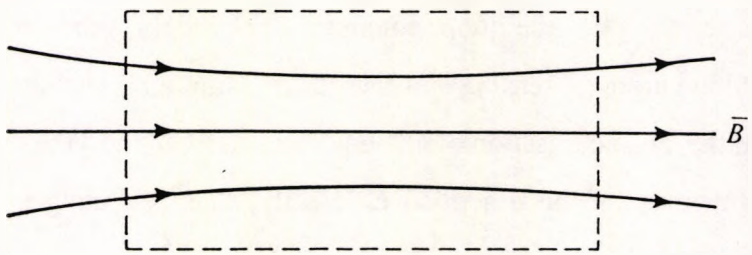


Fig. 2-4(d) Representation of Maxwell's equation - $\oint_s \mathbf{B} \cdot ds = 0$

2-4 PROPERTIES OF ANTENNAS

2-4.1 Introduction and Review

An antenna (or aerial) is a device for radiating or receiving electromagnetic waves and are the basic components of any electronic system which depends on free space as the propagation medium. Therefore, the antenna is the connecting link between free space and the transmitter and receiver, and as such, it plays an essential part in determining the characteristics of the system in which it is used. Thus antennas have always been associated with wireless communications.

Fundamentally, there is very little difference between a transmitting antenna and a receiving antenna, and by the *Reciprocity Theorem*, the same mathematical analyses applies.

In many systems of navigational or direction-finding purposes the operational characteris-tics of the system are designed around the directive properties of the antenna. In other systems the antenna may be used simply to radiate energy in an omnidirectional pattern in order to provide a broadcast type coverage. In other systems such as point-to-

point communications, the antenna may have a highly directional pattern to achieve increased gain and interference reduction.

Regardless of the systems application, all antennas are therefore associated with certain definite properties which can be well defined, and are common to them all.
Today, simple types of antennas, such as the loop antennas, are widely used in measurement applications, detection purposes, sensing and EMP/EMC immunity testing. Extensive work is taking place in the characterisation of antennas especially in the Time-Domain, in which wide band antennas can be described efficiently, thus providing a significant insight into an antenna's behaviour, (Allen and Hill 1993).

In a decade or so ago, antennas have been integrated as an essential part within the system along which they are designed. This is because it is important to know about the system performance as a whole rather than that of the antenna alone. For example, in a satellite ground station, the noise temperature of the whole system is a criterion of performance when it comes to receiving weak signals and not just the noise temperature of the antenna.

The type of antennas used in this experimental study are classified as loop sensors or loop probes and they function as receiving elements, to couple to pulses travelling on a transmission line. A novel approach is reported in the thesis on a modified loop antenna, that possesses unique features.

Nearly a century ago, Pocklington (1897), studied the excitation of a thin loop antenna by a plane wave. He used the Fourier series expansion method as appropriate for the geometry under consideration. Hallen (1938) and later Storer (1956), also used the same method. Wu (1968), studied the analyses and found that these authors made approximations that were not accurate enough. He formulated a different set of equations, based on the original, which appeared to remove some of the uncertainties from the previous equations.

Since antennas play a very important part in a communication system, it is essential to have a thorough understanding of the principles on which they perform their task efficiently. Hence this has led to the design and development of many different types of antennas, each suitable for a particular application.

Antenna Engineering is a very broad, yet specialised discipline, hence only a brief introduction to the subject is given. There are numerous reference books and papers that are readily available, which could provide in-depth knowledge to the subject.
In recent years antennas have been treated as an essential part of a system and are thus designed accordingly, since in most cases, it is the performance of the whole system that really matters. Antennas are therefore associated with certain common and definite properties, regardless of the systems application.

The following discussions are applicable to antennas used in the sense of both transmitting and receiving devices and these include the directional coupler, incorporating suitable loop probes. The properties of antennas which are most often of interest are:

- Radiation patterns (polar diagrams)
- Characteristics of simple patterns
- Polarisation
- Impedance
- Directivity
- Gain
- Bandwidth

2-4.2 Radiation Patterns

The radiation pattern of an antenna is generally its most basic requirement, since it determines the spatial distribution of the radiated electromagnetic energy.

Some common types of radiation patterns are as follows:

1. Omnidirectional (broadcast type)
2. Pencil-beam pattern
3. Fan-beam pattern
4. Shaped-bean pattern

The omnidirectional or broadcast type pattern is used for many broadcast or communication services, where all directions are to be covered equally well. The horizontal-plane pattern is generally circular while the vertical-plane pattern may have some directivity in order to increase the gain.

The pencil-beam pattern is a highly directional pattern which is used when it is desired to obtain maximum gain and when the radiation pattern is to be concentrated in as narrow an angular sector as possible. The beamwidths in the two principal planes are essentially equal.

The fan-beam pattern is similar to the pencil-beam pattern except that the cross-section of the beam is elliptical in shape rather than circular. The beamwidth in one plane may be considerably broader than that in the other plane. As with the pencil-beam pattern the fan-beam pattern generally implies a rather substantial amount of gain.

The shaped-bean pattern is used when the pattern in one of the principal planes is desired to have a specified type of coverage. A typical example is the cosecant type of pattern which is used to provide a constant radar return over a range of angles in the vertical plane. The pattern in the other principal plane is usually a pencil-beam type of pattern, but may also be of circular pattern as in certain types of beacon antennas.

In addition to the pattern types described here there are several other pattern shapes used for direction findings and other purposes which do not fall within the four categories listed. For those patterns which have particularly unusual characteristics, it is generally necessary to specify the pattern by an actual plot of its shape or by the mathematical relationship which describes its shape.

2-4.3 Characteristics of Simple Patterns

For antennas which have patterns of simple shape, the important characteristics of the patterns can be specified by the beamwidth and side-lobe level in the two principal planes, usually the *E*- plane and the *H*-plane. The *E*-plane is parallel to the electric- field vector and passes through the antenna in the direction of the beam maximum. The *H*-plane is perpendicular to the *E*-plane and also passes through the antenna in the direction of the beam maximum.

2-4.3.1 Radiation from Electric-Current Elements

A simple practical radiator is the *doublet*, or Hertzian dipole, which is frequently used in antenna practice. It is in the form of a short length of thin wire arranged in a linear configuration. If the current distribution on such a wire, assumed to be uniform and varies sinusoidally with time is known, then the radiation pattern and the radiated power can be found. This is based on the integration of the effects due to each differential element of the current along the wire.

It is therefore of interest to set down the complete expressions for the fields at any distance due to a differential element of current oriented along the *z*- axis as shown in Fig. 2-5.

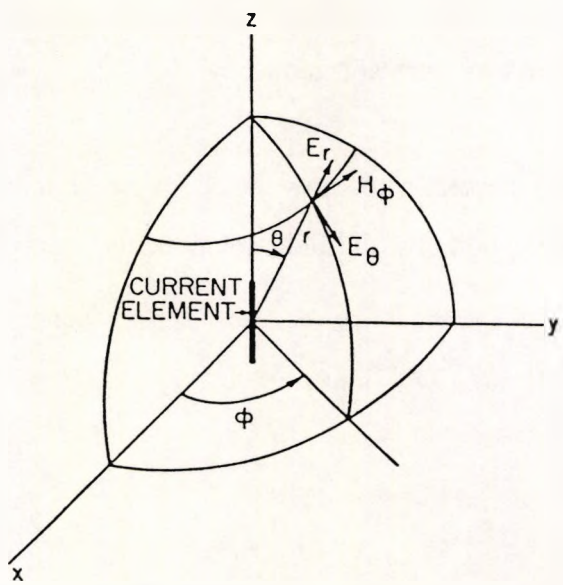


Fig. 2-5 Co-ordinate system for the electric dipole.

The rms electric- and magnetic-field components are given as follows:

$$E_r = 60\beta^2 Idz\left[\frac{1}{(\beta r)^2} - \frac{j}{(\beta r)^3}\right]\cos\theta e^{-j\beta r} \quad (2\text{-}22)$$

$$E_\theta = j30\theta^2 Idz\left[\frac{1}{\beta r} - \frac{j}{(\theta r)^2} - \frac{1}{(\beta r)^3}\right]\sin\theta e^{-j\beta r} \quad (2\text{-}23)$$

$$H_\phi = j\frac{\beta^2}{4\pi} Idz\left[\frac{1}{\beta r} - \frac{j}{(\beta r)^2}\right]\sin\theta e^{-j\beta r} \quad (2\text{-}24)$$

$$E_\phi = H_r = H_\theta = 0 \quad (2\text{-}25)$$

where,

Idz = moment of differential current (I given in rms and dz in metres)

r = distance in metres to the observation point

$\beta = 2\pi / \lambda$ [λ - the wavelength (m)]

E is the electric-field intensity (V/m)

and H - the magnetic-field intensity (A/m)

A time factor of $e^{-j\omega t}$ has been omitted, since in the general case of interest, it is assumed that the time-varying sinusoidal current is of constant frequency.

For most problems of interest it is only necessary to know the components in the far-field region, i.e. when $r >> \lambda$. Under these conditions, the field components are given simply by:

$$E_\theta = j\frac{30\beta Idz}{r}\sin\theta e^{-j\beta r} = j\frac{60\pi Idz}{r\lambda}\sin\theta e^{-j\beta r} \quad (2\text{-}26)$$

$$H_\phi = j\frac{\beta Idz}{4\pi r}\sin\theta e^{-j\beta r} = \frac{E_\theta}{120\pi} \quad (2\text{-}27)$$

2-4.3.2 Radiation from Magnetic-Current Elements

Another basic radiator which is frequently used in antenna practice is a magnetic-current element. Although magnetic currents do not exist in nature, there are a number of configurations which produce fields identical with those which would be produced by a fictitious magnetic current. For instance, a circular loop carrying electric current whose diameter is very small in terms of wavelengths, will produce fields which are equivalent to those of a short magnetic-dipole. The fields for any distance are given by the following expressions:

$$E_\phi = 30\beta^3 dm\left[\frac{1}{\beta_r} - \frac{j}{(\beta r)^2}\right]\sin\theta e^{-j\beta r} \tag{2-28}$$

$$H_r = \frac{\beta^3}{2\pi} dm\left[\frac{j}{(\beta r)^2} + \frac{1}{(\beta r)^3}\right]\cos\theta e^{-j\beta r} \tag{2-29}$$

$$H_\theta = -\frac{\beta^3}{4\pi} dm\left[\frac{1}{\beta r} - \frac{j}{(\beta r)^2} - \frac{1}{(\beta r)^3}\right]\sin\theta e^{-j\beta r} \tag{2-30}$$

$$E_r = E_\theta = H_\phi = 0 \tag{2-31}$$

whose co-ordinate system is shown in Fig. 2-6, and dm is defined as the differential magnetic-dipole moment.

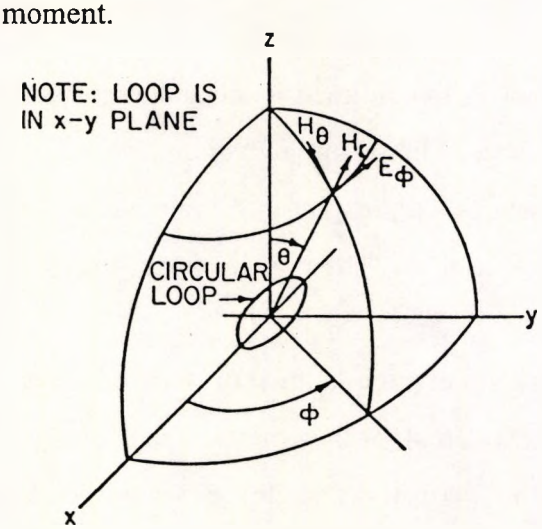


Fig. 2-6 Co-ordinate system for magnetic-dipole.

For a small diameter loop, the magnetic moment of the loop is equal to the electric current I, flowing through the loop *times* its area A.

For the far-field, when $r >> \lambda$, the field component is reduced to:

$$E_\phi = \frac{30\beta^2 dm}{r}\sin\theta e^{-j\beta r} \tag{2-32}$$

$$H_\theta = -\frac{\beta^2 dm}{4\pi r}\sin\theta e^{-j\beta r} = \frac{E_\phi}{120\pi} \tag{2-33}$$

It should be noted from the field expressions for the magnetic-current element are almost exactly analogous to those for the electric-field element, except for the interchange for electric and magnetic quantities.

2-4.4 Polarisation

The polarisation of an antenna is usually defined in terms of the orientation of the electric-field vector in the direction of maximum radiation. Thus a vertical dipole above ground will radiate vertical polarisation while a horizontal one will radiate horizontal polarisation. Although this simple arrangement is commonly used, it can become confusing for large angles above ground. Thus it is more precise to define the polarisation in terms of the E_θ and E_ϕ components in a polar co-ordinate system (Antenna Engineering Handbook - Jasik) as shown in Fig. 2-7.

The radiation pattern of an antenna is three-dimensional and requires field-intensity measurements over all angles of space. In taking radiation patterns, it is therefore necessary to specify various space angles with respect to the antenna under test. Fig. 2-7 describes the co-ordinate system in general use. The *xy* plane is the horizontal plane.

Radiation patterns may be taken either along the latitude or polar angle as a function of azimuth angle (these are conical cut patterns), or they may be taken along azimuth angle as a function of polar angle (these are vertical cut angle), depending on the application

and information desired. The orientation in space of the E vector is arbitrary, depending on the polarisation of the radiated field.

For elliptical polarisation, more than one orientation of the E vector is desirable. A complete set of measurements obtained from these methods, is often necessary for describing the radiation pattern of an antenna mounted on an irregularly shaped object. The direction of the polar axis of the co-ordinate system is generally taken as the local vertical.

In addition to linearly polarised antennas, the use of circularly polarised antennas has recently become quite common. Circular polarisation can be produced by two perpendicular linearly polarised fields which have a 90 degree phase difference. Depending on the sense of rotation, circular polarisation may be either right-handed or left-handed.

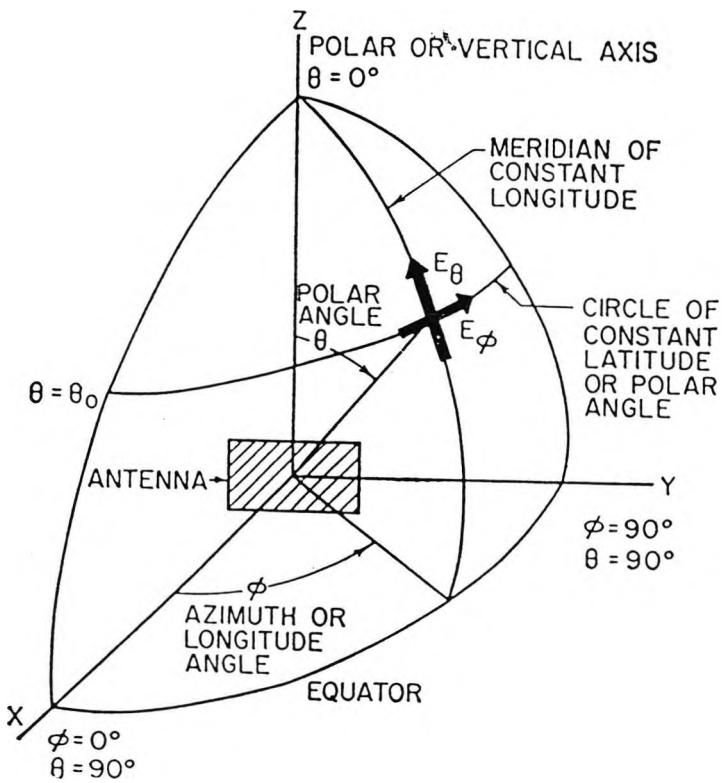


Fig. 2-7 Co-ordinate system for radiation-pattern measurements.

2-4.5 Directivity

The directional characteristics of an antenna are often expressed in terms of a gain function $G(\theta,\phi)$ where θ is the angle of co-latitude and ϕ is the polar angle (Fig. 2-5). The gain is commonly defined as the ratio of the maximum radiation intensity in a given direction *to* the maximum radiation intensity, produced in the same direction, from a reference antenna with the same power input.

Directivity is closely associated with gain and is defined as the ratio of the maxim radiation intensity to the average radiation intensity. If the radiation pattern of an antenna is specified in terms of the electric field $E(\theta,\phi)$, as a function of the polar co-ordinate angles θ and ϕ, then the radiation intensity is proportional to the square of the electric-field and the directivity D is expressed by:

$$D = \frac{4\pi E_{max}^{\ 2}}{\int_0^{2\pi}\int_0^{\pi} E^2(\theta,\phi)\sin\theta d\theta d\phi} \qquad (2\text{-}34)$$

in the *polar* co-ordinates. This expression defines directivity with reference to a lossless isotropic radiator.

2-4.6 Gain

The gain of an antenna is a basic property which is frequently used as a figure of merit. Gain is closely associated with directivity, which in turn is dependent upon the radiation patterns of an antenna. The gain is commonly defined as the ratio of the maximum radiation intensity in a given direction to the maximum radiation intensity produced in the same direction from a reference antenna with the same power input. That is:

$$G = \frac{power\ radiated\ by\ an\ antenna}{power\ radiated\ by\ reference\ antenna} \qquad (2\text{-}35)$$

The gain G is related to the directivity D by the expression:

$$G = kD, \tag{2-36}$$

where k is the efficiency factor of the antenna and is equal to unity if the antenna has no copper, dielectric or mismatch losses. For many types of antenna systems, the losses are very low and the value of the gain is essentially equal to the directivity. The reference antenna most commonly used is the isotropic radiator - a hypothetical lossless antenna which radiates uniformly in all directions.

Since gain denotes a concentration of radiated energy, high values of gain are associated with narrow beamwidths. For antenna that have no internal losses, the gain is the same as the directivity. However while directivity can be computed from ether theoretical considerations or from measured radiation pattern, the gain of an antenna is almost always determined by direct comparison measurement against a standard-gain antenna. The effective area of an antenna is directly related to its gain. The effective area is of interest when it is desired to compute the energy collected by a receiving antenna or to compute the transmission loss between two antennas in free space.

2-4.7 Impedance

The input impedance of an antenna system is of considerable importance since it directly affects the efficiency of energy transfer to and from the antenna. The over-all input impedance of an antenna system depends not only on the impedance of the individual antenna elements but also on the mutual impedance between elements as well as the transmission lines and transmission-line components which are used to interconnect the antenna elements.

The over-all design of a complex antenna system will therefore be governed as much by the details of the interconnecting transmission line, as by the characteristics of the individual antenna element. If a large operating bandwidth is desired, each element and component of the antenna system must have favourable impedance properties over the bandwidth of operation.

While it is possible to compute the properties of many transmission-line and wave-guide components, it is extremely difficult to theoretically determine the impedance characteris-tics of antenna element, other than those elements which have relatively simple geometric shapes. Even for the simple cases, many drawbacks exist, and it is generally preferable to use theoretical antenna impedance values, primarily for the purpose of interpreting and guiding the experimental measurement procedure. Also important is the radiation resistance which is associated with power radiating from the antenna.

To compute the radiation resistance, it is necessary to know the radiation field pattern of the antenna in terms of the current flowing at the point to which the radiation resistance is required. The total radiated is then computed by integrating the total power density passing through a sphere surrounding the antenna. This computation will be carried through very briefly for the case of a very short dipole having an effective length ℓ_e and carrying a current I_0. The electric-field intensity for this antenna can be deduced from Fig. 2-5 as:

$$|E_0| = \frac{60\pi I_0 \ell_e}{r\lambda} \sin\theta \tag{2-37}$$

The power density in the far-field is given by the Poynting vector, which is equal to $E_\theta^2 / 120\pi$, where the electric field is given in V_{rms} / m and the power density is expressed in *watts/m*^{2}. Integrating over a large sphere surrounding the antenna, the following expression is obtained:

$$P = \int_0^\pi \frac{E_0^2}{120\pi} 2\pi r^2 \sin\theta d\theta \tag{2-38}$$

$$= \frac{80\pi^2 I_0^2 \ell_e^2}{\lambda^2} \tag{2-39}$$

The radiation resistance R_e is obtained by dividing this result by I_0^2.

$$R_e = 80\pi^2 \frac{\ell_e^2}{\lambda^2} \tag{2-40}$$

2-4.8 Bandwidth

Unlike some of the properties which have been treated previously, the bandwidth of an antenna or antenna system does not have a unique definition. Depending upon the operational requirement of the system with which the antenna is to be used, the functional bandwidth of an antenna may be limited by any one or several of the following factors:

- change of pattern shape or pattern direction
- increase in side-lobe level
- loss in gain
- change of polarisation characteristics
- deterioration of impedance characteristics

For antennas where all of the factors mentioned are important, one of the factors, such as gain or impedance, will determine the low-frequency limit while another factor, such as change of pattern shape, will determine the high-frequency limit. In general, the only appropriate definition for the bandwidth of a particular antenna is that band within which the antenna meets a given set of specifications.

Despite the difficulty in uniquely specifying bandwidth, it is possible to make a few observations regarding the factors which tend to limit the bandwidth of certain simple antenna structures. For antenna with relatively small dimensions (i.e. when the linear dimensions are of the order of half wavelength or less), the limiting factor is most frequently the impedance performance. For many circularly polarised antennas, the polarisation characteristics prove to be the limiting factor on bandwidth. For end-field linear arrays, the pattern direction will deviate excessively long before the pattern shape or impedance characteristics deteriorate.

There are several situations where it is possible to make some firm estimates concerning bandwidth. One situation arises when it is necessary to face the problem of matching an antenna which has a known impedance variation over a given frequency range. By

determining the equivalent Q-factor of the antenna it is possible to determine the lowest theoretically obtainable standing wave ratio *(SWR)* over a required bandwidth with a given number of network elements. Conversely, it is possible to determine the maximum bandwidth for a permissible value of standing-wave ratio.

It should be noted that the bandwidth of an antenna is critically dependent on its value of Q; the higher the Q the lower the bandwidth. Or in other words, this indicates that the larger the stored reactive energy as compared to the radiated energy, the lower will be the bandwidth.

2-5 TIME-DOMAIN ANTENNA CHARACTERISATION

2-5.1 Introduction

The means by which an antenna's transmitting and receiving responses are described generally, is almost universally accomplished with the many defined and accepted frequency-domain characterisations. However, these characterisations become cumber-some when used to describe an antenna which can transmit and receive pulses whose duration is measured in the sub-nanosecond region. In such cases, the time-domain characterisation are more flexible and may provide greater insight into the antenna's behaviour.

A limited number of time-domain characterisation including directivity (Sengupta and Tai 1976), energy radiation efficiency, radiation resistance, slope patterns, effective aperture and peak amplitude (Harmuth 1984) have been reported.

Allen and Hill, (1993) used these existing characterisations and proposed a number of new time-domain characterisations that altogether, allow a more complete description of an antenna's behaviour to be made. Many of these bear the same name as existing frequency-domain characterisations because they have been derived from those characterisations and to some context, are similar in meaning.

2-5.2 Transient Response of an Antenna

A receiving antenna's response is defined as the output voltage waveform resulting from a given field incident upon the antenna. Its transmitting response is defined as the transmitted far-field resulting from a given voltage waveform driving the antenna element. Schmitt (1960), using the Rayleigh-Carson relationship, and Kanda (1986), using plane-wave scattering theory, have shown that an antenna's transient response is proportional to the time-derivative of its receiving response.

In the frequency-domain, high-fidelity reception of the transmission of wide-band signals is dependent upon the antenna having a flat amplitude response over the frequency band of interest, and a phase response that is a linear function of frequency. Deviation from either of these constraints will result in distortion of a transient signal. In the time-domain, an antenna's fidelity is a measure of how accurately the received voltage available at the antenna's terminals reproduces the behaviour of the transient field incident upon the antenna, or for the transmitting case, how accurately the time integral of the transmitted field reproduces the behaviour of the voltage applied to the antenna's terminals.

It is evident that an antenna's fidelity is specific to its waveform; i.e. an antenna may provide a high-fidelity reproduction for some waveforms and be unable to provide the same fidelity for many other waveforms.

2-5.3 Antenna Characterisation

Existing antenna characterisations are based on time-harmonics excitation of the antenna. However, is difficult for time-harmonics characterisation to provide a clear portrayal of the antenna's behaviour due to a transient field incident upon the antenna, or a transient waveform driving it. Allen and Hill (1993) formulated a set of time-domain characterisations, which are for most part, logical extensions of the existing time-harmonics characterisation described by Johnk (1988), Stutzman and Thiele, (1981) and Bronaugh and Lambdin, (1988).

The extension from time-harmonic characterisation to time-domain characterisation is in most cases, based on considering the energy content of the signal rather than its time-average power. Characterising an antenna based on an observable that is independent of the antenna excitation would be desirable. However as with frequency-domain characterisation, the time-domain characterisation are a function of the waveform exciting the antenna. These listed below are of interest in the experimental work:

2-6 THE LOOP ANTENNA

Fourier series expansion method is used in the analysis of loop antennas, in particular, those acting as electromagnetic field probes. Kanda (1984), proposed a theory based on rigorous mathematical concepts, of a loop sensor to perform simultaneous electric and magnetic field measurements. This analysis is outlined first then *modified* later in the text.

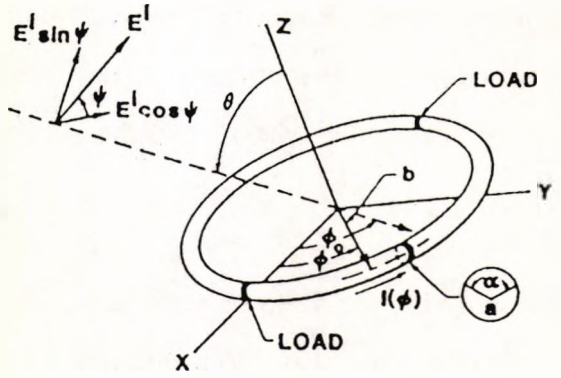


Fig. 2-8 Loop configuration of a near-field sensor for simultaneous E- and H-field measurements.

Fig. 2-8 shows the geometry and co-ordinate system for a loop antenna lying in the plane $z = 0$ and excited at $\phi = 0$ with a delta-function voltage source V_o. Assuming that a linearly polarised plane-wave E_ϕ^i, impinges onto the loop. The loop current $I(\phi)$ satisfies the integral equation:

$$V_o \delta(\phi) + b\, E_\phi^i(b,\phi) = \frac{j\varsigma}{4\pi} \int_{-\pi}^{\pi} L(\phi - \phi')\, I(\phi')\, d\phi' \quad . \qquad (2\text{-}41)$$

where,

$E_{\phi}^{i}(b,\phi)$ is the ϕ – component of the incident field at the point ϕ on the loop,

b is the loop radius, and

ς is the free space wave impedance.

The kernel in Eq. (2-41) may be represented in a Fourier series form as follows:

$$L(\phi-\phi') = \sum_{-\infty}^{\infty} a_n e^{-jn(\phi-\phi')} \tag{2-42}$$

with,

$$a_n = a_{-n} = \frac{kb}{2}(N_{n+1} + N_{n-1}) - \frac{n^2}{kb} N_n \tag{2-43}$$

$$N_n = \frac{b}{4\pi^2} \int_{\pi}^{\pi} d\alpha \int_{\pi}^{\pi} \frac{e^{jn(\phi-\phi')} e^{-jkr}}{r} d\phi \tag{2-44}$$

and:

$$r = \sqrt{\frac{4b^2 \sin^2(\phi-\phi')}{2 + 4a^2 \sin^2(\alpha/2)}} \tag{2-45}$$

Where k is the free space wave-number. Assuming that $a < b$ and $ka < 1$, Wu, (1964) has shown that N_n can be represented in terms of integrals of Bessel and Lommel-Weber functions, (Jahnke and Emde, 1945).

$$N_o = \frac{1}{\pi} \ln \frac{8b}{a} - \frac{1}{2}\left[\int_0^{2kb} \Omega_0(x)dx + j \int_0^{2kb} J_0(x)dx \right] \tag{2-46}$$

$$N_n = N_{n-1} = \frac{1}{\pi}\left[K_0\left(\frac{na}{b}\right) I_0\left(\frac{na}{b}\right) + C_n \right] - \tfrac{1}{2} \int_0^{2kb} [\Omega_{2n}(x) + jJ_{2n}(x)]dx, \quad n >> 1 \tag{2-47}$$

Where:

$$C_n = \ln 4n + \gamma - 2\sum_{m=0}^{n-1} \frac{1}{2m+1} \tag{2-48}$$

$K_0(x)$ is the modified Bessel function of the second kind,

$I_0(x)$ is the modified Bssel function of the first kind,

$\Omega_n(x)$ is the Lommel-Weber function,

$J_n(x)$ is the Bessel function, and

$\gamma \cong 0.5772$ is Euler's constant.

The loop current $I(\phi)$ can be expressed in the Fourier series:

$$I(\phi) = \sum_{-\infty}^{\infty} I_n e^{-j\phi} \tag{2-49}$$

and the electric field $E_0^i(b,\phi)$ in a Fourier series:

$$E_0^i(b,\phi) = E_0^i \sum_{-\infty}^{\infty} f_n e^{-jn\phi} \tag{2-50}$$

According to Fourier's theorem:

$$f_n = \frac{1}{2\pi E_0^i} \int_{-\pi}^{\pi} F(\phi) e^{jn\phi} d\phi \tag{2-51}$$

It becomes clear from Fig. 2-7 that the ϕ - component of the incident field at angle ϕ on the loop is:

$$E_\phi^i(b,\phi) = E_0^i[\cos\psi \cos(\phi - \varphi_0) - \sin\phi \sin(\phi - \phi_0)).\cos\phi] e^{ikb\cos(\phi-\phi_0)\sin\phi} \tag{2-52}$$

Using the integral representation of the Bessel function:

$$J_n(Z) = \frac{j^{-n}}{2\pi} \int_0^{2\pi} e^{jz\cos\phi} e^{jz\phi} d\phi \tag{2-53}$$

The following equation is obtained:

$$f_n = j^{n-1} \cos\psi e^{-jn\phi_0} J_n'(kb\sin\phi) + j^n \sin\phi.\cos\theta e^{-j\phi_0} \frac{nJ_n(kb\sin\phi)}{kb\sin\phi} \tag{2-54}$$

Using the orthogonality property of the function $e^{-jn\phi}$, the Fourier coefficient of the current can be obtained from (2-41), (2-42), (2-49) and (2-50):

$$I_n = -\frac{j}{\pi\zeta}\frac{V_0 + 2\pi b E_0^i f_n}{a_n} \tag{2-55}$$

2-6.1 Solving for the Inductance and Capacitance of the Loop Antenna

By setting $E_0^i = 0$ in (15), the admittance of the loop is given by:

$$Y = -\frac{j}{\pi\zeta}\sum_{-\infty}^{\infty}\frac{1}{a_n} = \frac{j}{\pi\zeta}\left(\frac{1}{a_0} + 2\sum_{1}^{\infty}\frac{1}{a_n}\right) \tag{2-56}$$

Assuming that currents of higher order than $n = 1$ in (15) are negligible due to the small size of the loop, the admittance for the magnetic-loop current ($n = 0$) can be defined as:

$$Y_0 = \frac{j}{\pi\zeta a_0} \tag{2-57}$$

And the admittance for the electric-dipole current ($n = 1$) as:

$$Y_1 = \frac{j2}{\pi\zeta a_1} \tag{2-58}$$

It will be shown later that the imaginary part (susceptance) of the loop admittance for the magnetic-loop current is generally negative and therefore is inductive. However, the susceptance for the electric-dipole current is generally positive and is therefore capacitive These form the slopes of the susceptance curves plotted against frequency, the quasi-static capacitance of the loop can be determined.

Imposing the quasi-static limit ($kb < 1$), to determine the admittance Y_0 for the quasi-static current, the following relationship is required:

$$a_0 = \frac{kb}{2}(N_1 + N_{-1}) = kbN_1 \tag{2-59}$$

$$K_0\left(\frac{a}{b}\right) \cong -\left(\gamma + \ln\frac{a}{2b}\right) \tag{2-60}$$

$$I_0\left(\frac{a}{b}\right) \cong 1 \tag{2-61}$$

$$\Omega_2(x) \cong -\frac{2x}{3\pi} \tag{2-62}$$

$$J_2(x) \cong \frac{x^2}{8} \tag{2-63}$$

To evaluate a_0, and neglecting the higher powers of kb , N_1 can be obtained from Eq.(2-47):

$$N_1 \cong \frac{1}{\pi}\left(\ln\frac{8b}{a} - 2\right) + 0(k^2b^2) \tag{2-64}$$

The quasi-static admittance of the magnetic-loop current can now be obtained from Eq. (2-57):

$$Y_0 \cong \frac{1}{j\zeta kb\left(\ln\frac{8b}{a} - 2\right)} = \frac{1}{j\omega L} \tag{2-65}$$

from which the inductance of the loop is:

$$L = \mu b\left(\ln\frac{8b}{a} - 2\right) \tag{2-66}$$

Where μ is the *permeability* of the medium.

This equation was used to calculate the inductance of a loop reported in the thesis.

The quasi-static capacitance of the loop can be obtained from Eq. (2-58):

$$a_1 = \frac{kb}{2}(N_2 + N_0) - \frac{1}{kb}N_1 \tag{2-67}$$

$$\text{Since } \Omega_0(x) \cong \frac{2}{\pi}x \tag{2-68}$$

$$\text{and } J_0(x) \cong 1 \tag{2-69}$$

N_0 can be obtained from Eq. (2-6), to the first order of kb.

$$N_0 \cong \frac{1}{\pi}\ln\frac{8b}{a} - jkb \tag{2-70}$$

Also with $\Omega_4(x) \cong \frac{2x}{15\pi}$ and $J_4(x) \cong \frac{x^4}{2^4 4!} \cong 0$, so that , neglecting higher orders of kb N_2 becomes :

$$N_2 = \frac{1}{\pi}\left[-\ln\frac{a}{b} - \gamma + C_2\right] + \frac{1}{2}\int_0^{2kb}\frac{2x}{15\pi}dx \tag{2-71}$$

$$\cong \frac{1}{\pi}\left[-\ln\frac{a}{b} - \gamma + C_2\right] \tag{2-72}$$

Where $C_2 = \ln 8 + \gamma - 8/3 \cong -0.010$

For N_1 given in Eq. (2-64), the leading term of the admittance for the electric-dipole current is:

$$Y_1 = -\frac{j2}{\pi\zeta a_1} \cong \frac{j2}{\pi\zeta}\frac{kb}{K_1} = \frac{j2}{\zeta}\frac{kb}{\left(\ln\frac{8b}{a} - 2\right)} = j\omega C \tag{2-73}$$

Thus the capacitance of the loop is given by:

$$C = \frac{2\varepsilon b}{\ln\frac{8b}{a} - 2} \tag{2-74}$$

This equation was also used to calculate the capacitance of the loop.

2-6.2 Electric and magnetic responses of the loop antenna

Consider the loop loaded with two equal impedances Z_L at diametrically opposite points, ($\phi = 0, \pi,$) in an incident plane-wave field, as shown in Fig. 2-8. Since the total current is the sum of the currents maintained by the electromagnetic forces (*EMFs*) at $\phi = 0, \pi$, and by the incident field E_0^i,

$$I(\phi) = 2\pi b E_0^i u(\phi) - I(0)Z_L v(\phi) - I(\pi)Z_L w(\phi) \tag{2-75}$$

where ϕ is the angular position around the loop

$I(0)$ and $I(\pi)$ are the currents through the two loads, b is the loop radius,

and:
$$u(\phi) = \frac{-1}{\pi\varsigma}\left(\frac{f_o}{a_o} + \frac{2f_1\cos(\phi)}{a_1}\right) \tag{2-76}$$

$$v(\phi) = \frac{-j}{\pi\varsigma}\left(\frac{1}{a_o} + \frac{2\cos(\phi)}{a_1}\right) \tag{2-77}$$

$$w(\phi) = \frac{-j}{\pi\varsigma}\left(\frac{1}{a_o} - \frac{2\cos(\phi)}{a_1}\right) \tag{2-78}$$

It is assumed here that currents of higher order than n =1 in Eq. (2-55) are negligible due to the small size of the loop. The current $I(0)$ and $I(\pi)$ can be determined by the simultaneous equations obtained from Eq. (2-75) with ϕ = 0 and π.

$$I(0) = 2\pi bE_0^i\left(\frac{f_0Y_0}{1+2Y_0Z_L} + \frac{f_1Y_1}{1+2Y_1Z_L}\right) \tag{2-79}$$

$$I(\pi) = 2\pi bE_0^i\left(\frac{f_0Y_0}{1+2Y_0Z_L} + \frac{f_1Y_1}{1+2Y_1Z_L}\right) \tag{2-80}$$

Where $Y_0 = G_0 + jB_0$ is the loop admittance for the magnetic loop response and

$Y_1 = G_1 + jB_1$ is the loop admittance for the electric-dipole response.

The following equations are obtained by taking the *sum* (Σ) and *difference* (Δ) of these currents:

$$I_\Sigma = \tfrac{1}{2}[I(0) + I(\pi) = 2\pi bE_0^i\left(\frac{f_0Y_0}{1+2Y_0Z_L}\right) \tag{2-81}$$

$$I_\Delta = \tfrac{1}{2}[I(0) - I(\pi)] = 2\pi bE_0^i\left(\frac{f_1Y_1}{1+2Y_1Z_L}\right) \tag{2-82}$$

It can be seen from Eqs.(2-81) and (2-82) that the sum current may be used to measure the magnetic-field whereas the difference current may be used to measure the electric-field

These results may be verified by considering the currents in the electric-dipole and magnetic-loop responses of the loop. The magnetic loop response adds to the electric-dipole response across one load, whereas across the other, it subtracts. Thus by taking the sum and difference of the currents across the loads, the magnetic-loop and electric-dipole responses can be separated. That is, the sum current gives a measure of the magnetic field, while the difference current gives a measure of the electric field.

2-6.3. Modification of these equations to allow for unbalanced loads

The mathematical theory of a single loop sensor for simultaneous measurements of the electric- and magnetic-field has been thus outlined above. The sensor uses an electrically small loop terminated with two identical load impedances Z_L at diametrically opposite points, $(\phi = 0,\pi)$. In practice it may be difficult and often inconvenient to use precisely matched loads to terminate the loop, especially when the sensor is to be used over a wide band frequency. The theory proposed by Kanda (1984), can be modified to allow for unmatched loads at the loop terminals. This analysis is intended for a semicircular loop as used in this experimental studies, but applies equally to a circular loop, since both loads are terminated on the earthplane so as to form a closed circuit.

Consider Eqs.(2-75) for the current at any point around the loop and Eqs. (2-76), (2-77) and (2-78). It is assumed in these latter equations that components of the loop current of higher order than 1 are insignificant due to the electrically small loop. The variable f_o relates the incident field E_0^i to the current induced in the loop by the magnetic field and similarly f_l relates to E_o^i to the current induced by the electric field, (Kanda, 1984). a_0 is related to the input admittance of the loop for magnetic loop current by:

$$Y_a = \frac{-j}{\pi Z_o a_o} \qquad (2\text{-}83)$$

where a_1 is related to the admittance for the electric-dipole current by:

$$Y_1 = \frac{-j2}{\pi Z_o a_1} \tag{2-84}$$

The first term on the right hand side of Eq. (2-75) is derived from the incident field on the loop, whereas the second two terms are related to the currents flowing through the two load impedances at $\phi = 0$ and $\phi = \pi$. Substituting unmatched impedances (Z_1 and Z_2) in Eq. (2-75) and solving for the currents through the two loads gives:

$$I_0 = 2\pi b E_0^i u(0) - I_0 Z_1 v(0) - I(\pi) Z_2 w(0) \tag{2-85}$$

$$I_\pi = 2\pi b E_0^i u(\pi) - I_0 Z_1 v(\pi) - I_\pi(\pi) Z_2 w(\pi) \tag{2-86}$$

Adding Eqs. (2-85) and (2-86) and substituting (2-76), (2-77), (2-78), (2-83) and (2- 84) gives:

$$I(0) + I(\pi) = 4\pi b E_0^i f_0 Y_0 - 2I(0) Z_1 Y_0 - 2I(\pi) Z_2 Y_0 \tag{2-87}$$

$$\Rightarrow 4\pi b E_0^i f_0 = \frac{I(0) + I(\pi)}{Y_0} + 2I_0 Z_1 + 2I(\pi) Z_2 \tag{2-88}$$

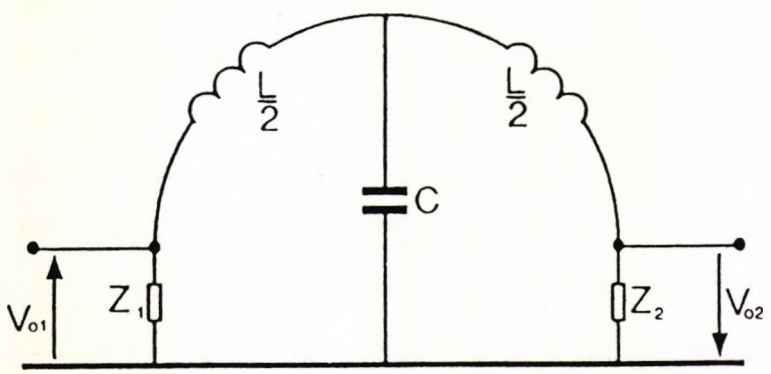


Fig. 2-9 Circuit model of a single loop sensor, showing output voltages and impedances, loop capacitance and inductance.

Fig. 2-9 shows an equivalent circuit diagram of the loop and it can be seen that the current through one load $I(0) = (V_{o1}/Z_1)$ and the other $I(\pi) = V_{o2}/Z_2$. Also the magnetic field admittance $Y_0 = \frac{1}{j\omega L}$.

$$\Rightarrow 4\pi b E_0^i f_0 = 2(V_{o1} + V_{o2}) + j\omega L\left(\frac{V_{o1}}{Z_1} + \frac{V_{o2}}{Z_2}\right) \tag{2-89}$$

and therefore,

$$H \propto 2(V_{o1} + V_{o2}) + j\omega L\left(\frac{V_{o1}}{Z_1} + \frac{V_{o2}}{Z_2}\right) \tag{2-90}$$

By subtracting Eqs. (2-85) and (2-86) and performing a similar set of substitutions, it can be shown that:

$$4\pi b E_0^i f_1 = 2(V_{o1} - V_{o2}) + \frac{1}{j\omega L}\left(\frac{V_{o1}}{Z_1} - \frac{V_{o2}}{Z_2}\right) \tag{2-91}$$

and hence

$$E \propto 2(V_{o1} - V_{o2}) + \frac{1}{j\omega C}\left(\frac{V_{o1}}{Z_1} - \frac{V_{o2}}{Z_2}\right) \tag{2-92}$$

Where V_{o1} and V_{o2} are the voltages at the two outputs of the loop. C is the loop capacitance to earth and L is the loop inductance. The capacitance of the loop can be calculated by first determining the impedance of the loop at one output, the other being open circuited. Similarly, the inductance can also be derived from the short circuited input impedance.

This method compares favourably with those calculated by Eqs. (2-74) and (2-66) and with the computer analysis.

The above equations for electric and magnetic field are valid for an arbitrary small semi-circular loop above an earthplane. Such loop and configuration are used in this experimental work.

2-6.4 Performance of Electric-field Transfer Standards

There are various standard antennas that can be used for the electric-field measurements, (Kanda 1994). The loading of these antenna is significant in these standards.

For an electrically short dipole antenna with a capacitive load, the transfer function is given by:

$$S(f) = \frac{V_L(f)}{E_i(f)} = \frac{h(\alpha / 2)}{1 + C / C_a} \tag{2-93}$$

where,

$$C_a = \frac{4\pi h}{v_0 \zeta_0 (\Omega - 2 - \ln 4)} \tag{2-94}$$

$$\alpha = \frac{\Omega - 1}{\Omega - 2 + \ln 4} \tag{2-95}$$

and,

- a antenna radius (m)
- C capacitance of load (F)
- C_a capacitance of antenna (F)
- E_i incident electric field (V/m)
- h half of physical length of dipole antenna (m)
- V_L output voltage of the antenna (V)
- ζ_0 free-space impedance (Ω)
- v_0 speed of light in free space (m/s)
- Ω antenna thickness factor $[i.e. \Omega = 2\ln(2h / a)]$

Since the input of an electrically short dipole is almost purely capacitive, it is possible to achieve a frequency-independent characteristic with a capacitive load, as indicated in Eq. (2-93). In practice the load is not purely capacitive, but may also have a resistive component which will cause a roll-off at the low end of the frequency range.

For resistive loading a FET amplifier with an input resistance of approximately 100 kΩ can be used. This would give a flat frequency response from 2 kHz to 400 MHz. Above

400 MHz the dipole becomes electrically long, therefore the theoretical expression given in Eq. (2-93) will not be valid. Given the present state of the art, however, it is not possible to build a balanced high-input impedance FET differential amplifier with a high common-mode rejection above 400 MHz. For this reason, it is a more common practice to use a high-frequency, beam-lead Schottky-barrier diode with a very small junction capacitance, (less than 0.1 pF) and a very high junction resistance (2 MΩ) for a standard antenna above 400 MHz.

2-6.5 Performance for Magnetic-field Transfer Standards

A magnetic-field probe consists of an electrically small balanced loop antenna, the response of which is directly proportional to the frequency. In order to make the response of the loop antenna flat over the frequency range of interest, the Q of the antenna is reduced through a loading resistor at the antenna terminal.

The voltage V_i induced in an electrically small loop antenna by an electromagnetic wave incident on the loop is determined by Maxwell's equations and Stoke's theorem, (Kanda, 1977) is given by:

$$V_i = \int E_i d\ell = j\omega\mu H_i NS \tag{2-96}$$

where: E_i is the tangential electric field around the loop

ℓ - the circumference of the loop

ω - the angular frequency of E_i

μ - the permeability of the loop core

H_i - the component of the magnetic field normal to the plane of the loop

N - the number of loop turns, and

S - the area of the loop

The induced voltage V_i of an electrically small loop antenna is proportional to frequency, the number of loop turns and the area of the loop. To make the response of the loop

antenna flat over the frequency range of interest, the Q of the antenna has to reduced through a loading resistor.

The response of an electrically small loop antenna, (Kanda 1977), is given by:

$$\frac{V_o}{V_i} = \frac{-j\frac{1}{\delta}}{\frac{1}{Q} + j(\delta - \frac{1}{\delta})} \tag{2-97}$$

where,

$$Q = \frac{R}{Z_0}$$

$$X_0 = J\omega_0 L = \frac{1}{j\omega_0 C}$$

$$\delta = \frac{\omega}{\omega_0},$$

$$\text{and } \omega_0 = \frac{1}{\sqrt{LC}} \tag{2-98}$$

Substituting for V_i in Eqs. (2-96) in (2-97), the following transfer function is obtained for an electrically small loop antenna:

$$S(f) = \frac{V_o}{H_i} = \omega_0 \mu NS \frac{1}{\frac{1}{Q} + j(\delta - \frac{1}{\delta})} \tag{2-99}$$

2-7 PHOTONIC PROBES

Properly designed photonic probes provide the wide bandwidth and low dispersion necessary to main the fidelity of time-domain signals, so that both amplitude and phase information can be retrieved. They are free from electromagnetic interference and there is minimum perturbation of the field being measured. These are systems in which the probe head contains no active components - electronics or power supplies. Light from a laser is launched into an optical fibre link and serves as a signal carrier. An electromagnetic-field incident on the probe head, induces a time-varying voltage across the modulator crystal

and changes its index of refraction. The resulting change in the propagation constant of the modulator crystal, changes the phase of the carrier as it traverses the crystal.

At the receiver end of the fibre link, the modulated light is detected by a photodiode and converted to an electrical signal suitable for analysis with a spectrum analyser, oscilloscope or other signal processor. The electro-optic interaction is weak, and except for very high fields, the gain of a small antenna is usually required to obtain an adequate signal.

For the measurement of a pulsed electric field, an antenna with a flat broadband response is most desirable. A restively loaded dipole gives a non-resonant frequency response and is therefore ideal for use in the time-domain measurement of electromagnetic fields. Electro-optical modulators which are driven by antenna feeds are characterised as a function of the voltage applied to their electrodes.

The physical characteristics of four modulators used in electromagnetic-field probes are shown in Fig. 2-10.

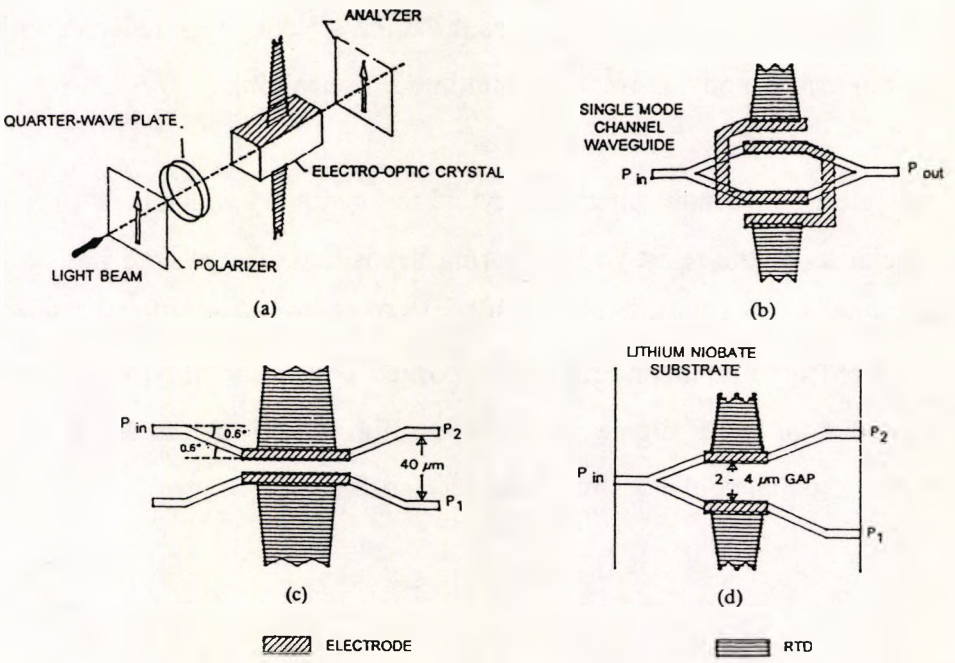


Fig. 2-10 Passive photonic modulators used in electromagnetic field probes.

The transfer functions of these passive photonic modulators are given in Table 2-1.

TABLE 1 Photonic E-field Measurement System

System	PEFM-2	PEFM-15	PEFM-15C
Source Wavelength	GaAlAs SRD 807 nm	GaAlAs Laser 830 nm	Diode Pumped YAG 1320 nm
P_d (dBm)	-22	-19	0
Fiber[1]	PM and MM	MM	PM and SM
Modulator	3-Port Coupler OGW $LiNbO_3$	Pockels Cell Bulk $LiNbO_3$	Pockels Cell Bulk $Bi_4Ge_3O_{12}$
V_π (V)	10	265	2100
S_m (dB)[2]	-15	-44.6	-62.6
Antenna	2 cm RTD[3]	15 cm RTD	15 cm RTD
S_a (dB)	-38	-23	-18
S_T (dB)	-23	-105	-104
Bandwidth (MHz)	0.02-1000[4] 500-3000	0.01-200	0.01-1000
NEF $V \cdot m^{-1} \cdot H^{-1/2}$	0.1	0.2	1.0
Dynamic Range (dB)	65	68	72

[1] MM = multimode, SM = single mode, PM = polarization maintaining.
[2] All dB values are for 20 log of the decimal values.
[3] RTD = resistively-tapered dipole.
[4] Band switched.

Photonic E-Field Measurement Systems - 15 (PEFM-15) has three 15 cm dipoles mounted orthogonally to each other to give an isotropic response, (Kanda 1986). The dipoles are fabricated on a planar fused silica substrate by geometrically tapering a thin film of resistive material. a single laser and detector are switched between the dipoles for the measurement of CW fields. Significant noise contribution are due to the receiver with its avalanche photodiode and modal noise in the multimode optical links.

PEFM-15C has a single 15 cm dipole antenna of cylindrical geometry which is fabricated by tapering the thickness of the resistive film during deposition. The system has been designed specifically for use at a high field level in an EMP environment. PEFM-2 has a 2 cm resistively tapered dipole antenna directly deposited onto a modified directional coupler (3-port) modulator. The dipole is of a thin-film nickel chromium and is geometrically tapered to obtained the desired resistance profile.

Chapter 3

A Mathematical Link between the Concepts of Circuit- and Field-Theory

3-1 INTRODUCTION

Both the concepts of field- and circuit-theory, using analytical methods based on differential and Maxwell's equations respectively, have been well documented in numerous texts and literatures. An attempt is made to establish a mathematical relationship between the concepts of field- and circuit-theory, since such relationship, although relevant and important to this work, does not appear to be documented in literatures.

The concepts of field- and circuit-theory are built on idealised models. The circuit-theory is built on circuit model of ideal sources and pure resistances, inductances and capacitances. In this case the basic quantities are voltages, currents, resistances, inductances and capacitances. The rules of operation are algebra, differential equations, Laplace transformations and the fundamental postulates are Kirchhoff's voltage and current laws.

Many relations and formulas can be derived from this rather simple model, and the responses of very elaborate networks can be determined. The validity of the model has

been amply demonstrated. In a like manner, an electromagnetic field-theory can be built on a suitable chosen electromagnetic model. The quantities on the electromagnetic model can be divided mainly into two categories: source quantities and field quantities. The source of an electromagnetic field is invariably electric charges at rest or in motion. However, an electromagnetic field may cause a redistribution of charges, which will in turn, change the field. Hence the separation of the cause-and-effect is not always so distinct.

Electromagnetics is of fundamental importance to the physicist and to the electrical, electronic and computer engineer. Electromagnetic theory is indispensable in understanding the atom smasher, cathode-ray oscilloscope, radar, satellite communication, television reception, remote sensing, radio astronomy, microwave devices, fibre optic communication, electromagnetic compatibility problems, instrument landing systems etc.

3-2 The Electromagnetics of Circuits

Much of the engineering design and analysis of electromagnetic interactions are done through the mechanism of lumped-element circuit. In general, circuit-theory deals with lumped-parameter system - circuit consists of components characterised by lumped-circuit parameters. In these, the energy-storage elements (inductors and capacitors) and the dissipative elements (resistors) are connected to each other and to sources or active elements within the circuit, by conducting paths of negligible impedance. There may be mutual coupling, either electrical or magnetic, but in the *ideal* circuit, these couplings are carefully planned and optimised. The advantage of this approach is that functions are well separated and cause-and-effect relationships are relatively simple to understand. Powerful methods of synthesis, analysis, and computer optimisation of such circuits have consequently been developed. When the source frequency is very low so that the dimensions of the individual conducting elements in an electrical circuit are small compared with their wavelength, the fields of the elements are *quasi-static*; that is

although varying with time, the electric- and magnetic-fields have the spacial form of static field distributions.

In this situation, the electromagnetic problem is simplified to a circuit problem where voltages and currents are the main variables. There are important distributed effects in many real circuits, but often they can be represented by a few properly chosen lumped coupling elements. In some circuits, in which the transmission lines are primary examples, the distributed effects are the major ones and must be considered from the beginning.

For DC circuits, the system variables are constant and the governing equations are algebraic equations. The system variables in AC circuits are time-dependent; they are scalar quantities and are independent of space co-ordinates. The governing equations are ordinary differential equations, while most electromagnetic variables are functions of time as well as space co-ordinates. Many are vectors (with both magnitude and direction) and their representation and manipulation require the use of vector algebra and vector calculus. Even in static cases the governing equations are, in general, partial differential equations.

However, it should be emphasised that circuit-theory is itself, a highly developed and sophisticated discipline. It applies to a different class of electrical engineering problems and is important in its own right.

A typical situation may arise to illustrate the limitation of circuit-theory concepts and hence the need for electromagnetic-field concepts. Consider the monopole antenna of a mobile telephone. On transmitting, the antenna is fed with an information carrying current at the appropriate carrier frequency. From a circuit-theory point of view, the source feeds an open-circuit, since naturally, the upper end of the antenna is not connected to anything physical; hence no current would flow resulting in no transmission.

Obviously this view point cannot explain why communications are established between mobile telephones at a distance apart. Therefore electromagnetic-field concepts must be used. That is, when the length of the antenna is an appreciable part of the carrier wave-length, a nonuniform current will flow along the open-ended antenna. This current radiates a time-varying electromagnetic-field in space, which propagates an electro-magnetic wave and induces time-varying currents in the other antenna at the distance.

3-3 Idealisations in Classical Circuit Theory

It is essential that circuit and circuit elements should be examined more closely from the point of view of electromagnetics, and to grasp the idealisation required to derive Kirchhoff's laws from Maxwell's equations. It is also possible to make certain extensions of the concepts when a simple idealisation do not apply. In particular, introduction of the retardation concept shows that a circuit may radiate energy when comparable in size with wavelength. The amount of radiated power may be estimated from these extended circuit ideas for some configurations.

For certain classes of circuits, it becomes impossible to make the extensions without a true field analysis.

9-4 Kirchhoff's Voltage Law

Kirchhoff's two laws provide the basis for classical circuit-theory. Consider the voltage law as a way of receiving the basic element values of lumped-circuit theory. The law states that for any closed loop of a circuit, the algebraic sum of the voltages for the individual branches of the loop is zero: i.e.

$$\sum_i V_i = 0 \qquad (3\text{-}1)$$

The basis for this law is Faraday's law for a closed path, expressed as:

$$-\oint \mathbf{E} \cdot \mathbf{dl} = \frac{\partial}{\partial t} \int_S \mathbf{B} \cdot \mathbf{dS} \qquad (3\text{-}2)$$

and the definition of voltages between two reference points on the loop,

$$V_{ba} = -\int_a^b \mathbf{E} \cdot \mathbf{dl} \qquad (3\text{-}3)$$

To illustrate the relationship between the circuit expression Eq. (3-1) and the field expressions Eqs. (3-2) and (3-3) consider first a single loop with applied voltage $V_0(t)$ and passive resistance, inductance and capacitance in series, shown in Fig. 3-1.

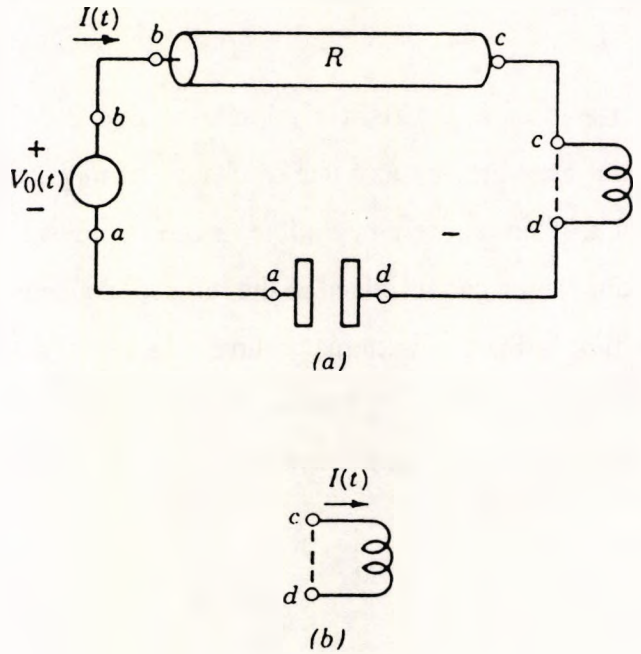


Fig. 3-1 (a) Series circuit with resistor, inductor and capacitor.
(b) Detail of inductor.

A convention for positive voltage at the source is selected as shown by the + and - signs on the voltage generator, which means by Eq. (3-3) that field of the source is directed from b to a when V_0 is positive. A convention for positive current is also chosen, as shown by the arrow on $I(t)$. The interpretation of Eq. (3-1) by circuit-theory for the basic circuit is then known to be :

$$V_0(t) - RI(t) - L\frac{dI(t)}{dt} - \frac{1}{C}\int I(t)dt = 0 \qquad (3\text{-}4)$$

A comparison can be made if the closed line integral is broken in Eq. (3-2), into its contributions over the several elements.

$$-\int_a^b \mathbf{E}\,.\,\mathbf{dl} - \int_b^c \mathbf{E}\,.\,\mathbf{dl} - \int_c^d \mathbf{E}\,.\,\mathbf{dl} - \int_d^e \mathbf{E}\,.\,\mathbf{dl} = \frac{\partial}{\partial t}\int_S \mathbf{B}\,.\,\mathbf{dS} \qquad (3\text{-}5)$$

or,

$$V_0(t) + V_{cb} = V_{dc} + V_{ad} = \frac{\partial}{\partial t}\int_S \mathbf{B}\,.\,\mathbf{dS} \qquad (3\text{-}6)$$

The right hand of Eq. (3-6) is not zero as is the right hand side of Eq. (3-4), but is recognised as the contribution to emf generated by any rate of change of magnetic flux within the path defined as the circuit. If not entirely negligible, it can be considered as arising from an inductance in the loop which can be added to the lumped element L, or a mutually induced coupling if the flux is from an external source. Hence, it would be considered as negligible or included in L so that the right hand side of Eq. (3-6) is zero. The three voltage terms related to the passive components R, L and C can now be examined separately.

9-4.1 Resistance Element

The field expression to be applied to the resistive material is the differential form of Ohm's law:

$$\mathbf{J} = \sigma\ \mathbf{E} \qquad (3\text{-}7)$$

so that the voltage V_{cb} is:

$$V_{cb} = -\int_b^c \mathbf{E}\,.\,\mathbf{dl} = -\int_b^c \mathbf{J}/\sigma\ .\ \mathbf{dl} \qquad (3\text{-}8)$$

where the path is taken along some current flow path of the conductor. Conductivity σ may vary along this path. At DC or low frequency, current I is uniformly distributed over the cross section A of the conductor, which can also vary with position. Thus:

$$V_{cb} = -\int_b^c \frac{Idl}{\sigma A} = -IR \tag{3-9}$$

where,

$$R = \int_b^c \frac{dl}{\sigma A} = \frac{l}{\sigma A} \tag{3-10}$$

This is the usual DC or low-frequency resistance. The situation is more complicated at higher frequencies because of the effect of the changing magnetic-fields on currents with-in the conductor. Current distribution over the cross section is then uniform, and the particular path along the conductor must be specified.

9-4.2 Inductance Element

The voltage across the terminals of the inductive element comes from the time rate of change of magnetic flux within the inductor, shown in Fig. 3-1 as a coil. Assuming first that the resistance of the conductor of the coil is negligible, consider a closed line integral of electric-field along the conductor of the coil, returning by the path across the terminals (Fig. 3-1(b). The distribution along the part of the path which follows the conductor is zero, all the voltage appears across the terminals:

$$-\oint \mathbf{E} \cdot \mathbf{dl} = \int_{c(cont'd.)}^{d} \mathbf{E} \cdot \mathbf{dl} - \int_{d(term.)}^{c} \mathbf{E} \cdot \mathbf{dl} - \int_{d(term.)}^{c} \mathbf{E} \cdot \mathbf{dl} \tag{3-11}$$

By Faraday's law, this is the time rate of change of magnetic flux enclosed:

$$-\int_{d(term.)}^{c} \mathbf{E} \cdot \mathbf{dl} = -V_{dc} = \frac{\partial}{\partial t} \int_S \mathbf{B} \cdot \mathbf{dS} \tag{3-12}$$

Inductance L is defined as the magnetic flux linkage per unit of current:

$$L = \int \mathbf{B} \cdot \mathbf{dS} / I \tag{3-13}$$

so the voltage distributed by this term, assuming L independent of time, is:

$$V_{cd} = \frac{\partial}{\partial t}(LI) = L\frac{dI}{dt} \tag{3-14}$$

Note that in computing flux enclosed by the path, a contribution is added each time followed by another turn around of flux. Thus for N turns, the contribution of induced voltage is N times that one turn, provided that the same flux links each turn. This enters into the calculation of L and will be seen specially when the inductance of the coil is found. If there is a finite resistance in the turns of the coil, the second term of Eq. (3-11) is not zero, but is the resistance of the coil R_L multiplied by current.

Therefore Eq. (3-11) becomes:

$$-\oint \mathbf{E} \cdot \mathbf{dl} = -R_L I - V_{dc} = \frac{\partial}{\partial t}\int_S \mathbf{B} \cdot \mathbf{dS} \tag{3-15}$$

or,

$$V_{cd} = R_L I + L\frac{dI}{dt} \tag{3-16}$$

Thus, as expected, another series resistance is added simply to take care of the finite conductivity in the conductors of the coil.

3-4.3 Capacitive Element

The ideal capacitor is one in which only electric energy is stored. Magnetic-fields are negligible, so there is no contribution to voltage from changing magnetic-fields, but only from the charges on the plates of the capacitor. The problem is then quasi-static and voltage is synonymous with potential difference between capacitor plates. In contrast to

the inductor, any path can be taken between the terminals of the capacitor for evaluation of voltage V_{da} , provided it does not stray into regions influenced by magnetic-fields from other elements.

$$C = \frac{Q}{V} \tag{3-17}$$

and from continuity,

$$I = \frac{dQ}{dt} = \frac{d}{dt}(CV_{da}) = C\frac{dV_{da}}{dt} \tag{3-18}$$

The last term in Eq. (3-18) implies a capacitance which is not changing with time. Integration of Eq. (3-18) will lead to:

$$V_{da} = \frac{1}{C}\int Idt \tag{3-19}$$

If the dielectric of the capacitor is lossy, there are conduction current to add to Eq. (3-18), which are represented in the circuit as a conductance $G_C = 1 / R_C$ in parallel with C. The value of R_C may be calculated from Eq. (3-10) by using conductivity of the dielectric and area of the capacitor plates.

3-5 Relation of Field and Circuit Analysis for Transmission Lines

Consider the transmission line as a distributed circuit. Fig. 3-2 shows a diagram of a parallel plate as a representation of a two-wire transmission line and the circuit model of the differential length of line.

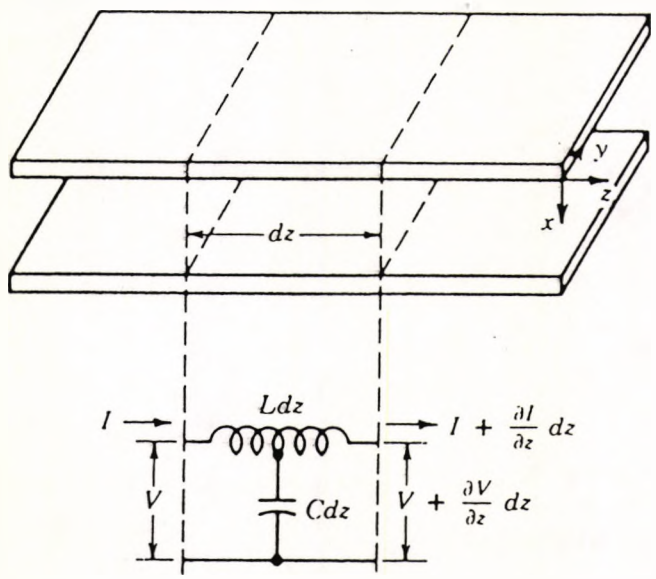


Fig. 3-2 Representation of a transmission line section and equivalent circuit for a differential length.

It can be shown that for such a differential length of line, the voltage change along it at any instant may be written as the length multiplied by the rate of change of voltage with respect to length. Then:

$$voltage\ change = \frac{\partial V}{\partial z} dz = -(Ldz)\frac{\partial I}{\partial t} \tag{3-20}$$

$$= \frac{\partial V}{dz} = L\frac{\partial I}{\partial t} \tag{3-21}$$

Note that time and space derivatives are written as partial derivatives, since the reference point may be changed in space or time in an independent manner.

Similarly, the change in current along the line at any instant is merely the current that is shunted across the distributed capacitance. The rate of decrease of current with distance is given by the capacitance multiplied by the time rate of change of the voltage.

$$current\ change = \frac{\partial I}{\partial z}dz = -(Cdz)\frac{\partial V}{\partial t} \tag{3-22}$$

$$= \frac{\partial I}{\partial z} = -C\frac{\partial V}{\partial t} \tag{3-23}$$

The distributed-circuit model for these transmission line equations can be related to the concept of field analysis. Consider the special case of a parallel-plane transmission line, as indicated in Fig. 3-2 with the conducting planes assumed wide enough in the *y*-direction so that fringing at the edges are not important. If the planes are assumed to be perfectly conducting, it is clear that a portion of a uniform plane wave with E_x and H_y, can be placed in the dielectric region between the planes. This will satisfy the boundary condition that electric-field enter normally to the perfectly conducting planes.
Such waves can be derived from Maxwell's equations, are:

$$\frac{\partial E_x(z,t)}{\partial z} = -\mu\frac{\partial H_y(z,t)}{\partial t} \tag{3-24}$$

$$\frac{\partial H_y(z,t)}{\partial z} = -\varepsilon\frac{\partial E_x(z,t)}{\partial t} \tag{3-25}$$

If the voltage can be defined as the line integral of -**E** between the planes at a given *z*,

$$V(z,t) = -\int_1^2 \mathbf{E}\cdot\mathbf{dl} = \int_0^a E_x dx = aE_x(z,t) \tag{3-26}$$

Current for a width *b*, with positive sense defined for the upper plane, is related to the tangential magnetic-field by:

$$I(z,t) = -bH_y(z,t) \tag{3-27}$$

With this results substituted in Eqs. (3-21) and (3-23), the identical relationship to Eqs. (3-24) and (3-25) are obtained.

where,

$$C = \frac{\varepsilon b}{a} \ F/\text{m} \quad \text{and} \quad L = \frac{\mu a}{b} \ H/\text{m}$$

The capacitance C and inductance L per unit length for a such a system of parallel-plane conductors, calculated from the static concept.

In this illustration, the field and circuit concepts are identical in the simple case.

3-6 Analogy of Wave Characteristics on Line and Waves in Lossy Medium

There is a close analogy between the general governing equations and the wave characteristics of a transmission line, and those of uniform plane waves in a lossy medium.

In a lossy medium with a complex permittivity $\varepsilon = \varepsilon' - j\varepsilon''$ and a complex permeability $\mu = \mu' - j\mu''$, the Maxwell's curl equations (*Chapter 2*) become:

$$\nabla \times \mathbf{E} = -j\omega(\mu' - j\mu'')\mathbf{H} \tag{3-28}$$

$$\nabla \times \mathbf{H} = j\omega(\varepsilon' - j\varepsilon'')\ \mathbf{E} \tag{3-29}$$

Assuming a uniform plane wave characterised by an E_x that varies only with z, Eq.(3-28) can be reduced to:

$$-\frac{dE_x(z)}{dz} = j\omega(\mu' - j\mu'')H_y$$

$$= (\omega\mu'' + j\omega\mu')H_y \qquad (3\text{-}30)$$

Similarly, from Eq. (3-29), the following relationship can be obtained:

$$-\frac{dH_y(z)}{dz} = (\varpi\varepsilon'' + j\varpi\varepsilon')E_x \qquad (3\text{-}31)$$

The time-harmonic transmission-line equations (explained in Chapter 2) are:

$$-\frac{dV(z)}{dz} = (R + j\omega L)I(z) \qquad (3\text{-}32)$$

$$-\frac{dI(z)}{dz} = (G + j\omega C)V(z) \qquad (3\text{-}33)$$

Comparing Eqs. (3-30) and (3-31) with Eqs. (3-32) and (3-33), it can be recognised immediately, the analogy of the governing equations for E_x- field and H_y-field of a uniform plane wave, and those for V and I on a transmission line, using circuit theory concepts.

Equations (3-30) and (3-31) can be combined to give:

$$\frac{d^2E_x(z)}{dz^2} = \gamma^2 E_x(z) \qquad (3\text{-}34)$$

and,

$$\frac{d^2H_y(z)}{dz^2} = \gamma^2 H_y(z) \qquad (3\text{-}35)$$

Equations (3-32) and (3-33) can be combined to solve for $V(z)$ and $I(z)$:

$$\frac{d^2V(z)}{dz^2} = \gamma^2 V(z) \qquad (3\text{-}36)$$

$$\frac{d^2 I(z)}{dz^2} = \gamma^2 I(z) \tag{3-37}$$

where

$$\gamma = \alpha + j\beta = \sqrt{(R + j\omega L)(G + j\omega C} \tag{3-38}$$

The field concept equations, (3-34) and (3-35) are distinctly similar to the circuit theory concepts of the time-harmonic transmission line equations, (3-36) and (3-37).

The propagation constant of the uniform plane wave can be shown to be:

$$\gamma = \alpha + j\beta = \sqrt{(\omega\mu'' + j\omega\mu')(\omega\varepsilon'' + j\omega\varepsilon')} \tag{3-39}$$

which bears a similar relationship with the that of the transmission line, Eq. (3-38).
The intrinsic impedance of the lossy medium (the wave impedance of the plane wave travelling in the + z-direction), can be shown to be:

$$\eta_c = \sqrt{\frac{\mu'' + j\mu'}{\varepsilon'' + j\varepsilon'}} \tag{3-40}$$

which is analogous to the expression for the characteristic impedance, Z_0, (derived in *Chapter* 2) for the transmission line:

$$Z_0 = \sqrt{\frac{R + j\omega L}{G + j\omega C}} \tag{3-41}$$

3-7 Resistance Calculations

Using the concept of circuit theory, the procedure of calculating the capacitance between the two conducting plates separated by a dielectric medium, can be deduced easily from Fig. 3-2. In terms of electric-field quantities, the basic formula for capacitance can be

written as:

$$C = \frac{Q}{V} = \frac{\oint_S D.ds}{-\int_L E.d\ell} = \frac{\oint_S \varepsilon E}{-\int_L E.d\ell} \tag{3-42}$$

where the surface integral in the numerator is carried out over a surface enclosing the positive conductor, and the line integral in the denominator is from the negative conductor to the positive conductor.

When the dielectric medium is lossy (having a small but non-zero conductivity), a current will flow from the positive conductor to the negative conductor, and a current density-field will be established in the medium. Ohm's law ($\mathbf{J} = \sigma\ \mathbf{E}$), ensures that the streamlines for J and E will be the same in an isotropic medium. The resistance between the conductors is:

$$R = \frac{V}{I} = \frac{-\int_L E.d\ell}{\oint_S J.ds} = \frac{-\int_L E.d\ell}{\oint_S \sigma E.ds} \tag{3-43}$$

where the line and surface integrals are taken over the same L and S as those in Eq. (3-42). Multiply Eqs. (3-42) and (3-43) gives the following interesting relationship:

$$RC = \frac{C}{G} = \frac{\varepsilon}{\sigma} \tag{3-44}$$

It can be shown that $LC = \mu\varepsilon$ (3-45)

Equation (3-44) is valid if ε and σ of the medium have the same space dependence or the medium is homogeneous (independent of space co-ordinates). In these cases, if the capactiance between the two conducting plates is known, the resistance (or conductance), can be obtained directly from the ratio ε / σ without recomputation.

3-8 Conclusions

In general, circuit-theory deals with lumped-parameter networks. Circuit concepts represents a restricted version, a special case of electromagnetic concepts. At DC, or when the source is very low, so that the dimensions of a conducting element are much smaller than its wavelength, a quasi-static condition arises, which simplifies the electromagnetic problem to one of circuit concepts. However, the concepts of fields and waves are essential in the explanation of action at a distance.

One important circuit having both distributed and propagation effects is the uniform transmission line, therefore circuit-theory can be extended in this case. Agreement with field solutions is exact for perfectly conducting transmission lines and very good with lines with small losses. This agreement for the transmission line parameters was verified experimentally in the studies.

Chapter 4

Devices and Apparatus

SYSTEMS DESCRIPTION AND TESTING

Introduction

The measurement system made use of the transmission line model (Rajroop and House, 1991) which was originally designed and constructed so as to study its performance due to fast travelling pulses. Incorporated within the measurement system was a mercury pulser and an SF_6 insulated high voltage pulser, which were used to inject fast pulses into the test line, during independent testings. Detection of these pulses as they travelled along the line was by directional couplers, incorporated suitable loop probes.
These apparatus and measuring devices were designed and built by the author and are described below.

The testing of the 1 kV mercury pulser is included in this section, and a preview of impulse voltage measurement is given, since the SF_6 pulser was used to simulate such impulse voltages. An introduction to electrode configurations and sulphur hexafloride (SF_6) gas, is also given.

4-1 THE TRANSMISSION LINE

The transmission line assembly consisted of the earthplane forming the return conductor and a conductor parallel to the plane, forming the open line. The earthplane is construct-ed in eight sections plus two curved end sections, one at the supply and the other at the termination end. Eight metal frames with supporting feet were made up with 18 mm square section material (mild steel) and are secured by *quick-fit* fixings. The tinned 18 *SWG* steel sheets were secured on the frames, one on each side, with a 35 mm lip all around. Holes were drilled on one side of the lip and slots made on the other side. The sections were held together using screws with winged nuts. This arrangement facilitates easy dis-assembling and assembling as may be required. The frames were held rigidly by the "quick-fit" fixings by friction due to plastic inserts. Braided links were made as necessary to provide electrical continuity throughout the fixings. One section of the earthplane is drawn to scale in Fig. 4-1(a) and (b).

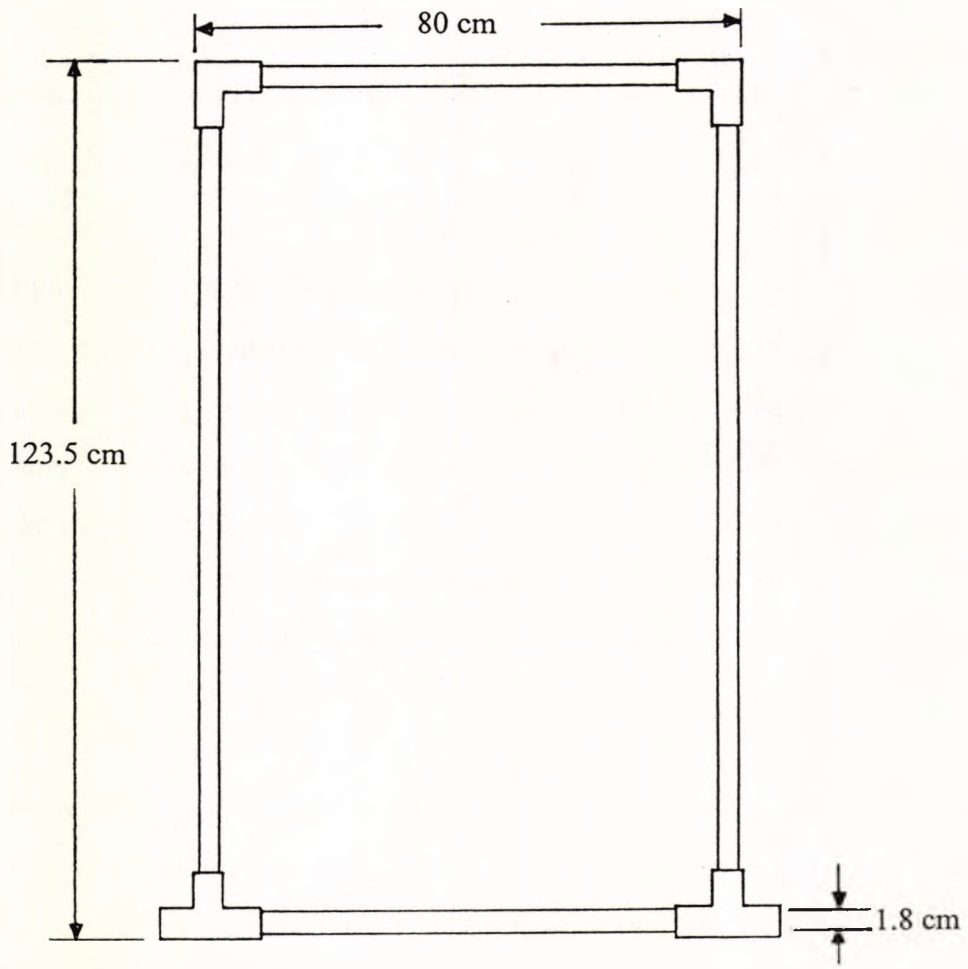


Fig. 4-1(a) Frame section of the earthplane.

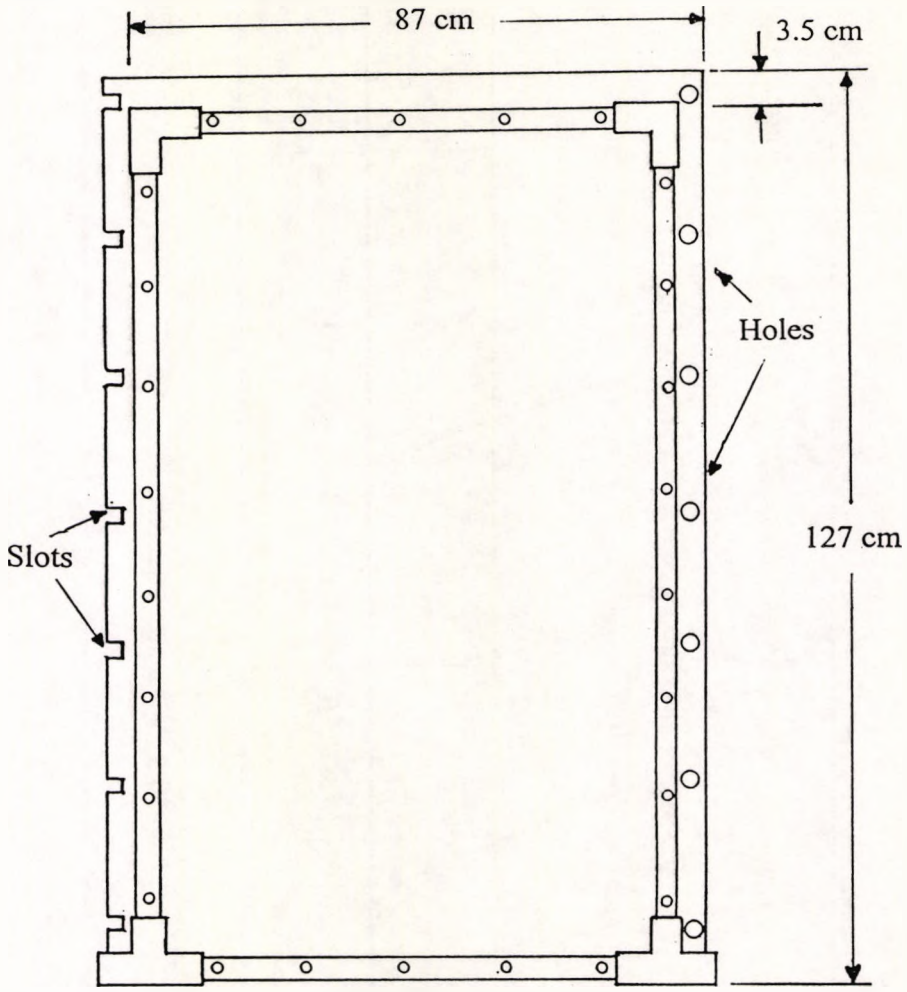


Fig. 4-1(b) Frame section with assembled tinned steel-plate.

The outer conductors were mounted on foam insulators, supported centrally on the sheets at one metre intervals, to form the line system in a balanced configuration. Being an open system, the dielectric medium is naturally air.

A drawing of the complete structure is shown in Fig. 4-2. and a photograph of the transmission system is shown in Fig. 4-3.

The foam insulators were glued on the surface of the earthplane with suitable adhesive and the conductor supported on the foam with plastic clips. Copper conductors, of 4 mm diameter were used for the line. Further calculations shown in Appendix 1, verify that this size is needed in order to withstand a voltage stress of ± 50 kV, for proposed high voltage testing.

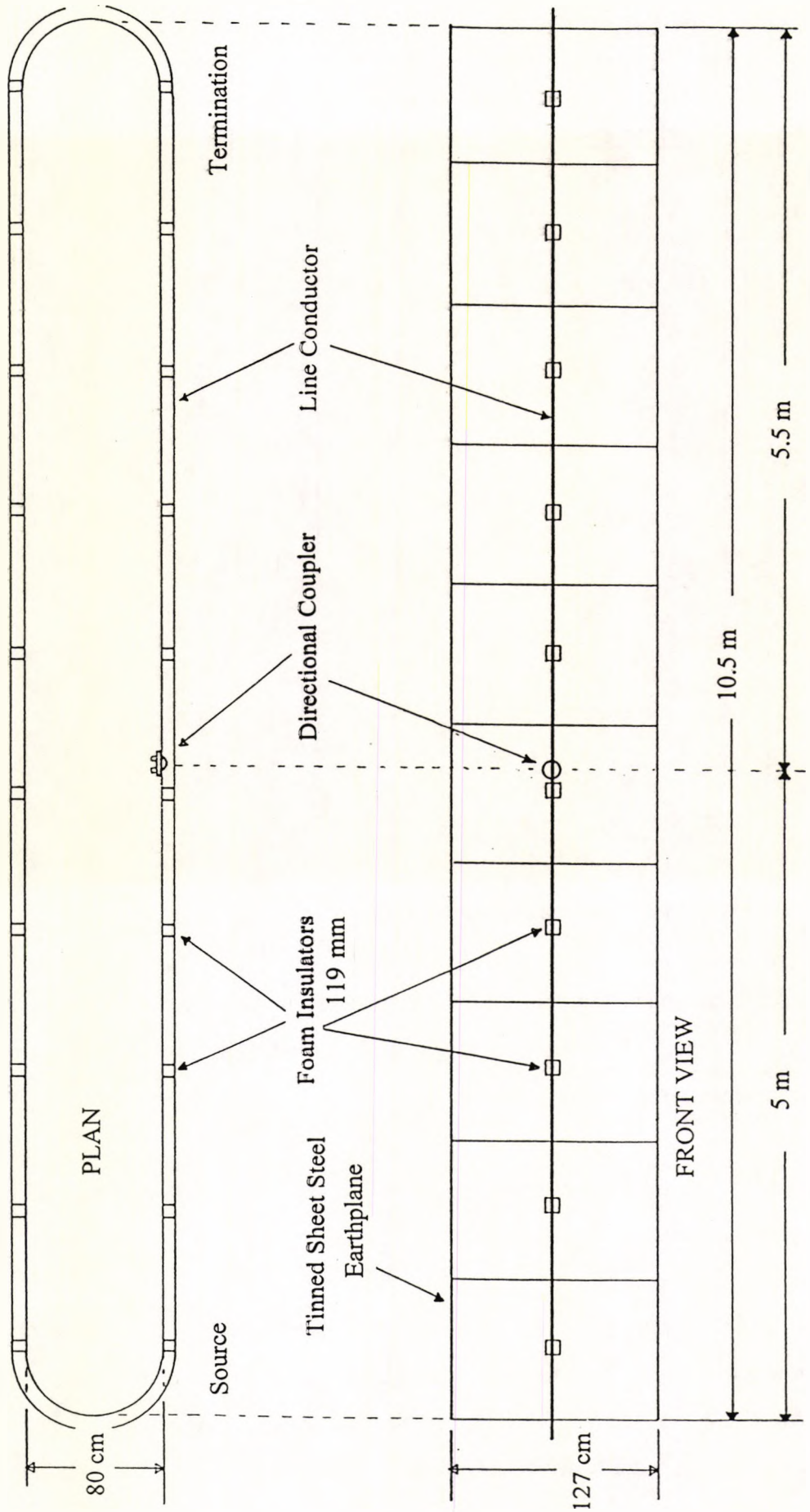


Fig. 4-2 Drawing of the line structure.



Fig. 4-3 Photograph of the transmission system.

Commercial dielectric materials have complicated molecular structures and show several absorption peaks. The behaviour of these dielectric can be represented by curves of permittivity and loss against frequency. At certain frequencies the loss curve would show a peak (the absorption peak) and the permittivity falls very sharply.

Foam was chosen for the insulators because it possesses a dielectric constant approximating to that of air. It was used in this application at frequencies outside the range of the absorption peaks. If the dielectric constant of the insulating medium is only slightly higher than air, small reflections will occur between the insulators as a result of the periodic structure and this will set up standing wave patterns.

Although on testing of the line, these reflections have been detected, their amplitudes were insignificant such that the material and design were considered to be satisfactory. Three directional couplers were installed in the structure of the earthplane. One near the source, one near the mid-section and one near the termination of the line. They were positioned in such a way that when the coupling loops were at 90 degree (or 270 degree), i.e. in the horizontal position, they were directly in parallel with the outer conductor. Correspondingly, when the loops were at the vertical (0/180 degree) position, they were at right angles to the line.

The dimensions of the earthplane were large enough with respect to the line conductor spacing, such that the plane may be regarded as being ideal. The configuration is analogous to that of a conductor above an earthplane.

4-2 THE DIRECTIONAL COUPLER

4-2.1 Introduction

An essential device in the measurement set-up for detection of the travelling pulses is the directional coupler, incorporating loop probes or single element antennas. The probes can be of square shape, but most of the testings were done with a single turn circular loop and semi-circular (half-turn) loops. The name given to this device, sometimes known as a reflectometer, in descriptive in the manner in which it can be adjusted so as to couple only to a pulse travelling in a given direction.

4-2.2 Descriptions

The directional coupler was constructed in three main sections namely:

1. A fixed threaded brass ring
2. A corresponding threaded (adjustable) centre, and
3. The coupling loop mounted on the centre.

The constructional details are shown in Fig. 4-4(a) and (b).

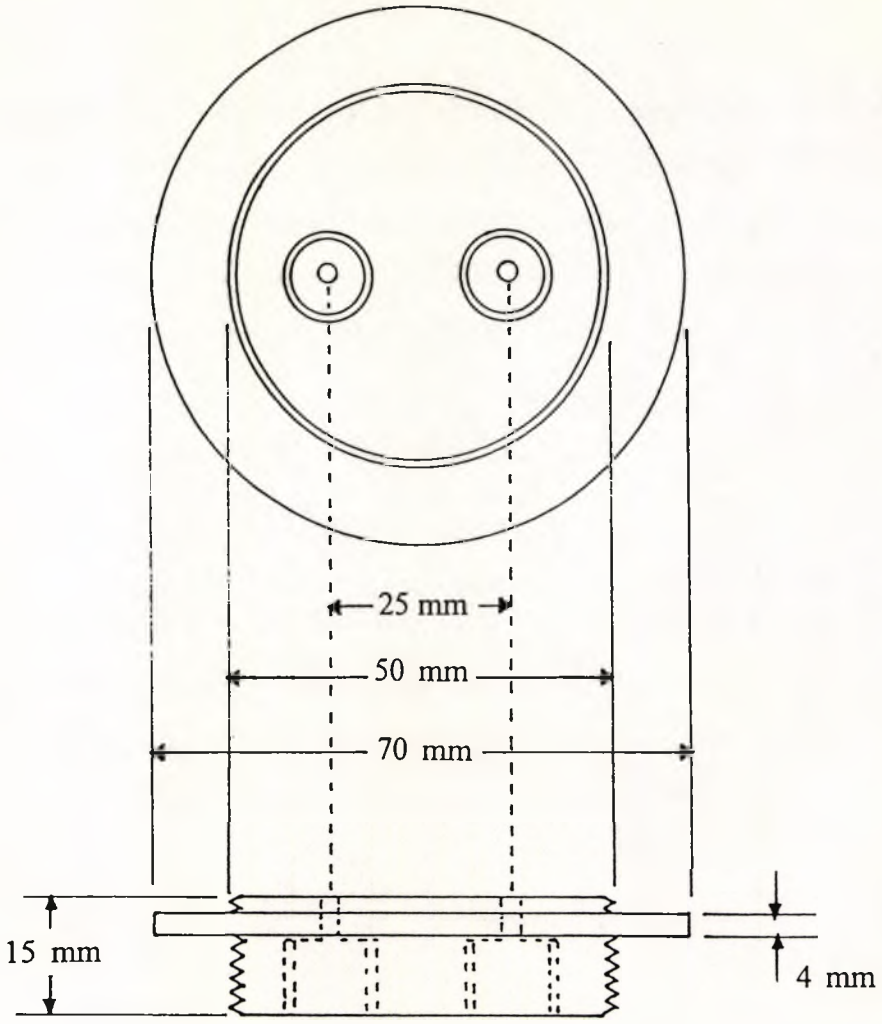


Fig. 4-4(a) Constructional details of the directional coupler.

A 70 mm brass ring of 50 mm internal diameter and 4 mm thickness was internally machined with fine (0.4 mm pitch) threads. The ring was soldered into a 52 mm hole on the earthplane. A 15 mm thick 50 mm diameter correspondingly threaded brass disc which incorporates the coupling loop, was screwed into the ring. This allowed 360° angular adjustment of the loop and the fine threads prevent any appreciable axial movement into the electromagnetic field, produced by the travelling pulses on the line.

Two threaded holes at 25 mm between centres were made into the rear surface of the disc to take standard *BNC* sockets. One socket is for a 50 ohm matching *BNC* load and the other for the output cable to the oscilloscope. On the front surface of the disc the holes were 3 mm diameter so as to clear the hollow pin connectors of the *BNC* sockets.

The loop was pressed firmly into these connectors and without the need for a soldered joint. This arrangement was quite useful as it readily allowed the interchanging of loops of different shapes and sizes. Assembled views of the directional coupler is shown in Fig. 4-4(b).

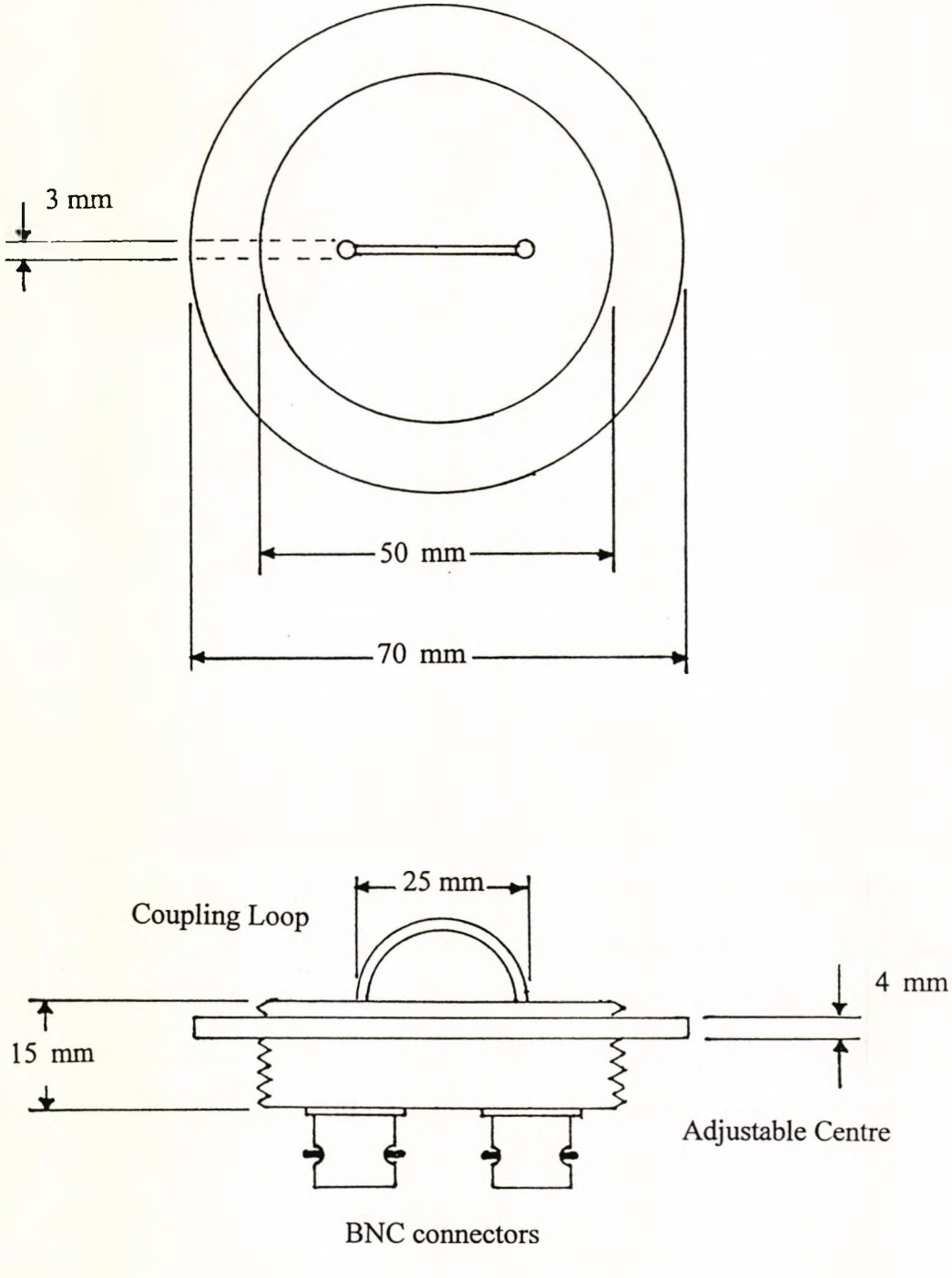


Fig. 4-4(b) Assembled views of the directional coupler.



Fig. 4-5 A photograph of the directional coupler.

4-3 THE 1 kV MERCURY PULSER

4-3.1 Introduction

In setting up fast equipment, it is often desirable or sometimes essential to have pulses with adequate amplitudes and fast risetimes. The steep wave front can be used to investigate the response time of measurement equipment and devices, and is useful in providing a reference for experiments where speed and jitter is under investigation.

An essential device in the testing and measuring techniques of the transmission system is a pulser, which was required to generate fast pulses for injection into the test line. Although these pulsers are available commercially, such as the Kenteck Range of Instruments, their high costs put them out of reach. Hence, the attempt to design and build a pulser to the suit the specific requirements for the experimental procedures.

Kentech Instruments Ltd. manufactures a wide range of very fast, high voltage pulse generators, mainly solid state, using advanced avalanche and *VMOS* technology. These pulsers can be configured to suit most loads and can drive short and open-circuit without damage. They are characterised into 50 ohm using *Barth* attenuators and transformers are

available to match the pulsers into low impedance loads, such as micro-channel plates. Applications of these pulsers are in high speed camera systems, laser pulse chopping, radar, time of flight mass spectroscopy, EMP simulation and cable characterisation.

4-3.2 Initial Development

The required pulse needed to propagate the line is of the Heaviside step-function and repetitive in order to make measurements using a digital sampling oscilloscope. The nature and properties of mercury (H_g), have been reported in many literatures. It seemed that a contact wetted with mercury, would produce the desired risetime pulse for the experimental study.

The initial work was based on the fact that a mercury gap, when stretched to its limit, breakdown in an extremely short time - (in the order of a few tens of pico-second). The making time is also correspondingly short. The same is true if the contacts of a switch wetted with mercury is used in a relay. This knowledge led to the testing of a mercury - wetted contact relay, incorporated in a dual-in-line (DIL) package.

The relay pulser was connected into a small discrete component circuit. In testing the device, it was discovered that the risetime response of the switch increased progressively with the increase in repetition rate of the relay up to a maximum of 1 kHz for stable operation. The risetime response at this frequency, measured to be in the region of 100 ns, was still relatively slow and therefore unsuitable for the application. A contributory factor to this slow response was due to the inductance inherent in the device. Attempts were made to reduce this by trying to pass the switch-contact return wire inside the relay coil. In this manner both the switch contact wires will be subjected to the same magnetic flux produced by the coil (Clifford and Lynch,1990).

This was not successful owing to the design and construction of the dual-in-line package. Further trials were made with different coils and switch-contacts arrangements in this configuration, in order to reduce the inductance, but without the desired results. This then led to the development of the pulser in its present successful coaxial form.

4-3.3 Description

The line pulser was constructed in a 50 ohm coaxial arrangement so as to match the impedance of the instrumentation and other ancillary devices. This arrangement also improved the risetime response of the pulser quite significantly and made it less vulnerable to outside interference sources. In order that the risetime of the output pulse is not degraded by multiple reflections due to mismatch in open circuit and short circuit testing, the entire measurement system was kept coaxial.

The vertical type of mercury wetted reed-switch capsule, manufactured by C.P. Clare Corporation, was chosen[1]. The principle involves a movable contact pivoted at the bottom connection which can vibrate (or switched) between the two stationary contacts at the top. The vibrating contact is constantly wetted with mercury drawn by capillary action from a pool of mercury at the bottom. A drawing of the mercury-switch capsule is shown in Fig. 4-6(a).

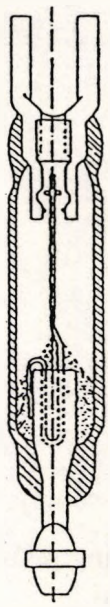


Fig. 4-6(a) Drawing of a mercury-switch capsule.

[1] Donated by the courtesy of British Aerospace, Sowerby Research Centre, Bristol.

The glass capsule containing the mercury-wetted contact switch was placed inside the continuous braided sheath of a 50 ohm 150 mm long coaxial cable. The inner core was broken so as to make connections to the switch terminals. The outer p.v.c. sheath was pushed back so as to allow the switch to form part of a continuous cable. A drawing of

this arrangement of the switch capsule inserted inside a section of a coaxial cable, is shown in Fig. 4-6(b).

The assembled '*cable switch*' was inserted into the hollow former of a relay operating coil and was placed inside a small screened box. Coaxial terminations were provided for the DC supply and switched output pulses. Capacitive 'feed through' insulators were used to bring in the repetitive signal to the operating coil and connections made using screened cables. These precautions were taken so as to minimise any possible interference problem.

This arrangement constitutes the line pulser, the photograph of which is shown in the experimental set-up in *Chapter* 5.

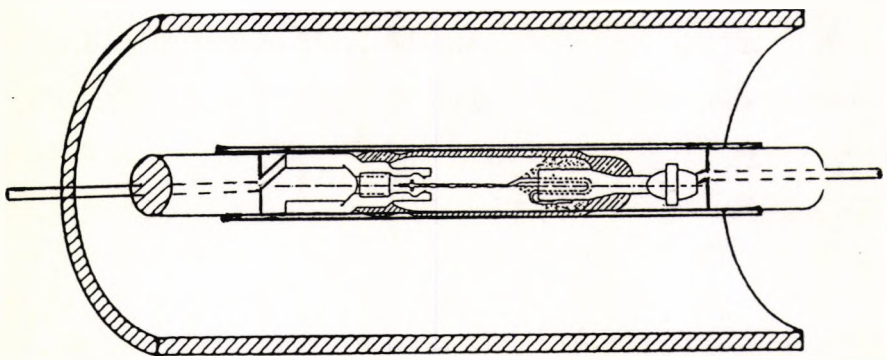


Fig. 4-6(b) Drawing of switch capsule inserted inside a section of a coaxial cable.

4-3.4 Testing of the mercury pulser

The circuit arrangement is shown in Fig. 4-7. The DC supply to the pulser was connected by a 50 ohm coaxial cable (cable *A*) through a limiting resistor *R*, to the power supply unit (PSU). The value of the resistor was chosen so that the reflection coefficient, (Γ) approximates that of an open-circuit, i.e. $\Gamma \cong {}^{+}1$. Cable *B* connected the switched output from the pulser to the measuring oscilloscope. The lengths of these cables were chosen to give the desired pulse width and hence known as the pulse forming cables. The signal generator repetitively drives the relay operating coil with rectangular pulses. The connection was made on the normally-open contact of the mercury switch.

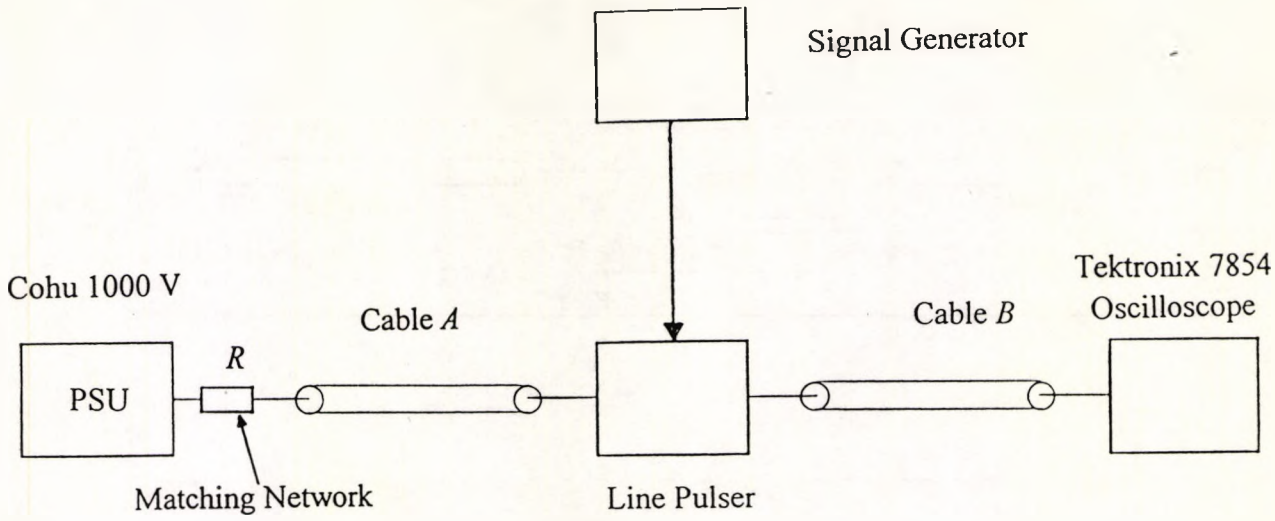


Fig. 4-7 Connection diagram for testing the pulser.

With the power supply switched ON, cable *A* was charged through the resistor *R* to a potential of V^+ volts. When the signal generator was switched ON - energising the operating coil and closing the contact - this charged potential on cable *A* was discharged into cable *B* with an amplitude of $V^+/2$ volts. The signal was aquired and the pulse risetime measured by the oscilloscope. Simultaneously a voltage of magnitude $V/2$ travelled back to the source so as to satisfy the transient state.

The measurement system and connections were kept coaxial and connection was made on the 50 Ω input of the oscilloscope, so as to minimise any possible reflections. The Bewley lattice diagram in Fig. 4-8 shows the pulse propagation and reflection pattern during the transient state.

Note that in the scale drawing only the two connecting cables, cable *A* and cable *B* are regarded as having finite lengths. The electrical lengths of other components are insignificant and therefore are not considered.

It is worthwhile to note that the pulse width is determined by cable *A* while cable *B* merely delays its time of arrival at the oscilloscope.

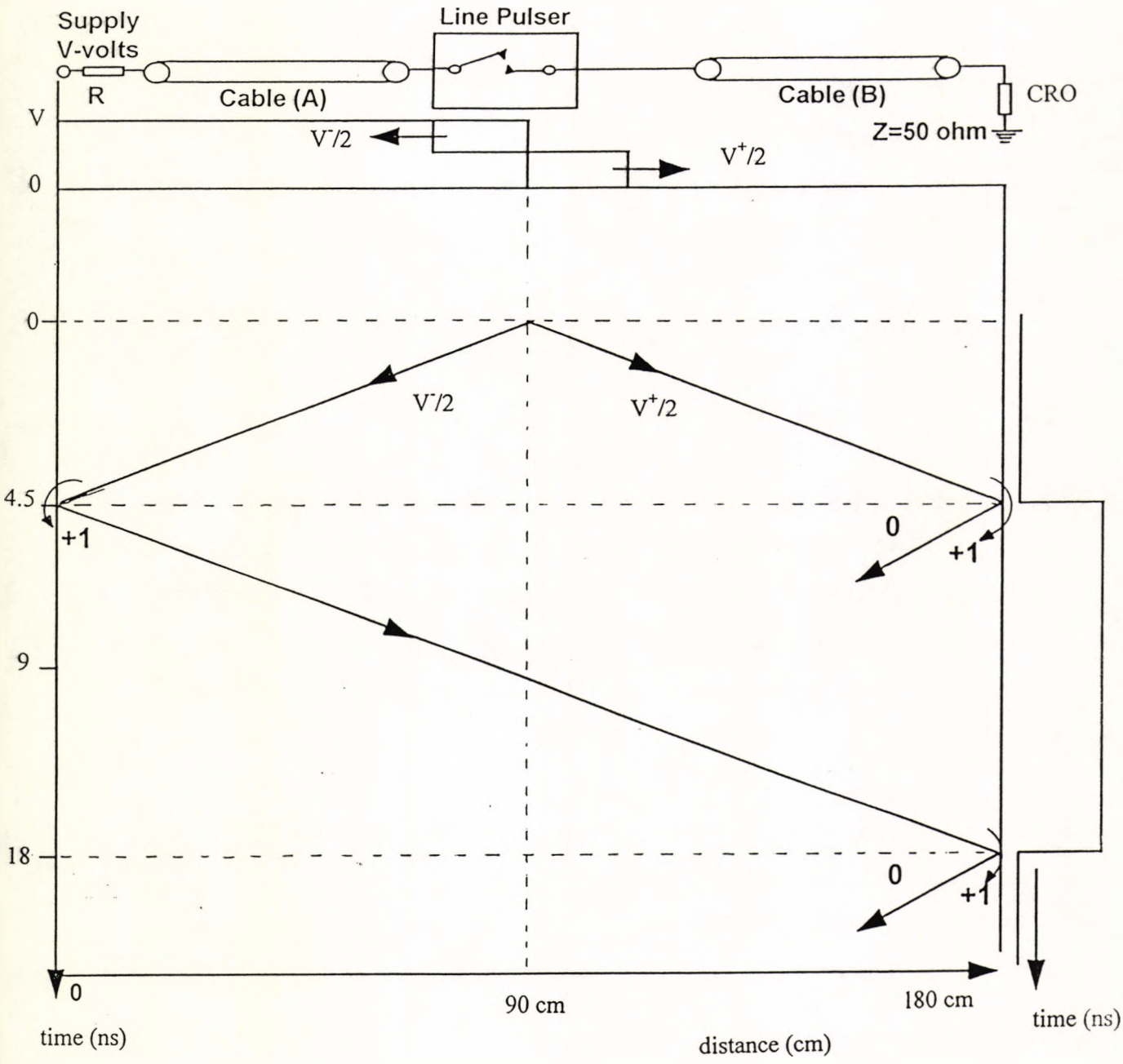


Fig. 4-8 Bewley lattice diagram of reflected pulses in testing the pulser.

On testing the pulser, it was found that the risetime decreased as the repetition rate of the driving signal was increased. The manufacturer's specification for the switch-contact is 200 Hz and 500 V maximum rating, but with careful adjustments of the ON and OFF

times of the driving signal, it was possible to obtain a switching frequency of up to 457 Hz.

This is shown in Fig. 4-9.

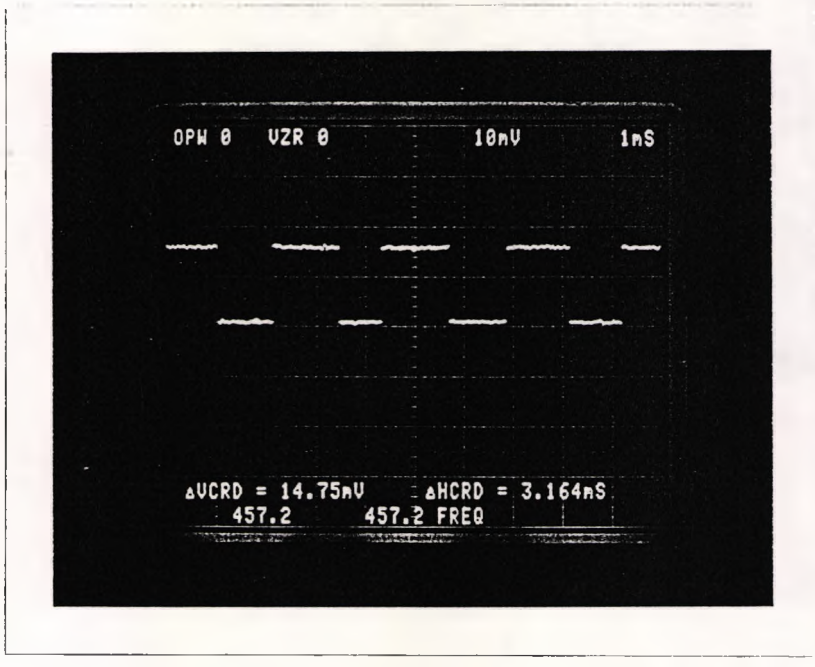


Fig. 4-9 Waveform of repetitive driving pulses.

Frequencies just above this value caused saturation whereby the contacts locked in a steady state position. The switched voltage range was also extended up to the limit of the power supply of 1 kV. The pulser functioned well at these extreme limits for short-time operation. The risetime was computed to be 298 ps, but a more meaningful definition of the slope is highlighted by cursors. Here, the risetime was computed to be 276 ps. These are shown respectively in Fig. 4-10.

Fast risetime mercury pulsers often integrated within the equipment, are also available commercially. Others working in the areas of fast pulse applications [(Thornton, British Aerospace), (Brunstein, Tel Aviv University), (Daum, G.E. Research Laboratory, N.Y.). *Personal Communications*], have designed pulser based on this principle, but not so compact and in a coaxial form.

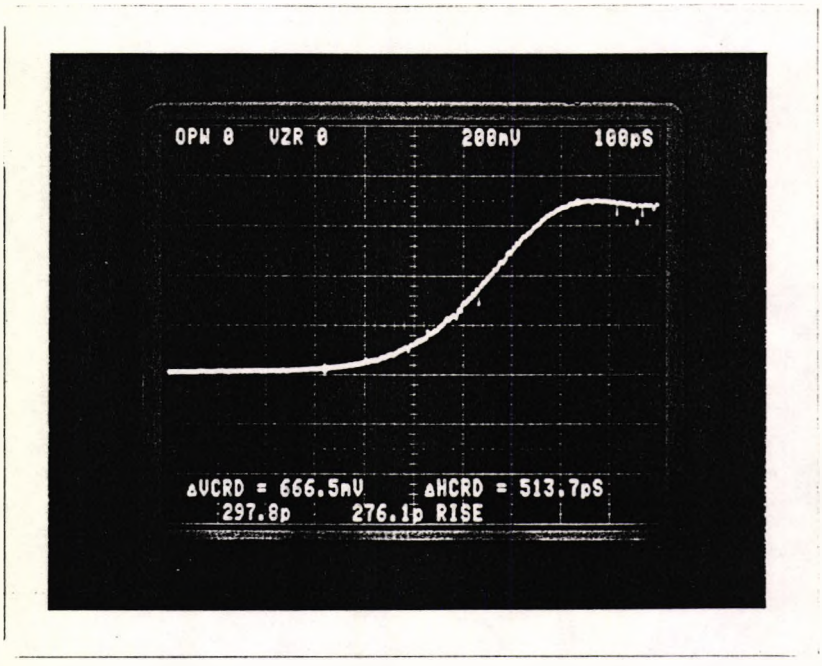


Fig. 4-10 Pulse risetime measurement.

4-3.5 Contact Protection

Arcing can considerably reduce the life expectancy of mercury wetted contacts. It may occur whenever a contact breaks a circuit with a source voltage greater than 12 V and current greater than 60 mA. Whenever these conditions exist, a contact protection network is required. The network which simply consists of a series combination of a resistor and capacitor, is placed across the contact.

The chart - C. P. Clare Corporation 220 (1990) shown in Fig. 4-11, is a valuable aid in quickly choosing these network components for a resistive load application.

The manufacturer's full specifications for mercury-wetted reed switches are shown in Table 4-1.

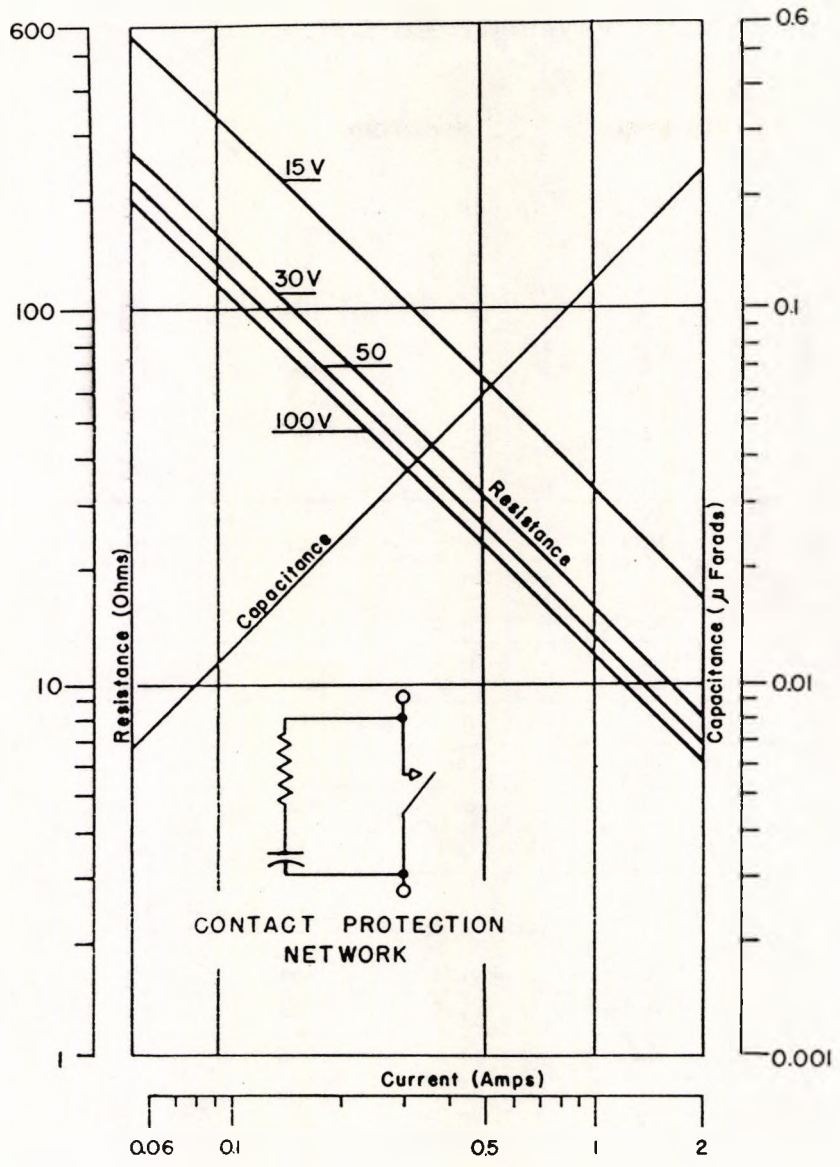
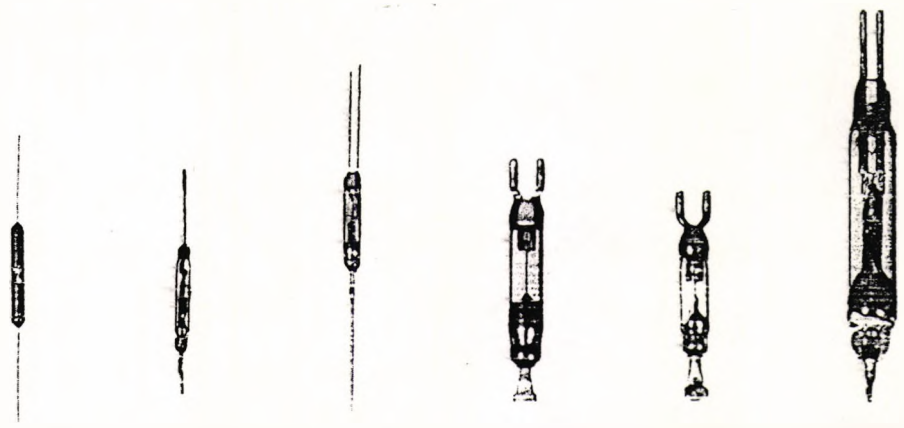


Fig. 4-11 Chart for selecting R-C network components.

The following precautions should also be observed:

- The network should be placed as close as possible to the contacts to be protected.
- Inductive resistors or metalised film capacitors should not be used.
- The rated working voltage of the capacitor should be at least twice the magnitude of the highest voltage that will be impressed across it.

TABLE 4-1 Specifications for Mercury Wetted Reed Switch



ngineering pecifications	MA1	MH2	MHC	HGR	HGW	HG1
ontacts ontact form	All Position Mounting 1 Form A	1 Form A	1 Form C	1 Form C, D	1 Form C	1 Form D
ontact Material	Mercury to Mercury	Mercury to Mercury	Mercury to Mercury	Mercury to Mercury	Mercury to Mercury	Mercury to Mercury
aximum power (VA)	30	50	50	100	100	250
aximum switched voltage (VDC)	350	350	350	500	500	500
aximum switched current (A)	0.75	1.00	1.00	2.00	2.00	5.00
aximum carry current (A)	2.00	3.00	3.00	5.00	5.00	10.00
lectrical Specifications itial contact resistance max. (Ohms)	0.075	0.030	0.030	0.030	0.030	0.030
ow level load electrical life ef. 10V. 10mA (Operations)	$200x10^6$	$1000x10^6$	$1000x10^6$	$1000x10^6$	$1000x10^5$	$1000x10^6$
inimum dielectric voltage (VDC)	1400	1400	1400	2100	2100	2100
apacitance (pF)	0.3	0.5	0.7			
inimum insulation sistance (Ohms)	10^8	10^8	10^8	$5x10^8$	$5x10^8$	$5x10^7$
peration Specifications ull-in ampere turns (NI)	35-70	30-65	35-70	60 max.		120-200
perate time milliseconds, max. t twice the operate NI)	1.5	2.0	3.0	2.0	1.25	4.0
elease time diode suppressed illiseconds, max.	1.5	2.0	3.0	2.0	1.25	3.0
perate frequency (Hz)	300	100	100	200	200	100
perating temperature	−38°C to + 125	−38°C to + 125	−38°C to + 125	−38°C to + 125	−38°C to + 125	
hysical Characteristics xternal lead finish** older plated	Nickel Iron Alloy	Nickel Iron Alloy	Nickel Iron Alloy	Nickel Iron Alloy	Nickel Iron Alloy	Nickel Iron Alloy
ounting Position	Any Position	Upright*	Upright*	Upright*	Upright*	Upright*
tandard Test Coil (MIL-S-55433, Coil A) oil resistance (Ohms)	3500	3500	3500			
umber of turns	10,000	10,000	10,000			
ire size	AGW48	AGW48	AGW48			
obbin diameter	4.2mm	4.2mm	4.2mm			

±30° of upright

4-4.1 Introduction

Digital Impulse Measurement System (DIMS) greatly simplifies impulse voltage measurements, whereby the graph of the wavefront and peak voltage can be obtained by the mere touching of a button. The DIMS automatically records, plots, analyses, displays and logs impulse waveforms, with the possibility of automated testing and signal processing. For these reasons, the use of digitizers in high voltage testing systems, is becoming a widespread practice.

Some systems have up to four input channels which are suitable for more extended impulse measurement analysis with the optional transfer function package. The transfer function measurement is evaluated by transfering two impulse oscillographs from the time-domain to the frequency-domain and then a comparison is made. The spectral representation provides information on the electrical oscillation characteristics of the equipment under test and in many cases, can contribute to the identification of effects.

4-4.1.1 Precision Impulse Measurement

Digital impulse measurement systems offer the following features:

- Precise, fully programmable input stages with wide bandwidth and drift compensation.
- Real simultaneous digital sampling in all measuring channels with flash converters.
- Large record length in each measuring channel for a constant high resolution and also for measuring long tails.
- Comprehensive software - for measuring, control of test sequence, evaluation and protocol, transfer function package.

The system is easy to use with menu-orientated operation, function keys programmed with user-specific test sequence; the load facility of pre-defined set-up files from the hard disk for the respective tests, allows a quick and error-free test performance.
The IEC-Standard on Digital Recorders for Measurements in High-Voltage Impulse Tests specifies the requirements for digital recorders and calibrations required to meet the measuring accuracies for measurement during high voltage and high current impulse tests in accordance with the relevant standards. The user in the test laboratory is obliged to use measuring equipment according to these standards.

To document the compliance, the equipment must be calibrated accordingly, with traceability to recognised standards, (Struss 1995).

However, resolution, differential non-linearity and internal noise are the most challenging requirements digitizers have to meet in high voltage impulse measurements, and as a result, not many equipment are suitable for this type of application. In addition, general purpose digitizers are becoming more and more sophisticated; the operations being performed on the original raw data before their availability on the interface bus, and the internal architecture of the converters are often so complex that it is difficult to judge the actual performance in this domain of application.

One drawback is that the digitizer of the instrumentation can only take a low input voltage. The actual input to the DIMS is much higher as the system incorporates high-voltage precision attenuators, mounted in a screened enclosure. Therefore extensive filtering has to be done if, for example, several mega volts has to be reduced to say, a few tens of volts. It is evident that this could impose serious errors and distort the wave shape.

4-4.2 The SF_6 Spark-gap Pulser as a Simulator for Impulse Voltages

This pulser was originally designed to study the corona distortion due to fast high voltage pulses travelling on the transmission system. It was of particular interest to observe the effects of the tin-plated steel sheets (which constituted the earthplane) on the pulse shape.

Extensive mathematical analyses on eddy currents losses and corona distortion on transmission systems were done by a colleague (Maksiejewshi, 1990a,b) working in this area and it was of interest to all concerned to compare calculated and experimental results.

Corona on overhead transmission lines plays an important role in determining the magnitude and waveshapes of over-voltages occurring in electrical power systems. Even though the phenomena has been studied for many decades, its physical complexity has prevented the development of a simple model for transient analysis. The study published by Clade *et al.* (1969) describes the application of physics for discharge laws and equations, to examine corona phenomena around electrical conductors. The basic mechanism of ionisation, displacement and recombination of charges are identified, and two methods to study the losses are proposed.

Wei-Gang (1987) and de Jesus (1994) undertook further investigations of corona using space charge techniques. The complexity of the physical phenomena involved and the lack of sufficient data in propagation under corona, means a good generic model of this nature is not available.

The mechanism of corona, which includes physical phenomena such as ionisation, displacement, diffusion and recombination of charges, is extremely complex. Two main problems have to be addressed to include corona effect in transient calculations. The first concerns the method to characterise the phenomena and the second is to incorporate this characterisation into the differential equation of the transmission line.

It was proposed to determine the surge propagation under corona condition on the transmission model by a routine based on the point-matched Time Domain Finite Element (TDFE) method and to make comparison with experimental results. Due to uncontrollable circumstances, it was not possible to pursue this investigation. However, the pulser was implemented as a simulator for an 80 kV impulse generator and the measurement of the high-voltage pulses was carried out in conjunction with a suitable designed loop probe.

4-4.3 Voltage Breakdown in SF_6

In an electro-negative gas, such as Sulphur Hexafloride (SF_6), the value of $(\alpha - \eta)/n$ increases very rapidly with E/n in the region of $(E/n)_{lim}$ with the result that in many cases corona inception or breakdown occurs when the maximum value of E/n in the gap exceeds $(E/n)_{lim}$ by only a small amount:

Where, α is the collisional ionisation coefficient (cm^{-1})

η the attachment coefficient (cm^{-1})

n the gas number density (cm^{-3})

E the electric field strength (kV cm^{-1})

$(E/n)_{lim}$ the limiting value of E/n in an electronegative gas (kV cm^{-1})

It was shown by Takuma and Watanabe (1970a,b,c) that:

$$E_s = n(E/n)_{lim} + H \qquad (4\text{-}1)$$

where H, (the magnetic field strength) which is independent of n is a correction term that allows for the non-uniformity and final length of the gap. For numerical values see Table 4-2 (Mattingly and Ryan, 1973).

Since the rapid increase of $(\alpha - \eta)/n$ with E/n is linear, it is relatively easy to derive a semi-empirical equation for E_s at least where the gap geometry is simple. Nitta and Shibuya, (1971) derived semi-empirical equations for sphere gaps and rod-rod gaps with hemispherically ended rods, and they fit their experimental results to these equations, (Table 4-2). Mosch and Hauschild (1974) discuss the case of coaxial cylinder geometry. Pedersen, (1970) discusses in detail the choice of a breakdown criterion suitable for the derivation of such semi-empirical formulae for SF_6, and presents calculations for sphere gaps that show good agreement with the impulse voltage measurement of Howard (1957) Because of the rapid variation of $(\alpha - \eta)/n$ with E/n, the onset of discharges in SF_6 is determined almost entirely by the maximum stress in the gap. For reason V_{si} is more

strongly dependent on the form of the electrodes than in other gasses such as air. This is illustrated in the results by Nitta and Shibuya shown in Fig. 4-12.

For high values of electric stress, discharges in SF_6 appear to be initiated with an applied electric field strength lower than that corresponding to $(E/n)_{lim}$, and therefore under condition where cumulative ionisation is theoretically impossible. The effect is usually explained in terms of local field enhancement resulting from the microstructure of the electrode surfaces or from solid particles in the gap.

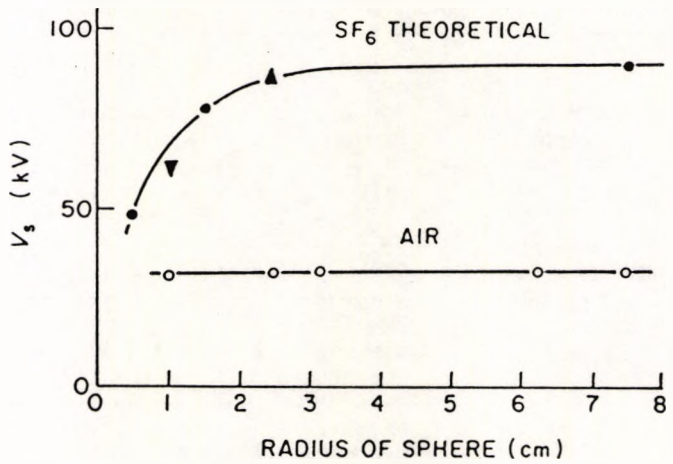


Fig. 4-12 Power frequency breakdown voltages of sphere gaps as a function of sphere radius (Nitta and Shibuya, 1971).

$d = 1$ cm, $n = 25.1 \times 10^{18}$ cm^{-3}.

- Measured value

Δ Howard (1957)

∇ McCormick and Craggs (1954)

Theoretical values were obtained using the equation in Table 4-2.

Another important feature to consider in voltage breakdown in SF_6 is corona stabilisation influenced by positive impulse voltages with various front times. To recognise the corona stabilisation a coaxial shunt (Thornton 1987), can be used to measure the large pre-breakdown current. Based on the fact that corona stabilisation is always accompanied by an intense space charge around the tip of the electrode, thus, by a practically continuous pre-breakdown current, breakdown events can be classified into two groups:

1. Breakdown with corona stabilisation and
2. Direct breakdown,

according to the current measurements and evaluated separately. Inception of the corona stabilisation also depends on the random effects such as the initiating electrons in a critical volume.

Table 4-2 Values for E_s for SF_6 (Mattingly and Ryan, 1973)

Table 6.14. Values of E_s for SF_6 (Mattingley and Ryan, 1973. Reproduced by permission of National Academy of Sciences)

Author	n (10^{18} cm^{-3})	Electrode geometry	Range of dimensions (cm)	Voltage waveform	Equation for E_s (kV cm^{-1})	Typical error range (per cent)
Zalesskii *et al.* (1970)	24–97	Coaxial cylinders	$0{\cdot}25 \leqslant r \leqslant 2{\cdot}5$ $3 \leqslant r_2 \leqslant 14$	50 Hz	$E_s = 53(1 + 0{\cdot}0186\,n) \cdot [1 + (0{\cdot}895 - 17{\cdot}9/n)r^{-\frac{1}{2}}]$	±6
Kawaguchi *et al.* (1971a, b)	24–97	Coaxial cylinders	$1{\cdot}9 \leqslant r \leqslant 10$ $10 \leqslant r_2 \leqslant 27$	50 Hz	$E_s = 1{\cdot}73\,n + 38$	
				Negative lightning impulse	$E_s = 2{\cdot}60\,n + 30$	
				Negative switching impulse	$E_s = 1{\cdot}86\,n + 35$	
	24–73	Sphere–sphere	$r = r_2 = 12{\cdot}5$ $2 \leqslant d \leqslant 8$	50 Hz	$E_s = 2{\cdot}48\,n + 23$	
	36–85			Negative lightning impulse	$E_s = 2{\cdot}72\,n + 26$	
Menju *et al.* (1972)	24–97	Coaxial cylinders	not specified, expected to be $1{\cdot}9 \leqslant r \leqslant 10$ $10 \leqslant r_2 \leqslant 27$	Positive lightning impulse	$E_s = 3{\cdot}30\,n + 10$	
Takuma and Watanabe (1970a, b, c)	24–145	Sphere–plane	$r = 1{\cdot}0$ $2 \leqslant d \leqslant 50$	Positive switching impulse	$E_s = 3{\cdot}55\,n + 104$	±7
			$r = 2{\cdot}5$ $2 \leqslant d \leqslant 50$		$E_s = 3{\cdot}55\,n + 26{\cdot}4$	
Nitta and Shibuya (1971)	24–120	Sphere–sphere	$r = r_2 = 7{\cdot}5$ $0 \leqslant d \leqslant 12$	50 Hz	$E_s = 3{\cdot}55[1 + 0{\cdot}876(nr)^{-\frac{1}{2}}]$	±7[a]
		Hemispherically ended rod–rod	$r = r_2$ $0{\cdot}5 \leqslant r \leqslant 1{\cdot}5$ $0 \leqslant d \leqslant 20$			

Table 4-2 shows equations representing the results obtained from various authors. These are empirical equations based on measured values of V_{si}, except for the equations due to Takuma and Watanabe and to Nitta and Shibuya. The equations due to Kawaguchi *et al.*(1971a,b) and to Mengu *et al.*(1972), are based on voltages that give a breakdown probability of 50%.

Mattingly and Ryan have fitted their own measurements, as well as those of other authors to empirical equations relating $E_s r$ and nr.

Figure 4-13 which is quoted from Nitta and Shibuya, shows 50 Hz values of V_{si} for rod-rod gaps in SF_6. These authors reported that there experimental results were in agreement with semi-empirical equation, as quoted in Table 4-1, for properly polished stainless-steel electrodes, at gap densities up to four times atmospheric and field strength of up to 300kV cm^{-1}. At higher values of n and E, the measured value of V_{si} were lower than that calculated, and the maximum values of E/n were below $(E/n)_{lim}$. When the electrodes have been roughened by repeated sparking.

Bornick and Cooke (1972) have studied the static-voltage breakdown of SF_6 between coaxial cylinders. They also investigated the effect of:

- fine wires wrapped around the inner conductor, which intensified the local field strength by a factor of 2.5.
- small metal spheres, both fixed to the electrodes and free to move, and
- of insulating coatings, both adhesive and nonadhesive, on the electrodes.

There results were comparable with a *similarity* law:

$$E_s = 3.552n\,[1+0.60(nr)^{-1/2}] \qquad (4\text{-}2)$$

for E_s in kV cm^{-1} and n in units of $10^{18}cm^{-3}$, (Compare Nitta and Shibuya, Table 4-2).

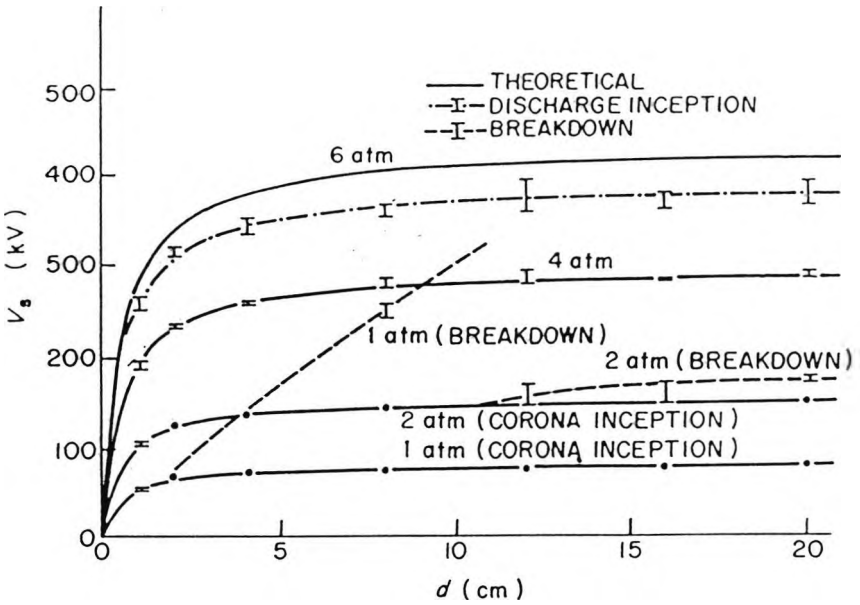


Fig. 4-13 Power frequency corona inception and breakdown voltages in rod-rod gaps in SF_6 (Nitta & Shibuya)
r = 0.5 cm. 1 atm. corresponds to $n \cong 24 \times 10^{18} cm^{-3}$
Theoretical values were obtained using the equation in Table 4-2.

4-4.4 Lightning Impulses

The response characteristics of gap electrodes were studied since in the thirties. For voltage risetimes of about 1 μs, the spark-over voltage of rod-plane and rod-rod gaps are linearly dependent upon the gap spacing for both positive and negative impulses, Allibone *et al.* (1934) and later by Walters and Jones (1964a), Paris and Cortina (1968) and Bahder *et al.* (1974). The exception to this study was possibly the long negative-rod/ earthplane gaps. This was investigated recently by the former author (Allibone *et al.* 1993)

4-4.5 Construction of the SF_6 pulser

In designing such pulser, a number of factors had to taken into consideration, one important one is the type of electrodes. There are several types of electrode configurations used to systematise the consideration of non-uniform field breakdown. Therefore a knowledge of electric field distribution in a non-uniform field system is clearly important

for any quantitative physical analysis of ionisation growth from initiation to arcing. Some of the common types of electrode configurations are:

- sphere-sphere
- sphere-plane
- conductor-conductor
- conductor-plane
- rod-rod and
- rod-plane

The configuration used in the design of the pulser is the cylindrical rod-rod of hemi-spherical ended electrodes, since from investigations, this possesses the best switching characteristics for the intended application. Steel electrodes of 25 mm diameter were used. (For voltage risetimes of about 1 μ s, such as for impulse voltages, the sparkover voltage of the rod-rod gap is linearly dependent upon the gap spacing). Other configurations in this profile are square section - cut square, conically tipped cylindrical rods and confocal paraboloids.

Pack (1991), described a similar SF_6 pulser with sphere-sphere electrodes, the pulser being metal enclosed to form a coaxial shielding. Although the pulser could only operate at voltages of up to 20 kV, very fast switching risetime was reported.

Extensive work on high voltage breakdown and corona studies using various electrode configurations (Allibone and Saunderson 1986,89,93) were carried out. [The former author had been conducting these experiments for some sixty years and only stopped because of the closure of the High Voltage Laboratory where he was last working]. Allibone *et al.* (1993), studied changes in the distribution of corona currents using rod/ plane configuration with very large gaps.

The electrodes are assembled in a cylinder filled with SF_6 pressurised gas. The cylinder constitutes a 100 mm long by 80 mm diameter 'transpalite' cast acrylic tube of wall thickness 6 mm. It is covered at both ends by aluminium discs (on which the electrodes

are attached) and sealed with *O*-rings. The adjustable electrode is also sealed with an *O*-ring. The discs are held together by six tufnol tie rods, each bolted at both ends. An inlet valve is fitted for the SF_6 gas and suitable terminals provided on the disc covers.

A drawings of the SF_6 pulser assembly is shown in Fig. 4-14 and the pulser can be seen in the photograph of the measuring set-up in Fig. 6-27.

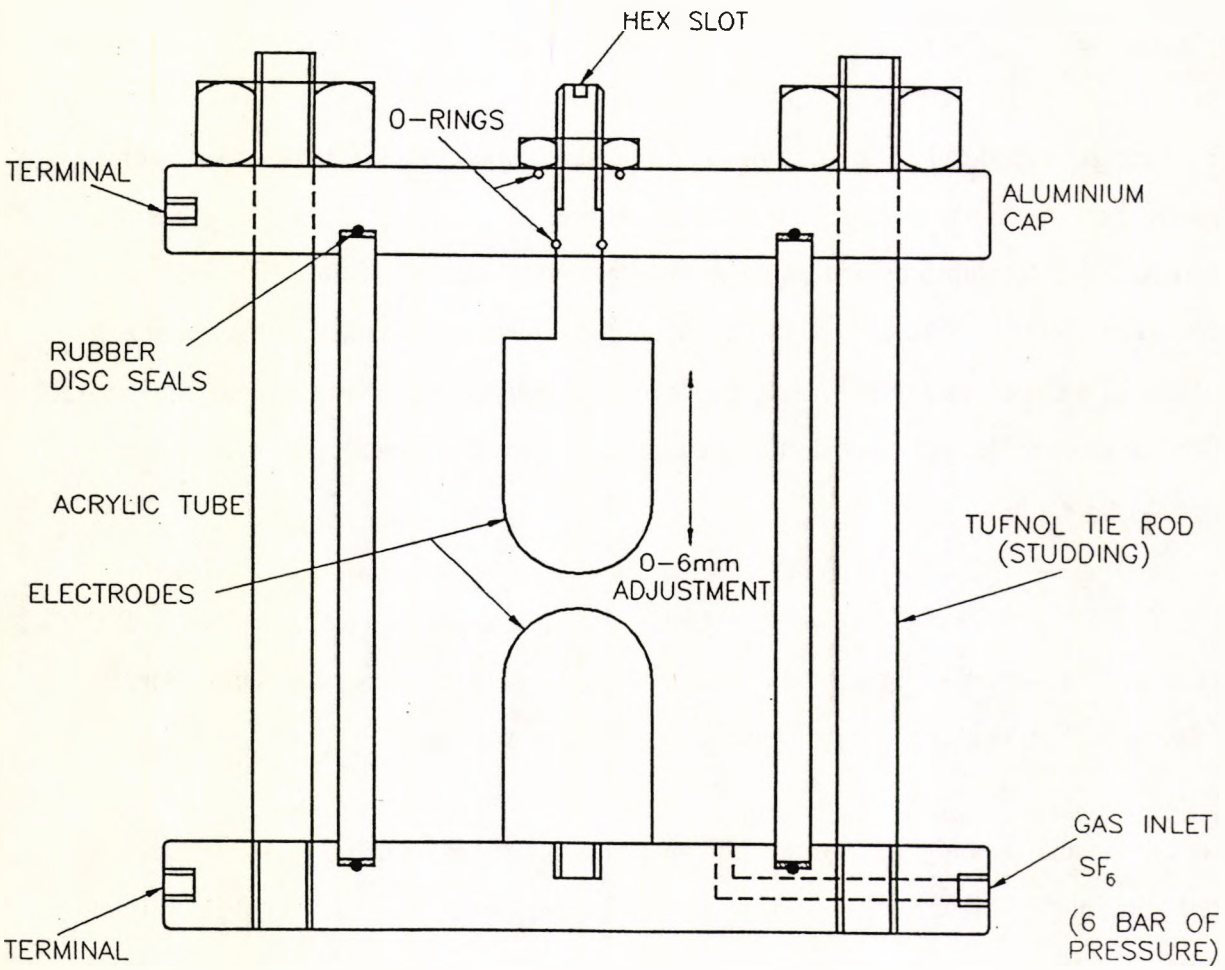


Fig. 4-14 Drawing of the SF_6 Pulser.

The most suitable materials in terms of their electrical and mechanical characteristics, were used in the design of the pulser and each component was carefully calculated. The pulser was first tested with air and then water at a pressure of 8 atm which was sustained for several hours. The results were excellent.

Chapter 5

Instrumentation and Measurement Technique

5-1 INTRODUCTION

Measurements are an essential part of human life in industrialised countries. Since trade, technology and science are world-wide, metrology, the science of measurements, must be pursued internationally.

Measurements of physical quantities serve to confirm our understanding of the nature of physical processes. However, our assessment of the methods of measurement is based on understanding the nature of the quantities measured. Therefore, improvements in the understanding of physical principles and improvements in methods in measurements, must proceed in parallel.

The command of Gallileo Gallilei:

"It is necessary to measure what can be measured and try to make measurable what cannot yet be measured,"

formulated four hundred years ago has been fulfilled in many fields since then, and has indeed, often been the motor of progress. Nevertheless, much and possibly even increasing effort is still devoted to measurements in science and technology, medicine, standards such as quantum based measurement standards, environmental protection etc.

Metrology has in world-wide co-operation, becomes a basic discipline for all areas of natural sciences.

In any measurement system, if the results are to have any real meaning, then the measurements should be carried out under ideal conditions, i.e. there should not be any interference or perturbing effects from adjacent or remote sources. If more than one instruments are used in the system, then they should be compatible with each other, especially in terms of input impedance and EMC compliance. The instruments should be selected so as to operate within their limiting ranges and thus preserving their accuracy. For specialised or precise accuracy, the measurements should be referenced to the appropriate relevant standards.

An oscilloscope, especially one which employs digital sampling technique and is equipped with an IEEE-488 interface, forms an integral part in most measurement set-up. Today, most users seem to consider sampling rate as the key specification on which to judge relative performance of digital oscilloscopes. However, the oscilloscope bandwidth is more important now than ever before as the clock speeds of digital systems continue to increase and signal risetimes are progressively decreasing in the sub-nanosecond region. An oscilloscope's risetime and its bandwidth are linked by virtue of the frequency response roll off. The measured risetime of a signal on an oscilloscope is a combination of the signal risetime and that of the oscilloscope's. That is:

$$\text{risetime } (r/t) \text{ viewed} = \sqrt{signal_{r/t}^2 + oscilloscope_{r/t}^2} \qquad (5\text{-}1)$$

The result can be very significant if instruments are not carefully chosen to match the characteristics of the signal that is to be measured. The graph in Fig. 5-1 shows the error in a risetime measurement for varying ratios of risetimes.

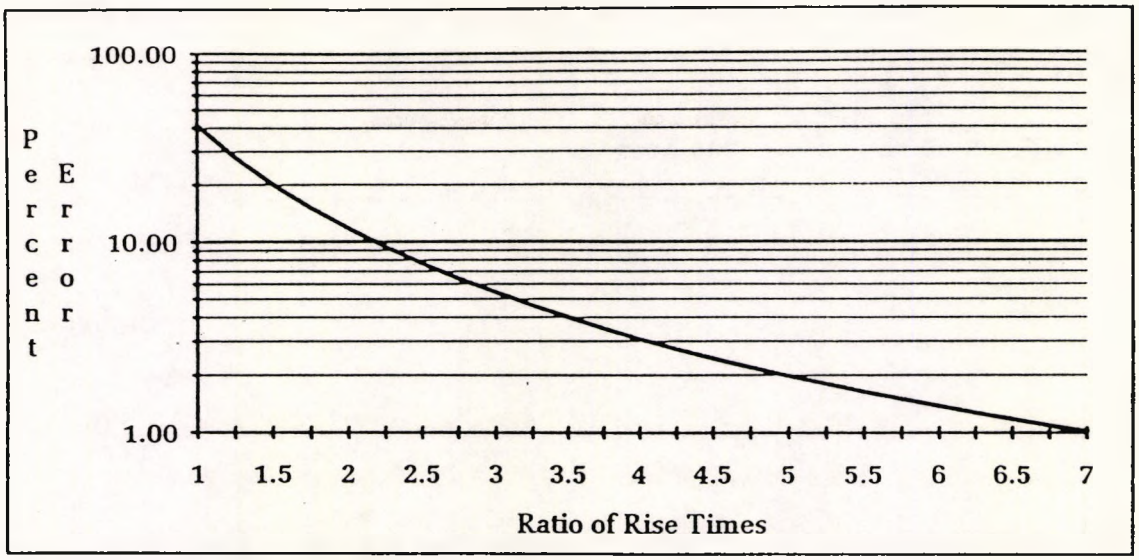


Fig. 5-1 Errors in risetime measurement.

As can be seen, even when the oscilloscope risetime is twice as fast as the signal that is to be measured, measurement errors through this source alone are above 10%. In order to reach acceptable levels of 2%, then the oscilloscope risetime needs to be 4 - times faster than the signal. This is not only of academic interests, but to everyone concerns with accurate measurements. The errors introduced by too slow an instrument affect almost all timing measurements.

In precision measurements, the risetimes of two signals that are being used in propagation delay measurements (as conducted in this investigation) will not be identical. This means that the degree to which each leading edge is slowed down on the oscilloscope screen will be different, and in turn shall distorts the timing relationship between the signals.

The graph in Fig. 5-2 shows a typical measurement of the extent of this delay between two signals.

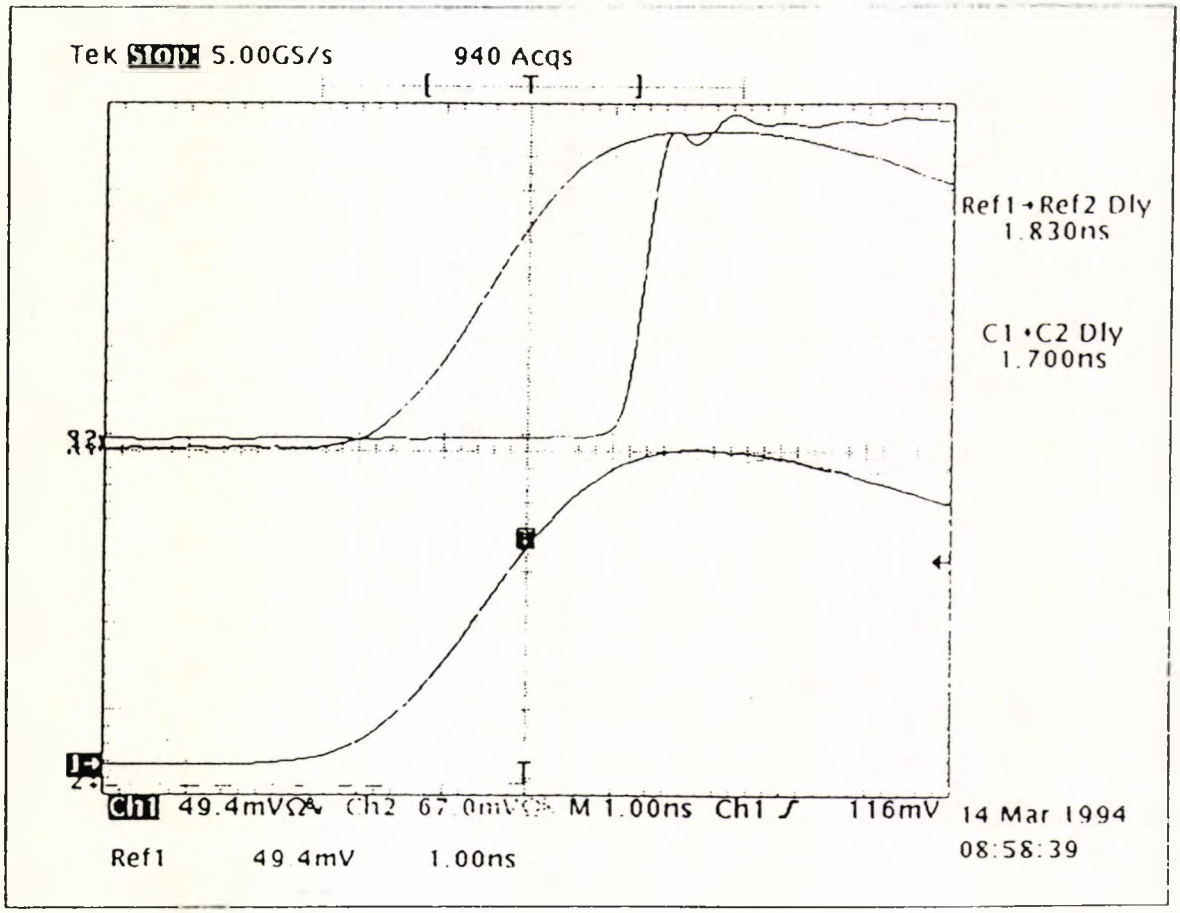


Fig. 5-2 Delay between two signals

The trace on bottom half was taken with the oscilloscope speed reduced by a factor of 4, i.e. the time-base running at 250 MHz.

The connecting probes (passive) also play an important part in the measurement accuracy and in checking specifications. The actual displayed risetime depends on all the elements in the acquisition of the system and in some measurements the probe bandwidth must be taken into consideration. In which case,

$$\text{risetime viewed} = signal_{r/t} + \sqrt{oscilloscope^2_{r/t} + probe^2_{r/t}} \qquad (5\text{-}2)$$

5-2 INSTRUMENTATION

The measurement equipment and instrumentation used in the investigations are as follows:

1. Tektronix 7854 digital sampling oscilloscope
2. Tektronix high speed camera
3. Datron autocal Digital Voltmeter
4. HP Spectrum Analyser
5. Cohu 1 kV Power Supply
6. Brandenburgh 80 kV Power Supply
7. Personal Computer
8. Precision inductive and capacitive bridges with ancillary devices.

A preview of the more specialised ones are given. Equipments 1, 3, 4 and 7 incorporate GPIB/IEEE-488 interface buses, some of which were interconnected during some of the testing. This technique is fully described in *Chapter* 6.

5-2.1 The Measuring Oscilloscope

This equipment formed an integral part of the experimentation from which all photographic results were taken. It combines the features of a high performance real-time oscilloscope with digital storage, and a 400 MHz waveform processor. When integrated with a wide range of plug-in units, it becomes a powerful measurement system. The Tektronix 7854 mainframe offers programmable measurement routines, GPIB interface for mass data and program storage, plus simultaneous display of real-time and stored waveforms. The on-board memory can store up to 40 waveforms and 2000 keystrokes.

Mainframe and calculator keyboard functions provide cursor control and waveform-parameter information at the touch of a button. The mainframe has facility to take a wide range and amplifier units with low ($50\,\Omega$) and high ($1\,M\Omega$) input impedance. An optical interface sampling unit (FO10) and a delay-line unit (7M11), can also be installed within the mainframe or externally through extender cables.

The 7S12 TDR/Sampler used is a dual purpose unit for measurements of recurring fast risetime signals or for time domain reflectometry. It combines a vertical and horizontal, double width sampling unit which can be used in any Tektronix 7000 series mainframe oscilloscope.

The 7S12 has two compartments and accepts a sampling and a pulse- generator plug-in heads, which determine the characteristics of the TDR measurement system. The left hand compartment (labelled SAMPLING on the front panel) accepts the *S*-series sampling heads which range from 1 GHz to 16 GHz. The right-hand compartment (labelled PULSE GENERATOR) accepts the pulse generator (*S*-52), trigger recognizer (*S*-53) and trigger count down (*S*-51) heads. Fig. 5-3 shows the 7S12 front panel with the installation of the S-6 sampling head and the S-52 pulse generator head, suitable for TDR.

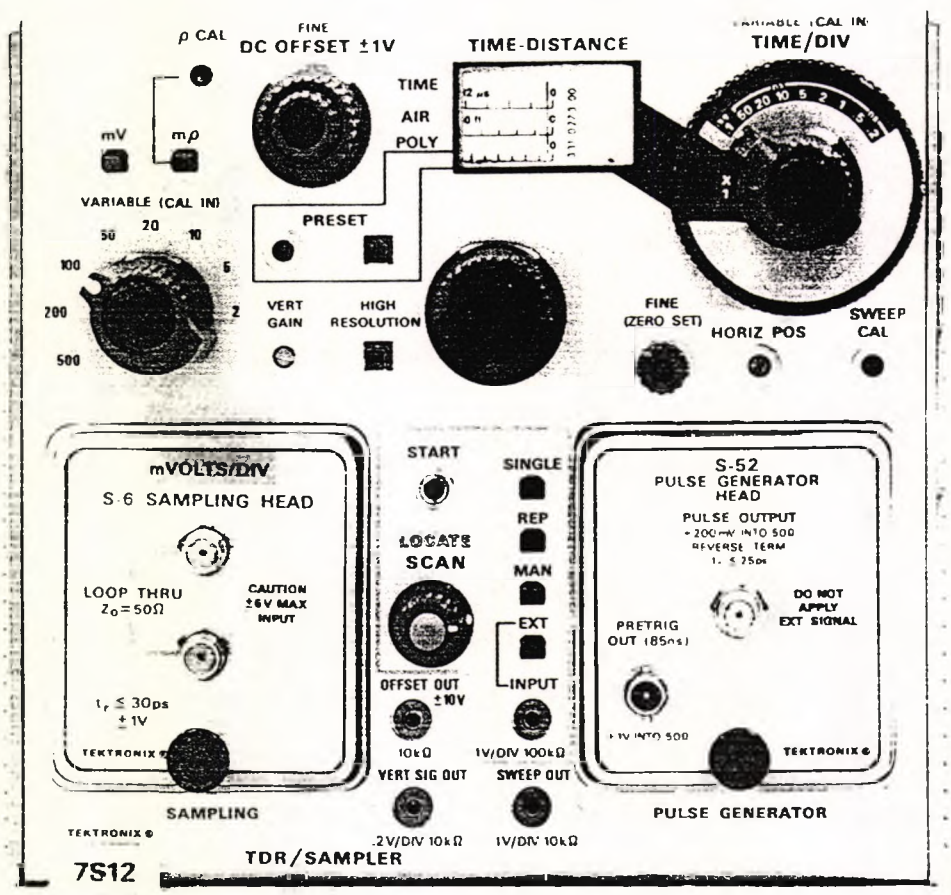


Fig. 5-3 7S12 front panel for TDR measurements.
(Tektronix Manual)

These sampling units can be used remotely from the mainframe through suitable extender cables. One example is that a signal can be sampled at its source and then digitally transmitted (with all the advantages compared with an analogue transmission) to the mainframe oscilloscope.

5-2.1.1 Features of the 7S12 TDR/Sampler

This unit has the following features: The vertical deflection factors, i.e. millivolts/ division and millirho/division are from 2 to 500 in a 1-2-5 sequence. The time/division is calibrated from 20 ps/division to 1 μ s/division in the same sequence. The DC OFFSET control offsets the display in a ± 1 V range. The HI RESOLUTION switch reduces the waveform noise jitter by signal averaging with a corresponding reduction of sweep rate. The LOCATE switch increase the time/div and intensifies a portion of the display to locate the time window, relative to the total waveform.

Front panel outputs include OFF- SET OUT (± 10 V range), VERTical SIGnal OUT and SWEEP OUT. Modes of sweep operation include SINGLE sweep, REPetitive sweep, MANual scan and EXTernal sweep IN.

The TIME-DISTANCE scale is calibrated for round-trip time measurements of 0 to 10 μ s and one-way distance measurements of up to 1500 m air dielectric or 975 m polyethylene dielectric. The POLY scale may be calibrated for transmission lines which have a velocity of propagation equal to or greater than that of polyethylene.

The electrical characteristics (performance requirements) of the 7S12 are given in Table 5-1 and the electrical characteristics (system performance requirements with S-6 and S-52) are given in Table 5-2.

TABLE 5-1 Electrical Characteristics - Performance Requirements

Characteristic	Performance Requirement	Supplemental Information
ERTical SIGnal OUT		
Amplitude		200 mV/div of signal display within 2% VARIABLE control must be in CAL position.
Source Resistance		10 kΩ within .5%
WEEP OUT		
Amplitude		1 V/div of horizontal deflection within 2%
Range		0 V to greater than 10 V
Source Resistance		10 kΩ within 1%
IME/DIV		
Accuracy	Within 3%	
Range		20 ps/div to 1 µs/div in a 1-2-5 sequence
ime/Div VARIABLE Range		Provides continuous coverage to at least 8 ps/div.
isplay Modes		
SINGLE Sweep		Each sweep is initiated by pushing and releasing the START button.
REPetitive Sweep		Normal resolution: sweep rate is continuously variable from at least 1 sweep in 20 ms to less than 1 sweep in 5 s. HI RESOLUTION: sweep rate is continuously variable from at least 1 sweep in 200 ms to less than 1 sweep in 50 s.
MANual Sweep		Any portion of the display may be observed by manual operation of the SCAN control.
EXTernal Input		
Deflection Factor		1 V/div within 5% to at least 15 V/div
Input Resistance		100 kΩ within 10%
Maximum Input Voltage		150 V (DC + peak AC)
INE (ZERO SET) Range		Moves an unmagnified waveform at least .9 div.

TABLE 5-1 Electrical Characteristics - Performance Requirements cont'd.

Characteristic	Performance Requirement	Supplemental Information
Deflection Factor		
Accuracy	Within 3%	
Range		2 units/div to 500 units/div in a 1-2-5 sequence. Units/div are labeled on the sampling head.
Units/Div VARIABLE Range		Provides continuous coverage from 1 to 770 units/div (mV or mρ)
ρ CAL Range		Allows calibrated reflection coefficient (ρ) with pulse generators supplying from 200 mV to 1 V pulse amplitude
DC OFFSET Range	Offsets display at least +1 V to −1 V.	
OFFSET OUT		
Range		At least +10 V to −10 V. OFFSET OUT = 10X (DC OFFSET) within 2%
Source Resistance		10 kΩ within 1%

TABLE 5-2 Electrical Characteristics Systems Performance with S-6 and S-52

Characteristic	Performance Requirement	Supplemental Information
Risetime	35 ps or less for the incident step, 45 ps or less for the displayed reflection from a short-circuited 1 ns test line	
Pulse Amplitude	At least +200 mV into 50 Ω	
Input Impedance		Nominal 50 Ω
Jitter	Less than 10 ps (without signal averaging)	
Aberrations	Not more than +7%, −7%, total of 10% P-P within the first 1.8 ns of the step edge with the reference level at 1.8 ns from the step edge; not more than +2%, −2%, total of 4% P-P after 2.5 ns from the step edge with the reference level at 0.3 μs from the step edge.	
TIME-DISTANCE Scale		Time scale indicates round-trip time. Distance scales (AIR and POLY dielectrics) indicate one-way distance. The usable TIME-DISTANCE range for TDR measurements are limited by the S-52 pulse duration.

TABLE 2 Electrical Characteristics Systems Performance with S-6 & S-52 cont'd.

Accuracy	TIME scale within 1% of full scale.	Distance scales are calibrated for the nominal velocity of propagation of the AIR and POLY dielectrics.		
		TIME-DISTANCE Multiplier		
		X.1	X1	X10
TIME Range		.1 μs	1 μs	10 μs
		Maximum of about 150 ns one-way cable delay.		
AIR Dielectric Distance Range		49 feet	490 feet	4900 feet
		15 meters	150 meters	1500 meters
		Maximum of about 150 feet (46 meters) cable length.		
POLY Dielectric Distance Range		32 feet	320 feet	3200 feet
		9.75 meters	97.5 meters	975 meters
		Maximum of about 100 feet (30 meters) cable length.		

5-2.2 The C-5C Camera

The Tektronix C-5C is a lightweight general purpose camera with a Polaroid-type CB101 back. It features a battery-operated electronic shutter with fixed focus and an f/16 aperture opening. The camera can be mounted directly on most models of Tektronix oscilloscopes and small monitors. Adapter hoods are provided that permits mounting to others. An interchangeable lens-shutter assembly and spacer section, provide an object-to-image ratio (magnification factor) of either 1:0.67 or 1:0.85. With these ratios, photographs taken on instruments with either an 8 cm by 10 cm or 9.8 cm by 12.2 cm display, cover the usable area of the film surface. The camera's major sections are high-impact resistant, injection-moulded plastic. A viewing door is provided which can be opened so as to observe the cathode ray tube (crt) display without removing the camera.

5-2.2.1 Specifications

The optical characteristics of the camera, presented in Table 5-1 are valid only if the camera is operating at an ambient temperature between 0° and +50°. Electrical characteristics listed in Table 5-2 are valid when the camera has been adjusted within an ambient temperature between +20° and +25° for at least 10 minutes.

Table 5-3 Optical Characteristics

Characteristics	Performance Requirements	Supplemental Information
Relative Aperature	Fixed at f/16.	
Focal Length	58 mm nominal.	
Object-to-Image Ratio (Magnification Factor)	1:0.67 or 1:0.85 within ±5%.	Changeable by repositioning the lens-shutter assembly in one of two possib positions.
Geometric Distortion	±1% or less.	
Resolving Power	At least 6 lines/mm at center. At least 3 lines/mm at corner.	

Table 5-4 Electrical Characteristics

Characteristics	Performance Requirements	Supplemental Information
Timed Shutter Mode	Shutter speed continuously variable from 0.1 through 5 seconds ±20%.	
Minimum Time Interval	0.1 second ±20%.	Minimum shutter time interval must have been adjusted to 0.1 second wit the camera at ambient temperature between +20 to +25° C for at least 1 minutes.
Open Shutter Mode	Shutter opens on actuation and closes on actuation at any time interval greater than 0.1 second.	
Graticule Flash Unit		
Recycle Time	2 seconds nominal.	
Energy Input	Adjustable from 0.04 to 0.2 joules.	

5-2.3 The Digital Voltmeter

An accurate digital voltmeter was necessary so as to make comparative measurements during very small changes and for measuring resistance values. A Datron 1061A autocal DVM was used for the measurements. This is a high precision multi-function micro-processor controlled instrument featuring exceptionally high stability and systems capability. The basic instrument provides full DC measurement capability, computation facilities, self check routines and calibration memory.

The self-check feature is initiated on power up.

The model used for the testing incorporates an IEEE-488 interface, a feature which was utilised in the measurement technique, whereby the oscilloscope measured the waveform of the signal and the DVM simultaneously measured the peak voltage.

With the IEEE-488 interface option, the AUTOCAL series instrument provides a wider range of Bus controlled measurement functions. In addition to the normal measurement functions of DC or AC voltage or current and resistance, the 1061A provides DC coupled AC voltage or current and most other front panel controlled functions. This allows the use on the interface bus, of such features as:

- error readout
- dB
- Autocal
- Keyboard
- Maths
- Limits
- Ratio
- Superfast
- Selftest and
- Input zeroing.

5-2.3.1 Self Test

The most reliable instruments can be exposed to extreme conditions beyond its design specifications. Components no matter how carefully screened and tested before being integrated within the instrument, can sometimes fail prematurely. The 1061A has a built-in self-test procedure which verifies correct functioning of the instrument. Pressing the *TEST* key starts the self-test program during which a sequential routine:

- Checks in turn, all the display segments, characters and legends
- Verifies the correct functioning of individual measuring circuits
- Checks the non-volatile calibration memory

On completion of the test, the instrument returns automatically to the last selected function and range to provide rapid return to measurement. In the event of a failure, it displays an appropriate error code.

In its basic version, the 1061A is a precision DC voltmeter. A wide range of additional measurement capabilities in the form of plug-in cards are then fitted by the manufacturer. With all the measurement options added, the instrument provides the following measurement functions:

- DC Voltage
- DC Current
- True RMS AC Voltage
- True RMS AC Current
- DC coupled True RMS AC Voltage
- DC coupled True RMS AC Current
- Resistance
- dB
- Ratio
- Full Remote Control

Whilst the Autocal DVM is widely used as a general purpose multi-function instrument, the Selfcal DVM is used for standards measurements. The performance of precision digital multimeters used mainly for calibration and standards laboratory applications has been limited by the basic stability of certain critical components in their analogue measurement circuits. The most significant of these components are the gain defining resistor network used in signal conditioning amplifiers, and the zener devices which form the instrument's basic voltage reference.

In order to push the state of the art beyond some of these limitations, a new design of precision digital multimeter (DMM) makes extensive use of internal calibration - Selfcal - to remove the effects of time and temperature drift in all areas except those due to the zener references.

Edwards (1987), gave the internal calibration procedure and outlined the resulting benefits of Selfcal as follows:

1. A 35% improvement in performance over the identical instrument when use without Selfcal. This is of obvious use to the standards and calibration engineer who is always striving to achieve better margins of uncertainty over the equipment that has to be maintained. Alternatively, this addition margin may be used to justify extending the calibration period of the DMM, reducing the frequency with which it needs to be calibrated.

2. A 2:1 improvement in temperature coefficient. This means that standards laboratory type performances can be obtained in uncontrolled factory floor or ATE environment.

3. Internal calibration necessarily involves highly accurate internal measurements which may also be used for very high accuracy selftesting. In general, Selfcal can provide a superb instrument selftest of measurement accuracy.

Simple to use, the process can be activated with a single key press or use of the IEEE-488 command and require no external calibration sources.

5-3 TEST METHODS

The sampling heads used in this experiment are the S-6 which is a 50 ohm feed-through unit for high speed (<30ns/11.5 MHz bandwidth) applications and the S-53 trigger recognizer head which produces stable pulses from the input signal. The fast (sub-nanosecond) pulse was unable to trigger the oscilloscope, therefore the measurements had to be carried out using a delay-line pre-trigger arrangement.

In this technique the signal that is to be measured first arrived at the trigger recognizer head and initiated triggering. The signal was then teed off and travelled through a fixed delay-line unit which imposed a delay of 75 ns before it reached the sampling head. The test arrangement is shown in Fig. 5-4.

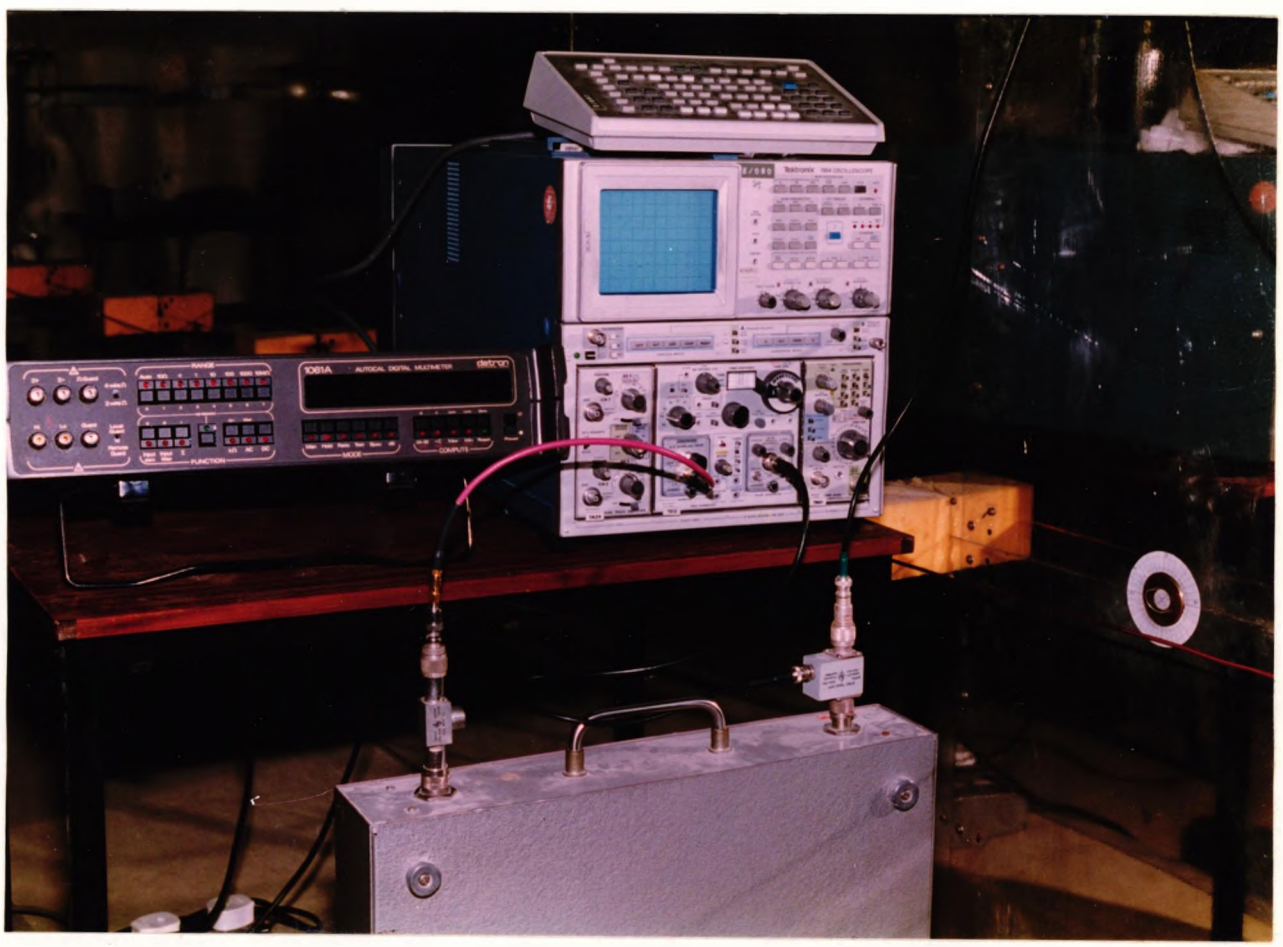


Fig. 5-4 Photograph of measurement set-up.

This was measured both with TDR, using the facility of the oscilloscope, and the fast output from the mercury pulser. Although there was some attenuation imposed on the pulse amplitude, there was negligible degradation to the pulse front.

5-3.1 Signal Acquisition Method

The waveform of the signal must be repetitive in order that it can be sampled by the digitiser and stored in a memory register. Having been displayed and properly positioned on the screen, the real-time waveform can then be placed in memory. This is done by simply pressing the signal acquisition command (*AQR*) button which will give a one time averaging. Ten, one hundred and one thousand times averaging can also be obtained.

Equivalent-time random sampling is used to construct the waveform into memory from as many repetitions of the real-time waveform as required. The reconstruction of a pulse from a repetitive real-time signal is shown in Fig. 5-5.

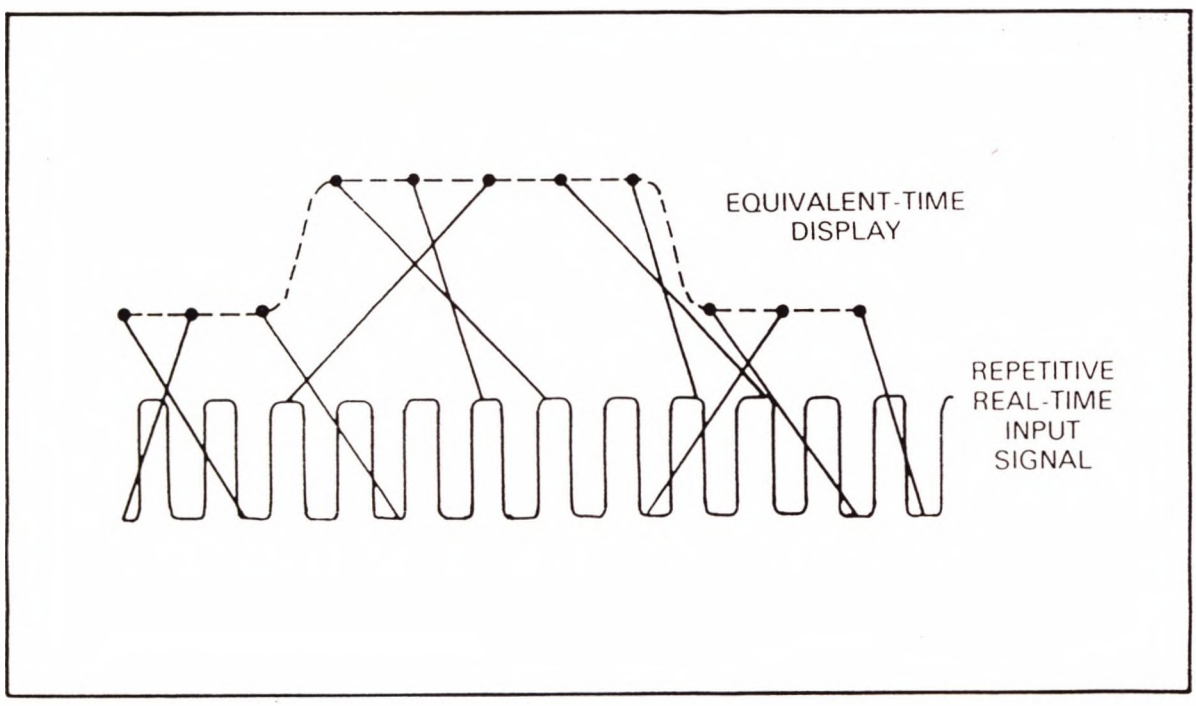


Fig. 5-5 Reconstruction of an input pulse from equivalent-time random sampling.

The digitiser simultaneously samples and quantizes the repetitive real-time signal. This sampling is asynchronous with respect to the sweep and only the samples acquired within the horizontal limits of the graticule while the waveform is visible are considered valid. During digitising most of the waveform points will have sampled more than once , while some may not have been filled at all. The most recent data is retained in memory.

Waveform acquisition is terminated when at least 99% of all valid points have been sampled and stored into memory and atleast one complete sweep has occurred, or when a STOP command is received.

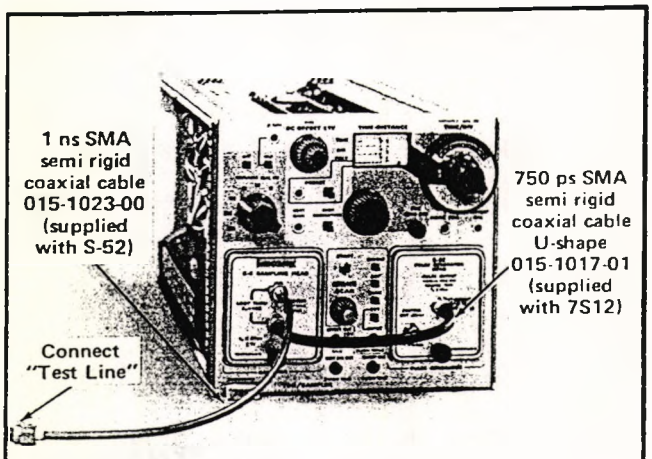
The waveforms were digitised at the appropriate sampling rate and them stored in the oscilloscope. The information is also stored in the computer through the GPIB link. Mathematical functions and wave analyses were then performed as necessary.

With suitable plug-in modules the oscilloscope can also be used to aquire a single sweep waveform. This may be necessary when the required signal to be stored is not repetitive because of varying amplitude, waveshape or repetition rate. In this method the processor uses real-time sampling to sequentially sample and store 512 points of the single sweep waveform.

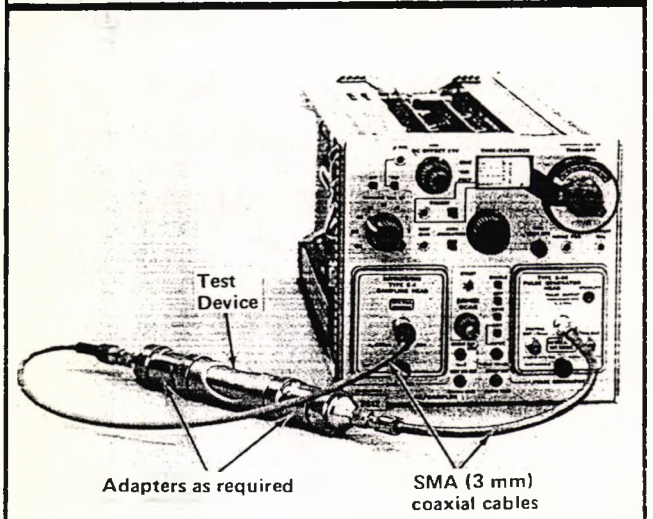
5-3.2 Time Domain Reflectometry (TDR) Measurements

Time domain reflectometry is widely used in microwave stripline evaluation, computer backplane measurements, printed circuit board testing and lines. This measurement technique is also suitable in transmission systems, e.g. risetime and attenuation, and for cable testing. With *TDR*, a pulse is sent down a conductive path and measured as it reflects back from any impedance changes in the device under test (DUT). Any impedance variations in the path cause a corresponding signal to be displayed on the scope. The precise location and type of impedance such as open circuit, short circuit or step change, in the conductive path or line, can be measured on the display.

In order to illustrate the technique in time domain reflectometry measurements, a 7S12 TDR/Sampler incorporating the S-6 sampling head and an S-52 Pulse Generator can be used in several configurations, as shown in Figs. 5-6, 5-7 and 5-8.



(A) "Loop Thru" connections for short and medium length cable TDR measurements. The "Test Line" is connected to the end of the 1 ns semi rigid line for minimum aberrations and fast risetime. Use the 7S12 Multiplier settings of X.1 and X1 (limited by the S-52 pulse duration).



(B) "In Line" connections for short length cable TDR measurements. The transmission system under test must have two ports with low attenuation between them. SMA (3 mm) semi rigid cables are used with the proper adapter to the device under test. Use the 7S12 Multiplier setting of X.1.

Fig. 5-6 Application connections for "Loop Thru" and "In Line" TDR measurements.

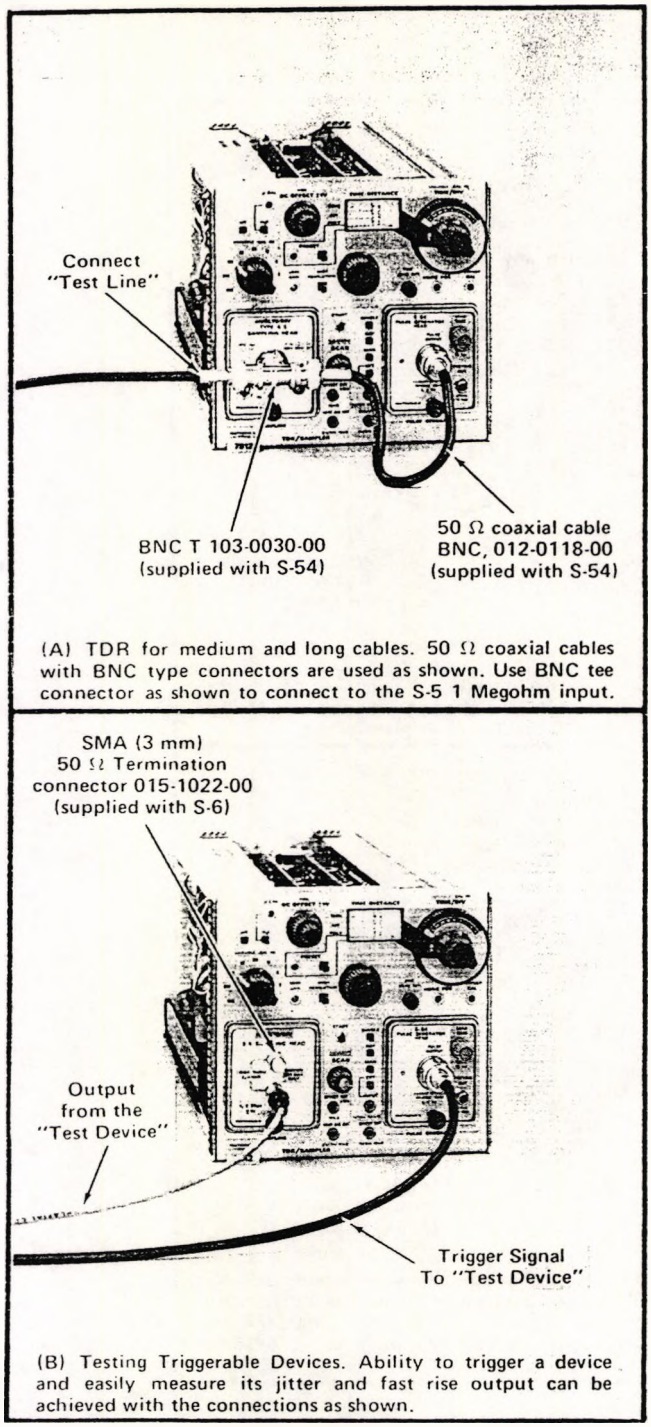
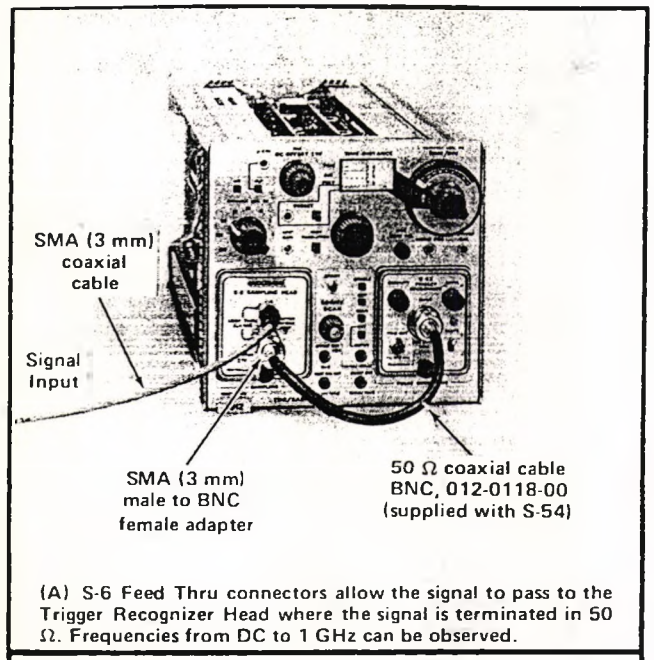
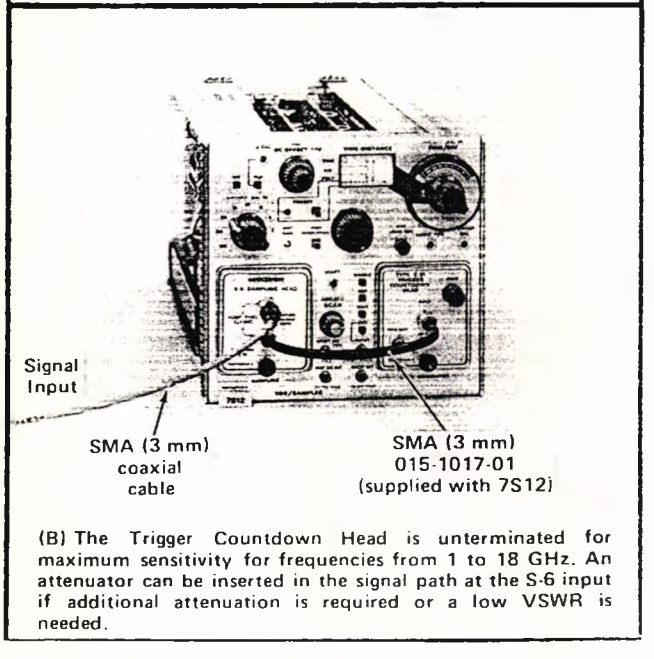


Fig. 5-7 Application connections (A) for TDR measurements with medium and long cables.

(B) for testing triggerable devices.



(A) S-6 Feed Thru connectors allow the signal to pass to the Trigger Recognizer Head where the signal is terminated in 50 Ω. Frequencies from DC to 1 GHz can be observed.



(B) The Trigger Countdown Head is unterminated for maximum sensitivity for frequencies from 1 to 18 GHz. An attenuator can be inserted in the signal path at the S-6 input if additional attenuation is required or a low VSWR is needed.

Fig. 5-8 High Frequency Signal Application.

5-3.2.1 Experimental - Distance Measurement of the Line using TDR

The test was conducted to measure the travel time of the pulse on the line, with the termination open-circuited. The output from the pulse generator was connected to the line and a display of the pulse reflection pattern obtained. Cursors were placed at the source position so as to exclude the cable connection and at the termination just before

reflection of the pulse. Twice the travel time of the pulse on the line was computed by the oscilloscope to be 70.12 ns. Using the velocity of propagation:

$$v = 3 \times 10^8 \text{ m/s} \tag{5-3}$$

for an electromagnetic pulse in free space, this is in good agreement with the actual physical length of 10.5 m for the line.

Although the developed mercury pulser has a much faster risetime and higher amplitude, the pulse generator incorporated in the oscilloscope is very convenient and can find use in many practical applications. Fig. 5-9 shows the result of the TDR measurement.

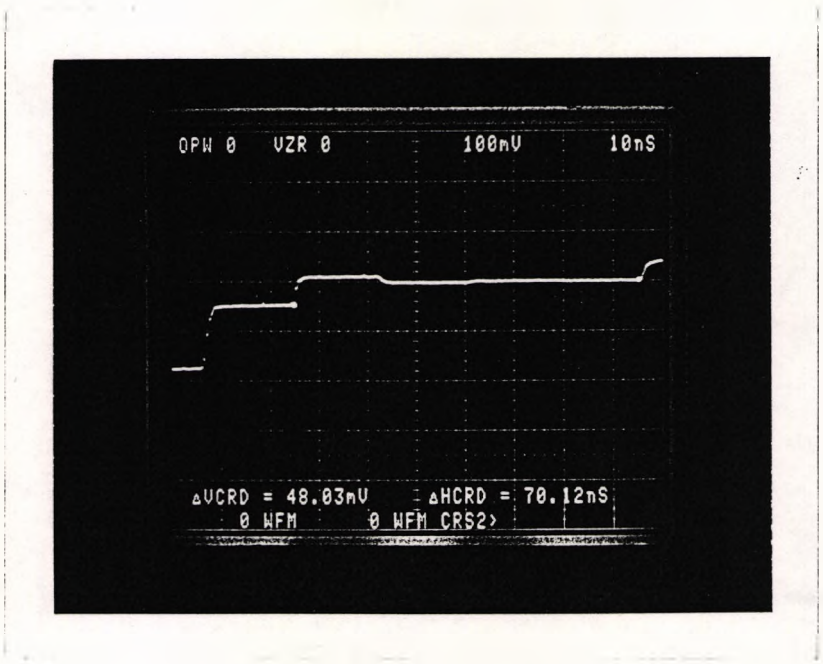


Fig. 5-9 TDR measurement of the line.

Whilst TDR measurement techniques are useful for general purposes, there are severe limitation for longer lengths of cables such as sections of a transmission line or distribution feeders. The main reason is due to the low amplitude output from the pulse generator.

5-3.3 Voltage Reflection Coefficient

TDR measurements can also determine the value of the voltage reflection coefficient of a transmission line from which the load resistance (R) can be calculated. As shown in Fig. 5-10, the reflection coefficient (Γ) is taken from the top of the incident pulse launched from the S52 pulse generator.

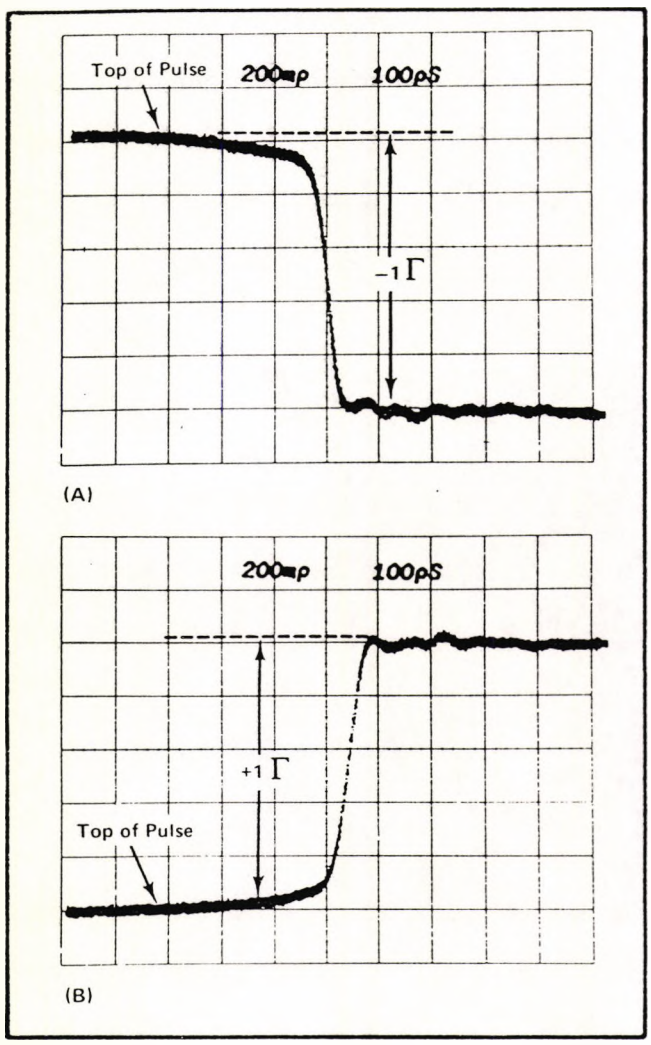


Fig. 5-10 (A) Display of a short-circuit terminated line and (B) and unterminated line.

A positive reflection (referenced from the top of the incident pulse) indicates an impedance greater than the impedance of the line. A negative reflection indicates an impedance less than the impedance of the line.

With a known reflection coefficient Γ, the resistance of the load can be found by the following equation:

$$R_{load} = Z_0\left(\frac{1+\Gamma}{1-\Gamma}\right) \tag{5-4}$$

5-3.4 Time or Distance Measurement Procedure

Using the 7S12 front panel with the S6 and S52 sampling heads, the propagation time or distance to a discontinuity can easily be made. There are three general methods:

1. On the c.r.t. screen, where measurement points are located a short distance apart.
2. Between two points on the *time-distance* dial.
3. From dial zero on the *time-distance* dial.

5-3.4.1 The On-Screen Method

The distance between two measurement points or discontinuities on the screen may be determined more readily than from the TIME-DISTANCE dial - just by measuring the time separation on the c.r.t. screen and applying the velocity of an electromagnetic wave for the particular dielectric medium.

In the measurement set-up, the 1 ns semi-rigid coaxial line was used when making time or distance measurements, because the S-6 and S-52 waveform discontinuities are in the first 2 ns. The junction of the transmission line and the sampling head connector can be found by partially disconnecting the line under test from the sampling head connector to produce an inductive discontinuity at the junction. This is shown in Fig. 5-11. Adjustment of the FINE control is made so as to place the discontinuity (or bump) at a convenient reference point for the measurement. The connection is then fully installed. Note that cursors can be placed on the trace of the c.r.t. screen at the discontinuity and at the point of reflection, and the time computed by the oscilloscope by invoking the relevant command. This technique is shown in **5-3.5.**

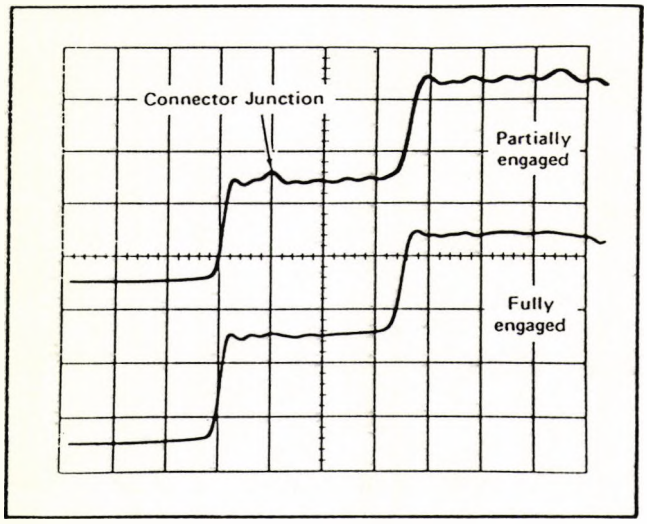


Fig. 5-11 Test line connector junction location obtained by partially engaging the line to the connector.

5-3.5 TDR Measurements using the Line Pulser

5-3.5.1 Preview

A pulse may be considered as the sum of a positive going and equal, but time displaced negative step function. The voltage and current pulse travel away from the source without any distortion, i.e. maintaining their waveshapes as a function of either distance or time. The surge energy of the travelling pulse is stored equally in the electric and magnetic fields.

The angular settings of the directional coupler immersed in the electromagnetic field created by a pulse travelling on the line is of significant importance since it forms the basis of the tests and investigations. The loop dimensions were chosen so that the amplitude of the induced voltage due to the component of the magnetic coupling is greater that that due to the component of the electric coupling, as in the general case. The amplitude of the induced voltage throughout the testing is generally always the resultant value of the electric- and magnetic-field coupling. Since at the 0/180 degree position of the directional coupler, there is no influence of the magnetic coupling of the loop, then the induced voltage at these settings must be due only to the electric coupling.

Hence, a means is established such that the directional coupler is able to distinguish between, and independently measure these electromagnetic coupling effects.

5-3.5.2 Connections of the Measurement System

The system was connected as shown in the diagram, Fig. 5-12(a) and the photograph in Fig. 5-12(b) shows the arrangement. The pulser was connected to the line though a simple line matching network so that the 50 ohm measuring system matched the characteristic impedance of the line. Details and calculations are shown in Appendix 2.

There is always the problem of mismatch when a coaxial system is connected to a line with a different impedance as in the experimental work. Although the system was properly matched and the network was made as small as possible, the physical insertion of the network was sufficient to cause a small reflection. This is an inherent problem in such interconnection, but in this case the reflection at this junction was characterised.

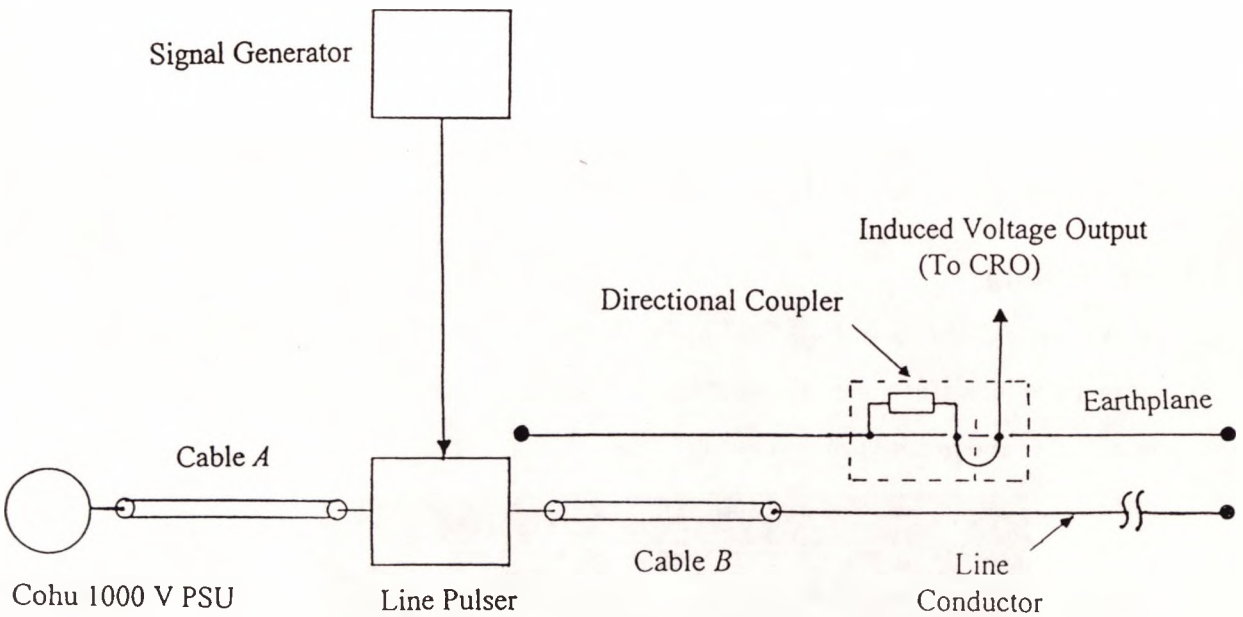


Fig. 5-12(a) Connection diagram.

A directional coupler was mounted on the earthplane near the mid section of the line, at a distance of 5 m from the supply end and 5.5 m from the termination. These are arbitrary distances as the directional coupler had to be mounted at a suitable and convenient position on the earth-plane, i.e. away from the frame support. Each of the two connecting cables has a propagation delay time (PDT) of 4.5 ns. This was calculated and confirmed by time domain reflectometry (TDR) measurement using this feature of the oscilloscope.

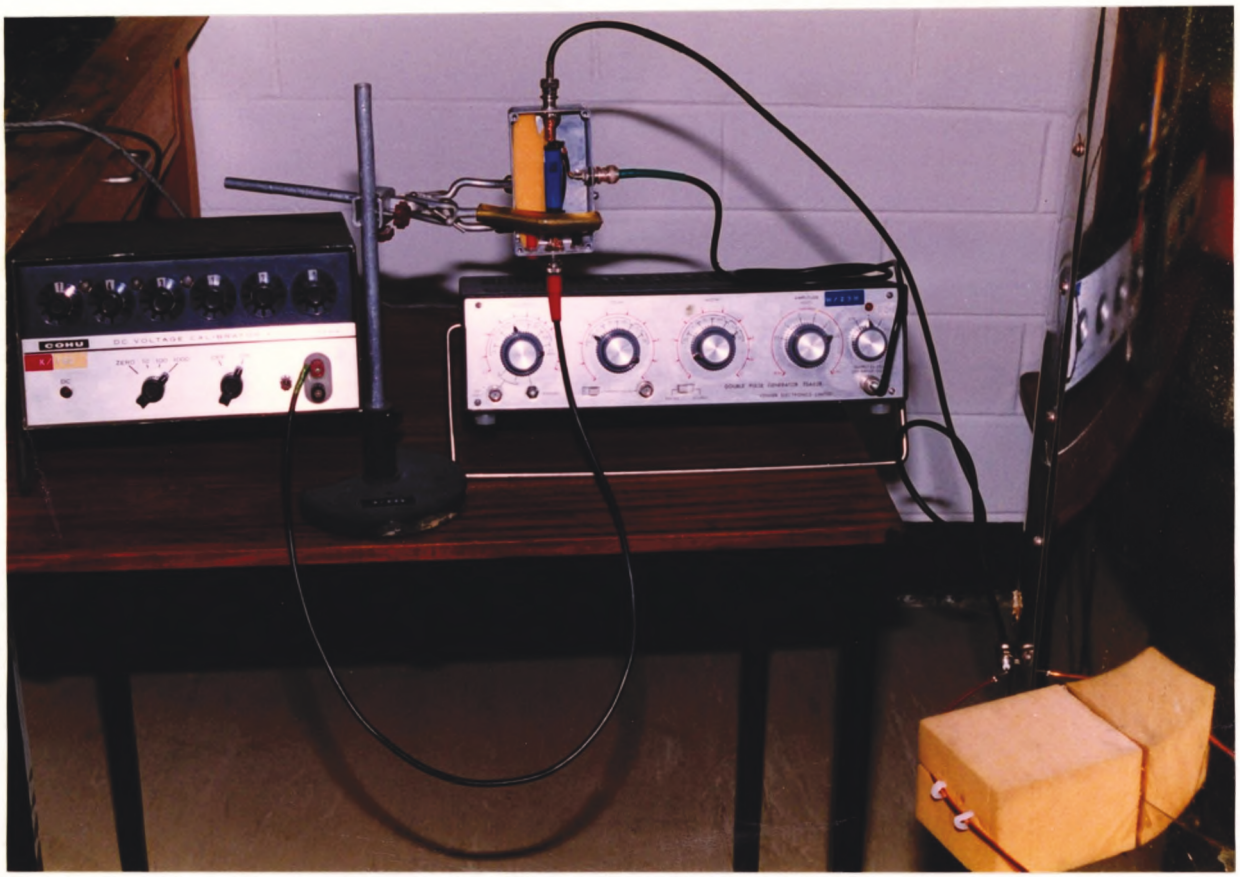


Fig. 5-12(b) Photograph of the pulser and ancillery equipment.

5-3.6 Initial Testing

The circuit was connected as in Fig. 5-12(a) with the line termination open-circuited. The directional coupler was then adjusted for maximum magnetic coupling at the 90 degree position, and the result is shown in Fig. 5-13.

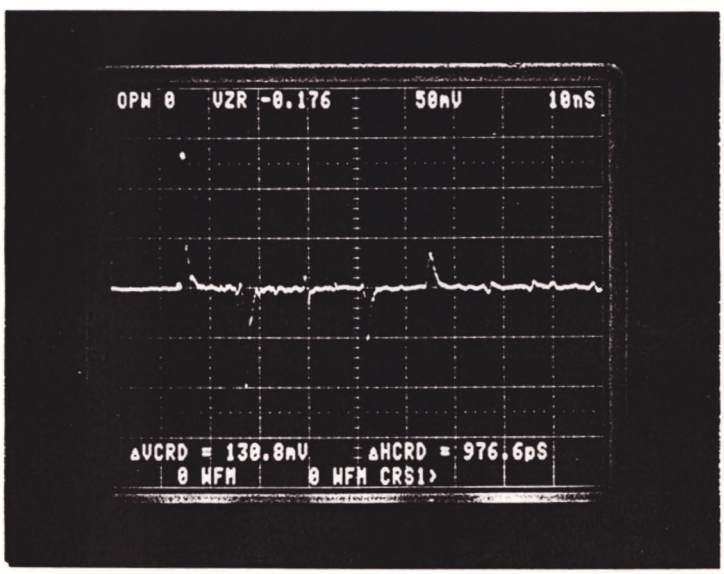


Fig. 5-13 Pulse reflection pattern with maximum coupling.

This result suggested an alternative method and shows how the length of a line can be found simply by the TDR principle, described in **5-3.2**. Although there is a limitation on distance measurements using the pulse generator of an oscilloscope, there is a very good agreement between these two methods. This technique is described fully in *Chapter* 7, as a possible application for use as a fault locator on a transmission line.

The induced voltage in the loop due to the component of the forward travelling positive V^+ pulse was observed to be of positive polarity [shown in Fig. 5-14 (a)] and for the forward travelling negative V^- pulse, it was reversed. This negative pulse was reflected from the high limiting resistor on the PSU output terminal and delayed by 9 ns due to its travel time in the pulse forming cable *A*. The waveform is shown in Fig. 5-14(b).

Having reached the end of the line the V^+ pulse was then reflected at the open circuit termination and travelled back to the source with the same phase. On interacting with the loop again, it induced a voltage of the negative polarity, shown in Fig. 5-14(c).

Conversely, the delayed V^- pulse reflected from the termination, travelled back with the same polarity, and on interacting with the loop, caused a positive voltage to be induced. This is shown in Fig. 5-14(d). Fig. 5-14(a) illustrates in principle the induced voltage polarity in the loop due to a forward travelling pulse. Fig. 5-14(b), that due to the pulse reflected from the supply. Fig. 5-14(c), the reflection from the termination and Fig. 5-14(d), the induced voltage due to the delayed reflection from the termination.

Since the reflected pulse at the open circuit termination travelled back with the same phase, the polarity of the induced voltages should be the same as that of a forward travelling pulse. This reversal in polarity shown in the result is simply due to the reflected pulse when travelling back to the source, interacted with the loop in a different configuration, that is, displaced by 180^o.

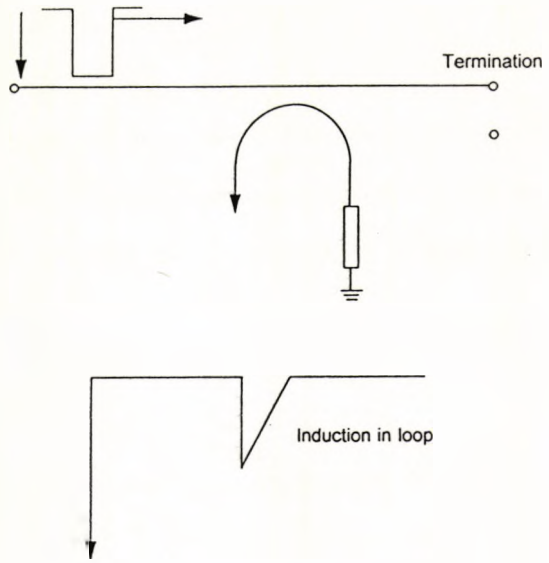


Fig. 5-14(b) Induced voltage due to a pulse reflected from the supply.

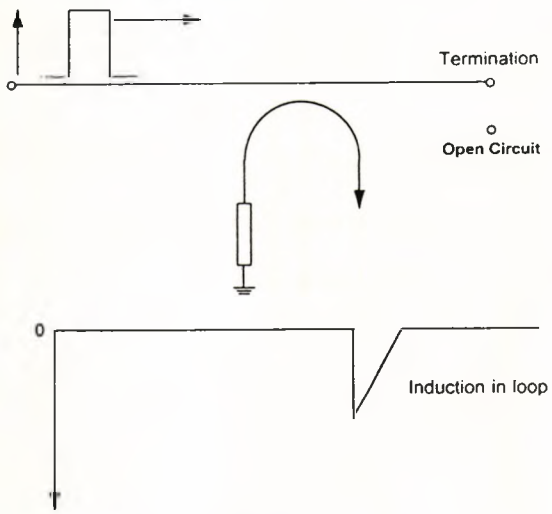


Fig. 5-14(c) Induced voltage due to a pulse reflected from the termination.

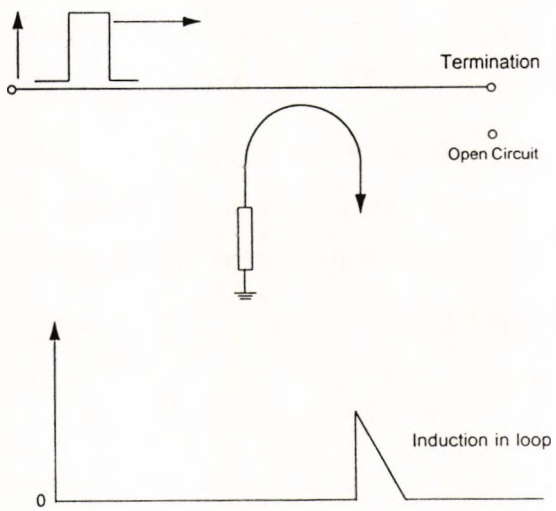


Fig. 5-14(d) Induced voltage due to a delayed pulse reflected from the termination.

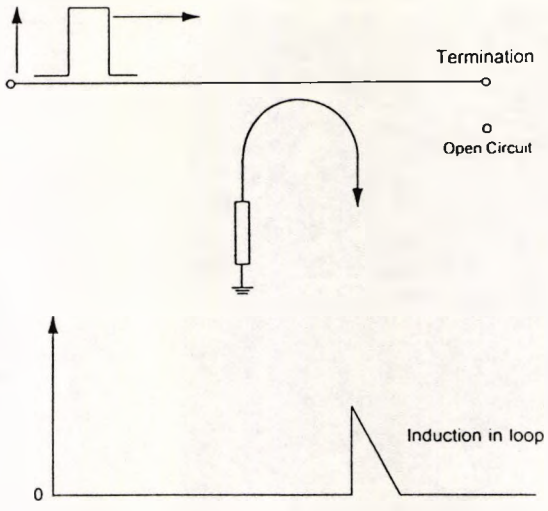


Fig. 5-14(d) Induced voltage due to a delayed pulse reflected from the termination.

For a short circuited termination, the polarity of these induced voltages (due to reflections from the termination) will be changed in accordance with the sign of the reflection coefficient. That is, they will be of opposite as for the case of open circuit condition.

The directional coupler was then displaced by 180 degree, i.e. set for maximum coupling but now at the 270 degree position. In this configuration there was an interchanging of position between the output of the coupling loop and its matching load resistor. The tests were repeated and the results shown in Fig. 5-15.

Note the complete reversal of polarities of the induced voltage, marked (a), (b), (c) and (d) as compared with the results in Fig. 5-13.

These polarities of the induced voltages satisfy Lenz/Faraday Laws.

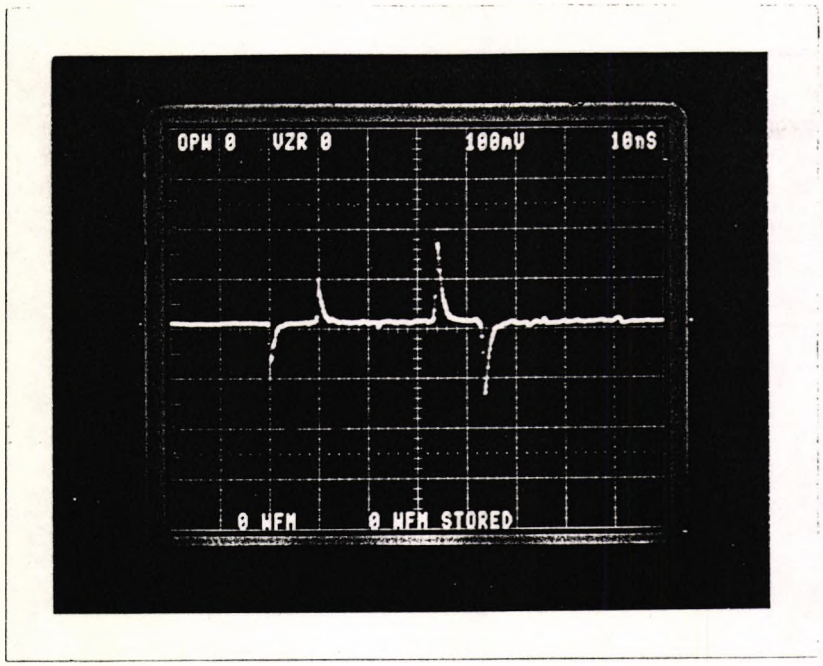


Fig. 5-15 Induced voltage due to 180° displacement of the directional coupler.

5-4 THE BEWLEY LATTICE (REFLECTION) DIAGRAM

The preceding reflective pulses from the source and termination tends to become tedious and difficult to visualised when it is necessary to consider many of such reflected pulses. In such cases, a graphical construction of a reflection diagram is very helpful.

The Bewley lattice diagram is a very useful illustration in evaluating the potential distribution of pulses on lines at specific instances of time. The propagation of a wave (or pulse) is represented as a directed segment, the horizontal component representing distance travelled and the vertical component, the time elapsed after a change in circuit condition.

The voltage reflection diagram for the transmission line circuit in Fig. 5-16 is given in Fig. 5-17.

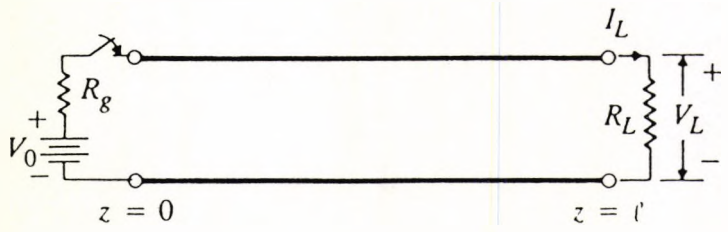


Fig. 5-16 A d-c source applied to a lossless transmission line.

Consider a wave V_1^+ at $t = 0$, travelling from the source (z = 0) in the +z-direction with a velocity $u = 1/\sqrt{LC}$. This wave is represented by the directed straight line marked V_1^+ from the origin. This line has a positive slope equals to $1/u$. When the V_1^+ wave reaches the load at $z = \ell$, a reflected wave $V_1^- = \Gamma_L V_1^+$ is created if $R_L \neq R_0$. The V_1^- travels in the -z-direction and is represented by the directed line marked $\Gamma_L V_1^+$ with a negative slope equals to $-1/u$.

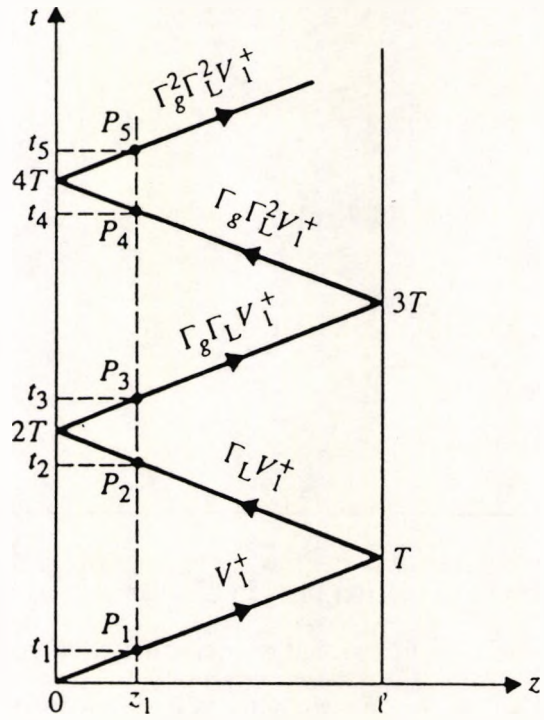


Fig. 5-17 Voltage reflection (Bewley) diagram.

This method of illustration is used throughout the results in the testing, and is further explained in *Chapter* 6.

Chapter 6

Test Sequence on the Transmission Line and Experimental Results

6-1 INTRODUCTION

The discussions of wave characteristics on transmission lines in *Chapter* 2, was based on steady-state, single frequency, time-harmonic sources and signals that involve voltage and current phasors. Quantities such as reactance, wavelength, wavenumber and phase constant would loose their meaning under fast switching or transient conditions. However there are important practical situations in which sources and signals are not time-harmonic and the conditions are not steady state.

Chapter 3 shows a relationship between electric/magnetic fields and voltages/currents. Antenna theory is applicable to the loop probe, since the probe extracted energy from an incident electromagnetic wave and delivered it to a load. In the following tests, the quantity measured was the induced voltages and currents of the probe.

In the past antenna theory had almost always concerned far field predictions which are easier to characterise. Important observations can be made on these far-zone fields, e.g.,

- E_φ and H_ϕ are in space quadrature and time phase, and their ratio, $E\varphi / H\phi = \eta_o$ is a constant equal to the intrinsic impedance of the medium.
- The far-zone fields then have the same properties as those of a plane wave, since at very large distances from the dipole, a spherical wavefront closely resembles a plane wavefront.
- The far-fields varies inversely with the distance from the source.

Due to stringent emission regulations for the use of electronic equipment, characterisation of emitted interference is a problem of immense interest to the EMI/EMC community. During recent years, the tendency is to predict far-field values from near-field measurements, since a better insight to an antenna's behavior can be obtained. Based on comuputational technique and numerical methods, Bucci (1990), explored the possibility of calculating the far-field from near-field amplitude measurements. An algorithm for the near-field to far-field transformation was proposed by Laroussi and Costache (1994).

6-1.1 Transients on Transmission Lines

In this section, the testing concerns the transient behaviour of a lossless transmission line due to fast switching pulses, injected into the line, and the transient response of loop probes that couple to the electromagnetic fields produced by these pulses. For such lines (R=0, G=0), the characteristic impedance becomes the characteristics resistance, $R_o = \sqrt{L / C}$, and the voltage and current waves propagate (*in phase*) along the line with a velocity $\mu = 1 / \sqrt{LC}$. A simple case is used in this experimental procedure where a DC voltage source V_0 is applied through a resistance R_g at $t = 0$ to the input of a lossless line, terminated into a characteristic impedance of R_0. This is shown in Fig. 6-1(a).

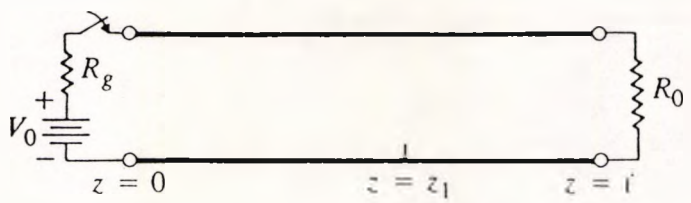


Fig. 6-1(a) Line terminated in its characteristic resistance - switch closed at $t = 0$

Since the impedance looking into the terminated line is R_o, a voltage wave of magnitude:

$$V_1^+ = \frac{R_o}{R_o + R_g} V_o \qquad (6\text{-}1)$$

travels down the line in the $+z$-direction with a velocity $\mu = 1/\sqrt{LC}$. The corresponding magnitude I_1^+, of the current wave is:

$$I_1^+ = \frac{V_1^+}{R_o} = \frac{V_o}{R_o + R_g} \qquad (6\text{-}2)$$

If the voltage across the line is plotted at $z = z_1$ as a function of time, a delayed step function is obtained at $t = z_1/\mu$ as in Fig. 6-1(b).

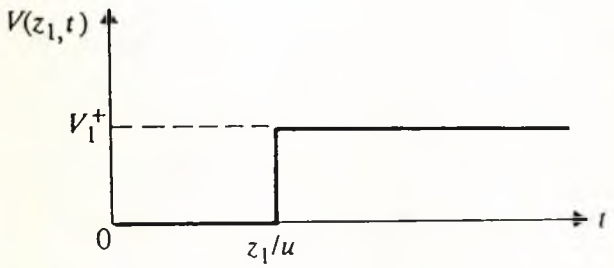


Fig. 6-1(b) Line terminated in its characteristic resistance - voltage at $z = z_1$

The current in the line at $z = z_1$ has the same shape with a magnitude I_1^+, given in Eq.(6-2). When the voltage and current waves reach the termination at $z = \ell$, there are no reflected waves because the reflection coefficient, $\Gamma = 0$. A steady state condition is established and the entire line is charged to a voltage equal to V_1^+.

If both the series resistance R_g and the load resistance R_L are not equal to R_0 as in Fig. 6-1(c), then the situation is more complicated.

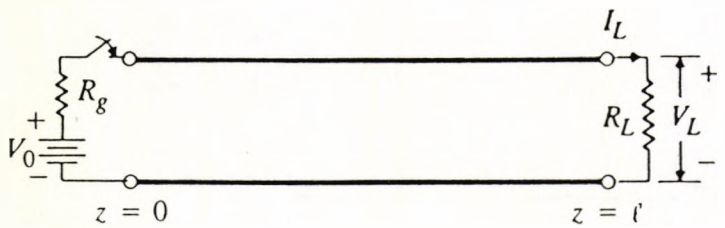


Fig. 6-1(c) A d.c. source applied to a terminated lossless line at $t = 0$ (general case).

When the switch is closed at $t = 0$, The d.c. source sends a voltage wave of magnitude:

$$V_1^+ = \frac{R_o}{R_o + R_g} V_o \qquad \text{(as in Eq. 6-1)}$$

in the +z-direction with a velocity of $\mu = 1/\sqrt{LC}$ as before, because the V_1^+ wave has no knowledge of the length of the line or the nature of the load at the other end. It proceeds as if the line is infinitely long. At $t = \mathrm{T} = \ell / \mu$, this wave reaches the load end, $z = \ell$. Since $R_L \neq R_0$, a reflected wave will travel in the -z direction with a magnitude of

$$V_1^- = \Gamma_L V_1^+ \tag{6-3}$$

where,

$$\Gamma_L = \frac{R_L - R_0}{R_L + R_0} \tag{6-4}$$

is the reflection coefficient of the load resistance R_L. This reflected wave arrive at the input end, or source, at t = 2T, where it is reflected by $R_g \neq R_0$. A new voltage wave having a magnitude V_2^+ then travels down the line, where:

$$V_2^+ = \Gamma_g V_1^- = \Gamma_g \Gamma_L V_1^+ \tag{6-5}$$

In Eq. (6-5),

$$\Gamma_g = \frac{R_g - R_0}{R_g + R_0} \tag{6-6}$$

is the reflection coefficient of the series resistance R_g. This process will go on indefinitely with waves travelling back and forth being reflected at each end at $t = n\mathrm{T}$ (n = 1,2,3,..). Two points are worth noting here. First, some of the reflected waves travelling in either direction may have a negative amplitude, since Γ_L or Γ_g (or both) may be negative. Second, except for an open-circuit or a short-circuit Γ_L and Γ_g are less than unity. Thus the magnitude of successive reflected waves becomes smaller and smaller, leading to a convergent process.

The progression of the transient voltage waves on lossless lines in Fig. 6-1(c) for $R_L = 3R_0 (\Gamma_L = \frac{1}{2})$ and $R_g = 2R_0 (\Gamma_g = \frac{1}{3})$ is illustrated in Fig. 6-2(a, b and c) for the three different time intervals. The corresponding current waves are given in Fig. 6-2(d,e and f), which are self explanatory. The voltage and current at any particular location on the line in any particular time interval are just the *algebraic sums*,

$$(V_1^+ + V_1^- + V_2^+ + V_2^- + \ldots.) \text{ and } (I_1^+ + I_1^- + I_2^+ + I_2^- + \ldots.) \text{ respectively.}$$

It is interesting to check the ultimate value of the votage across the load, $V_L = V(\ell)$, as t increases indefinitely. This leads to the following (for a converging series):

$$V_L = V_1^+ + V_1^- + V_2^+ + V_2^- + V_3^+ + V_3^- + \ldots.$$
$$= V_1^+(1 + \Gamma_L + \Gamma_g\Gamma_L + \Gamma_g\Gamma_Z^2 + \Gamma_g^2\Gamma_L^2 + \Gamma_g^2\Gamma_L^3 + \ldots.)$$

Can be shown to be:

$$= V_1^+\left(\frac{1+\Gamma_L}{1-\Gamma_g\Gamma_L}\right) \tag{6-7}$$

For this present case, $V_1^+ = V_0/3$, $\Gamma_L = \frac{1}{2}$ and $\Gamma_g = 1/3$

From Eq. (6-7),

$$V_L = \tfrac{9}{5}V_1^+ = \tfrac{3}{5}V_0 \qquad (\text{as } t \to \infty) \tag{6-8}$$

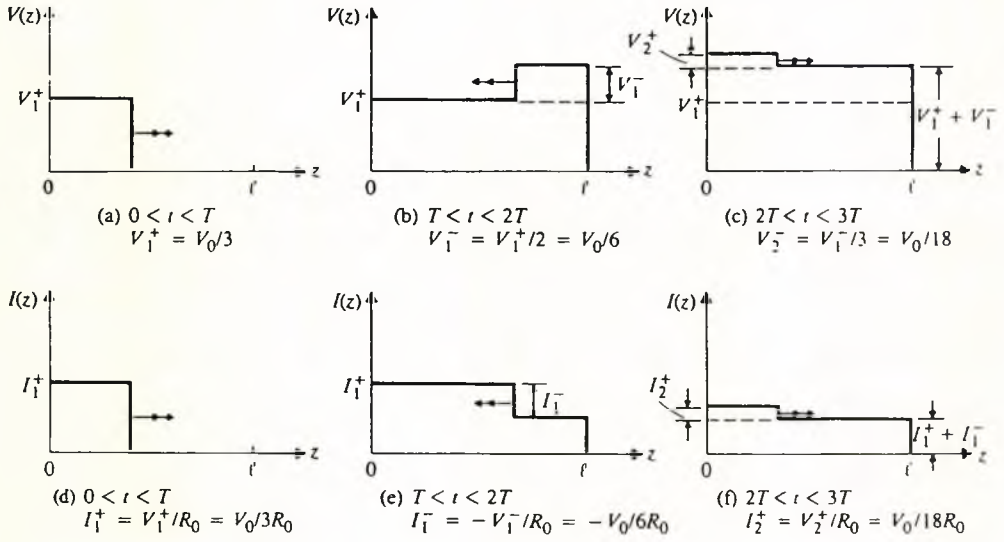


Fig. 6-2 Transient voltage and current waves on transmission line shown in Fig. 6-1(c).

This result is obviously correct, because in the steady state, V_0 is divided between R_L and R_g in the ratio of 3 to 2.

Similarly,
$$I_L = \left(\frac{1-\Gamma_L}{1-\Gamma_g\Gamma_L}\right)\frac{V_1^+}{R_0} \tag{6-9}$$

which yields,

$$I_L = \frac{3}{5}\left(\frac{V_1^+}{R_0}\right) = \frac{V_0}{5R_0} \qquad \text{(as expected)} \qquad (6\text{-}10)$$

The voltage injected into the line is of a transient step function, because from a pulse repetition frequency of , say 500 Hz, the pulse width would be 1 ms, compared with the short travel time of 35 ns for an electromagnetic wave on the line. The step function is given by:

$$v_g(t) = V_o U(t), \qquad (6\text{-}11)$$

where $U(t)$ denotes the step function,

$$U(t) = \begin{cases} 0 & t<0 \\ 1 & t>0 \end{cases} \qquad (6\text{-}12)$$

6-1.2 Pulse Excitation

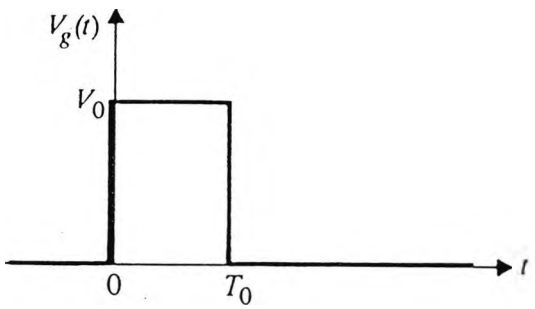


Fig. 6-3 A rectangular pulse.

In many instances, such as in computer networks and phase modulation systems, the excitation may be in the form of pulses and this is indeed true for all pulsed power applications. The analysis of the transient behaviour of a line with pulse excitation, however, does not present any special difficulties because a rectangular pulse can be decomposed into two step functions. For example, the pulse of amplitude V_0 lasting from $t = 0$ to $t = T_0$ shown in Fig. 6-3 can be written as:

$$v_g\ (t) = V_o[U(t) - U(t - T_0)] \qquad (6\text{-}13)$$

If $v_g\ (t)$ in Eq. (6-3) is applied to a transmission line, the transient response is simply the superposition of the result obtained from a DC voltage V_0 applied at $t = 0$ and that obtained from another DC voltage - V_0 applied at time $t = T_0$.

The following experimental set-up and test methods are the same in this section. The investigation involved adjustments of the orientation of the directional couplers which were places at different locations in the transmission system. The tests being conducted with open circuit, matched and short circuit conditions on the termination.

6-2 EXPERIMENTAL - TESTING WITH OPEN CIRCUIT TERMINATION

6-2.1. Electric (D) coupling

The circuit was connected as in Fig. 6-4, with the end of the line open-circuited in this case. The directional coupler was then adjusted to the zero degree or *reference* position where there was no effect , due to the magnetic coupling on the loop, since negligible flux linkages is assumed. Therefore the induced signal was produced only by the effect of the electric-field coupling.

For this angular setting, the loop was vertically orientated so that its 50 ohm matching load was at the 180 degree position and the signal output connector at the corresponding 0/360 degree positions on the directional coupler. This arrangement is shown in Fig. 6-5.

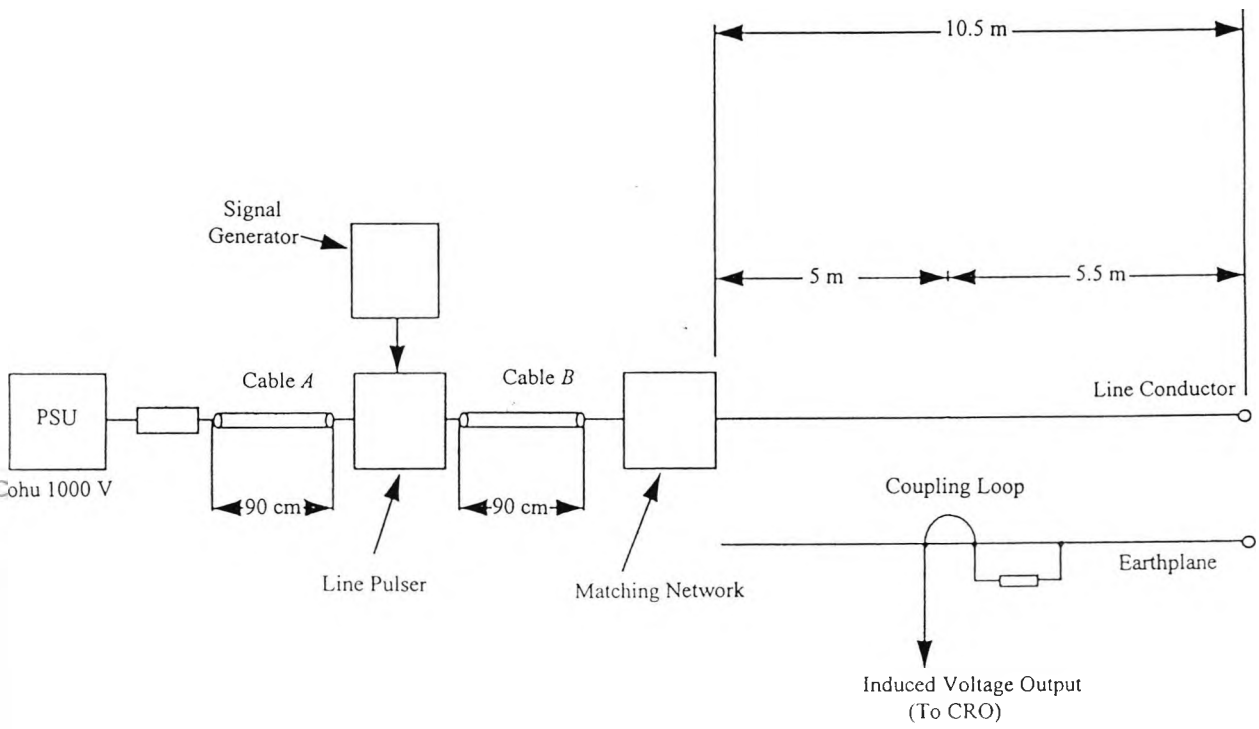


Fig. 6-4 Connection diagram of the measurement system.

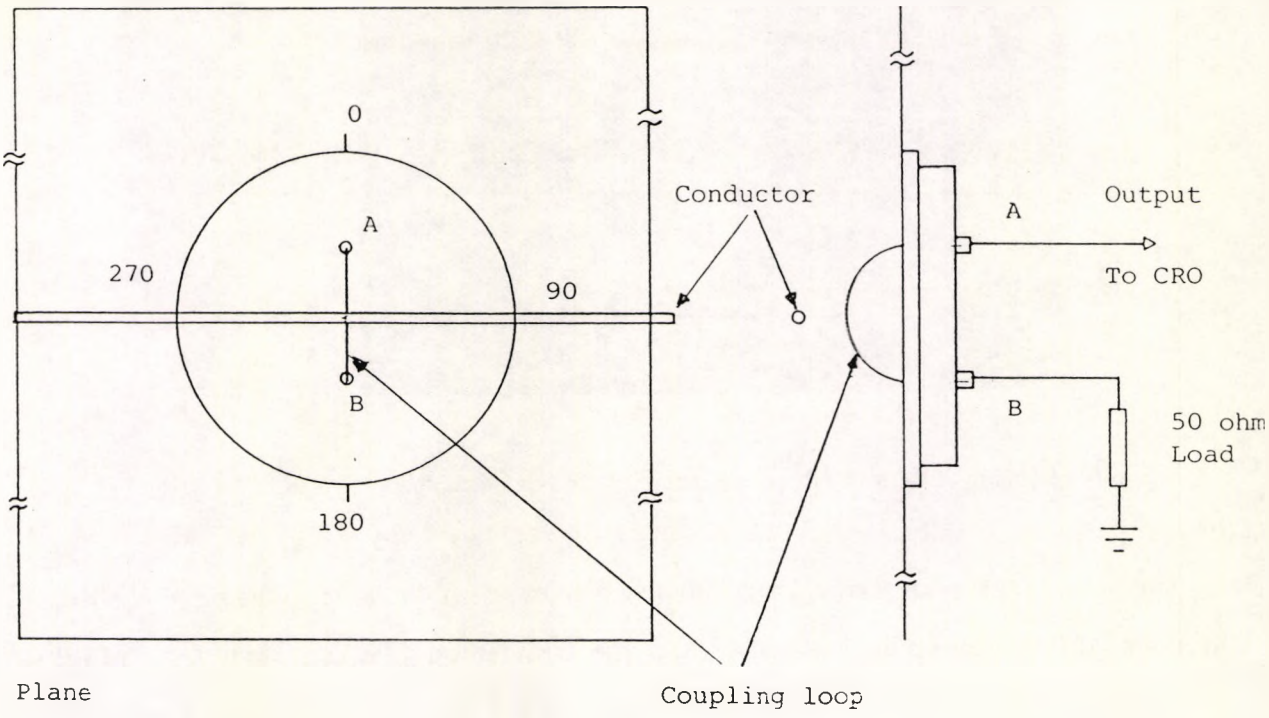


Fig. 6-5 Orientation of the directional coupler for electric-field coupling.

With open-circuited line termination, the power supply and line pulser were switched on. The output from the power supply unit (PSU) was then raised to 700 volts and a pulse of this amplitude was injected into the transmission line and allowed to propagate.

The induced voltage in the loop, due to the component of the electric-field coupling of the travelling pulses, was sampled and stored in the oscilloscope. The oscillograph result in Fig. 6-6 shows the induced signal waveform and the consecutive induced voltage pulses are marked (*a*), (*b*), (*c*) and (*d*). Their amplitudes can be estimated from the result.

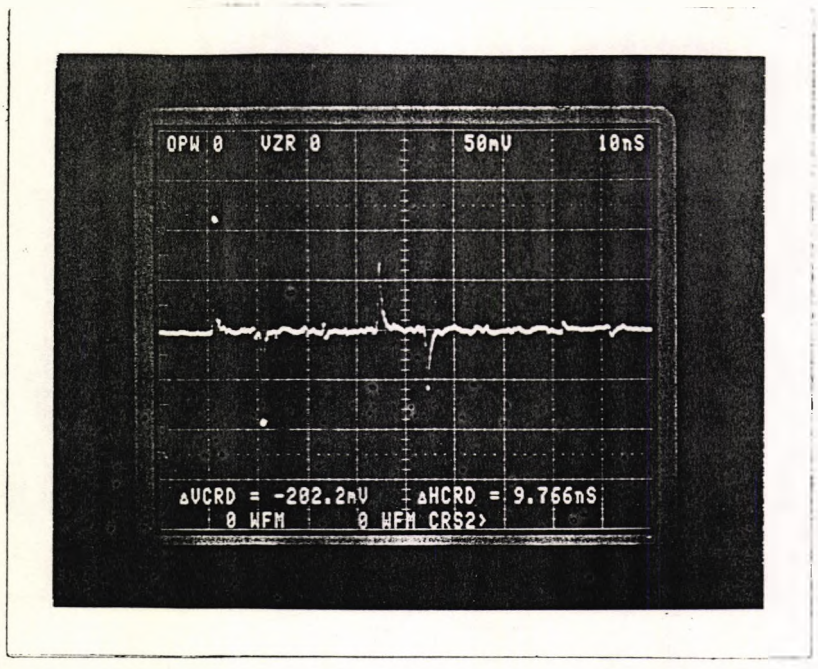


Fig. 6-6 Waveform of induced voltages due to the electric-field coupling.

The forward travelling ($V^+/2$) pulse induced a voltage in the loop of the same positive polarity as the same pulse reflected from the termination. That is, signal (*a*) is of the same polarity as signal (*c*). Conversely, the delayed forward ($V^+/2$) travelling pulse reflected from the supply, induced a negative polarity signal in the loop, as did the same pulse when reflected from the termination. That is, signal (*b*) corresponds to signal (*d*).

No changes in the amplitude nor polarity, (as expected), of the induced voltage occurred when the directional coupler was adjusted to the 180 degree position. In fact, the electric-field coupling is always present in the electromagnetic field and the coupling effect of the induced voltage is of the same amplitude and polarity, regardless of the angular position of the loop. However, the induced output voltage of the loop can vary with its conductor dimensions. This is explained later in the text.

It is easy to observe or measure this output voltage at the zero or 180 degree position, where the effect of the magnetic-field coupling is negligible. Thus the polarity of an induced voltage in this case, due to a pulse travelling on the line, is independent of the direction of travel and is not influenced by the orientation of the matching load resistor of the loop, with respect to its signal output connector. In general terms, a positive travelling pulse would induced a positive signal in the loop, and negative, for a

the matching load resistor of the loop, with respect to its signal output connector. In general terms, a positive travelling pulse would induced a positive signal in the loop, and negative, for a corresponding negative travelling pulse. Refer to the Bewley lattice diagram in Fig. 6-7(a) for the pulse distribution on the line.

Associated with the voltage pulse Eq. (6-1), there is also a current pulse Eq.(6-2), the value of which is the amplitude of the voltage pulse divided by the surge impedance (*resistance in this case*) of the line.

The capacitive (electric) coupling effect is created by the voltage pulse and the inductive (magnetic) coupling effect, by the current pulse.

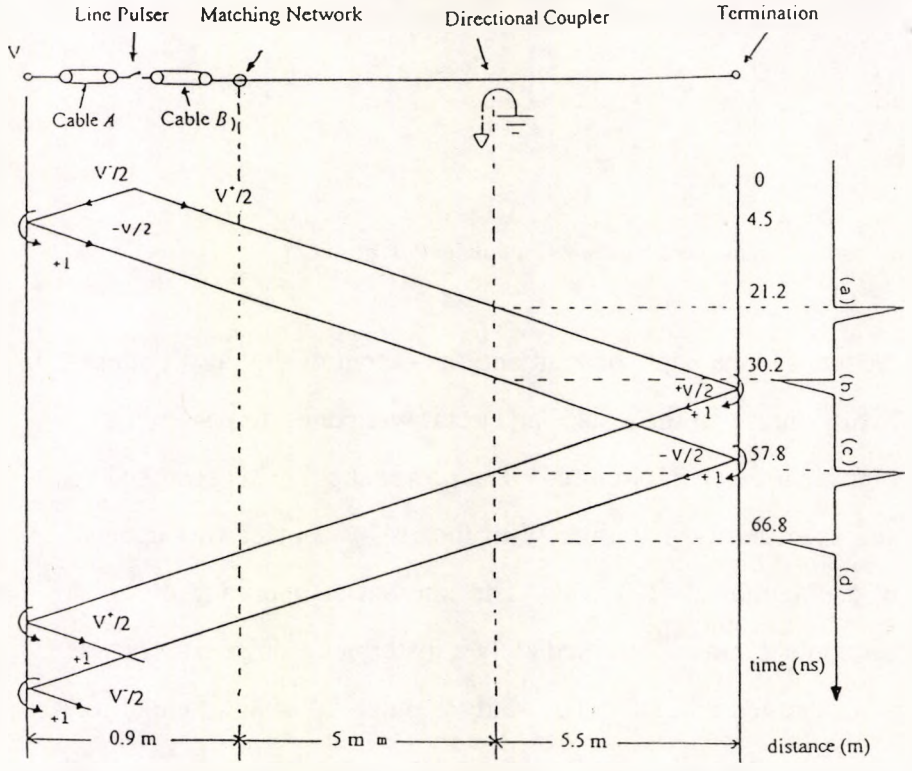


Fig. 6-7(a) Pulse reflection (Bewley) diagram for electric-field coupling.

6-2.2 Maximum (B+ D) Coupling

The directional coupler was now adjusted to the 90 degree position with respect to the vertical axis and hence perpendicular to the magnetic field, and the experiment was repeated. This is the condition for maximum magnetic coupling. Fig. 6-7(b) shows the arrangement.

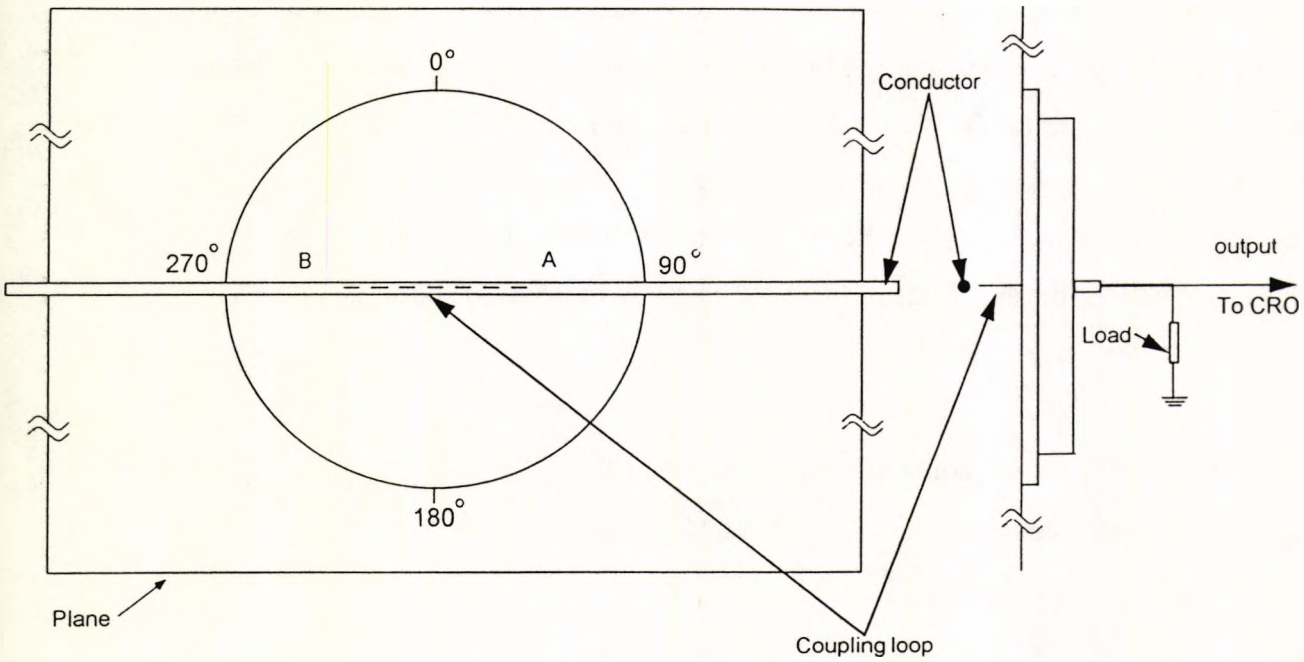


Fig. 6-7(b) Orientation of loop for maximum electromagnetic coupling (90° position)

Note that the switching frequency was kept constant and the output of the power supply was set for the same 700 volts during all the tests. The circuit was connected as in Fig. 6-4 as before, but with the termination open-circuited. The power supply was switched on and the voltage set for the specified (V^+) value. With the relay contact was opened, cable (A) was charged to a potential of (V^+) volts. The line-pulser operating coil was energised and the switch - contact closed. Immediately a disturbance pulse pattern was created. Cable (A) then discharged into cable (B) and a pulse of magnitude ($V^+/2$) volts travelled through the line. Simultaneously the pulse of magnitude ($V/2$) volts travelled back to the supply, so as to satisfy the transient condition:

$$(V^+/2) + (V/2) = 0 \qquad (6\text{-}14)$$

That is, as soon as the line pulser contacts were closed the voltage at that point dropped to zero. The forward ($V^+/2$) pulse travelled down the line, setting up transverse electric **E** and magnetic **H** fields, and on interacting with the loop probe, caused a signal voltage of positive polarity to be induced in the loop. This is marked (a) in Fig. 6-8.

Since a pulse cannot anticipate the impedance condition at the end of the line, the forward ($V^+/2$) pulse must travelled to the end termination. Since this was open-circuited, the pulse was reflected and travelled back to the source in the same phase . The imping-ing pulse, on interacting again with the loop, induced another voltage, but of the opposite (negative) polarity in the loop. This is marked (*c*) in the waveform in Fig. 6-8.

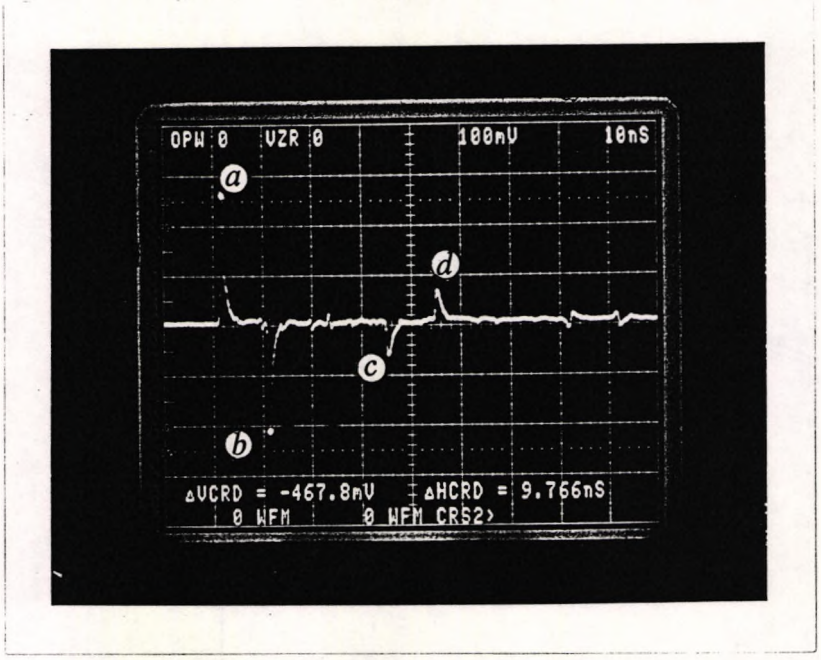


Fig. 6-8 Result of maximum electromagnetic coupling.

When the ($V^+/2$) pulse was injected into the line, the ($V/2$) pulse simultaneously travelled through cable (*A*) to the supply. Since this was grossly mis-matched by the resistor *R*, the pulse was reflected and travelled through cable (*A*) and cable (*B*) into the line. On impinging on the loop it also caused a signal to be induced but delayed by 9 ns. This delay was because the ($V/2$) pulse had travelled twice through cable (*A*), (i.e. from the pulser to the supply and back) and the propagation delay of each cable is 4.5 ns. This induced signal is marked at (*b*). Similarly the same pulse was then reflected at the termination and travelled back to the source with the same phase. This caused a signal of negative polarity [marked (*d*) in the photograph] to be induced in the loop. These markings of the waveform corresponds to similar markings on the Bewley lattice diagram in Fig. 6-9.

The switching transient conditions are the same for all the tests.

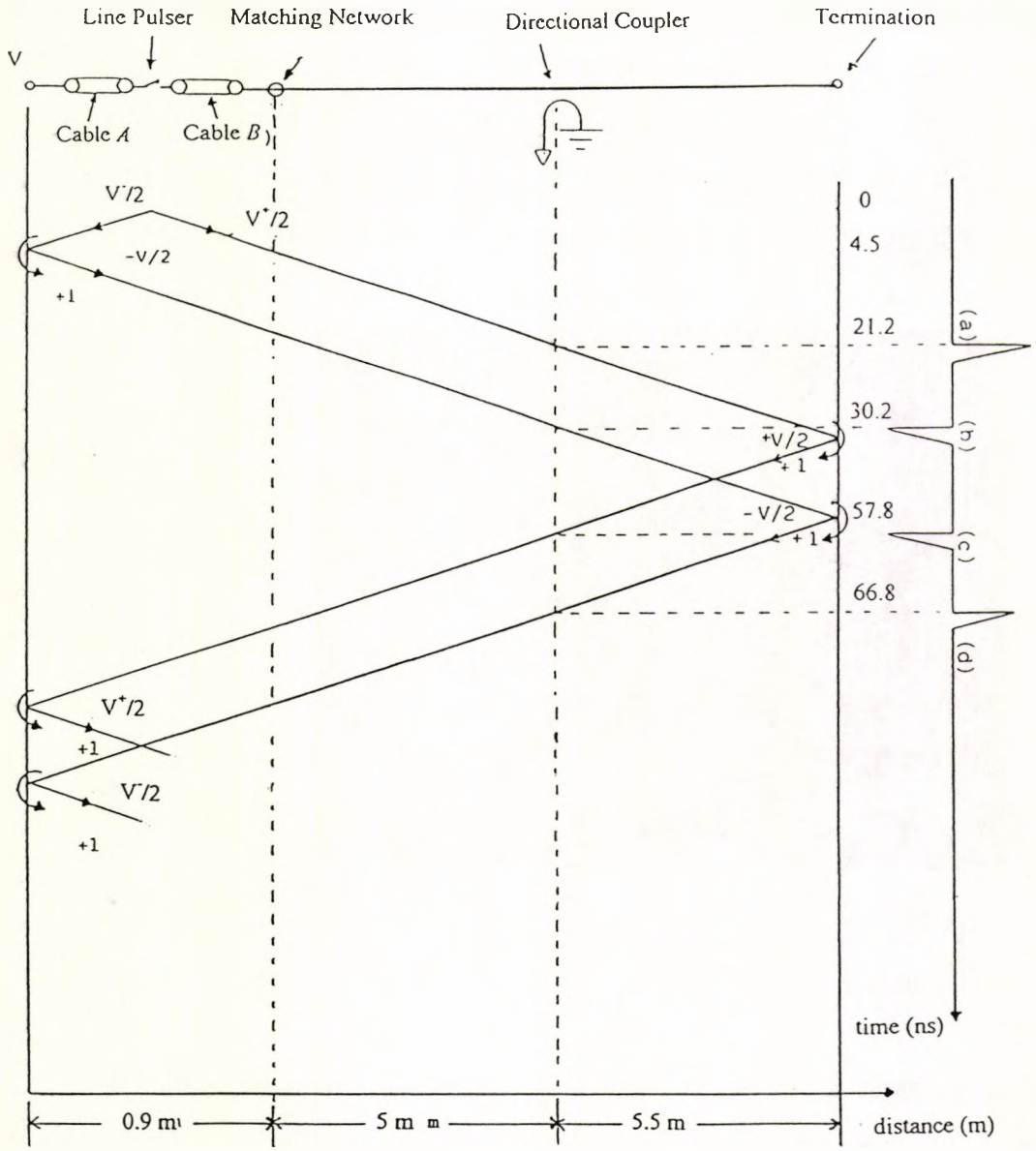


Fig. 6-9 Bewley lattice diagram of reflections with open-circuit termination.

6-2.3 Results with brief remarks

The induced signal in the loop [marked (*b*) on the photograph of Fig. 6-8] was due to the interaction of the $(V^-/2)$ pulse reflected from the supply, (first reflection). It is slightly lower in amplitude than the induced signal [marked (*a*)], which was due to the forward $(V^+/2)$ pulse. The main contributory factor to this is the attenuation in the coaxial cable (*A*), although there was a small reduced reflection coefficient at the supply, i.e. $\Gamma \neq 1$. Consideration must also be given to radiation losses along the open line conductor.

Induced signals marked (*c*) and (*d*) are significantly reduced in amplitude compared with the initial induced signals marked (*a*) and (*b*). This is mainly due to the cancelling effects of the inherent electric-field coupled induced signals (shown in Fig. 6-6) being of opposite polarty, due to the change in the direction of travel of the pulse reflected from the termination.

The maximum induced signal of 250 mV in the loop [marked (*a*) in the results in Fig. 6-8], was due to the coupling effects of both the electric- and magnetic-fields, produced by the forward travelling ($V^+/2$) pulse. The electric-field coupling from the same pulse induced 120 mV, measured on (*a*) in Fig. 6-6 results. (Note scale change).

It can be deduced that the maximum magnetic-field coupling alone caused 130 mV (250 mV-120 mV) to be induced in the loop. The corresponding induced signal of -60 mV [marked (*c*)], due to the same pulse reflected from the termination, is of opposite polarity and of amplitude equal to the *algebraic* sum of the magnetic- and electric-field components. That is:

$$-60\ \text{mV} - (+70\ \text{mV}) = -130\ \text{mV}. \qquad (6\text{-}15)$$

The +70 mV was measured from the correspondly induced voltage from Fig. 6-6. This explains these results in terms of magnitude and direction, but reference should be made to Fig. 5-14 for a graphical representation for the pulse propagation pattern.
The Bewley lattice diagram in Fig. 6-9 shows that the ($V^+/2$) pulse, on leaving the pulser had travelled through the coaxial cable *B* and into the line, a total distance of 6.35 m before impinging on the loop and causing the voltage marked (*a*) to be induced. The same pulse had travelled an additional distance of twice 5.5 m, i.e. reflected at the termination, when voltage marked (*c*) was induced. The travel time of 35 ns can be estimated from the results and was accurately measured using *TDR*, shown in Fig. 5-9.

Since total (100%) reflection cannot be easily achieved in practice, (except for a short circuit where $R \to 0$ or an open circuit where $R \to \infty$), it is assumed that there was also a reduction in the magnitude of the ($V^+/2$) pulse at the termination, and possibly, some radiation loss.

Although small losses should have been encountered, these were not easy to determine due to the fact that the transmission system exhibited a kind of pulse sharpening condition which resulted in an increase in voltage. This phenomena will be explained later the text.

It was shown that in an open circuit condition the voltage pulse, on reaching the termination, reflected back to the source with the same polarity. In this case there can be no current flowing in the open-circuit so that the reflected pulse must cause a current, equal and opposite to the forward (I^+) current to flow back to the source.

To create this equal and opposite current, the voltage of the reflected pulse must be of the same magnitude and polarity as the forward pulse. Thus during the reflection the voltage at the end of the line rises momentarily to double the forward pulse voltage. This is shown in Fig. 6-10. The reflection pattern continued until the distrubance ceased, and the line reached a steady state condition.

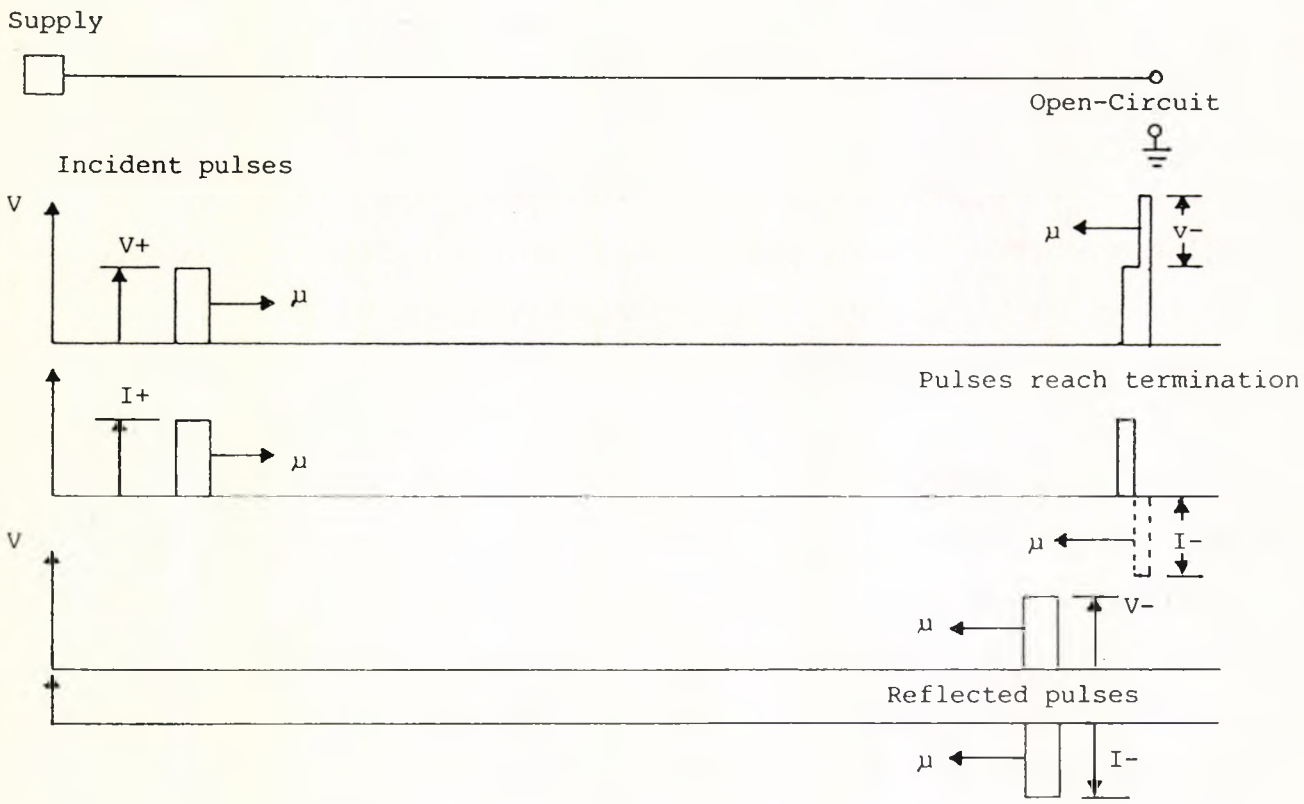


Fig. 6-10 Pulse propagation on line with open-circuit termination.

6-2.4 Maximum coupling (270° position)

In this test, the directional coupler was adjusted to the 270 degree position again set for maximum magnetic field coupling, but with the reversal of the matching load resistor of the loop with respect to its signal output connector. The arrangement is similar as shown in Fig. 6-7, but with a 180 degree displacement of the loop.

The results in Fig. 6-11 shows a complete reversal in polarity of the induced signals compared with a similar test at the 90 degree angular position. This is because the orientation of the directional coupler is now reversed, causing the field coupling effects of the same travelling pulse to induce voltages of the opposite polarity in the loop.

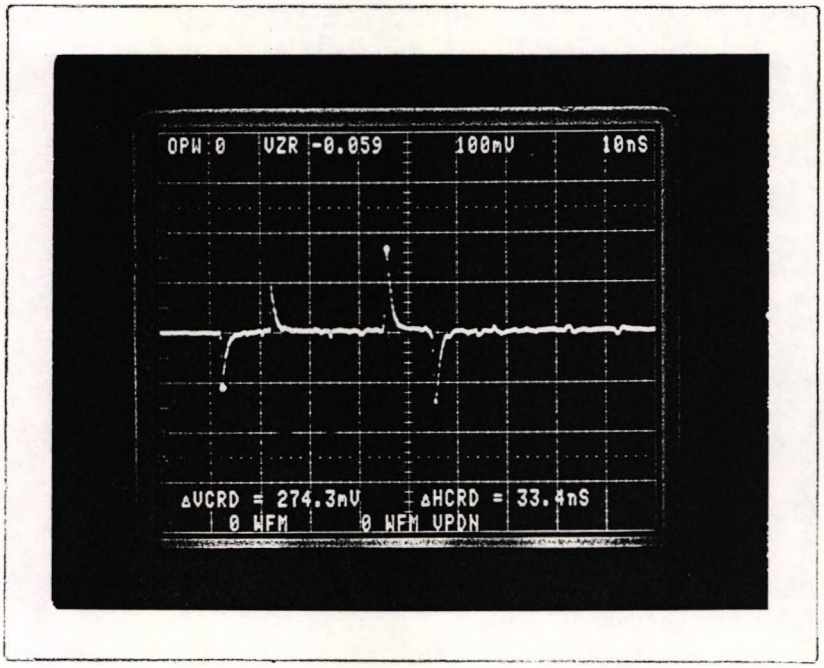


Fig. 6-11 Results of maximum coupling of induced voltages at 270° position.

This is a unique feature of the directional coupler and in this orientation it coupled to the **E** and **H** - field component of the pulse travelling in the reverse direction and gave summation of the two induced signals. At the same time it algebraically added those induced signals associated with the forward travel pulse. The pulse propagation and reflection pattern is as before, shown in the Bewley lattice diagram in Fig. 6-7, but with opposite polarity of the induced voltages.

6-2.5 Cancelling Effects of Electric-field Coupling

6-2.5.1 Reflections from the Termination

The directional coupler was now adjusted until complete algebraic cancellation of the induced signals (*c*) and (*d*) were obtained. This occurred at an angular position of 25 degrees for the nearest satisfactory results. The **E** and **H** components of the travelling pulse, reflected from the open-circuited termination of the line, induced signals of equal and opposite polarity in the loop, for cancellation.

This result is shown in Fig. 6-12.

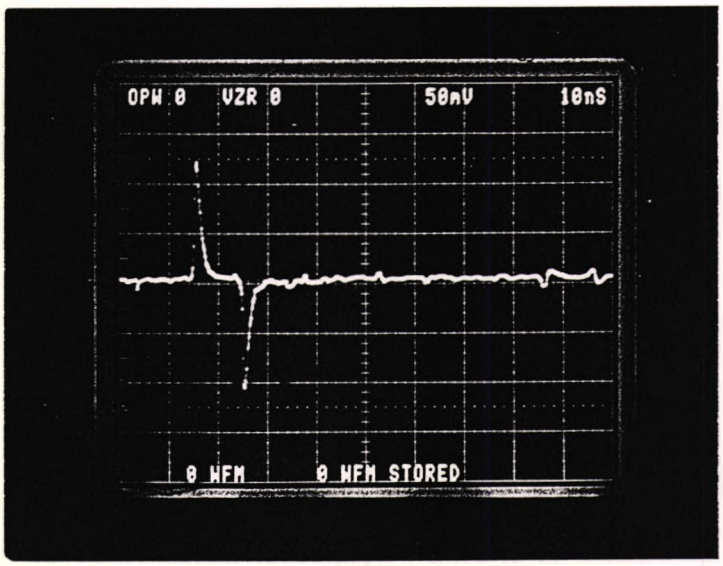


Fig. 12 Cancellation - Reflections from termination.

6-2.5.2 Reflections from Source

The directional coupler was adjusted for the best cancellation of the induced signals (*a*) and (*b*), this time from the effects of the components of the pulses travelled from the supply. This was obtained at the angular position of displacement π , of the loop, i.e. at the 205 degree position. The result is similar as for the reflections from the termination except for a reversal in polarity, which made it possible for cancellation of induced voltages *a* and *b* instead.

The impinging **E** and **H** - field components of the pulse leaving the pulser and travelling down the line, induced voltages in the loop of the opposite polarity to that of the inherent electric-field component. This polarity reversal is due to the 180 degree displacement of the loop. For the angular setting in this test, there was *algebraic* cancellation of the induced voltages due to the component of the forward travelling pulse and the pulse reflected from the source.

These effects are consistent with the same constant electric-field coupling ($\dot{D}$) induced signals and a reduction (by virtue of the relevant angle of the directional coupler) magnetic-field coupling ($\dot{B}$) induced signal.

Complete cancellation was not possible in this case, since the amplitude of a few millivolt is the minimum value that is required for the triggering of the oscilloscope. A slight angular turn of the directional coupler resulted in a loss of synchronisation and the consequent time-shift of the displayed waveform on the oscilloscope. This problem can be overcome by external triggering of the oscilloscope from the line pulser. This was not attempted owing to the long distance from the oscilloscope to the line pulser would be introduced additional time-delay and attenuation that in the measurement.

These tests on cancellation clearly demonstrate that the directional coupler can be adjusted so as to detect only pulses travelling in one direction, and hence the device is descriptive by its name.

6-3 LINE TERMINATED INTO ITS CHARACTERISTIC IMPEDANCE

For this test the directional coupler was again adjusted to the 90 degree position for maximum magnetic-field coupling. The circuit was connected as in Fig. 6-3 as before. The characteristic impedance of the line was calculated using line constants, to be 287 ohm. The transmission line was first characterised by connecting suitable resistors in this region, one at a time, at the termination and observing the induced signal caused by the reflections from these resistive elements.

A very low inductance, high stability carbon resistor was constructed so as to terminate the line into its characteristic impedance. The initial value was measured to be 280 ohms and was adjusted by slightly rubbing off some carbon compound until there was not any noticeable reflection. This value of resistor closely agreed with the calculated characteristic impedance of 287 ohm for the line. A computer program calculated the value of 290 ohm. Details and calculations are shown in Appendix 2.

The results are shown in Fig. 6-13.

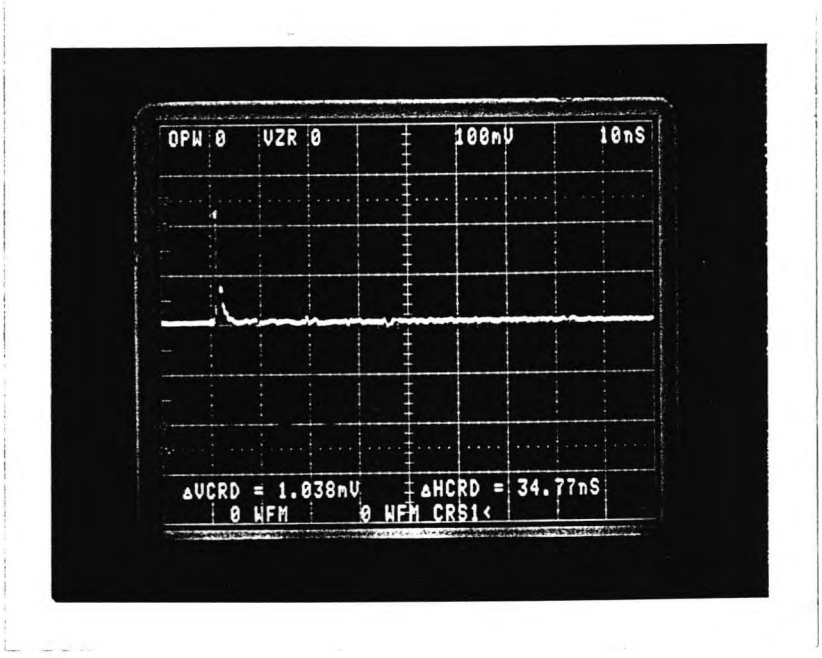


Fig. 6-13 Line terminated into its characteristic impedance.

This test shows that when a transmission line is adequately terminated in its characteristic impedance, the forward travelling pulse is smoothly absorbed, and its energy dissipated in its load resistor in the shortest possible time. Although the line was adequately matched to its characteristic impedance, the small reflection shown on the result was due to the physical insertion and connecting links of the resistor between the line and earthplane.

Note that in this test, the pulse reflected from the pulser was suppressed. This was done by connecting a longer cable between the supply and pulser such that twice the travel time of the pulse in the cable is greater than that on the line.

The reflection coefficient, $(\Gamma) = \frac{V_r}{V_f} \cong 1$ (6-16)

6-3.1 The Line Matching Resistor

A matching resistor for terminating the line into its characteristic impedance must be such that its transit time is not affected by its size and yet be able to absorb the full transient power. Also its inductance should be extremely low so as not to interfere with the circuit parameters.

The resistor, constructed in the laboratory, was designed to satisfy these requirements. It consists of a 100 mm long by 10 mm diameter plastic (tufnol) tube on which a sheet of paper, after being impregnated with a mixture of carbon compound and distilled water was stuck onto the tube. Conducting rings were placed at both ends to which flying leads were connected. Adjustment of the resistance was made by gently rubbing off a thin coating of the carbon uniformly over the entire length. The final adjustment was made and measurements checked with the Datron digital multimeter (*DMM*) to meet the calculated value of the characteristic impedance.

The resistor was handled with care so as not to alter its value. A protective coating was applied later to prevent the carbon from rubbing off, which would alter the resistance value.

6-3.2 Transmission Line Impedance Matching

Transmission lines are used mainly for the transmission of electrical power and information. For radio-frequency transmission, it is highly desirable that the lines are nearly matched as possible so as to prevent unwanted reflections. It may not always be possible to ensure that the load impedance is exactly equal to the characteristic

impedance of the line, and in such cases, measures must be taken to improve the matching so that the standing-wave ratio is close to unity.

For information transmission, mismatched loads at junctions will result in echoes and will distort the information-carrying signals. Proper matching does not only saves energy of any reflected wave, but also prevents any action by a reflected wave on the generator, although there is little consequence to power frequency transmission, since these lines are generally very short in comparison to their wavelengths. Power frequency lines are usually analysed in terms of equivalent lumped electrical networks.

6-3.2.1 Quarter Wavelength Matching

A simple method of matching a resistive load R_L to a lossless transmission line of a characteristic impedance R_0 is to insert a quarter-wave transformer with a characteristic impedance $R_0^{'}$ such that:

$$R_0^{'} = \sqrt{R_0 R_L} \tag{6-17}$$

Since the length of the quarter-wave line depends on wavelength, this matching method is frequency-sensitive as are the *Stub* matching to be discussed. The arrangement of a quarter-wavelength matching is shown in Fig. 6-14.

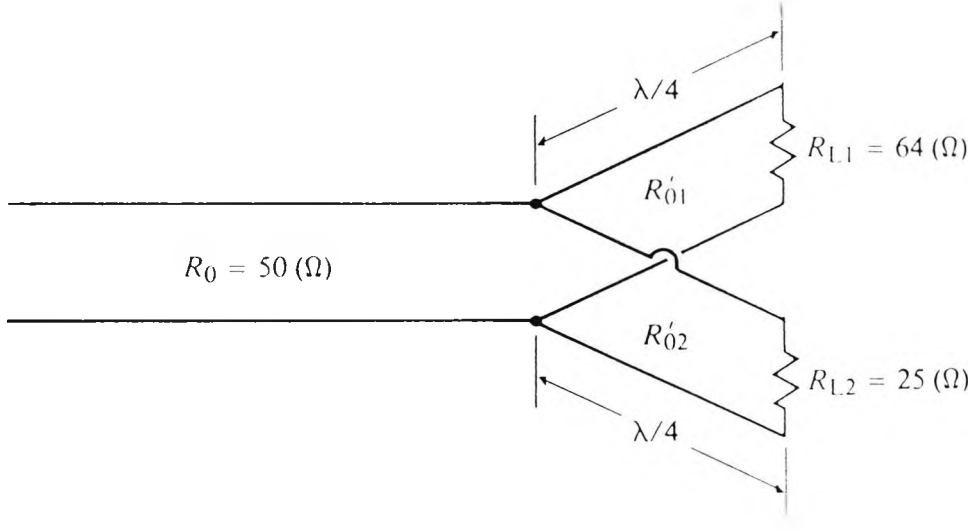


Fig. 6-14 Impedance matching by quarter-wave lines.

Ordinarily, the main transmission line and the matching line sections are essentially lossless. In this case, both R_0 and $R_0^{'}$ are purely real, and therefore Equation (6-5) will have no solution if R_L is replaced by a complex Z_L.

Hence quarter-wave transformers are not useful in matching a complex load impedance to a low-loss line.

6-3.2.2 Tapered Line

If the spacing of the conductors is varied, the impedance of a line varies. A line in which the spacing varies uniformly from the input, provides a gradual impedance transformation along its length. Tapered lines may be constructed so that the characteristic impedance varies exponentially. Impedance matching can be achieved by interposing a suitably designed tapered line between the load and the main transmission line. An advantage of a tapered line is that it is less frequency selective than a quarter-wavelength line.

6-3.2.3 Stub Matching

If a short section of a loss-free line is connected across a main transmission line, it will introduce at the point of attachment, a reactance, the value of which will depend on the length of the section and on the condition of the end, remote from the line. Such sections of line, referred to as *stubs*, may be used for impedance matching. Since a stub is connected in parallel with the main transmission line, it is preferable to treat the question of impedance matching by stubs in terms of admittances rather than impedances. A loss-free stub of variable length should therefore be considered as a device which has zero input conductance and a susceptance which varies with the stub length.

If the terminal load on a transmission line is not equal to the characteristic impedance, then the input admittance of the line will vary with distance from the load. If a stub is placed at a point on the line where the input conductance at that point is equal to the characteristic impedance of the line, and the stub length is adjusted to provide a

susceptance which is equal in value, but opposite in sign to the input susceptance of the line at that point, then the total susceptance at the point of stub attachment will be zero. The combination of stub and line will thus present a conductance which is equal to the characteristic conductance of the line, i.e. the main length of a high-frequency transmission line will be matched. If the length of the line is several wavelengths long, there will be multiplicity of points at which the stub may be placed, but it is normally positioned at a point nearest to the load. In which case, the longest possible length of line is operated in a matched condition.

Stubs may have the end remote from the main line, open-circuited or short-circuited. The short-circuited stub is generally preferred in practice since it permits a simpler mechanical construction and adjustment.

6-3.2.4 Single Stub Matching

For single stub matching, it is first of all necessary to find the correct place of attachment, i.e. the value of the distance ℓ.

Consider the problem of matching a load impedance Z_L to a lossless line that has a characteristic impedance R_0 by placing a single short-circuited stub in parallel with the line, as shown in Fig. 6-15.

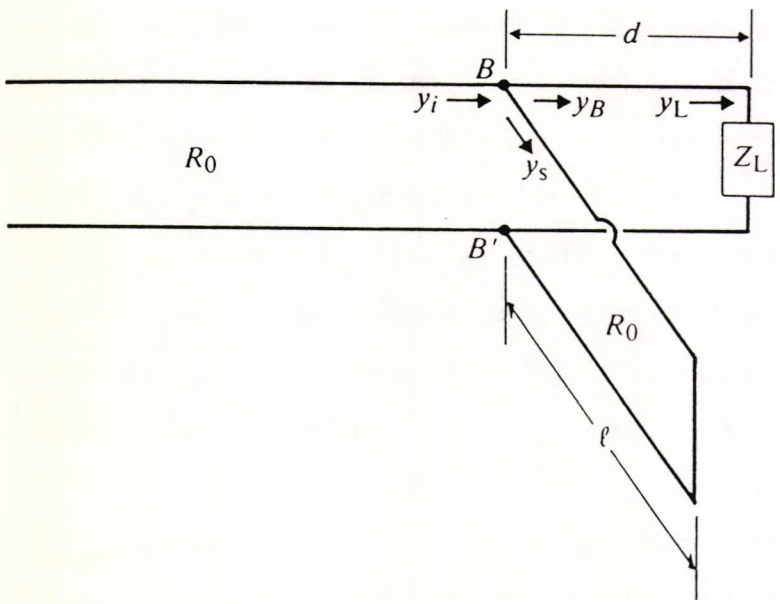


Fig. 6-15 Impedance matching by a single-stub method.

This is the *single stub method* for impedance matching. It is necessary to determine the length ℓ of the stub and the distance d from the load such that the impedance of the parallel combination to the right of the points $B - B'$ equals R_0. Short-circuited stubs are usually used in preference to open-circuited stubs because an infinite terminating impedance is more difficult to realise than a zero terminating impedance for reasons of radiation from the open end and coupling effects with neighbouring objects. Moreover, a short-circuited stub of an adjustable length and a constant characteristic resistance is much easier to construct than an open-circuited one. The difference in the required length for an open-circuited stub and that for a short-circuited stud is an odd multiple of a quarter-wavelength.

The parallel combination of a line terminated in Z_L and a stub at points $B - B'$ in Fig. 6-15 suggest that it is advantageous to analyse the matching requirements in terms of admittances. The basic requirement is:

$$Y_i = Y_B + Y_s \qquad (6\text{-}18)$$
$$= Y_0 = \frac{1}{R_0}$$

In terms of normalised admittances, Eq. (6-6) becomes:

$$1 = y_B + y_s \qquad (6\text{-}19)$$

where $y_B = R_0 Y_B$ is for the load section and $y_s = R_0 Ys$ is for the short-circuited stub. However, since the input admittance of a short-circuited stub is purely susceptive, y_s is purely imaginary. As a consequence, Eq. (6-7) can be satisfied only if:

$$y_B = 1 + jb_B \qquad (6\text{-}20)$$

and

$$y_s = -jb_B, \qquad (6\text{-}21)$$

where b_B can be either positive or negative. The objectives then, are to find the length d such that the admittance y_B of the load section looking to the right of terminals

$B - B'$ has a *unity real part* and to find the length ℓ_B of the stub required to cancel the imaginary part.

Using the Smith chart as an admittance chart shown in Fig. 6-16 , the single-stub matching can be found.

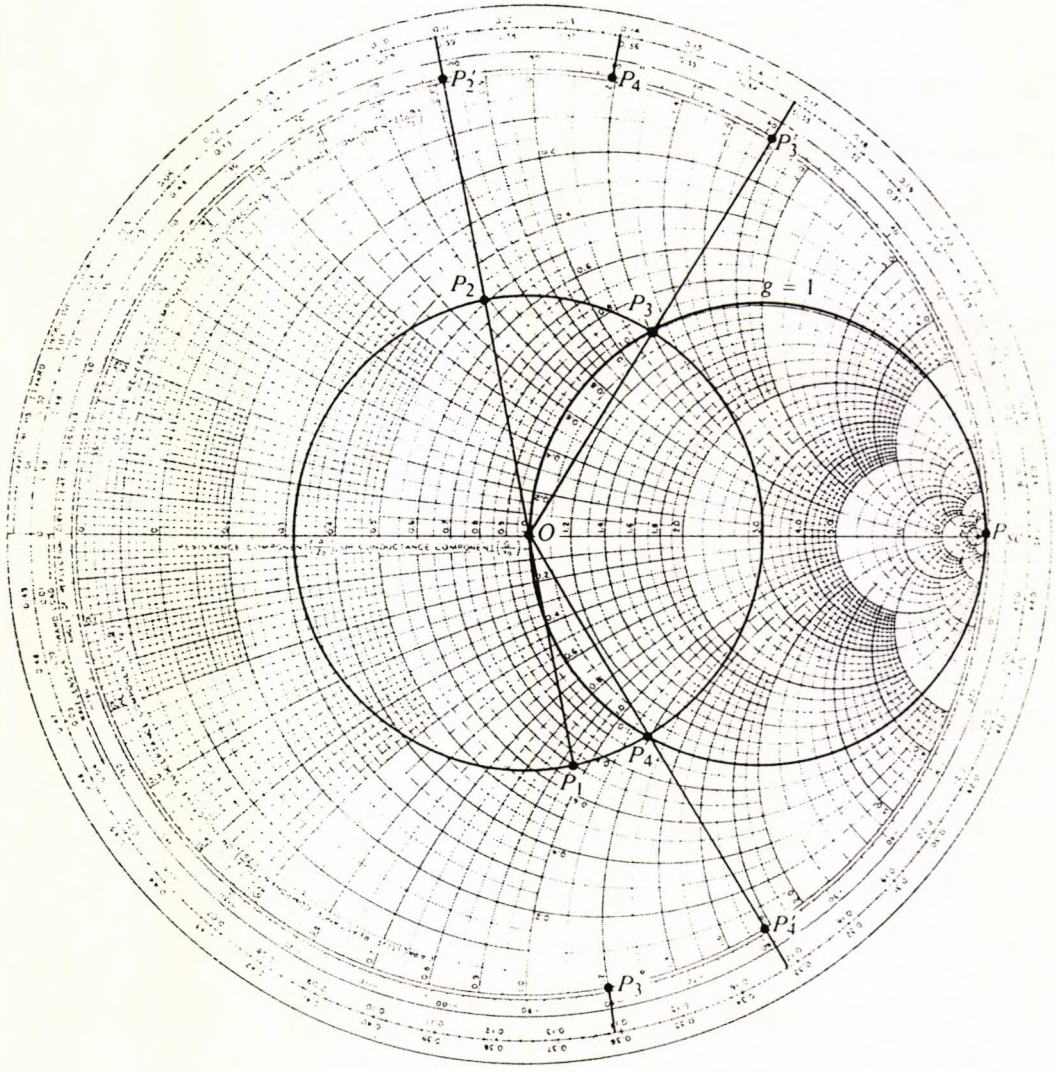


Fig. 6-16 Construction of single-stub matching on Smith admittance chart.

6-3.2.4 Double-Stub Matching

Single-stub method requires that the stub be attached to the main line at a specific point, which varies as the load impedance or the operating frequency is changed. This requirement often presents practical difficulties because the specific junction point may occur at an undesirable location from a mechanical point of view. Furthermore, it is very difficult to build a variable-length coaxial line with a constant characteristic impedance. In such cases an alternative method for impedance-matching is to use two short-circuited stubs attached to the main line at fixed positions, as shown in Fig. 6-17.

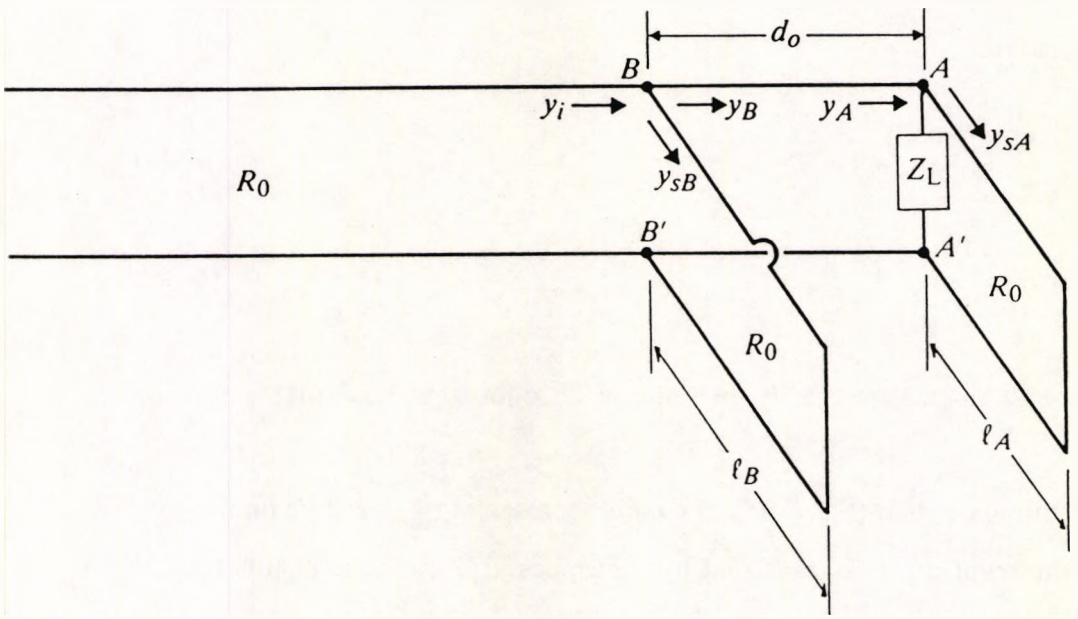


Fig. 6-17 Impedance matching by double-stub method.

Here the distance d_0 is fixed and arbitrarily chosen (such as $\lambda/16, \lambda/8, 3\lambda/16, 3\lambda/8$, etc) and the length of the two stub tuners are adjusted to match a given load impedance Z_L to the main line. This scheme is the *double stub method* for impedance matching.

In the arrangement in Fig. 6-17, a stub of length ℓ_A is connected directly in parallel with the load impedance Z_L at terminals $A - A'$, and a second stub of length ℓ_B is attached at terminals $B - B'$ at a fixed distance d_0 away. For impedance matching with a main line

that has a characteristic resistance R_0, the total input admittance at terminals $B - B'$ look- ing towards the load, to equal the characteristic conductance of the line; that is:

$$Y_i = Y_B + Y_{sB} \tag{6-22}$$

$$= Y_0 = \frac{1}{R_0}$$

In terms of normalised admittances, Eq. (6-14) becomes:

$$1 = Y_B + Y_{sB} \tag{6-23}$$

Now since the input admittance Y_{sB} of a short-circuited stub is purely imaginary Eq. (6-15) can be satisfied only if:

$$y_B = 1 + jb_B \tag{6-24}$$

and, $$y_{sB} = -jb_B \tag{6-25}$$

Note that these requirements are exactly the same as those for single-stub matching.

On the Smith admittance chart (Fig. 6-18), the point representing Y_B must lie on the $g = 1$ circle. This requirement must be translated by a distance d_0 / λ "wavelengths towards load"; that is Y_A at terminals $A - A'$, must lie on the $g = 1$ circle rotated by an angle $4\pi d_0 / \lambda$ in the counter-clockwise direction. Again, since the input admittance Y_{sA} of the short-circuited stub is purely imaginary, the real part Y_A must be solely contributed by the real part of the normalised load admittance g_L.

The solution (or solutions) of the double-stub matching problem is then determined by the intersection (or intersections) of the g_L- circle. The problem of a double-stub matching can be solved using the Smith admittance chart.

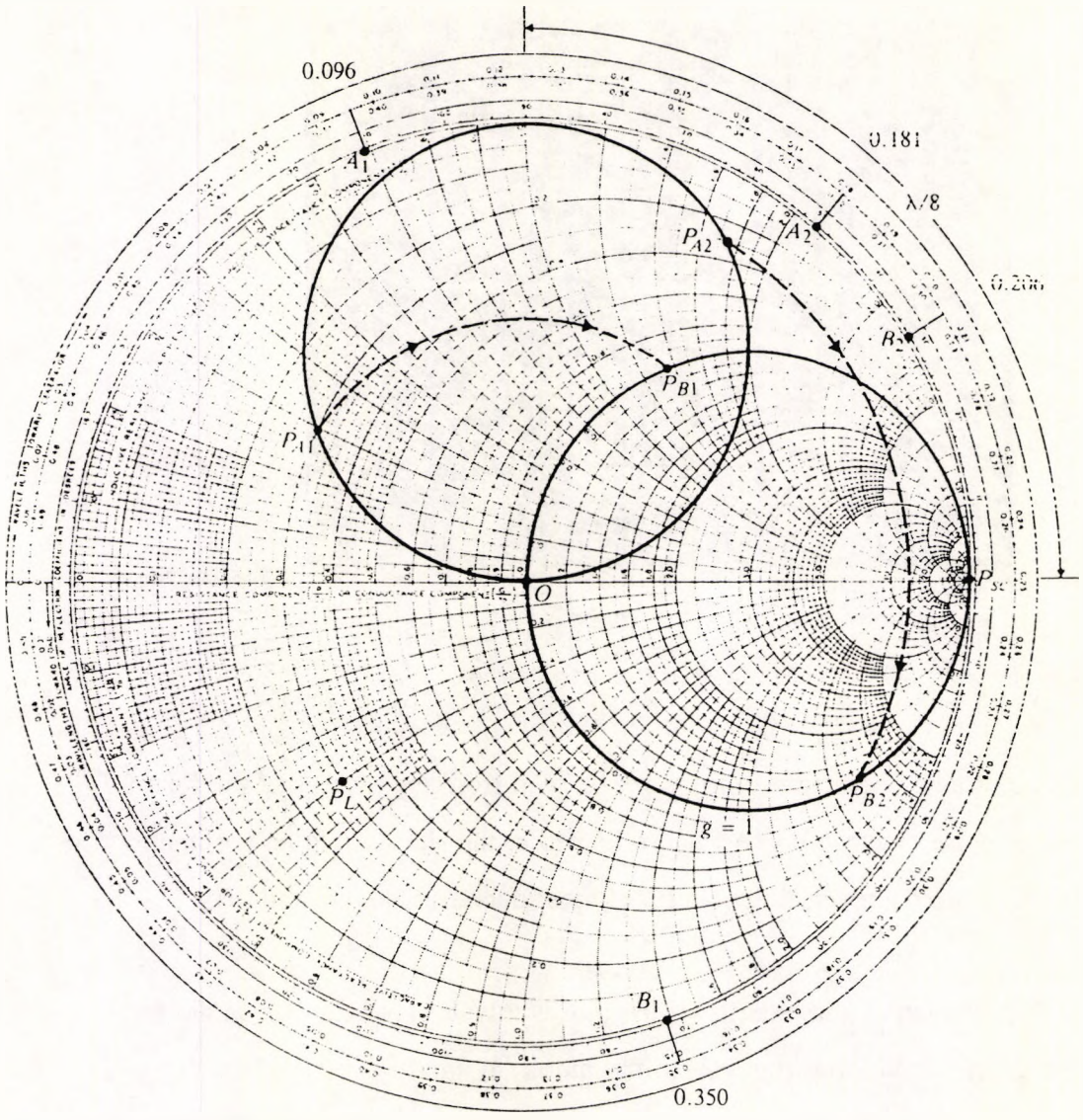


Fig. 6-18 Construction of double-stub matching on Smith's admittance chart.

6-4 TESTING WITH SHORT-CIRCUITED TERMINATION

6-4.1 Electric-Field Coupling

The matching load resistor of the line was now removed and the termination short-circuited using a metal sheet. The loop was adjusted to the zero-degree or reference position, (as in Fig. 6-5) again for only electric-field coupling. The result is shown in the Fig. 6-19.

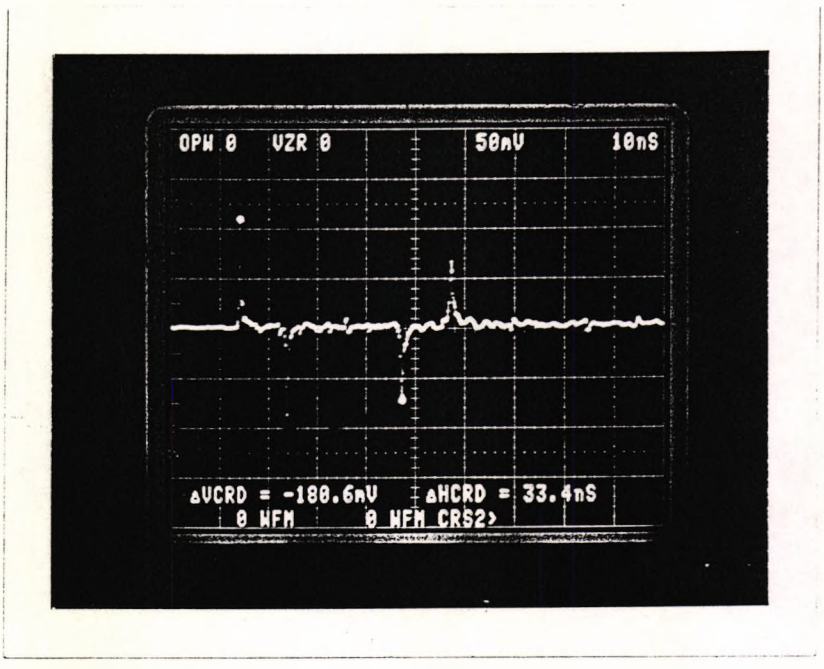


Fig. 6-19 Results of electric-field coupling with short-circuit termination.

Compared with the open-circuited testing, it can be seen from the result that the forward travelling voltage pulse changed phase when reflected at the short-circuited termination. This consequently caused a reversal in polarity of the induced signals (*c*) and (*d*).

The direction of propagation and polarity of the pulses travelling on the line is the same throughout the short-circuited testing. Hence the amplitude and polarity of the induced signals now only depends on the orientation of the directional coupler. No changes (as expected) were observed when the loop was set at the 180-degree. position. The induced signal due to the electric-field coupling of the forward pulse is 120 mV as before.

6-4.2 Maximum Electromagnetic Coupling at 90° Position

The directional coupler was adjusted to the 90-degree position and once again set for maximum magnetic-field coupling. The difference in this test compared with similar testing with the open-circuited condition (Fig. 6-8), is the reversal of the signals marked (*c*) and (*d*), and follows similar explanation.

This result can be seen in Fig. 6-19.

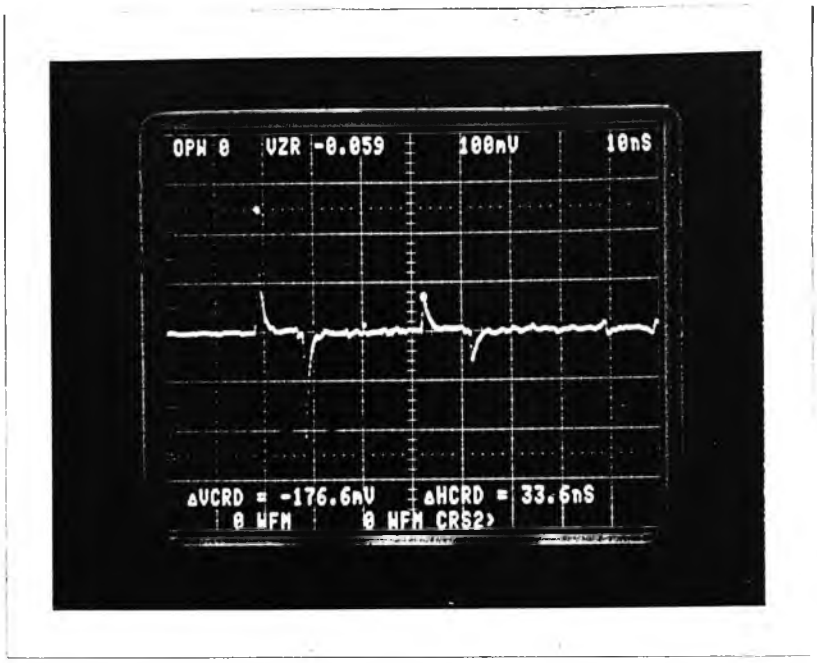


Fig. 6-19 Results of maximum EM coupling at 90° with short-circuited termination.

6-4.3 Maximum Electromagnetic Coupling at 270° Position

The directional coupler was once again set for maximum magnetic-field coupling at the corresponding 270-degree position, but this time with the termination short circuited . As in the open-circuited testing (Fig. 6-11), the loop orientation with regards to its matching load resistor and signal output connector, was reversed. The results in Fig. 6-20(a) shows a complete reversal of the signals marked (*c*) and (*d*), to that of a similar test (Fig. 6-11) with open circuit termination. The magnitude and direction of the pulse travel [shown in Fig 6-2(b)] is as given before with the same explanation applies.

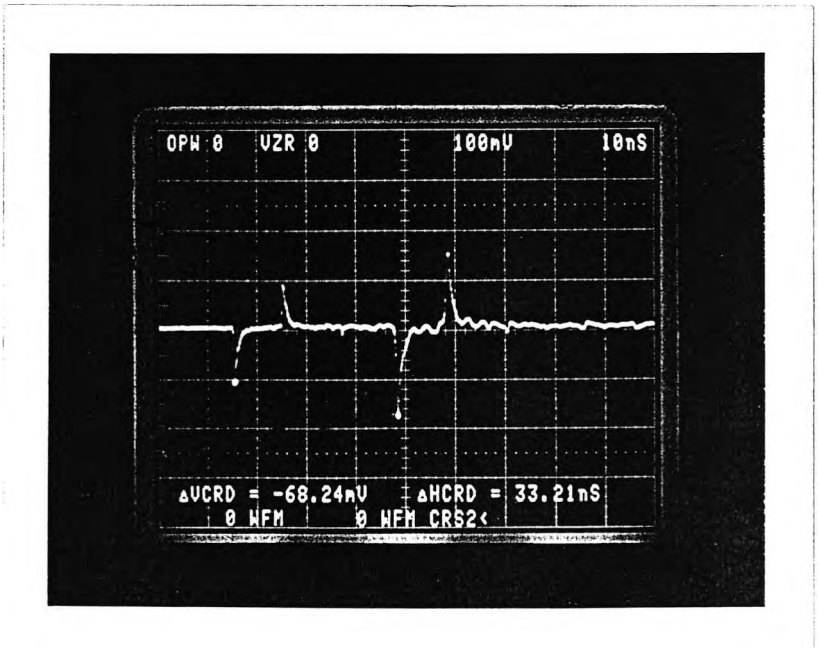


Fig. 6-20(a) Maximum Coupling at 270° position with short-circuit termination.

These tests further emphasised the significance of the orientation of the matching load resistor of the coupling loop with respect to its signal output connector.

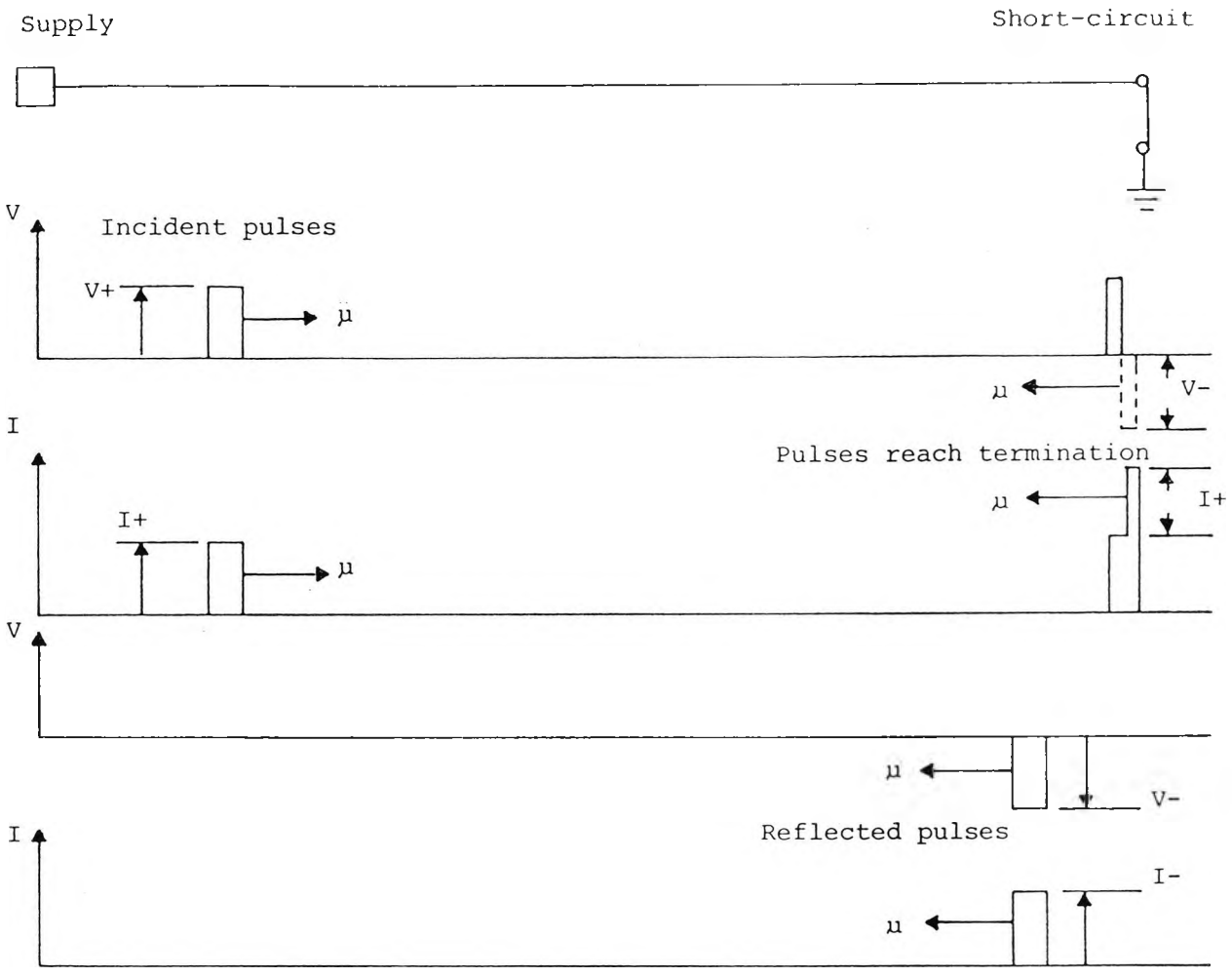


Fig. 6-20(b) Pulse propagtion on line with short-circuit termination.

6-5 MIS-MATCHED CONDITION AT SOURCE WITH O/C TERMINATION

In this test a mis-matched condition was introduced in the system by removing the matching resistor network from the junction of the open line conductor and the coaxial cable. The results in Fig. 6-21 shows the degree of unbalanced condition and emphasised the need for matching when two lines with different impedances are connected together.

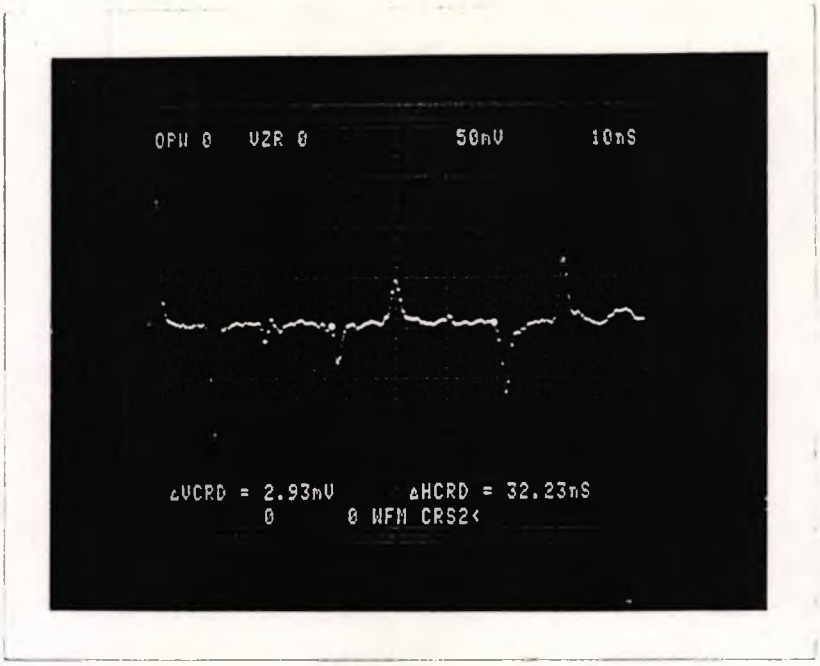


Fig. 6-21 Reflections due to a mis-matched condition at source.

Measurements using TDR technique, of the travel time on the first part of the line (5 m long - junction of coaxial cable and open line at source to the directional coupler near mid-section) was not possible before. Whereas in all previous tests, there were very small reflections from the junction to pulses travelling back from the termination. In this case, i.e. with the matching network removed, complete reflections can be seen in the results.

This demonstrates the effectiveness and necessity of the line matching network. Note the cursor positions on the photograph that indicate a travel time of 32.23 ns, which is from the line junction to the directional coupler and back. This is also represented in the Bewley lattice diagram in Fig. 6-22.

From the propagation time of 1 ns/30 cm for an electromagnetic wave travelling on an open line, the travel time in this 5 m length of line would be just over 16 ns. Any small discrepancy in the result is attributed to the short connecting leads which was not accounted for in the measurements, and to the positioning of the cursors.

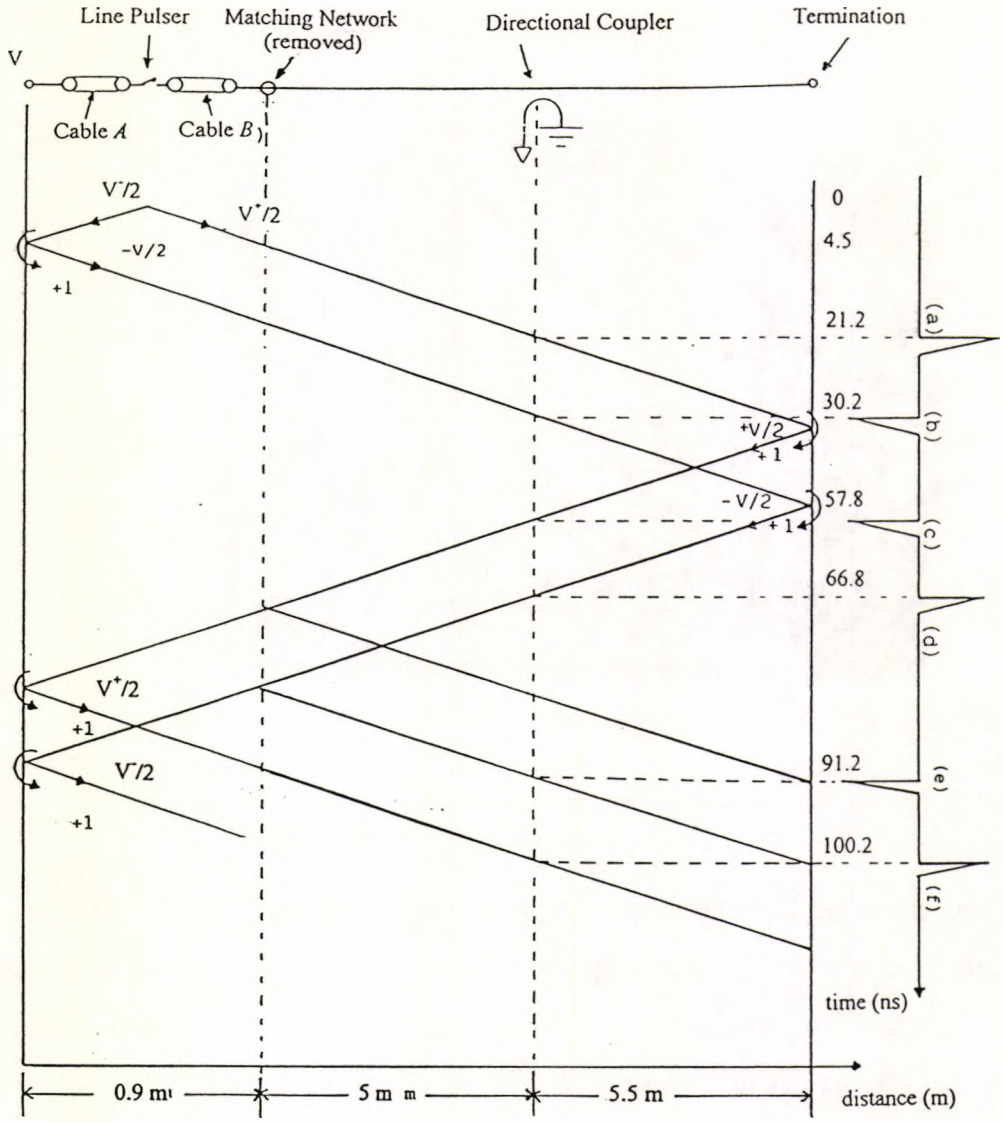


Fig. 6-22 Bewley lattice diagram of mismatched condition.

6-6 ANALYSIS OF THE RESULTS ON CANCELLATION

6-6.1 Effects from Pulses Reflected from Termination

Since the measurement was made only from the first induced voltage in the loop, due to the forward travelling pulse on the line, the condition of the line termination and hence phase of the reflected pulses are not of importance. This analysis therefore applies to the testing with both open-circuited termination [section **6-1.2**] and short-circuited termination [section **6-3.2**]

Cancellation of signal (*c*) and (*d*) occurred when the directional coupler was adjusted at the angular position of 26-degree.

The electric field change ($\dot{D}$) coupling induced 120 mV in the loop, (Fig. 6-6), and is always independent of the angular position of the loop. The sum of the maximum magnetic field ($\dot{B}$) and electric field ($\dot{D}$)) coupling induced 250 mV (Fig. 6-8).

i.e. $\dot{B}_{max}$ + $\dot{D}$ coupling induced 250 mV (*measured*)

$\dot{D}$ coupling induced 120 mV (*measured*)

Therefore $\dot{B}$ coupling induced 130 mV (*by deduction*)

From the cancellation results of open-circuited testing (Fig. 6-12), the positive polarity induced voltage is measured to be 125 mV when cancellation occurred at the 26-degree positions.

i.e. $\dot{B}_{max}$ + $\dot{D}$ coupling induced 125 mV (*measured*)

As before $\dot{D}$ coupling induced 70 mV (*measured*)

Therefore $\dot{B}$ coupling induced 55 mV (*by deduction*)

This net magnetic ($\dot{B}$) induced signal cannot be measured, only the angle of the directional coupler when cancellation occurred was measured. This value of 55 mV can be shown to be consistently correct as the calculation below demonstrates.

From,

$$E = V \cos \varphi \qquad (6\text{-}26)$$

$$E = 125\ [\cos (90\text{-}26)]$$

$$E \cong 55 \text{ mV}$$

Although the maximum magnetic field ($\dot{B}$) induced signal is not a direct measured value, which is used in the above calculation, there can be no ambiguity in its accuracy, owing to the method in which the measurements were made.

6-7 CONCLUSIONS

The results for these initial tests are consistent which demonstrated the versatility and sensitivity characteristic of the coupling loop. Even at the higher repetition rate of operation of the pulser, the switching pulses were jitter-free which caused stable induced voltages. Although some results showed almost perfect agreement while with others,there are some discrepancies, it should be pointed out that, apart from the usual measurement errors, the directional coupler could only be adjusted to within a half of a degree.

Using the concept of field-theory, to preserve the fields in strictly transverse planes, a perfect conducting sheet, capable in extent to cover the region of appreciable field at right angles to the transmission system, must be used. The sheet connected solidly between the earthplane and the line.

To leave the line disconnected does not ensure that the fields are reflected in a plane. There would be distortion in the fields at the open circuit termination, which would not behave as an infinite impedance, but as a small capacitance. When the wavelength is comparable with the cross-sectional dimension of the line conductor, the open circuit behaves as a resistance and energy is dissipated at the termination. As always there would be small copper loss, radiation loss and loss due to the *skin effect,* due to the very sharp risetime pulses injected into the line. These losses could not have been characterised as were intended, due to a special condition imposed on the line, which resulted in a *gain* that was measured. This is described later.

When the line was terminated in its characteristic impedance, the matching resistor, in particular its flying leads, gave rise to a small reflection. The actual resistor which was purposely made, was perfectly matched. A similar effect occurred at the junction of the coaxial cable and the open line. The matching network was made as small as possible and the values of the components are very accurate, since they were selected from a batch and measured with a precision DMM. The physical insertion into the circuit gave rise to a small reflection which was accounted for.

6-8 REFLECTIONS FROM CURVATURE OF THE TRANSMISSION SYSTEM

It was shown in the above experiments that reflections occur at discontinuities such as an open circuit, a short circuit or when a line is connected to another one with a different impedance, e.g. a coaxial cable connecting to the open line, as in this work. Whilst trying to characterise an *unknown* reflection, it was discovered that the small change in impedance due to the curvature near the termination of the transmission system, consequently gave rise to a series of small reflections. Note the position of the directional coupler (i.e. induced voltage) and the open end of the line (induced voltage due to reflection) are highlighted by cursors. Twice the travel is computed to be 10.2 ns which is in agreement of the actual distance measured of 1.5 m.

The curvature is greatest between the directional coupler and the end of the line. The small reflections due to the change in impedance, is shown exactly between these two points in Fig. 6-23.

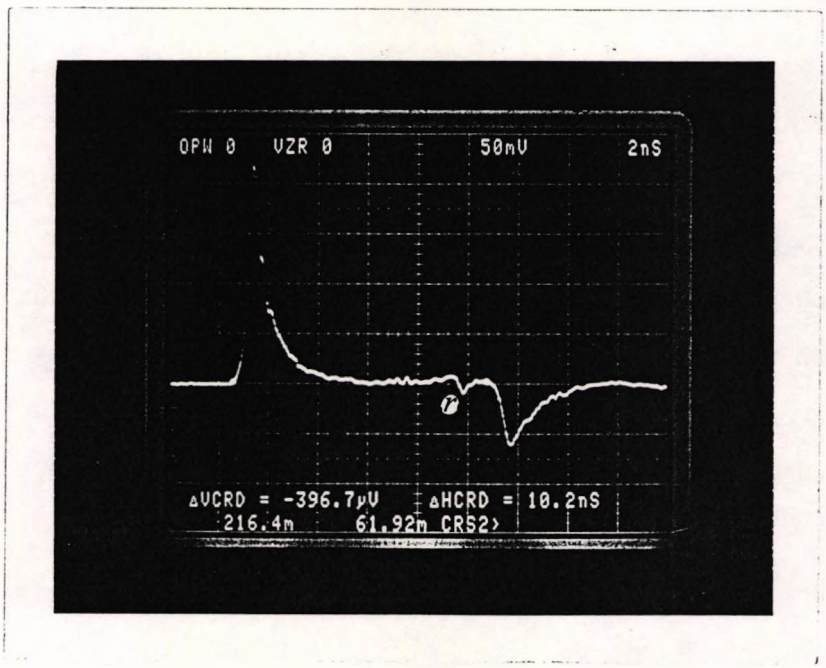


Fig. 6-23 Reflections from the curvature of the line system.

This test was done with the directional coupler mounted near the end of the line, at a distance of 1.5 m from its termination. This *unknown* pulse (denoted by *r* in Fig. 6-16) appeared to come from a line insulator since the measured travel time corresponded to the exact location of the insulator. The insulator was removed and the line suspended by nylon string.

The test was repeated with the same result. It was then verified that what appeared to be an unknown reflected pulse was actually a reflection at the junction of the coaxial cable and the open line, although these two lines were matched by a resistive network. It was coincidental that the travel time of the pulse from the directional coupler (near the termination of the line) to the said insulator is the same as the travel time from the cable connecting the pulser and the line. Therefore, what appeared as a reflection near the termination was infact an induced voltage pulse caused by a delayed travelling pulse which was first reflected at the junction of the coaxial cable and open line, and back again at the pulser open contact.

The reflections at the curvature at the beginning of the line was also verified in a similar manner.

6-8.1 Possible EMC application

The sensitivity of the measuring devices and set-up, developed and used in this experimental studies are demonstrated clearly. It is envisaged that, with further development, this important discovery can be applicable in EMC measurements where it is difficult or almost impossible, to place a radiating antenna inside a sealed enclosure. By the ability to detect small reflected pulses, the technique may be used to predict flaws in shielding seams and enclosures.

6-9 ELECTROMAGNETIC PROPERTIES OF MATERIALS

There is no scope in this thesis to fully discuss the properties of electromagnetic materials. Just an introduction and a review on ferrite is given, since a composite of this material used in the structure of the earthplane, exhibited a feature of much interest, under fast pulse application.

6-9.1 Introduction

Materials react to applied electromagnetic fields in a variety or ways including displacement of both free and bound electrons by electric fields and the orientation of atomic moments by magnetic fields. In most cases, these responses can be treated as *linear* (proportional to the applied fields) over useful ranges of field magnitudes. Often the response in independent of the direction of the applied field; the material is called *isotropic.* The responses of these linear isotropic materials to time-varying fields may depend to a significant extent upon the frequency of the fields. Therefore these linear isotropic materials can be represented by scalar values of ε and μ for analysis at a given frequency. Common dielectric such as glass, quartz and polystyrene and common conductors such as copper, aluminium and brass behave in this manner for a vast majority of applications.

The terms *dielectric*, *conductor* and *magnetic material* is used to indicate the character of the dominant response. In all solids and liquids the permittivity differs appreciably from that of free space as a result of the behaviour of the bound electrons in the constituent atoms. In a conductor, however, the movement of the free electrons in response to the electric field produces an electromagnetic response which overwhelms that of the bound electrons.

Similarly, ferromagnetic materials are mostly rather highly conductive but are referred to as magnetic materials as that property is most significant in their application. All materials have some response to magnetic fields but, except for ferromagnetic and ferrimagnetic types, this is usually small, and differs from μ_0 by a negligible fraction.

6-9.2 Diamagnetic and Paramagnetic Responses

All materials have some response to magnetic fields. Except for certain categories (ferro -magnetic and ferrimagnetic), their magnetic responses are very weak. Magnetic response can either decrease or increase the flux density for a given **H**. If **B** is decreased, the material is said to be *diamagnetic*, and if increased, it is called *paramagnetic*.

Atoms have a diamagnetic response that arises from changes of the electron orbits when the magnetic field is applied. From Faraday's law, an electric field is produced by a changing magnetic field that induces currents which, in turn, produce a magnetic field that opposes the change. The response of the electron orbits in an atom is of this kind. The effect produces fractional changes of μ and μ_0 by only 10^{-8} to 10^{-5}.

The diamagnetic response is usually obscured in materials having natural net magnetic dipole moment. such materials give a paramagnetic response which can arise from dipole moments in atoms, molecules, crystal defects and conduction electrons. The dipole moments tend to align with the magnetic field but are deflected from complete alignment by their thermal activity. The fields resulting from the partially aligned dipoles add to the applied field.

For certain materials the permittivity can be changed through application of an electric field. For liquids such as carbon disulphide and nitrobenzene, and for centrosymmetric solids, the effect is proportional to the square of the electric field and is known as the *Kerr effect.* For certain noncentrosymmetric solids such as lithium niobate and gallium arsenide the change may be directly proportional to the applied field and is known as the *Pockels effect.* Both these linear effects in crystals are relatively small for practical values of electric field, but the latter is especially important in a number of modulators, switches and deflectors.

6-9.3 Ferrite Magnetic Material

A group of materials, called ferrites, have the important characteristics of low loss and strong magnetic effects at microwave frequencies. These are solids with a particular type of crystal structure made up of oxygen, iron and another element which may be lithium, magnesium, zinc, etc. The important factors in the study of wave propagation in ferrites are that the losses at microwave frequencies are small, the dielectric constants are relatively high (within a factor of 2 of ε_r =15), and anisotropic behaviour of permeability results when the ferrite is subjected to a steady magnetic field.

A complete description of the energy state of an atom requires specifications of both the orbits and spins of the electrons. In the language of quantum mechanics, there are orbital and spin quantum numbers, both of which must be given to define the energy state of an atom. A strong magnetic moment is associated with electron spin. In paramagnetic substances these magnetic moments are randomly oriented with respect to those neighbouring atoms, but in ferromagnetic, anti-ferromagnetic and ferrimagnetic (ferrite) materials, there exists a strong coupling between spin magnetic moments of neighbouring atoms, causing parallel or antiparallel alignment.

Ferrite core is an indispensable tool in an EMC laboratory, and ferrite devices have found important uses in microwave applications for both waveguides and striplines. In microwave application ferrite devices such as the microwave gyrator, microwave isolator, microwave circulator and wave rotation of waves in two directions in magnetised ferrite rod are used. In stripline devices, a stripline Y-junction circulator can also be used as a switch or isolator.

Ferrite pulse sharpener is widely used in wave shaping applications (Seddon and Thornton 1988). Lai *et al.* (1994) applied a concept of using ferrite at high frequencies in developing a protection scheme.

A preliminary report is given on this condition, as encountered in the experimental studies.

6-10 PULSE SHARPENING PHENOMENA

Since no practical transmission medium is completely loss-free, it was intended to characterise the losses due to attenuation, radiation and conduction (copper) as the pulse travelled along the line. This could not be carried out easily because the line system exhibited some kind of pulse sharpening condition, whereby the pulse risetime decreased progressively as the it travelled along the line. This resulted in an increasing induced voltage amplitude so as to satisfy the condition:

$$v = \frac{d\Phi}{dt} \tag{6-27}$$

This test was conducted with an output pulse amplitude from a range of 100 V to 1kV and the induced loop voltages measured by the three directional couplers, situated at the beginning, mid-section and near the end of the line. Individual reading of the induced voltage amplitude was taken after the waveform was acquired and stored in the oscilloscope. The P-P (peak to peak) function then gives a digital readout of the induced voltage. When a small reflection was observed on the oscillograph trace, the cursors were used to marked off the peak voltage, since this will introduce an error in the automated computation.

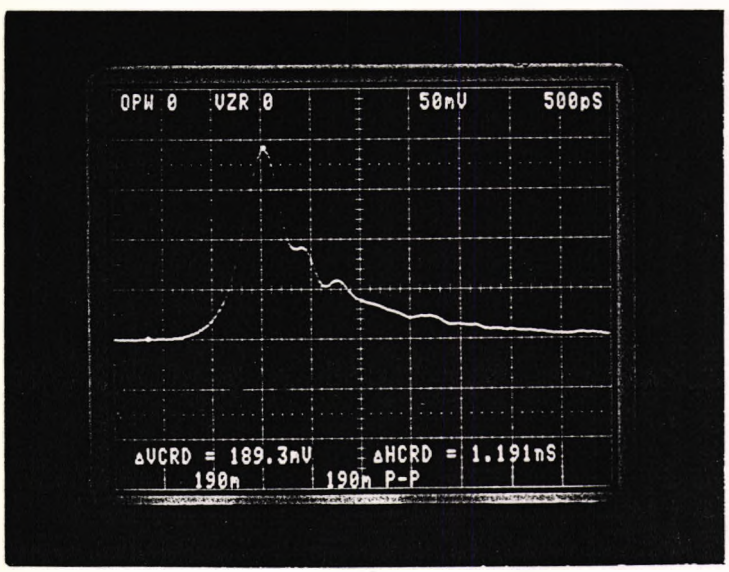


Fig. 6-24 Peak voltage measurement due to pulse sharpening condition.

A typical result is shown in Fig. 6-24 so as to demonstrate this measuring technique. It can be seen that there is no difference between the value of 190 mV computed automatically and the computed value when marked with the cursors. The oscilloscope is able to distinguish 0.1 mV within a range setting for the maximun input of 1 volt *peak- peak.*

Periodically checks were made during the test to ensure there was no change in the risetime of the excitation pulse. The result in Fig. 6-25 shows a typical pulse front after integration of an induced voltage. It illustrates the sharp rising edge which is an indication of the fast pulse entering the line.

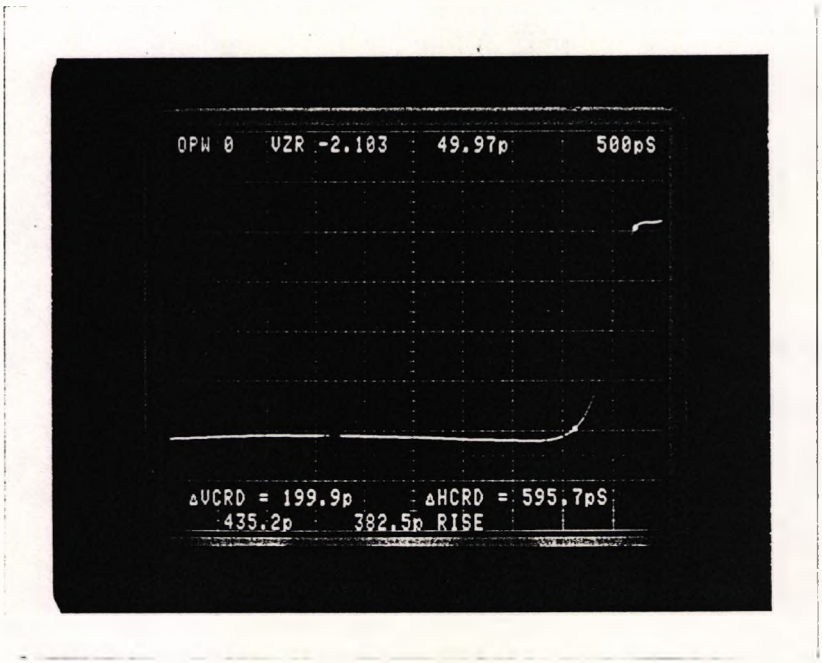


Fig. 6-25 Pulse front measurement.

The results are tabulated (Table 1) and graphs were plotted for the three sets of readings, with all the plots showing a linear relationships. Graphs drawn in Fig. 6-26, illustrates this linear relationship.

Table 6-1 Results of Induced Voltages due to Pulse Sharpening

Impulse Voltage (V)	Loop Induced Voltage (mV)		
	Source	Mid-section	Termination
100	32	34	35
200	64	67	69
300	94	99	101
400	127	132	135
500	157	166	169
600	190	199	204
700	222	232	238
800	253	266	272
900	284	300	306
1000	317	333	343

Although ferrite-line pulse sharpening is used in wave shaping, it was not anticipated when the system was designed that the effect on the transmission system would have been so noticeable. This is a direct result of the fast pulse penetrating the metal of the transmission system. Further investigations into this condition are pursuing.

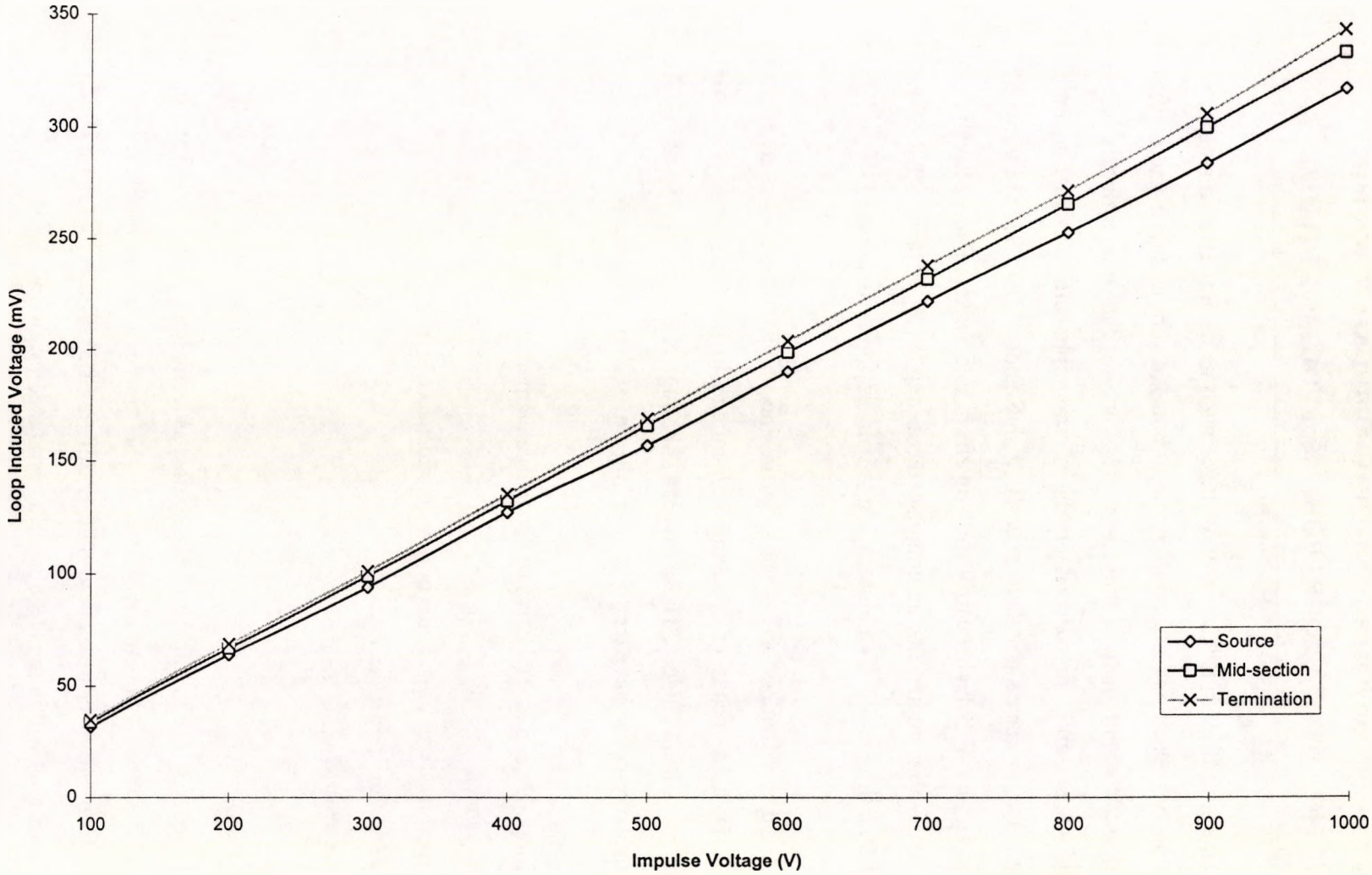


Fig. 6-26 Graph of induces voltages due the effects of pulse sharpening phenomena.

6-11 THE SF_6 PULSER AS A HIGH-VOLTAGE SIMULATOR USED IN CONJUNCTION WITH A LOOP PROBE AS A VOLTAGE DIVIDER

A divider for recording high transients over voltages such as an impulse voltage, may consists of resistors or capacitors (or a combination of both) in various stages and configurations. The essential requirement is that the wave shape of the voltage that is to be measured should be faithfully reproduced on the oscillograph, with a reduction ratio accurately known. The impulse shape is defined (British Standard 923:1972) in terms of two time values T_1 and T_2 which qualify the wavefront and wavetail respectively. A T_1/T_2 impulse shape thus represents an impulse increasing from 30% to 90% of its maximum value in a time of $0.6\ T_1$ and decaying to half-amplitude in a time T_2.

Resistive and capacitive dividers are always used (since high voltage measurements were first reported), as a means of reducing the voltage to an acceptable level for connecting to the measuring devices. These dividers, although are always primarily used in high voltage measurements, have the following inherent technical problems:

- 1. Residual inductance in any resistive or capacitive element.
- 2. Stray capacitance.
- 3. Voltage drop on circuit impedance of device under test.
- 4. Oscillations in the divider circuit.
- 5. Capacitive and Restivtive loading.
- 6. Flashover.

The technique proposed in this experimental studies is completely different from the conventional dividers and is much less prone to the above inherent problems. The approach is based on the electromagnetic-field coupling of a suitable calibrated loop probe, which is immersed within the electric-field, produced by an impulse voltage.

The versatility of the capacitive loop lends itself to the application of a non-perturbing voltage divider. With proper calibration it can be used as a simple divider in a digital impulse measurement system (DIMS), that is, reducing the output from a capacitive

divider to an acceptable input. This method in voltage reduction does not suffer from the limitations and technical problems of resistive and capacitive dividers outlined in **(5-3.2)**.

6-11.1 Experimental - High Voltage Divider

A novel attempt was made to implement the coupling characteristic of the loop probe used in the experimental studies, as an **E**-field sensor. It was found experimentally that the response of the probe configured as an **E**-field sensor is faster than that of an **H**-field sensor. Adjustment of the probe as an **E**-field sensor is important for accurate measurements. This was easy to set up in the testing as the 0/180 degree position (where the influence of the magnetic-field coupling is assumed negligible) was calibrated. In practice, this position could be found by measuring the response time when the probe is at or very near the 0/180 degree position.

Experimentally, the response was found to be fastest at this position.

6-11.2 The Test Procedure

The available measuring equipment does not have a fast enough writing speed for single shot measurements, therefore an oscillatory trigger circuit had to be designed and built so as to pulse the output voltage repetitively at a few hundred hertz. This repetitive voltage was necessary so that the oscilloscope (Tek 7854) using digital sampling techinque, could be used for the measurements.

The charge line was connected to the unit through a charging resistor and large smoothing capacitors were used to ensure a short charging time and a low ripple DC component. The high voltage source was from a 80 kV (bench) power supply unit. The measurement set-up is shown in the photograph of Fig. 6-27.

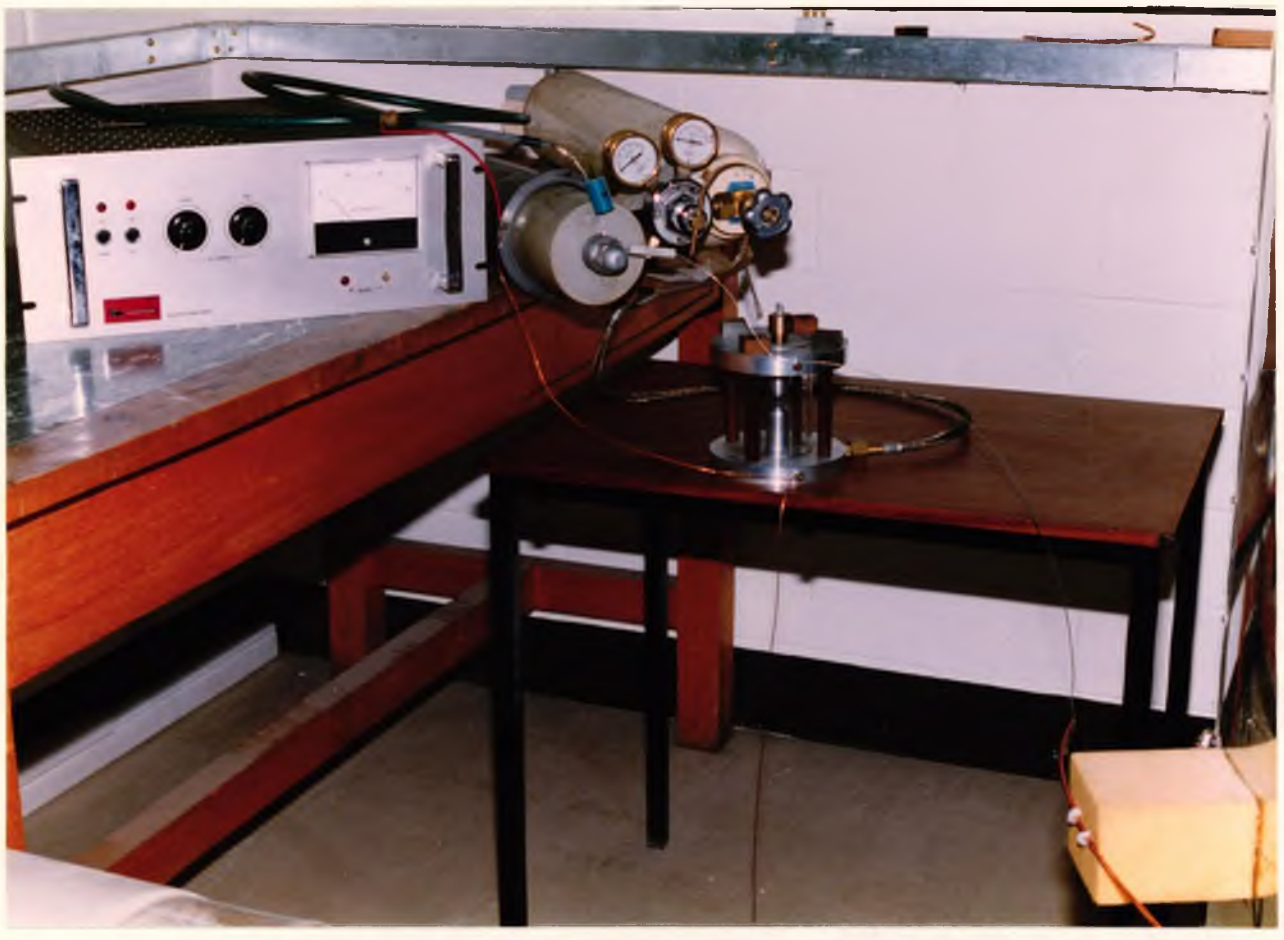


Fig. 6-27 Experimental set-up of the SF_6 pulser as a high voltage simulator.

Although the SF_6 pulser worked well at lower switching frequencies, the switching of the high voltage pulses at the required repetitive speed for triggering the sampling oscilloscope, was not stable enough for successful operation. Therefore an alternative measuring technique was adopted, ustilising the features of a computer with an IEEE-488 interface and a device with a similar interface. These readings are tabulated (shown in Table 6-2 below) with a typical result shown in Fig. 6-28.

A graphical representation with an almost linear relationship between the applied impulse high voltage and the loop induced voltage, is also shown in Fig. 6-29.

TABLE 6-2 Results of Impulse Voltage Measurement

Pulser Voltage (kV)	Loop Induced Voltage (mV)
5	72
10	141
15	212
20	282
25	352
30	420
35	496
40	570
45	641
50	718

This experiment clearly demonstrated a unique method of how an impulse voltage can be reduced for measurement using a general purpose oscilloscope, or alternatively for connection to a digital impulse measurement system.

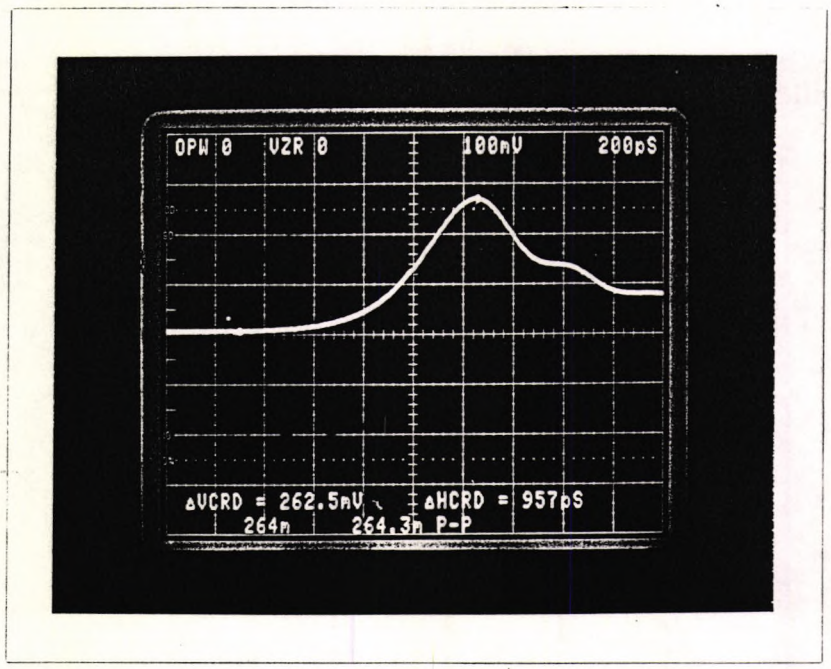


Fig. 6-28 Representation of a peak high-voltage measurement.

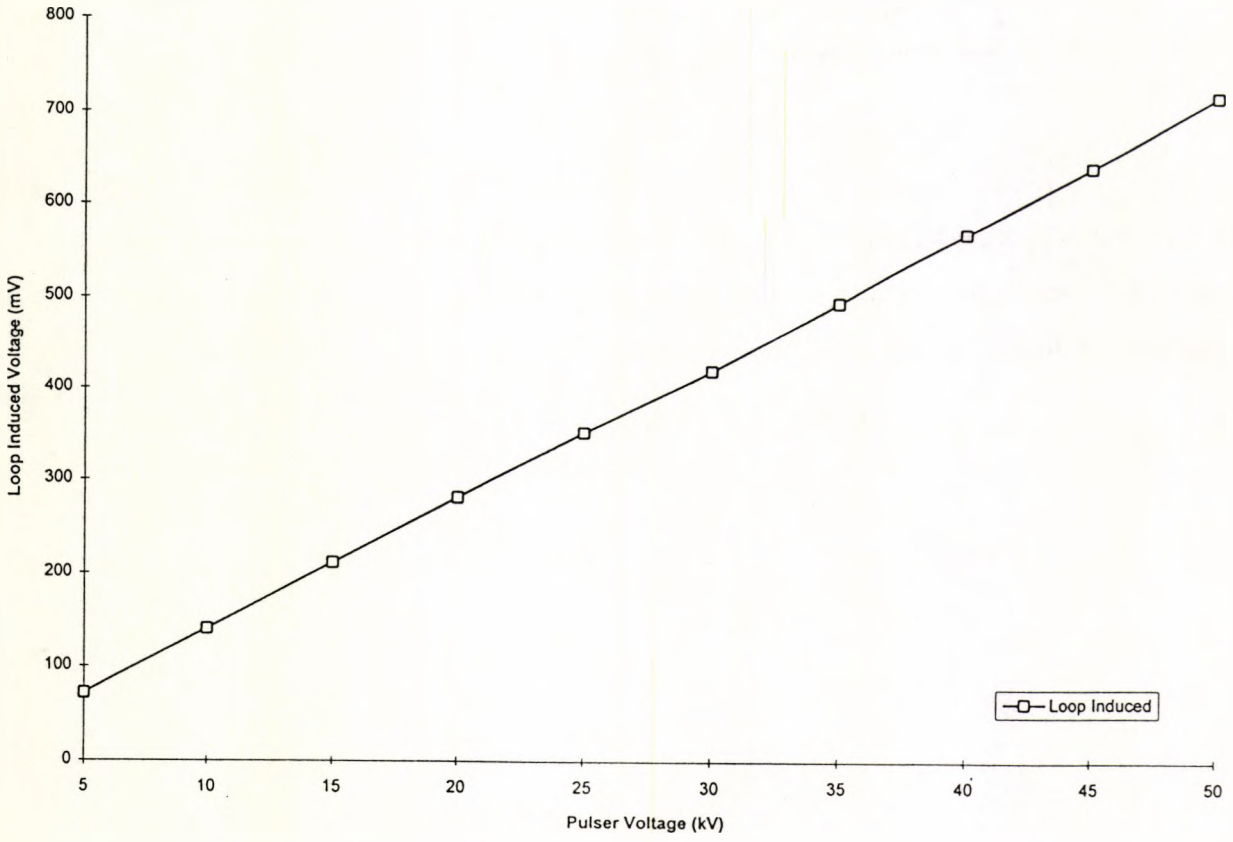


Fig. 6-29 Graph of relationship of the probe as a voltage divider.

6-12 Impulse Voltage Measurement

An introduction to the SF_6 Pulser as a simulator for impulse voltage measurement is given in *Chapter* **4-3.** The experimental set-up was in conjunction with that used for high voltage divider measurements and the procedures were similar.

The technique is simply to connect the output from the loop probe (optically if necessary, as used in the experiment) to a suitable measuring oscilloscope, placed in a less hostile electromagnetic environment. The results of the displayed waveform can then be taken photographically or through an interface device to a computer. Both of these approaches were utilised. With proper calibration, an accurate peak impulse can be determined.
The electrode gap and SF_6 gas pressure of the pulser were adjusted until the output waveform approximates that of a lightning impulse voltage. Several readings were taken within a safe voltage working range. A typical result of a lightning impulse voltage wave-form is shown in Fig. 6-30.

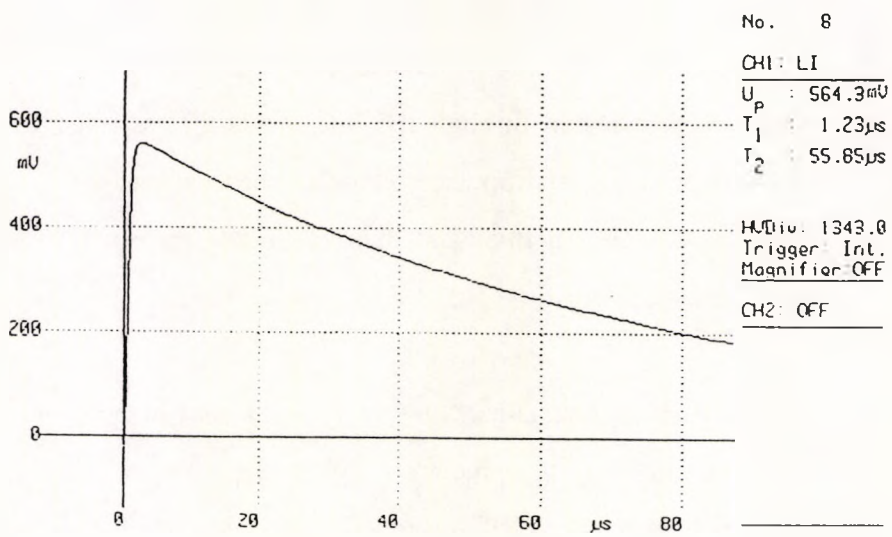


Fig. 6-30(a) Impulse voltage measurement - magnification off.

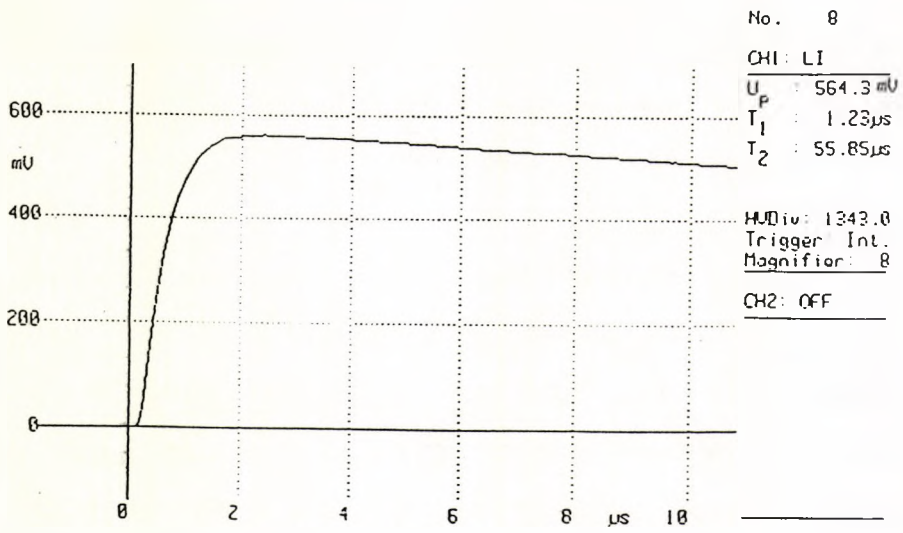


Fig. 6-30(b) Impulse voltage measurement - 8 x magnification.

6-13 Conclusions

The electromagnetic-field into which the loop probe was coupled, was not of the free-field nature, as associated within the vicinity of high voltage equipment, such as an impulse generator, since the pulse was propagated through the line. Nevertheless, the experiment demonstrated clearly that in principle, an impulse voltage can be reduced first without any physical connection to the source generator and then accurately measured simultaneously using a general purpose oscilloscope.

Although capacitive and resistive dividers have long since come to maturity, they are still the standard, acceptable as granted, the only way in reducing a high voltage source for measurements. The National Physical Laboratory (NPL), United Kingdom, and their counterpart, the Physikalisch-Technische Bundesanstalt (PTB), Germany, are looking for alternative methods in impulse voltage measurements to meet new standards, laid down by the MIL-Specifications. These specifications largely concern the accurate measurement of lightning impulse voltages relating to studies of lightning strike on air-craft.

In general, any loading of a circuit will cause a reaction to its source generator, the effects depending mainly upon the type of load and the generator itself. When the quantity of interest is the wave front, the the loading must be of paramount importance if appreciable errors are to be avoided. The impulse generator and its capacitive and resistive dividers are no exception. Hence, there is tremendous potential in this alternative measurement technique, proposed in this thesis.

Even with the advent of sophisticated digital impulse measurement systems, this proposed field coupling technique of reducing the impulse voltage could be an indespensible means of connection to such a measurement system. The output from the loop probe can be transmitted digitally to a measurement system, thereby offering total isolation, the freedom from earth loops, and the elimination of possible interference problems.

The system has to be calibrated against a known traceable reference. The coupling coefficient k can be measured from the high voltage graph and hence the measurement of an induced voltage in the loop due to electric-field produced by an impulse voltage, is a direct relationship to the peak impulse voltage.

The calibration and final implimentation of the measurement system, is proposed for the continuation of the work.

Chapter 7

Further Investigations and Applications using the New Developed Probing Measurement System

7-1 THE DIRECTIONAL COUPLER AS AN ACCURATE FAULT LOCATOR

7-1.1 Introduction

The constant call for papers on increased measurement accuracy for fault detection and location on transmission lines and distribution feeders, has led to a great deal of activity in this area. This section reports an investigation on a fault location method using the pulse injection principle. The measuring technique made use of the versatility of the directional coupler, in conjunction with the sub-nanosecond mercury pulser, which was used to transmit the pulse into the test line.

The results are presented in photographic form taken from the high speed digital sampling oscilloscope.

7-1.2 Review

There has been a significant expansion in power transmission and distribution over the last decade. Consequently, this has led to the search for more effective protection devices. This area of research is not new as investigations in fault diagnostics on

transmission lines and feeders using digital protection, have progressed since the early sixties, (Wedepohl 1963).

The use of non-power frequency components for power system protection is dated as far back as 1937 (Logan and Richardson, 1937), but since then there has not been any degree of significant development. The improvement of microprocessor technology over recent years has led to the development of more sophisticated digital protection systems, (Mansour and Swift, 1985).

There are considerable interest and activity in fault detection and location. More recent work on monitoring non-power frequency components of current waveform for the detection of low level faults in power distribution systems, is reported by Aucoin and Russell (1987), and Russell *et al.* (1988a,b). Johns and Agarwal (1990) investigated techniques of monitoring high frequency components of currents and voltages in a typical 400 kV transmission network. A different approach on detecting fault-induced high frequency components on distribution feeders, was reported by Johns *et al.* (1991).

Most of the algorithms currently employed in fault detection are based on either the fundamental power frequency parameter evaluation or travelling wave theory, (Ibe and Cory, 1985). One recent approach is to inject a fast pulse into the faulty section of the line. The other method is to record the voltage and current waveforms at suitable points on an energised line, almost immediately (a few millisecond) after the fault condition has occurred. More recently Artificial Neural Network (ANN) and Genetic Algorithms (Lai, *et al.* 1992/93) are being integrated in fault diagnosis. These methods are progressing rapidly in this as well as other areas of technology. A *tutorial* on Fault Diagnostic using Neural Networks in HVDC Transmission Systems is proposed (Sood Et al. 1996).

From the investigations carried out in this area, a simple, yet accurate method of fault location may is presented. It made use the pulse injection principle, but instead of a travelling wave, a very fast (sub-nanosecond) risetime pulse is injected into the faulty section of the line. Any response from the line due to a fault impedance, (between zero impedance and infinity) will result in a backward travelling reflected pulse, which will interact with a suitable placed **B**-dot/**D**-dot coupling probe, (Rajroop and Lai 1993a).

7-1.4 Open-Circuit Fault Condition

The same experimental set-up was used as in the connection diagram, Fig. 6-4 and in the photographs in Figs. 5-4 and 5-12(b).

When the power supply was switched-ON, cable *A* was charged through resistor *R* to a potential of V^+ volts. The signal generator was then switched-ON and energised the operating coil. When the contacts were closed, this charged potential on cable *A* was discharged into cable *B* at a potential of $(V^+/2)$ volts and was then injected into the test line.

Simultaneously a pulse of $(V/2)$ volts travelled back to the source where it is reflected by the high resistance of *R*. It then travelled in the negative direction in the line, delayed by 12 ns, due to the travel time in cable connections. When the pulse impinged on the loop sensor, the field change created caused a signal *b* to be induced in the loop. Signal *d* is the induced signal caused by this same pulse when it reflected at the line termination.

When the forward travelling pulse impinged on the loop, a voltage was induced and is shown as *a*. Since a pulse cannot anticipate the load condition, it travelled to the end of the line, encountered an open circuit and was reflected. It then travelled in the forward direction and induced signal *c* as it impinged on the loop once again. These induced signals are shown in Fig. 7-2.

7-1.5 Calculation of Distance to Fault

For the measurement of a fault location, only the forward pulse travelling in the fault section of the line is meaningful. Therefore the induced signals *b* & *d* can be ignored.
The cursors mark the beginning of induced signals *a* & *c*, shown in the result in Fig. 7-2.

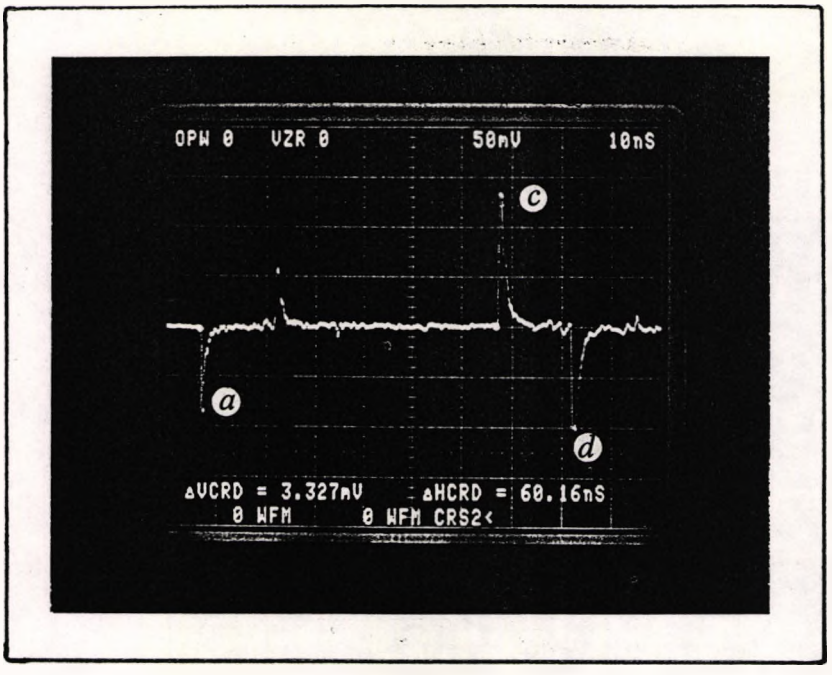


Fig. 7-2 Waveform of induced voltages for open-circuited condition.

The travel time between these two points is computed to be 60.16 ns which is the time from when the pulse induced the first signal, travelled to the assumed fault location, and reflected back. Therefore the actual time of travel to the fault location is half of this value.

The velocity (v) of an electromagnetic wave travelling in free space is given by:

$$v = 3 \times 10^8 \text{ m/s}, \qquad (7\text{-}1)$$

$$\text{or } v = 30 \text{ cm/ns}$$

Using a steel tape, the distance from the directional coupler to the open ended condition was measured to be 9 meters, [(1/2 of 60.16 x 30 = 9.024 m).

This is in good agreement with half of the recorded time of 60.16 ns.

The line termination was short-circuited and the test procedure repeated. The results are shown in Fig. 7-3.

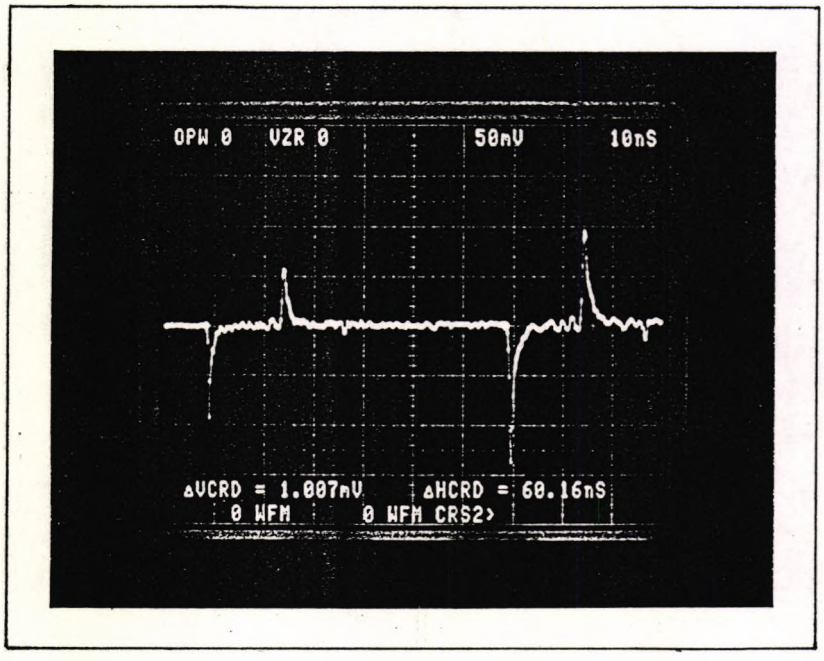


Fig. 7-3 Waveform of induced voltages for short-circuit condition.

Since the fault is imposed at the same point in the line, the travel time would be the same as expected, and is shown in the result. It is interesting however, to note that induced signal *c* is now of negative polarity.

These tests demonstrate how the directional coupler can be applied in such a unique manner. At a glance on the waveform one can tell the direction of the fault with respect to the reference direction coupler position, (i.e. 90 degree or 270 degree angular setting) and whether the fault is an open-circuit or a short-circuit one.

7-1.7 Detection of an Impedance Fault

For the following tests, the pulse which would have been reflected from the source was suppressed, since it had no relevance in the results. This was achieved by connecting a longer cable from the pulser to the power supply so that the delay imposed is greater than the pulse propagation time for the line.

7-1. Low Impedance Fault

A low impedance (100 ohm) fault condition was imposed at an arbitrary point in the line. Using the same test procedure, the following results were obtained, shown in Fig. 7-4.

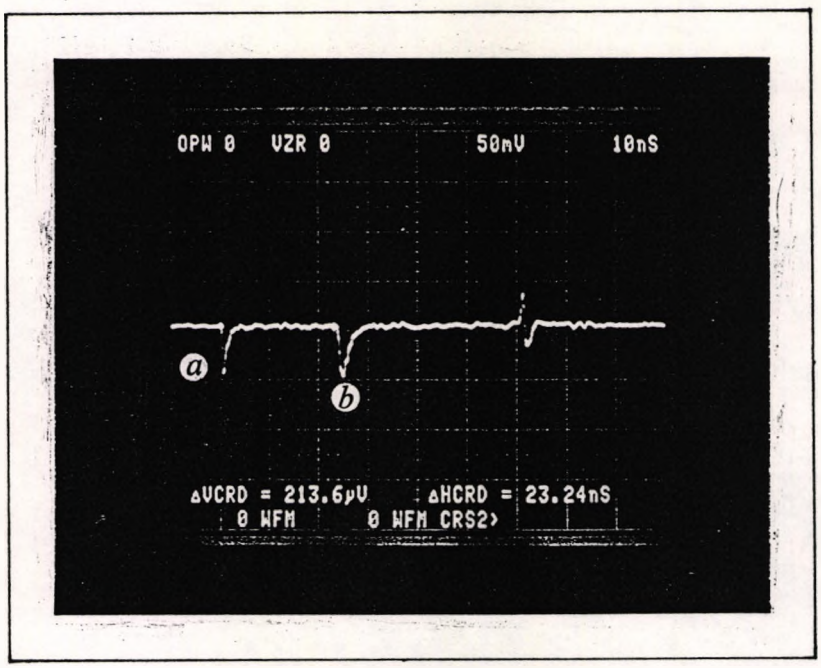


Fig. 7-4 Detection of low impedance fault condition.

7-1.9 High Impedance Fault

The results due to a high impedance (2.2 MΩ) fault imposed at the same point in the line is shown in Fig. 7-5.

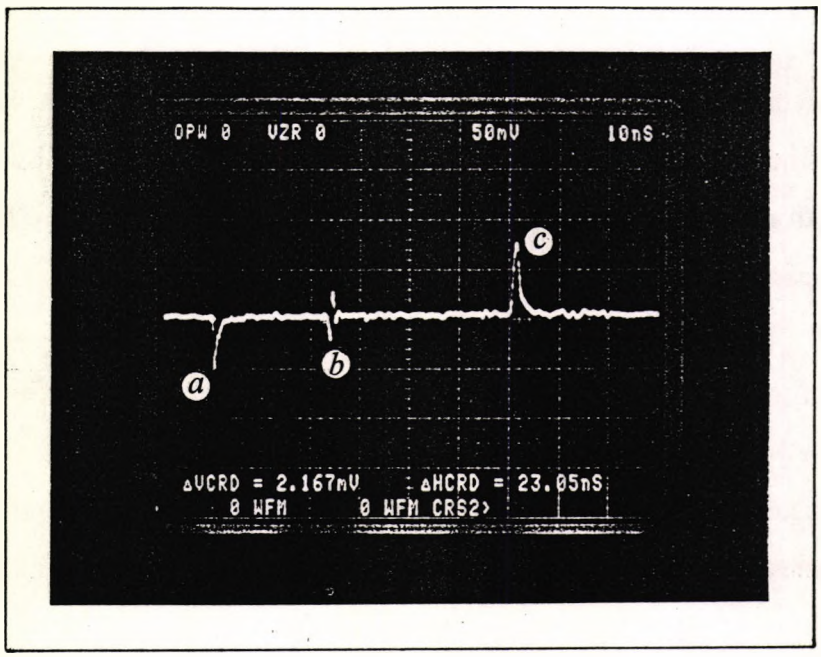


Fig. 7-5 Detection of high impedance fault.

7-1.10 Intermediate Impedance Fault

Finally a random intermediate fault impedance of 100 kΩ was imposed again at the same point in the line. The results are shown in Fig. 7-6.

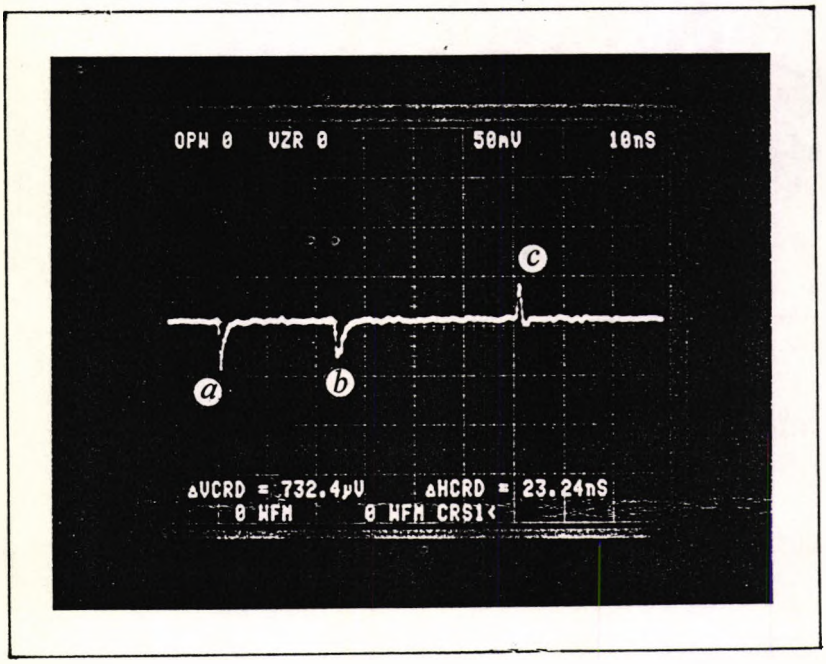


Fig. 7-6 Detection of an intermediate impedance fault.

7-1.11 Discussions

From Figs. 7-2, 7-3 and 7-4, the first *(L to R)* induced signal (marked *a*) is regarded as the reference signal from which the distance to fault is measured. This is also the same in Figs. 7-5 and 7-6, where the last induction was due to reflection from the line termination, and the middle induced signal, from reflection of a pulse from a fault impedance along the line. Cursors marked the points on the reference signal and the fault reflection induced signal. Twice the travel time was computed to be slightly greater than 23 ns. Using the velocity of propagation for an electromagnetic wave as before, this value coincides with the actual measured distance of approx. 3.5 metres. For simplicity in the illustrations, all the faults were imposed at the same point, but the fault conditions could have been imposed at any point in the line with the same measuring technique applied.

It is interesting to note from the relationship between the second and third signals (marked *b* and *c* on Figs. 7-4, 7-5 and 7-6) on the waveforms, that a rough estimation as to the nature of the fault can be determined. For a given orientation of the directional coupler, a comparison of the induced voltages (marked *b*) showed a significant increase in the induced voltage amplitude for a low impedance fault, than that of an intermediate impedance fault. The high impedance fault (with a reflection coeffic-ient, $\Gamma \rightarrow 1$) gave rise to a very steep reflected pulse which caused a corresponding transient overshoot response from the output of the loop probe. This is marked *b* and is shown in Fig. 7-5.

Although open-circuit and short-circuit faults and their relative directions are easy to determine, this fast response feature of the directional coupler could be useful in detecting impedance faults such as insulator breakdown.

7-1.12 Conclusions

The application of the directional coupler as an accurate fault locator on a transmission line is described. It is appreciated that on a long transmission line the errors would increased, but with skilful operation and measuring techniques, these errors can be kept to a minimum. Due to the sensitivity of the directional coupler and the fast response time of the directional coupler, marking the induced signals with the cursors is extremely

accurate. Any discrepancy in the marking is due to the time displacement between two adjacent points with regards to the number points per division.
It could be advantageous if sections of the line are first checked under no-fault conditions and the acquisition of data stored for comparison.

This technique can be digitally automated so that when a fault occurs, an audible alarm is sounded and the distance to fault is then a matter of simply pushing a button on the measurement system. The displayed waveform of the reflected pulse, when referenced to stored information, can predict the type of fault. With the application of Artificial Neural Network (ANN) the system will learn and update itself each time a fault occurs, continually giving more accurate predictions, (Swarup *et al.* 1993).

A significant advantage of the technique is that the directional coupler can be adjusted to detect pulses travelling only in one direction, and hence indication of the direction of the fault. The technique is limited to a two-terminal network, but further work is proposed to extend this measuring technique to a three-terminal network.

Because of the sensitivity characteristics of the directional coupler and its ability to detect very small changes in impedance, the technique can be extended to predict and locate faults in a complex bus-bar system, including an insulated network of bus-bar.

7-2 NEW LOOP-PROBE DESIGN FOR EQUAL B-dot/D-dot COUPLING

7-2.1 Introduction

A single loop sensor having properties so that it can respond equality to the electric ($\dot{D}$) field and magnetic ($\dot{B}$) field change, is of significant practical importance. In the continuation of work on the modelling and design of small loop sensors and antennas, it was shown mathematically that it is possible to alter a loop coupling characteristics by adding resistors to its circuit , (Kanda, 1984). Tests were conducted using this principle and comparison made with a method proposed by the author of the thesis.

In general, the magnetic-field response of a $\dot{B}/\dot{D}$ probe sensor, due to an electro-magnetic field change, is greater than that created by the electric-field. If the probe, or loop is loosely coupled within the electromagnetic field, it can be adjusted to such an angular position, so that it can only couple to a pulse (producing this field) travelling in a given direction. In this case the magnetic-loop response is reduced by virtue of the angular displacement of the loop, to equal that of the electric-dipole moments. The thesis illustrates a new and effective method in achieving this same condition of equality, but without the need for any angular adjustment.

The measuring system made use of the transmission line model which was originally designed and constructed to study the performance of fast travelling pulses. This was used in conjunction with the line pulser and directional coupler which incorporates the loop probe (Rajroop,1990). These measuring devices are already described in *Chapter* 4.

The technique presented in this thesis does not depend on the addition of resistor in the loop circuit. The approach is based on the change of loop geometry which was kept to a minimum size, thereby giving an added advantage of reducing the loop inductance. It also enables the directional coupler in its original form to be used.

The unique feature of the coupling loop is its directional properties and hence is known as the directional coupler. These directional properties are described in **7-1** and in *Chapter* 6. This equal response coupling is of significant practical importance when it occurs at the fixed angle for maximum coupling..

7-2.2 Experimental Procedure

In further study of the properties and behaviour of fast pulses on lines, and the coupling characteristics of directional couplers, it was decided to make the effects of the magnetic-field coupling equal to that of the electric-field coupling. The first method was by altering the loop impedance in accordance with the theory, (Kanda 1984). Since it is difficult to accurately define all the parameters and established precise boundary conditions within the system, only an approximate calculation could be made.

These investigations were carried out as outlined in the test sequence of the line, described in *Chapter* 6.

7-2.3 Loop Termination with Identical Loads

It can be shown by calculations that for a specific condition, a 68 ohm resistor connected in each arm of the loop would enable the condition of equality to be obtained. This test was carried out with 0.25 W 68 ohm high stability metal film resistors connected at the ends into a 25 mm diameter semi-circular loop made with 1 mm copper wire. The following experimental results were obtained:

$\dot{B}_{max} + \dot{D}$ coupling induced 160 mV (measured at 90 degree position)

$\dot{D}$ coupling induced 80 mV (measured at 0 degree position)

Hence $\dot{B}_{max}$ induced 80 mV (*by deduction*)

Where $\dot{B}$ and $\dot{D}$ are the magnetic and electric field coupling respectively. This clearly satisfies the condition for equal ($\dot{B} = \dot{D}$) coupling.

7-2.4 Termination with one Resistor in Loop Circuit

It was found that the condition of equality can also be met with a resistor connected only in one arm of the loop. In this case a resistor of value calculated to be 56 ohms was inserted in the loop circuit, in series with the 50 ohm matching *BNC* load. The test was repeated as before with the following results obtained.

$\dot{B}_{max} + \dot{D}$ coupling induced 180 mV

$\dot{D}$ coupling induced 90 mV

Hence $\dot{B}_{max}$ induced 90 mV

This test shows that the condition ($\dot{B} = \dot{D}$) is met again.

7-2.5 Loop without a Load Termination

Finally, a test was carried out without any resistor connected to the original loop. The following result shows the degree of unbalanced condition.

$\dot{B}_{max} + \dot{D}$ coupling induced 230 mV

$\dot{D}$ coupling induces 75 mV

$\dot{B}_{max}$ induces 155 mV (*by deduction*)

Comparison with the previous tests has shown that a voltage drop occurred in the loop resistors which had the effect of reducing the induced voltage due to the $\dot{B}_{max}$ coupling. The component of the $\dot{D}$ coupling does not change quite so significantly. It should be pointed out that the $\dot{D}$ component which is always present, can readily be observed at the zero degree or reference position, where the component of the magnetic coupling is assumed negligible.

7-2.6 Equality Condition Obtained by Altering the Loop Geometry

It can be shown by calculations that the coupling characteristic of the loop can also be changed by increasing the loop conductor diameter, so as to make the electric-field coupling greater and equal that of the maximum magnetic-field coupling. For a given electric-field change, the induced voltage varies according to the conductor diameter of the loop, and for a given magnetic-field change, the induced voltage varies according to the area of the loop.

This is a new practical approach in obtaining an equal response coupling. By making approximations, simple calculations showed that a 25 mm diameter semicircular loop of conductor diameter, 6 mm, should satisfy this condition of equality.

For these measurements one of the original directional couplers was modified to accommodate the new loop.

A loop probe designed with the above dimensions gave the following results:

$\dot{B}_{max} + \dot{D}$ coupling induced 398.4 mV (see Fig. 7-3)

$\dot{D}$ coupling induced 200.2 mV (see Fig. 7-4)

Therefore $\dot{B}_{max}$ induced 198.2 mV (*by deduction*)

This test result [Fig. 7-7(a) and (b)] shows a good agreement in equality condition for the electric- and magnetic- field response.

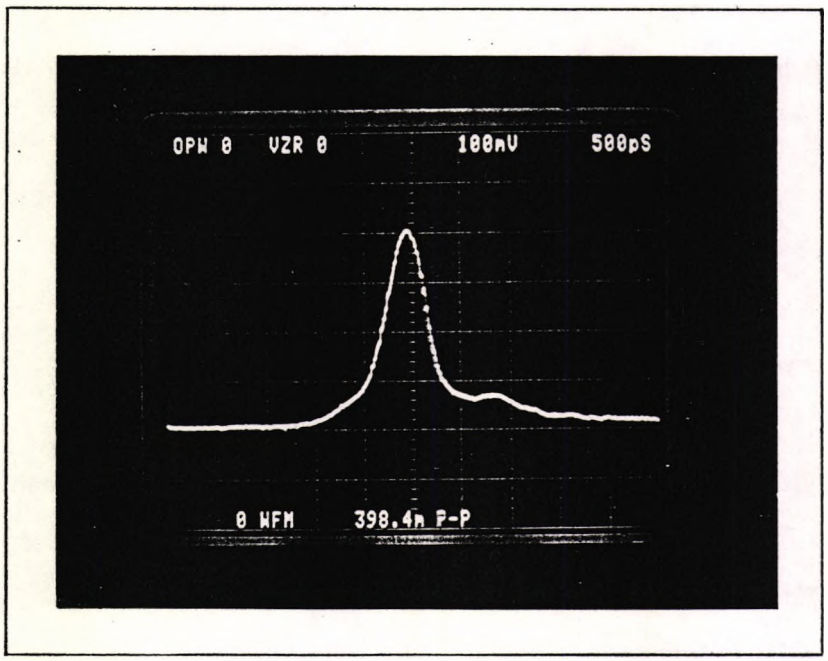


Fig. 7-7(a) Cursor set at peak induced voltage of 398.4 mV, **B**-dot coupling.

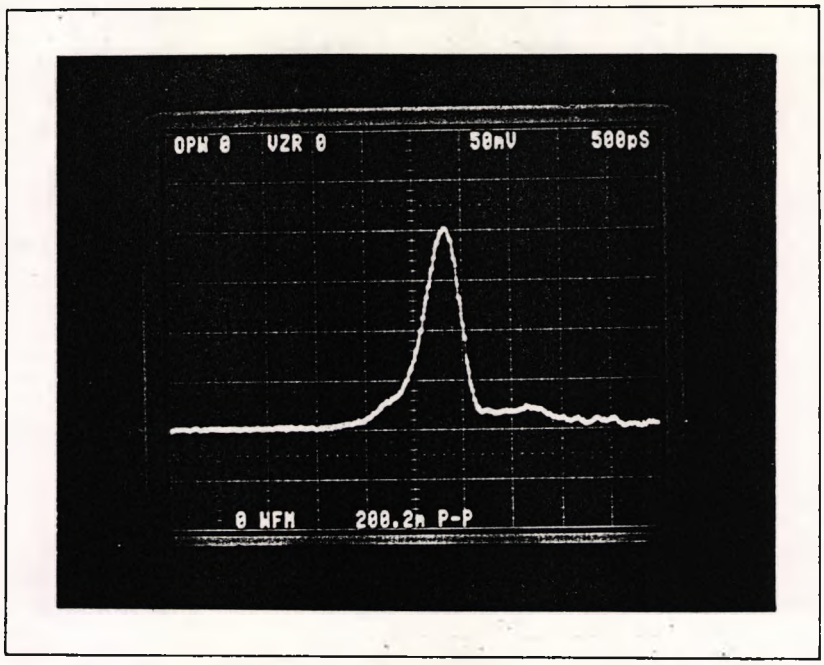


Fig. 7-7(b) Cursor set at peak induced voltage of 202.2 mV, **D**-dot coupling.

7-2.7 Calculation of Loop Inductance and Capacitance

It was shown in *Chapter* 2 that the inductance (L) and the capacitance (C) of the loop can be expressed by the following equations:

$$L = \mu b\left(\ln\frac{8b}{a} - 2\right) \tag{7-2}$$

and

$$C = \frac{2\varepsilon b}{\ln\left(\frac{8b}{a}\right) - 2} \tag{7-3}$$

Where μ is the relative permeability of the medium

ε is the relative permittivity

b is the loop radius

and a, its conductor radius

For the loop chosen for equal electric and magnetic coupling, the following results were calculated:

Loop Inductance (L) = 32 nH

Loop Capacitance $(C) \cong 0.2$ pF

These values compared favourably with those measured with reference-series capacitive and inductive bridges. From the equation:

$$f = \frac{1}{2\pi\sqrt{(LC)}} \tag{7-4}$$

the frequency response of the loop was calculated to be >2 GHz. Although the risetime of the wavefront leaving the pulser was measured to be < 300 ps, this sharp front was degraded at the junction of the coaxial line and the open line conductor, matched by a resistive network. The 10% - 90% risetime of an exponential (RC) system to a step function is 0.35 of the period of the sine wave signal at its 3 dB point applied to the same system. Using this criterion, the measured value shown in Fig. 7-8 does not agree with the calculated value due to the limitation of the pulse risetime as it coupled with the loop.

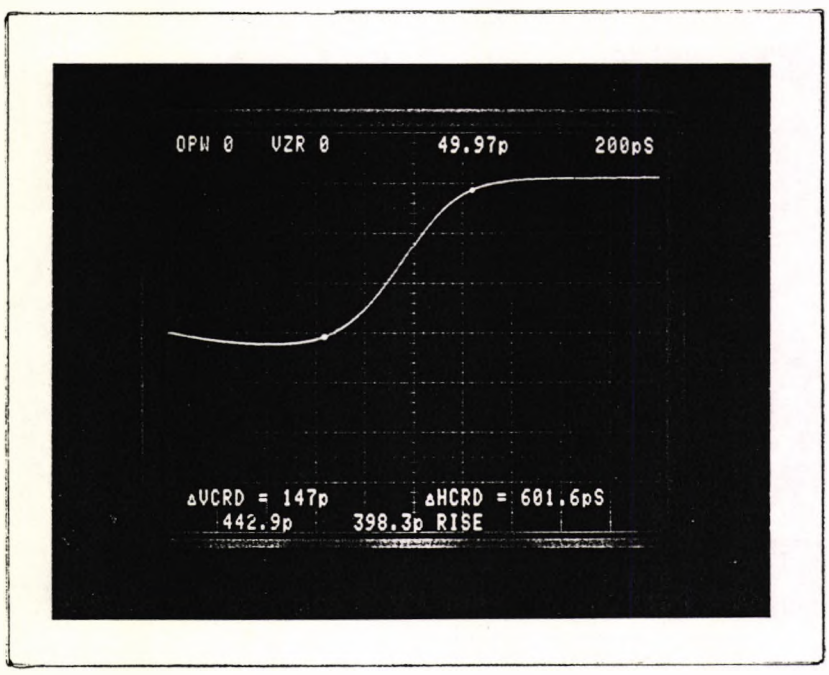


Fig. 7-8 Pulse front risetime measurement (derivative of induced loop voltage).

Although the values of L and C would seem extremely small, it must be considered that only a small piece of wire was used to construct the loop.

7-2.8 Discussions

Simultaneous measurements of the electric- and magnetic-field components are of significant practical importance. The method described in this test, enables these components to be measured and distinguished at the angle for maximum coupling.

Although the results show very close values in the equality conditions ($\dot{B} = \dot{D}$), it should be pointed out that there could be some small discrepancies in the measurements. This is particularly so when the induced voltage, due to the electric-field coupling was measured. An angular error of a degree can give rise to a few millivolt change. The arrangement is such that it is difficult to obtain an accuracy better than half of a degree in angular adjustment. Moreover, the results were taken under ideal conditions due the to experimental set-up and measuring technique.

Mathematical functions are performed by a software incorporated within the mainframe oscilloscope. The risetime is computed with respect to the specifications of the program. The value of 443 ps for the derivative of the induced voltage response of the loop is shown in the result in Fig. 7-8. From the waveform (which initially rises and tails off relatively slowly) a more meaningful measurement of the risetime is high lighted by the cursors, i.e. the fastest rate of change. This is computed to be 398 ps, also shown in the result.

This method of making the electric and magnetic-field response equal, is much preferred since the loop is matched on one side to the oscilloscope impedance, thereby preventing the setting-up of small reflective pulse patterns. Also a higher signal output is obtained since there is no voltage drop in the loop resistor. This is very useful in low signal strength areas.

The coupler is small as was originally designed. Only the loop conductor diameter was made larger to obtain the equality condition. This compactness prevents any possible perturbation of the field when the loop is immersed in such fields. It is envisiged that by constucting a much smaller loop probe with SMA connector configuration, the overall response could be at a few tens of Gigahertz range.

The technique is simplicity in itself and the devices described are inexpensive, easy to set up and use and are very accurate.

Although Kanda's (1984) theory was verified experimentally, it is felt that in some practical application e.g. Frequency Swept Measurements, it may not be possible to match the load termination of the loop accurately enough, using his method. Hence this new approach.

It is envisaged that the loop sensor described, may be used to measure the polarisation ellipses of the electric- and magnetic-field vectors in the near-field region. It may also be used to measure the time-dependent Poynting vector from which it should be possible to describe the energy flow.

7-3 PROBES FOR ELECTROMAGNETIC PULSE (EMP) MEASUREMENTS

7-3.1 Introduction

The widespread use of large scale integration (LSI) and (VLSI) circuits in telecommunications systems and information technology, has notably increased their EMP vulnerability. EMP hazards can originate from a number of sources such as lightning discharges, high power switching transients and nuclear EMP, etc. To improve the EMP immunity of electronic devices, it is necessary to carry out continuous investigations. These include the parameter of EMPs coming from a variety of sources as mentioned, and those produced by the simulators themselves, which are widely used in immunity testing.

Measurement of EMP parameters generally involve electrically small linear antennas or loops that act as measuring probes. The majority of probes, however, can only measure one field component - electric or magnetic. This drawback can be eliminated by the use of a double-loaded loop probe.

7-3.2 Loop Analysis

It should be pointed out that the loop used in the experimental studies is loaded on one side so as to match the oscilloscope impedance on the other, therefore it may be regarded as a double loaded loop. Hence the following analysis applies.

The properties of a double-loaded loop antenna which can act as a probe for measurements of electromagnetic pulses, is analysed. This probe can perform independent measurements of the electric- and magnetic-field components of an electromagnetic pulse. A mathematical analysis on a similar double-loaded loop, proposed by Kanda (1984), is given in *Chapter* 2. An attempt is made here to extend the analysis such that the ratio of the electric-field strength to the magnetic-field strength may be obtained.

This is an important requirement in EMC applications

Use of the Fourier series expansion method in the analysis of a loop (in particular, one acting as electromagnetic-field probe) immersed in an electromagnetic field, is carried out.

Consider a small circular loop (similar as in Fig. 2-8) arbitrarily loaded by L impedances Z_l at points $\varphi = \varphi_l$ (l = 1,..,L), and is immersed in an electromagnetic-field of an arbitrary structure. The algebraic sum of the currents flowing in the loop depends on both the electric $E_s^1(\omega)$ and the magnetic $H_z^1(\omega)$ component of the travelling wave. These currents are given by:

$$I(\varphi,\omega) = -j\omega\mu\pi b^2 H_Z^1(\omega)W(\varphi,\omega) - 2\pi b E_S^1(\omega)X(\varphi,\omega)$$

$$+\sum^{L} I(\varphi_l)Z_l V(\varphi-\varphi_l,\omega) \qquad (7\text{-}5)$$

where,

$W(\varphi,\omega)$ is the function describing the relationship between the even component of the magnetic field at the loop centre and the electric field tangential to the loop surface.

$X(\varphi,\omega)$ the function describing the relationship between the even component of the electric field (which is equal to the odd component of the magnetic field by virtue of Maxwell equations) at the loop centre and the electric field tangential to the loop surface.

$V(\varphi,\omega)$ the function describing the normalised distribution of currents in the loop.

Probes designed for independent measurements of electromagnetic field components involve antennas loaded at $\varphi = \varphi_1$ and $\varphi = \varphi_2 = \varphi_1 + \pi$ with identical impedances Z_1. Substituting $\varphi = \varphi_1$ and $\varphi = \varphi_2$ in Eq. (5), the following equations for currents flowing in the loop antenna and its loads are obtained:

$$I(\varphi_1,\omega) = \frac{-j\omega\mu\pi b^2 H_Z^1(\omega)W(\varphi_1)}{1+2Y_0Z_1} - \frac{2\pi b E_S^1(\omega)X(\varphi_1)}{1+2Y_1Z_1} \tag{7-6}$$

$$I(\varphi_2,\omega) = \frac{-j\omega\mu\pi b^2 H_Z^1(\omega)W(\varphi_1)}{1+2Y_0Z_1} + \frac{2\pi b E_S^1(\omega)X(\varphi_1)}{1+2Y_1Z_1} \tag{7-7}$$

where:

$$Y_0 = \frac{1}{j\pi\zeta}\left[\frac{1}{a(0)} + \sum_{n=1}^{\infty}\frac{2}{a(2n)}\right] \tag{7-8}$$

and,

$$Y_1 = \frac{2}{j\pi\zeta}\sum_{n=1}^{\infty}\frac{1}{a(2n-1)} \tag{7-9}$$

The term $a(n)$ represents the coefficients of the Fourier series expansion of the kernel of the integral equation describing the current in the loop, and ζ denotes the characteristic impedance of the medium in which the loop antenna is immersed.

From the relationship in Eqs.(7-6) and (7-7), it follows that the summation of the currents (or voltages) across the load of the loop yields a signal which depends upon the

magnetic- field change ($\dot{B}$) alone. Subtracting of the currents or voltages gives a signal depending on the electric-field change ($\dot{D}$).

Thus the designed loop probe in such configuration enables independent measurements of these two components to be made. Therefore, it follows that the sum of the currents flowing in the loop is a measure of the magnetic-field response, while the difference is a measure of the electric-dipole response.

With a double loaded loop antenna, thus described, and acting as a probe sensor, it is possible to measure the two field components separately, both in the frequency domain and in the time domain.

7-3.3 Application of the Double-Loaded Matched Probe

It is proposed that a double-loaded loop, thus analysed and used in this experimental study, can find application in determining the real shape of the magnetic and electric EMP components at the loop centre. In order to achieve this, it is necessary to measure the sum $U_a(t)$ and the difference $U_S(t)$ of the voltages across the loads and as well to know the transfer functions which relate these voltages to the magnetic- and electric-field in the loop centre. The real shapes of the EMP components can be obtained by numerical evaluation, using a method based on the hybridisation of the calculation domain.
Hence:

$$H(t) = \frac{1}{2\pi} \int_{-\infty}^{\infty} \frac{U_a(\omega)}{2P_H(\omega)} e^{j\omega t} d\omega \qquad (7\text{-}10)$$

$$E(t) = \frac{1}{2\pi} \int_{-\infty}^{\infty} \frac{U_S(\omega)}{2P_E(\omega)} e^{j\omega t} d\omega \qquad (7\text{-}11)$$

where:

$P_H(\omega)$ is a transfer function describing the relationship between the components of the voltages across the loads and the magnetic field at the loop centre,

$P_E(\omega)$ is a transfer function describing the relationship between the load voltages and the electric field at the loop centre, and

$U_a(\omega), U_S(\omega)$ are spectra of the voltages $U_a(t), U_S(t)$ respectively.

The transfer function $P_H(\omega)$ and $P_E(\omega)$ incorporated in Eqs. (10) and (11) depend on the following:

- The transfer function of the transmission line $P_l(\omega)$ and the transfer function of the dividers $P_d(\omega)$.
- The transfer function of the antenna for the magnetic field $P_{aH}(\omega)$ and the electric field $P_{aE}(\omega)$.

Thus $P_{aH}(\omega)$ and $P_{aE}(\omega)$ take the form:

$$P_{aH}(\omega) = \frac{\in_H(\omega)}{H_Z^1(\omega)} = -j\omega\mu\pi b^2 Z_0 H_Z^1(0) W(\varphi_1) \qquad (7\text{-}12)$$

and

$$P_{aE}(\omega) = \frac{\in_E(\omega)}{E_s^1(\omega)} = 2\pi b Z_1 E_s^1(0) X(\varphi_1) \qquad (7\text{-}13)$$

Where:

$\in_H(\omega)$ is the electromotive force (*EMF*) at the antenna terminals induced by the magnetic-field and,

$\in_E(\omega)$ is the EMF induced by the electric-field.

7-3.4 Experimental

The characteristics and performance of the new designed semicircular loop approximates that of a half-turn double-loaded loop, when loaded to match the impedance of the measurement equipment. Using this loop, it was possible to provide an independent measurement of the EMP components at an arbitrary point in a measuring volume.

The sum transfer function $P_H(\omega)$ [Figs. 7-9(a)], is the relationship between the sum of the voltages across the loads and the magnetic field at the loop centre.

The differential transfer function $P_E(\omega)$, [Fig. 7-9(b)] is the relationship between the difference of the voltages across the loads and the electric current at the loop centre.

Knowledge of these transfer functions and measured values of the load voltages, (Figs. 7-10(a) sum of load voltages and Fig. 7-10(b) difference of load voltages), enable reconstruction of the real EMP shape, using computer analysis.

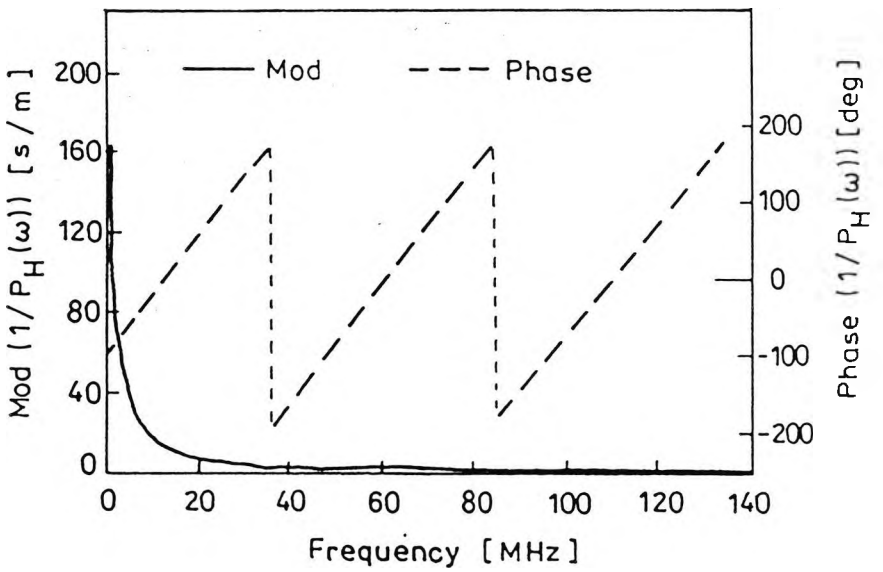


Fig. 7-9(a) Sum transfer function: *Relationship between the sum of the voltages across the load and the magnetic-field at the loop centre.*

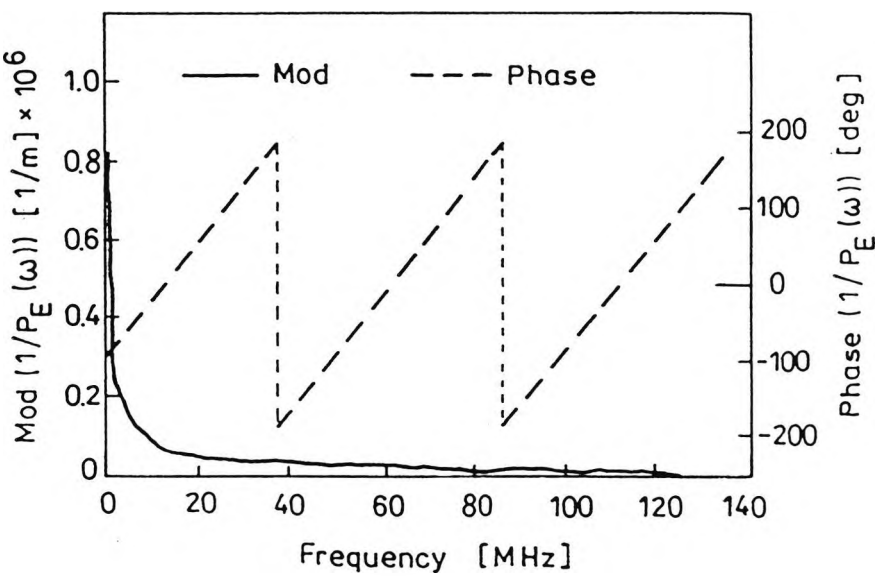


Fig. 7-9(b) Differential transfer function: *Relationship between the difference of the voltages across the load and the electric-field at the loop centre.*

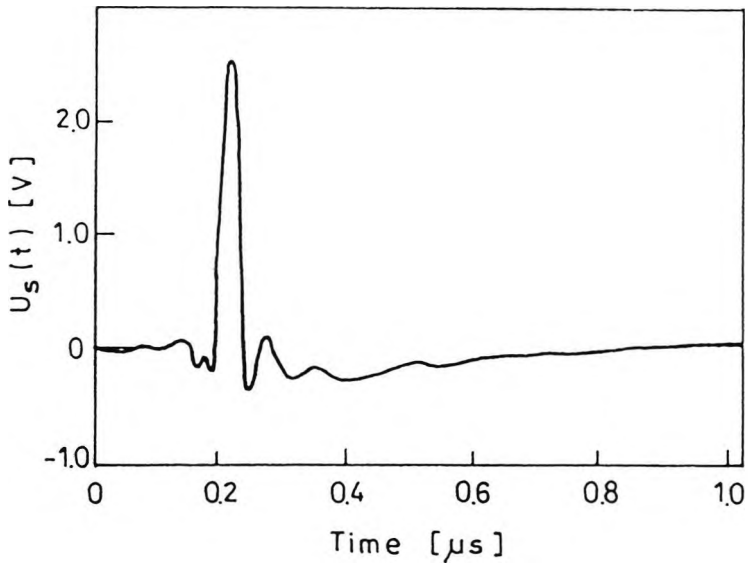


Fig. 7-10(a) Results of measurements:

Sum of the load voltages (probe with double-loaded loop antenna).

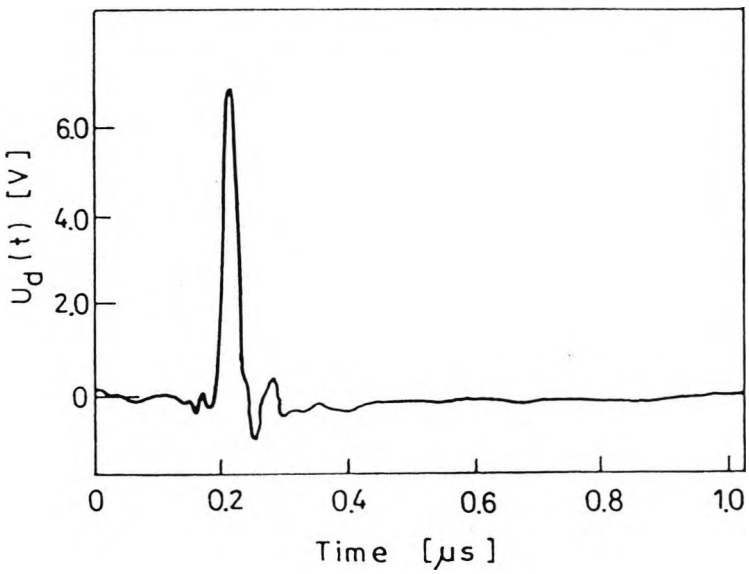


Fig. 7-10(b) Results of measurements:

Difference of the load voltages (probe with double-loaded loop antenna).

The appropriate numerical method enabled reconstruction of the real field shape. In this method, the real EMP shape can be reconstructed by hybridisation of the calculation

domain and making use of the fast Fourier transform (FFT). The results, based on this method, are shown in Fig. 7-11 below:

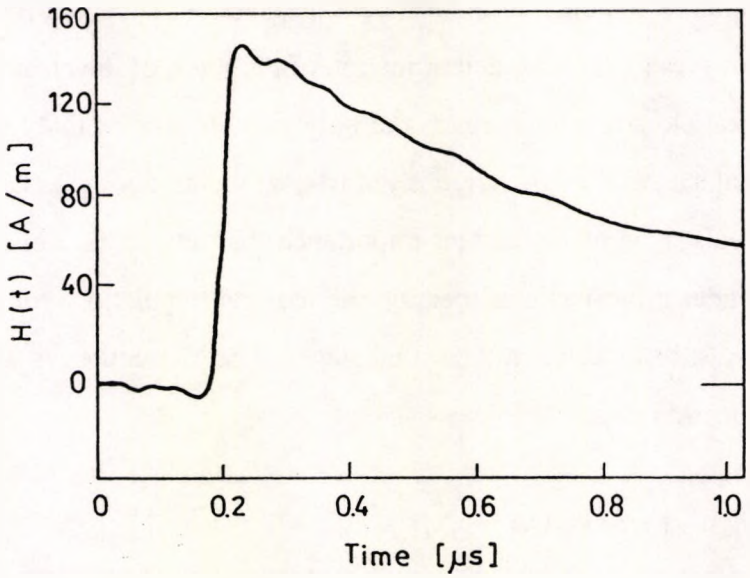


Fig. 7-11(a) Magnetic pulse shape reproduced from the sum of the load voltages shown in Fig. 7-10(a).

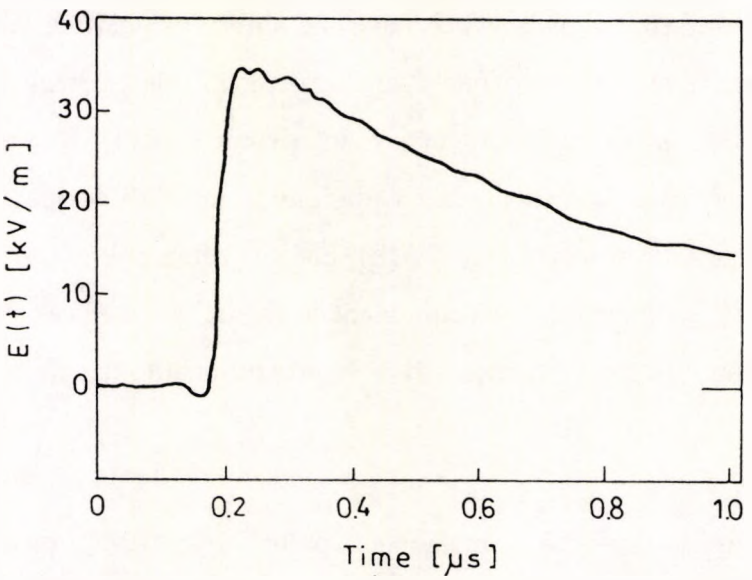


Fig. 7-11(b) Electric pulse shape reproduced from the difference of the load voltages shown in Fig. 7-(b).

7-3.5 Summary

In terms of electromagnetic field metrology, probes with double-loaded loops are particularly attractive. They enable, not only an independent measurement of both EMP components (shown in previous tests), but also determination of the ratio of the electric-field strength to the magnetic-field strength. Perhaps the only reliable tool available to the EMC engineer at the initial stages of a product design, where crucial decisions have to be made, are modelling tools. It is of paramount importance that any feature in the product design which may render it incapable of meeting the required regulations for its intended operation and use, must be detected at the initial stages. The consequences will be disastrous at a later or production stage.

7-4 LOOP PROBES IN EMP/EMC MEASUREMENTS

7-4.1 Introduction - The EMC problem

Electrical and electronic devices and equipment, especially when interconnected together to form a complete system, may emit signals which have the ability to interfere with other devices, or with themselves. These signals are known as electromagnetic interference (EMI) or sometimes as radio frequency interference (RFI) sources. Conversely, the ability of a device to withstand such emissions from other devices or from itself, is called electromagnetic susceptibility (EMS). EMS is often referred to as immunity. Susceptibility of equipment to electromagnetic-fields, as well as the possibilities of biological hazards, is generally assumed to be proportional to the electro-magnetic fields.

The effect of the European directives on Electromagnetic Compatibility (EMC) on the design of many electrical and electronic products, may be summarised, in principle, as both the minimisation of unwanted emissions from the equipment and of the effects of incident radiation on the equipment.

As the number of devices in society and the working environment grows, so does the potential for these devices to interfere in the operation with each other. EMC is a measure of how well they share their EM environment without adverse effects from EMI. The EMC problem, or goal, is to construct electrical equipment with sufficiently low emission and sufficiently high immunity to guarantee electromagnetic compatibility. The definition of sufficiently high and sufficiently low, thus becomes a matter of standards and regulations. In fact, when a reference is made on EMC compliance, it generally means the ability of a system or device to meet standards regulating the amount of EMI that it can emit, and its immunity to EMI.

It is evident that there is a permanent need for companies to reduce a product's time to market, while maintaining, or building on, a reputation for quality. One method of achieving this is to avoid post-prototype modifications by utilising advanced design method and computer-based tools. It is therefore clear that a product has to be designed to conform to the required regulation with regards its intended application at the beginning of production. European legislation (EC Directive 1989), for example, requires all electrical equipment and devices to meet certain EMC criteria. It is here that the powerful packages now available for electromagnetic simulation come into force.

7-3-2 Computational Modelling Techniques

Two well known modelling techniques which are almost always used in EMI analysis are:

1. Transmission line modelling(TLM), and
2. Numerical Electromagnetic Code (NEC)

These modelling techniques are based on the methods of moments, the finite-element method, the finite-difference time-domain method, the transmission line matrix and the generalised multipole techniques. An examination of typical EMC environment shows that three broad features are found in all problems.
These are:

1. Electromagnetic interference originates from non-ideal sources of complex structure. Although it is sometimes possible to assume a plane wave incident on the object or device, subject to an electromagnetic hazard (EMH), [and thus the actual details of the source can be ignored] it is, in general, necessary to take into account the exact nature of the source. This is particularly true for EM coupling calculations in the near-field region.
2. Radiation couples through structures of complex shape, e.g. apertures, slots and various wire penetrations. Analytical solutions are possible in some simple systems, while in others which are not, the complex nature of electromagnetic coupling must be taken into account.
3. Propagation of electromagnetic energy in real systems may take place in a multi-conductor environment, where coupling, cross-talk and non-linear loads contribute to the nature and severity of electromagnetic interference.

It is clear that a numerical simulation method must be capable of describing arbitrary shapes in a variety of materials, includes lossy materials. It must also have comprehensive excitation and output facilities. It must be computationally efficient and since EMC modelling problems are complex and can often only be solved after approximations have been made, it must remain physically meaningful to the user.

Every EMC laboratory must be equipped with certain tools that are considered more or less essential. Spectrum analysers or specialised EMI receivers, for example, are standard equipment. High speed oscilloscopes, field probes, copper tape and ferrite cores are also basic tools. However, these items are only useful when the user has some type of representative.

During the initial product design phases, where many crucial decisions have to be made, the only tools available to the EMC engineer are modelling tools. Computer modelling tools can be particular helpful for anticipating and analysing a variety of EMC problems. To this end, focus is made in EMC applications of Numerical Modelling Technique. The term *numerical techniques* encompasses methods that solves integral and differential equations numerically in order to calculate field quantities.

Most of the development work and research in numerical modelling has been driven by the needs of antenna and microwave engineers, who rely heavily on numerical electromagnetic modelling tools to analyse and help to evaluate new designs or design modifications. The widespread use of these techniques has spawned a growing electromagnetic software industry.

Unfortunately, numerical modelling codes have not yet had the same impact in the field of EMC that they have had in other areas of electromagnetics. A major reason for this is the complexity of most EMC problem configurations. A printed circuit card, for example, might have well over a hundred components. It is not practical to model every detail, and yet it is difficult to predict which details can be neglected. Another problem has been that most numerical modelling codes were developed for antenna or microwave applications. These codes may lack the necessary features to analyse even relatively simple EMC configurations.

Each numerical modelling technique is best suited for a particular class of application. Peng and Balanis (1993) described two of the most widely used moment method codes in modelling the interference between two wire antennas on a helicopter of complex shape. The numerical electromagnetic code (NEC) and the electromagnetic surface patch (ESP) codes can be used to analyse a variety of configurations consisting of wires, plates and lumped-circuit elements.

Djordjevic and Sarkar (1993) and Aksun and Mittra (1993) described method moment techniques applied to analyse different aspects of integrated circuit and printed circuit board geometries. Naishadham and Nutison (1993) also applied this technique with particular emphasis on the *asymmetric* or *common-mode* radiation.
Leuchtmann and Bomholt (1993), described a more recent code based on generalised multipole technique where the expansion functions are analytic solutions of the fields generated by multipole sources. The finite-element method is a widely used EM modelling technique. Laroussi and Costache (1993) introduced this technique and some of its EMC applications.

Two time-domain techniques, namely, the transmission line matrix method and the finite-difference time-domain (FDTD) method have been the object of much attention recently because of their exceptional power and flexibility. Christopoulos and Herring (1993) presented an overview of transmission line matrix method and showed how it could be used to model EMC configuration. Tirkas *et al.* and Li *et al.* (1993) described the FDTD method and its application to two different EMC problems. (Omick and Castillo (1993), presented a new electromagnetic modelling technique. It is a finite-difference technique, operated in the time-domain, but is designed to have fewer dispersion problems than standard FDTD techniques that are based on the Yee algorithm.

This new technique could potentially be applied to a number of EMC problems involving fast transients that are difficult to model with existing methods.

7-4.3 The Nature of EMI

Basically, EMI is any unwanted or undesirable signal, or any signal that can cause undesirable effects on the performance of a system or device. Such signal can arise intentionally or unintentionally.

Whenever the voltage or current in a circuit is altered, an electromagnetic signal is created. The circuit does not have to be man-made and in the case of a nuclear explosion or lightning strike, a tremendous amount of EMI can be generated. The signal may propagate along the conductive components of the circuit and from there via any power or interconnecting cables to other circuits, or it may be emitted into free space as radio-frequency radiation.

Generally, equipment can be divided into two main categories:

1. Intentional radiators consists of devices such as broadcast radio and television transmitters, citizen's band and amateur radio transceivers, mobile and cellular telephones, radar and navigation systems, etc., wherein a radio-frequency (RF) signal is deliberated emitted.

2. This category consists of unintentional radiators such as computers, domestic appliances, video, stereo and TV, office electrical equipment, electronics test equipment, fluorescent lamps, dimmer switches, power tools (with or without variable speed control) and power lines.

In the consideration of EMC it is quite common to think only of the interference caused by continuous repetitive phenomena such as unmodulated radio frequency (RF) signals, but other quasi or non-repetitive waveforms exists and the direct measurement of these waveforms are also desirable.

7-4.4 EMC Measurements

Presently, there is a considerable amount of interest in developing a new method to measure the radiated emissions from devices and equipment. Ideally, such measurements should be carried out in open space. However, open space test ranges are not only expensive to maintain, but also suffer from the effects of ground reflections.

The widespread use of LSI and VLSI circuits in telecommunications and information technology has noticeably increased their EMP vulnerability. To improve the electromagnetic susceptibility of electronics devices it is necessary to carry out continuous investigations. These include the parameters of EMI originating from a variety of sources, already mentioned and those produced by the simulators themselves which are widely used in EMS testing.

Measurements of EMS parameters generally involve electrically small linear antennas or loop probes. The majority of probes, however, enable measurements of one field component only to be made, (i.e. electric or magnetic). Simultaneous measurements of both field components are often necessary, and hence the design of the new resistively loaded loop antenna. This kind of loop can also determine the electric to the magnetic-field strength ratio. Knowledge of this ratio in the measuring volume of a simulator, permits investiga- tion of how the device under test (DUT) affects the electromagnetic field distribution.

7-4.5 Shielding Performance

The importance of EMC in the design of high-speed and high frequency electronic devices is continuously increasing. In this context, electromagnetic shielding for protection of electronic equipment and systems against EMI, is a matter of growing concern to the industry.

In practical situations, the most important factors in degrading the shielding efficiency are apertures for cable interconnections, displays and for ventilation. In general, the degrading effects of apertures, slots and seams on the total shielding efficiency is some order of magnitude larger than, for example, the effect of the finite conductivity of the shield. Moreover, far-field conditions are often not fulfilled in practical shielding applications; for instance a high frequency connector shield, where the outgoing electromagnetic radiation may be concentrated. This results in a near-field region with localised high field strength which must be taken into account.

Therefore, in order to obtain a good understanding of the near-field shielding behaviour of perforated shields, a near-field analysis of a periodic structure of apertures in a conducting flat screen should be considered. Two major difficulties arising from this analysis are:

(1) An objective near-field characterisation method for shielding performance is needed and should be based on clear, unambiguous criteria, and

(2) Accurate experimental evaluation of the shielding efficiency should be relatively simple to perform.

As far as the characterisation procedure is concerned, this is rather straightforward when the far-field conditions are met. Analysis of flat perforated screens have been carried out over the last decade, (Chen, 1970), (Cwik and Mittra, 1985) and (Scott, 1989), using the concept of shielding effectiveness.

7-4.6 Shielding Effectiveness

A shielding effectiveness (SF) may be defined by considering two consecutive situations. First a reference geometry is calculated and/or measured, where the shield is omitted. Next the same geometry is considered but with the shield placed between the two loops, one acting as a radiator and the other as a detector. The ratio of the maximum field intensity in the shielded configuration *to* the field intensity at the same position in the unshielded configuration, gives a measure of the near-field shielding performance. That is:

$$SE(f) = \left(\frac{\left| e_{emf}[f, x_{\max}, y_{\max}, z_1] \right|_{unshielded}}{\left| e_{emf}[f, x_{\max}, y_{\max}, z_1] \right|_{shielded}} \right) \qquad (7\text{-}14)$$

where,

$x_{\max}$ and $y_{\max}$ are the co-ordinates at which e_{emf} reaches a maximum in the shielded configuration and for a fixed z value $(z = z_1)$.

The measured position with maximum field strength is derived from the two-dimensional field patterns, although other extensions are possible. The measurements can be repeated for different positions of the radiating loop to define the worst configuration in shielding effectiveness. Moreover, scanning data over a complete plane allows, by way of integration, to derive the corresponding far-field data, (Laroussi and Costache 1994).

A near-field analysis, despite its necessary practical applications, has not received much attention so far. Only a few cases of near-field shielding problems have been investigated. Bannister(1968) and Moser (1988) studied the electromagnetic leakage through infinite, homogeneous shields (without apertures) due to electric and magnetic dipole sources. This geometry was also analysed by Yang and Mittra (1985) and Nishikata and Sugiura (1992) using an alternative technique which is based on the plane-wave spectral representation of the radiated fields of the dipole sources. Later, Criel *et al.* (1994) extended this geometry to the application of perforated screens. In all these cases, a basic geometry as defined and used in this experimental work, was considered..

7-4.7 Experimental

In some types of EMC testing of enclosures for shielding performances, a radiating antenna could be placed inside the enclosure and a receiving antenna or detector, placed outside. If there is any electromagnetic leakage then this will be detected by the coupling antenna and measured. The existing line set-up was used for this work with only a slight modification. The directional coupler, mounted near the mid-section on the earth plane was removed (centre part unscrewed) thereby leaving a hole (the aperture). A similar corresponding ring was soldered onto a sheet which was attached to the earthplane and the centre part (with facility to accommodate a loop probe) was screwed back again. [Refer to constructional details of the directional coupler in *Chapter* 4]. The co-ordinate origin is chosen in the centre of the aperture and the co-ordinate axes were parallel.

The geometry, in principle, is shown in Fig. 7-12.

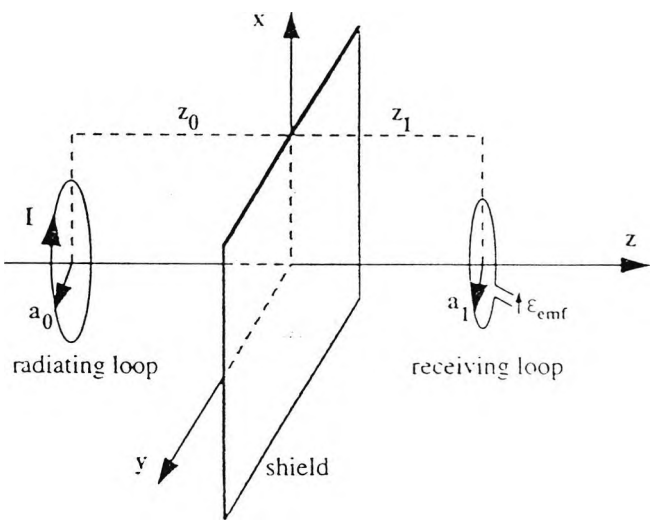


Fig. 7-12 Geometry of coupling through an aperture for shielding measurement.

The line was matched into its characteristic impedance and then excited with a fast transient pulse which was allowed to propagate along the line. When the pulse impinged on the loop, the fields created caused a small voltage to be induced in the loop.

The principle is similar to the previous tests on the line , only in this case, the voltage induced in the loop is small due to the field coupling through the small aperture. A result is shown in Fig. 7-13 for a pulse excitation of 1 kV on the line.

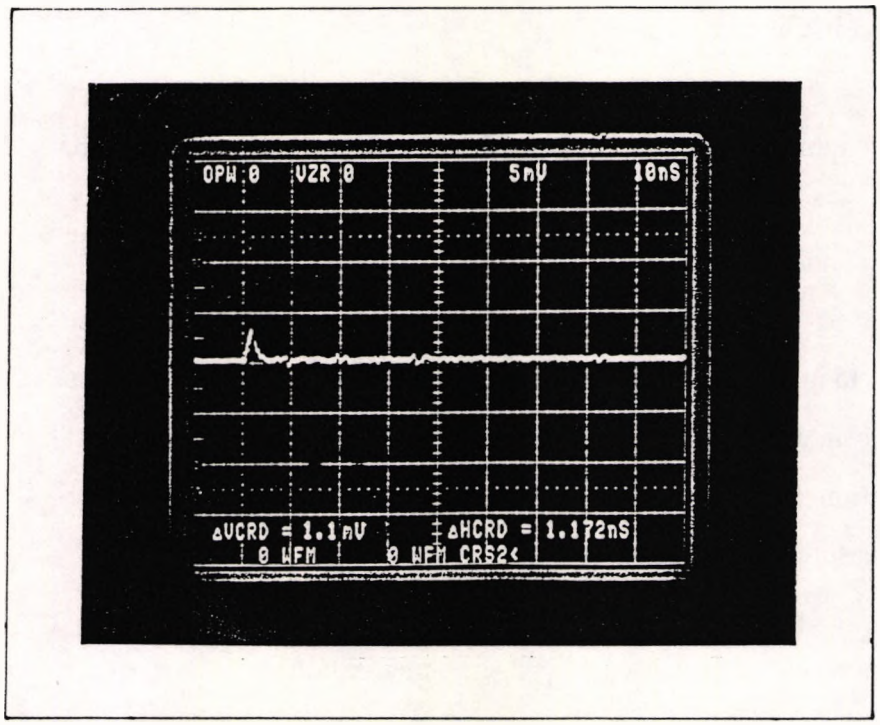


Fig. 7-13 Results of electromagnetic coupling through an aperture.

Apertures are widely used as efficient antennas (Elliot 1981), (Cockrell 1976), but owing to this characteristic, they are sources of electromagnetic interference problems, both for radiated emission and for susceptibility. In fact slots used for cooling purposes and cable connections, degrade the shielding effectiveness of the metal enclosures.

There is at presently, considerable interest in the continued development of analytical and numerical methods to approach this electromagnetic problem, which demonstrates the importance of accurate prediction of electromagnetic-field coupling through apertures.

Approximation can sometimes be effectively used according to the geometry of the wavelength. At low frequencies, a quasi-static approach (Casey 1981, 1985), allows an accurate analytical description of the field penetration inside the shielded region.

Although the work reported here in not conclusive, it demonstrates another important application of the loop probe in detecting unintentional radiation from an enclosure. Further work is continuing in this area.

Criel *et al.* (1994) extended this technique in a laboratory based fully automatic measurement system, in which a three-dimension positioning robotics arm was able to move/adjust the device under test, using a workstation control unit. During the measurements, the radiating loop was excited by the signal generator at discrete frequencies. The second loop was attached to the positioning system, converting the transmitted field pattern into the corresponding output voltages which was post-processed by the workstation. In this way, three dimensional field patterns and the near-field performance was measured with high accuracy and flexibility.

Fig. 7-14 show a good agreement of the measured and simulated results.

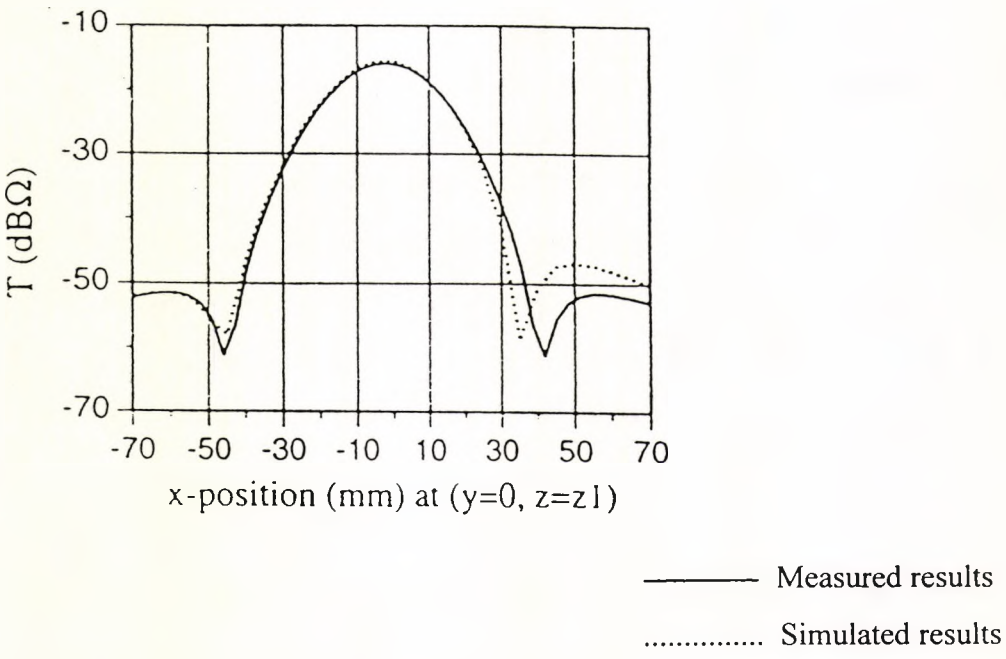


Fig. 7-14(a) Reference geometry: intersect parallel to the *x*-axis.

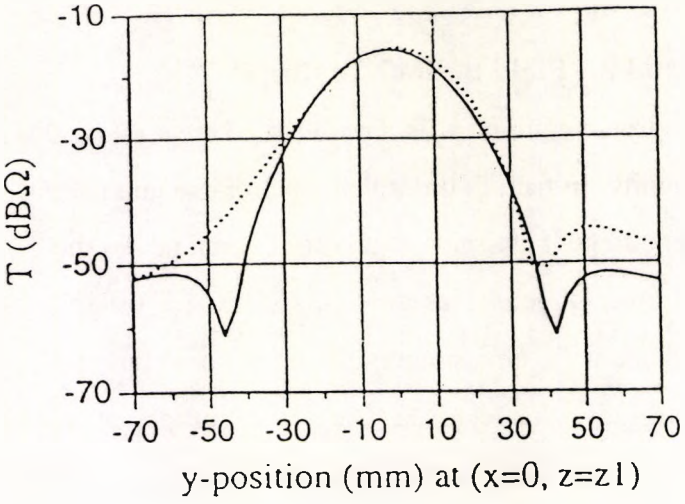


Fig. 7-14(b) Reference geometry: intersect parallel to the *y*-axis.

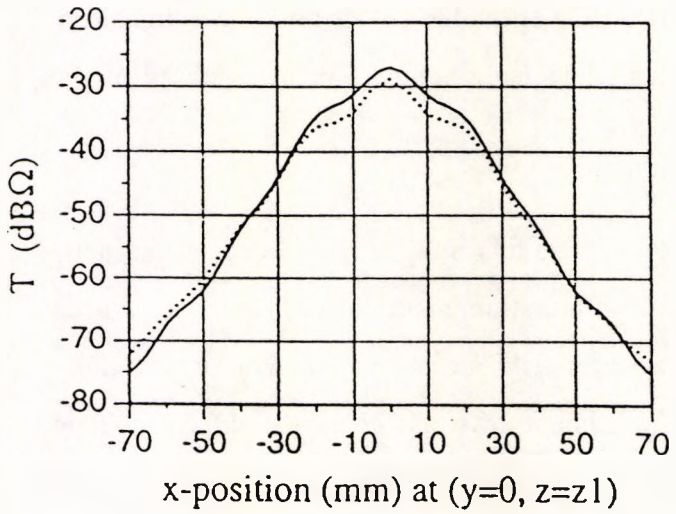


Fig. 7-14(c) Shielded geometry: intersect parallel to the *x*-axis.

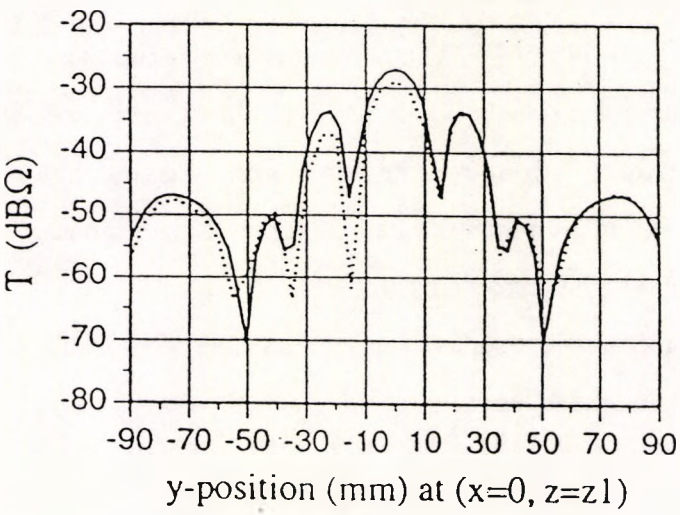


Fig. 7-14(d) Shielded geometry: intersect parallel to the *y*-axis.

7-4.8 Discussions on Near-Field and Far- Field in EMC Testing

Characterisation of interference from electronic equipment is a problem of great interest to be addressed by the EMI/EMC community. In fact, in order that electronic equipment be approved for use, it must comply with stringent emission regulations contained in the FCC Part 15 rules for the US, and such other directives as the 89/336/EEC for the EC and the VCCI program in Japan. Compliance with emission regulation requires that the radiation from electronic equipment be fully characterised when the equipment is operating under normal conditions. These regulations, among other things, require that the radiated parasitic field levels be kept under specified maxima over a range of distances. Depending on the device under test (DUT), these distances can fall anywhere between the near-field (NF) and the far-field (FF) of the DUT. It is possible to transform emitted field levels from one initial set of field measurements in the vicinity of the radiating equipment to any distance away from it.

The theory and best manner to proceed to achieve this transformation depend on many factors. Several approaches, depending on configuration, nature of DUT, etc., have been developed to predict far-field values from near-field measurements. This is especially true for antenna characterisation. An algorithm known as the near-field to far-field transform was developed by Laroussi and Costache (1994), which shows several advantages in this approach. The amount of measurement data is reduced to only one set in the NF from which the rest of the information can be computed. The extent to the areas that have to be scanned to sample the field are mush smaller when they are closer to the DUT (i.e., the NF) than when they are in the FF. The computed results can also pinpoint localised maxima that may otherwise never be identified with direct measurements in the far-field. The computation of FF from NF measurements bypasses the problems and requirements of direct FF measurements such as open range, good characterisation of the sight attenuation and logistic problems.

Sarkar (1990), used an approach based on equivalent surface currents reconstructed from the field measurements on a sphere enclosing the antenna.

In both EMI/EMC testing and antenna characterisation, the radiation takes place in homogeneous space where the analysis greatly simplifies the theoretical part of deriving an NF-FF transfer algorithm. In most cases however, due to the complexity of the radiating structure itself, the algorithm has to be implemented numerically.

Chapter 8

Signal Interface Methods

As an extension to the research programme schedule, two interface methods, namely, the General Purpose Interface Bus (*GPIB*) and an Optically Coupled (*OC*) Interface, were developed to enhance the measuring technique in terms of accuracy, efficiency, convenience and economy. These are described as follows:

8-1 GENERAL PURPOSE INTERFACE BUS (GPIB)

8-1.1 Introduction

The GPIB interface, also known as the IEEE-488 interface, is a hardware device and a valuable addition, designed to be installed in a slot of a personal computer (PC). The interface system uses sixteen lines as follows:

- eight *data* lines
- three *handshake* lines and
- five *bus* management lines.

Information is transferred over the bus in a bit-parallel, byte serial format using an asynchronous 'handshake' procedure. This handshake allows communication between instruments with different transfer rate, if they conform to the handshake state diagrams and other protocols defined in the IEEE-488 standard.

The data transfer rate is effectively limited by the slowest active instrument (talker or listener) on the bus. This ensures the accurate transfer of data to and from all active instruments.

The GPIB system can be connected in either a star or linear configuration, or in a combination of both. This is illustrated in Fig. 8-1. To maintain the electrical characteristics of the bus, a device load must be connected for each two metres length of cable, and atleast half of the devices connected to the bus must be powered up.

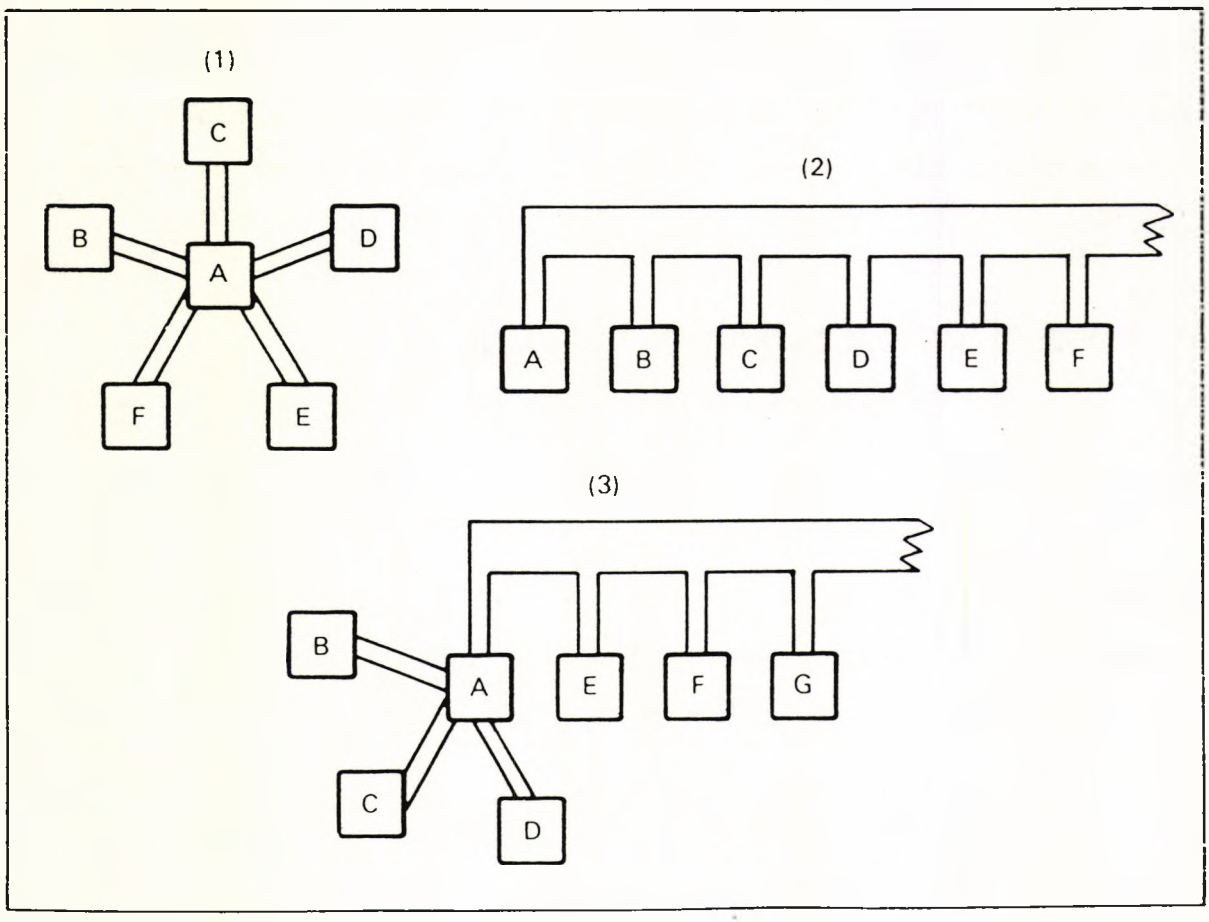


Fig. 8-1 GPIB system configurations.

The minimum requirement for a GPIB system would consists of the device and a GPIB controller. The controller detects all command and data transfer on the GPIB. A large GPIB system may consist of up to fifteen instruments distributed over a total cable length of up to 20 metres. These instruments may include, in addition to the device and controller, other talkers (e.g. counters, digital multimeter, oscilloscope, etc.) and other listeners (e.g. line printer, tape drive, programmable signal generator, etc.).

8-1.2 GIPB Interface Messages

All of the many possible messages that may be sent over the GPIB can be divided into two main classifications:

1. Interface messages
2. Device-dependent messages

Interface messages are sent by the GPIB controller to the other instruments on the bus to control the functions of each instrument's GPIB interface. Device-dependent messages (e.g., instruments commands, data, etc.) may be sent by any instrument on the bus, to any other instrument (s) on the bus. This arrangement is shown in Fig. 8-2.

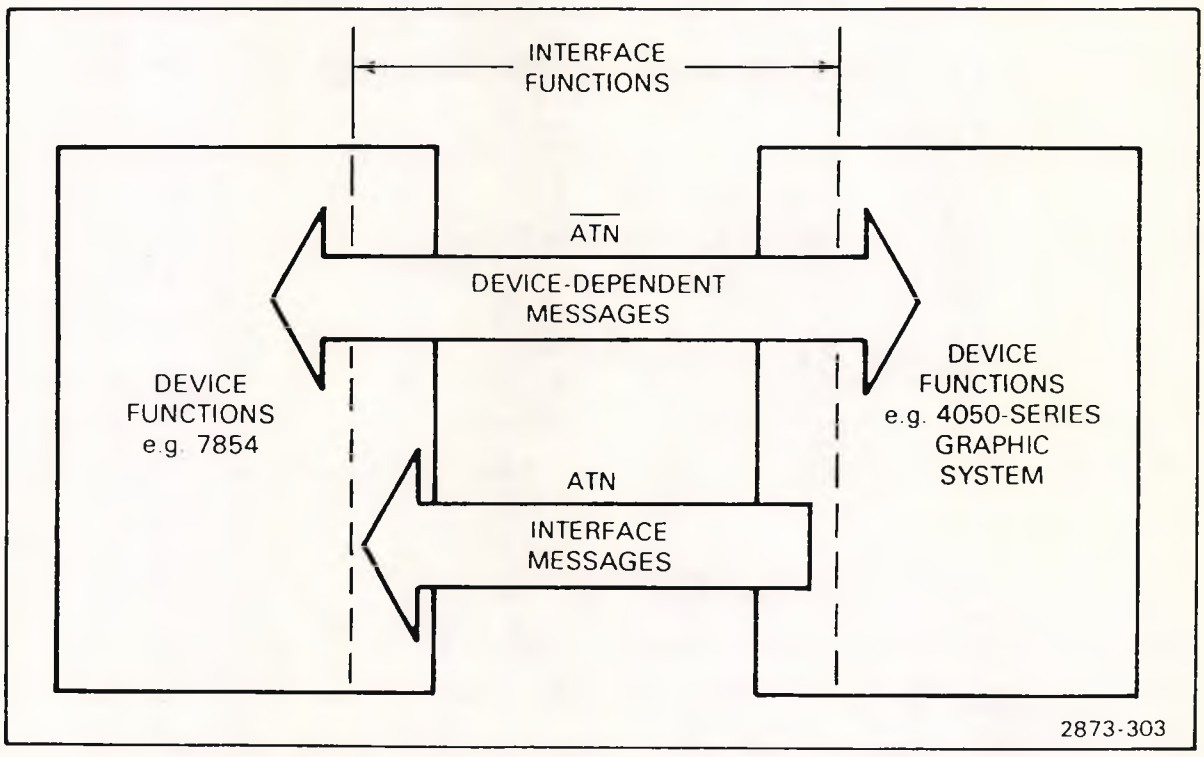


Fig. 8-2 Device-dependent messages versus interface messages.

The IEEE-488-1978 standard that the IEEE-488 card implements, is the most widely used international standard for information transfer between computer and electronic instruments. These standards are well documented in numerous articles, publications and user reference manuals, (PCL-848A/B IEEE-488 Reference Manual).

8-1-3 (GPIB) Theory

The Standard IEEE 488-1978 is a complete description of the GPIB interface. A brief description is summarised below:

8-1.3.1 Signal Lines

The GPIB contains three groups of signal lines, namely,

1. Data
2. Handshake
3. Bus control

The eight data lines (DI0 through DI8) are used to carry both interface messages and device-dependent messages.

The asynchronous, three-wire handshake is controlled by these lines:

- DAV (Data Valid) - asserted by the transmitting device.

- NRFD (Not Ready For Data) and NDAC (Not Data Accepted) - asserted by the receiving device.

The five interface control lines are used for the following functions:

- ATN (Attention) - specifies how data on the DI0 lines is to be interpreted: as interface messages when asserted or device-dependent messages when unasserted.

- IFC (Interface Clear) is used to initialise the interface functions of all instruments and return control to the systems controller.
- SRQ (Service Request) is used to request service from the controller.
- REN (Remote Enable) allows remote control of devices on this bus.
- EOI (End Or Identify) indicates the last byte of a message.

8-1.2 The Handshake

The data and handshake lines are used for the source and acceptor handshake. Infact, there are two parts of the same handshake. Fig. 8-3 shows the states of these lines as they are set by a talker using the source handshake, and a listener, using the acceptor handshake. Note that the timing diagram relates the electrical signals on the bus to the states of the source and acceptor handshakes. By looking at both, it may be easier to grasp the sequence of the interlocked handshakes than to absorb, by themselves, the state diagrams in the standard.

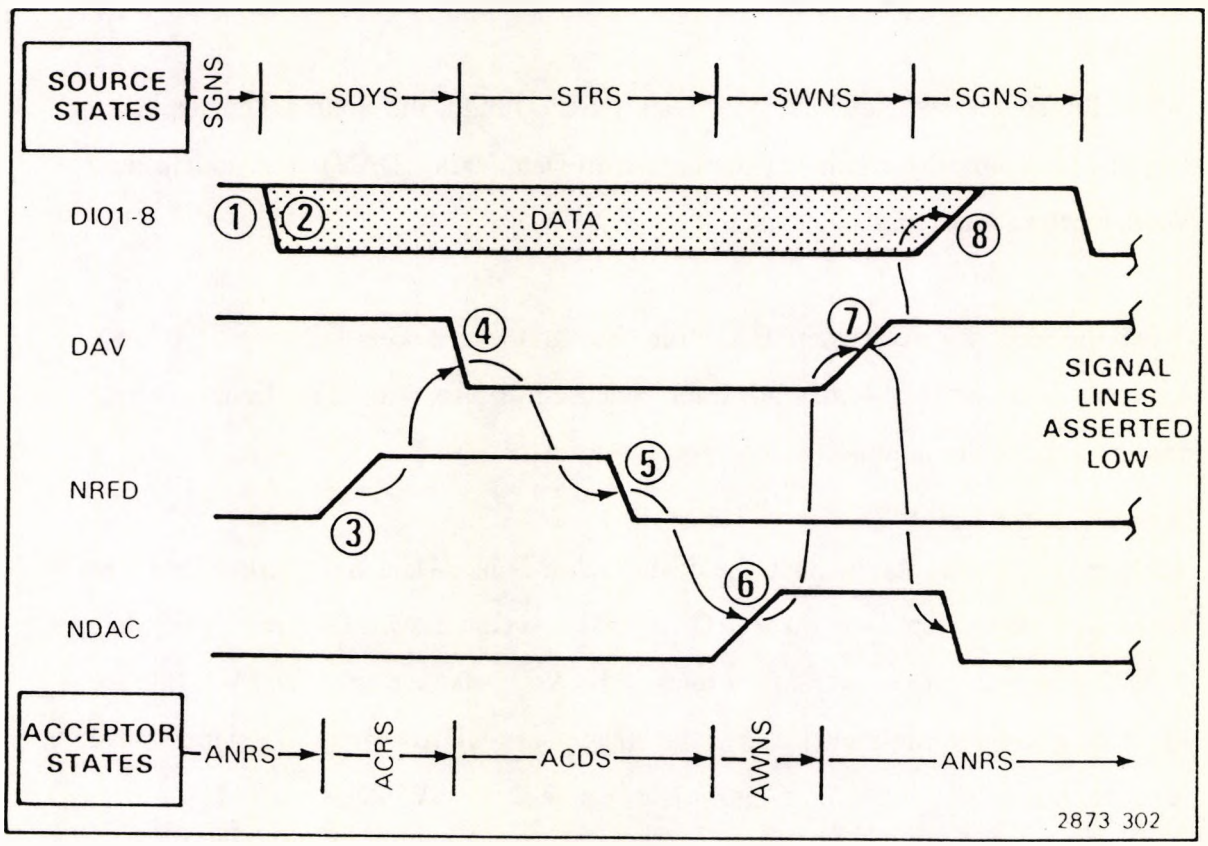


Fig. 8-3 Source and acceptor handshake sequence.

1. To commence, the source goes to the Source Generate State (SGNS). In this state, the source is not asserting a data byte on the data lines or Data Valid (DAV). When no bus data is asserting a line, the line rises to a high level set by the bus terminating network. The acceptors are in the Acceptor Not Ready State (ANRS), asserting both Not Ready For Data (NRFD) and Not Data Accepted (NDAC). In this condition, NRFD and NDAC are both low (asserted).

2. The source sets the data byte on the data lines and enters the Source Delay State (SDYS). If this is the last data byte in the message, the source asserts the End Or Identify (EOI) line at the same time. The source waits for the data to settle on the line and for all acceptors to reach the Acceptor Ready State (ACRS).

3. Each acceptor *says*, "I'm ready" by releasing Not Ready For Data (NRFD) to move to the Acceptor Ready State (ACRS). This is one of the points in the handshake designed to accommodate slower listeners. Any acceptor can delay the source handshake by asserting NRFD.

4. When the source *see* Not Ready for Data (NRFD) high, the Source Transfer State (STRS) is entered by validating the data with Data Valid (DAV). The source then waits for the data to be accepted.

5. When the receiving devices *see* DAV true, they go to the Accept Data State (ACDS). Each device asserts Not Ready For Data because it is busy with the current data byte and is not ready for another.

6. As each device accepts the data, the device releases Not Data Accepted (NDAC) to move from the Accept Data State (ACDS) to the Acceptor Wait for New Cycle State (AWNS). Again, all receivers must release the Not Data Accepted (NDAC) line for the source to see a high level. When the source sees NDAC high (all listeners have accepted the data), the Source Wait for New Cycle State (SWNS) is entered.

7. In the SWNS, the source unasserts Data Valid (DAV). This causes the acceptors to proceed to the Acceptor Not Ready State (ANRS), their initial state in the handshake. In ANRS, they asserts Not Data Accepted (NDAC).

8. The source continues to the Source Generate State (SGNS), its initial state in the handshake, to prepare a new byte for transmission.

The IEEE-488 interface card provides the hardware (electrical and mechanical) and software for interfacing a PC to the IEEE-488 bus. The software is packaged in read-only-memory (firmware) to provide versatile and easy to use IEEE-488 function extensions for current programming language or operating system. Firmware cannot be accidentally erased or overwritten and it is always available for use by application programs.

A program was written for this purpose. There are several advantages in this set-up, one obvious one is that more than one instruments can be connected at different points within a network and measurements taken simultaneously. High accuracy in obtained in this manner since changes such as supply fluctuations and contact problems can take place during disconnecting and reconnecting the instruments' test probes/leads.

8-1.4 The Test Procedure

The line set-up as before was used for this test, with the output from the loop probe connected to the oscilloscope. GPIB cables were used to interface a Datron Autocal precision digital voltmeter (DVM) and the Tektronics 7854 sampling oscilloscope (both fitted with corresponding GPIB connectors) with a computer for the measurement control. The devices were connected in a linear configuration as shown in Fig. 8-1(2).

On testing, the oscilloscope measured the waveform while the DVM measured the peak output voltage simultaneously. A typical result of a 415 ps pulse front is shown in Fig. 8-4. Although these readings are comparable, the digital voltmeter gave a more accurate reading than could be measured from the waveform.

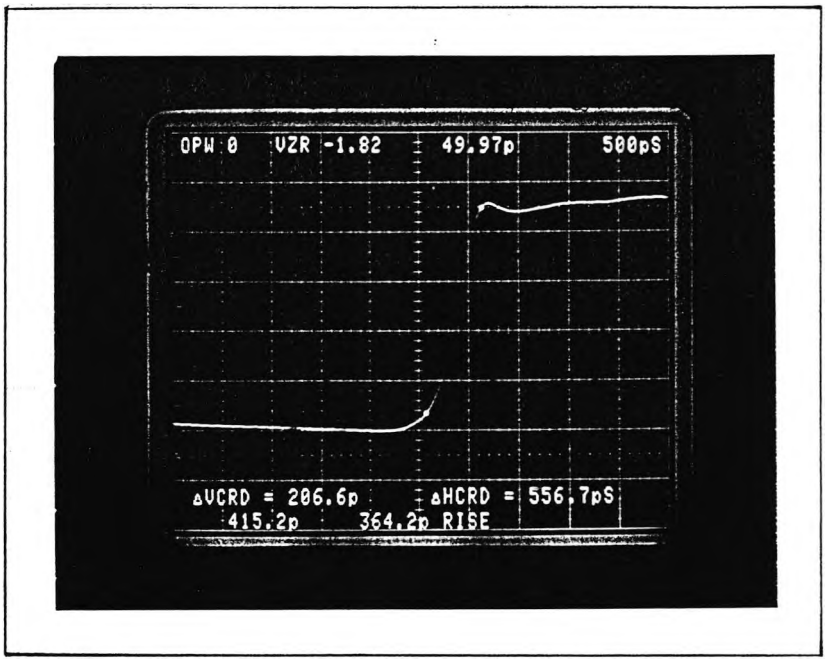


Fig. 8-4 Pulse front measurement.

8-1.3 Summary

This technique was found to be very useful especially when comparative measurements in small changes, such as for attenuation losses and variations due to pulse sharpening condition were made. Large numbers of results can be taken, stored in memory then plotted as necessary to give hard copies which are very cheap compared with expensive polaroid photographs. Once in the computer's memory, relevant mathematical functions and analyses can be performed. These calculated results and waveform data can be easily sent via the *E*-mail (electronic mail) link to other interesting parties working or collaborating in the area of study.

The author is presently communicating on a regular basis with two such parties, Dr. W. Daum from General Electric Research Laboratory, Schnectady, New York and Prof. Dr. A. Braumstein, Tel Aviv University, Israel.

The Tek 7854 used in the measurement in this experimental work embodies a software package and waveform calculator and thus is capable of performing waveform parameter analyses. With simple programs written, these analyses were also performed on a P.C.

8-2 OPTICALLY COUPLED (*OC*) INTERFACE

8-2.1 Introduction and Review

In an optical system, the signals are transmitted in the form of photon (light) which have no electrical charge, and therefore cannot be affected by the electric-fields as experienced in high voltage environments, during lightning discharges, or high power switching transients. Similarly, high magnetic-fields from electrical machines, transformers, etc. have no adverse effect on optical transmission. There are no problem of crosstalk, as the leakage flux which may occur at the fibre boundary interface is retained by the opaque primary jacket, ensuring that optical signals cannot interfere with each other when fibres are in close proximity.

This factor also guarantees security of transmission, for the signal cannot be detected externally throughout the length of the fibre.

Optical technology has progressed at a rapid pace during recent years. Its applications have extended into most medical and industrial fields focusing primarily on data communications for measurement and control. Research and development are now being conducted in many related technology areas.

Protective systems operated exclusively by digital technology and information networks are being widely employed in power distribution systems using optical local area network (LAN). As a result there is a growing need for the development of systems using sensors that can be easily mounted on existing equipment.

Fast current and voltage pulse measurements are now being incorporated in optical technology.

8-2.2 Features of Optical Communications

The following features of fibre optics communications may be summarised:

- Freedom from electromagnetic interference
- Freedom from crosstalk
- Security in transmission
- Elimination of sparking and fire hazard
- Electrical isolation
- Absence of ground loops
- Low weight coupled with high strength
- Increased bandwidth and lower losses at high frequencies than in coaxial cables.

The inert nature of optical fibres means they can tolerate most kinds of weather and be immersed in many different fluids. Their low weight and small size is useful in many applications. Complete electrical isolation is a distinct benefit, giving more freedom in the design of the transmitter and receiver and ensuring the elimination of ground loop problems. However, and probably by far, the major advantage is bandwidth. In either coaxial or parallel-conductor cable, the bandwidth varies inversely as the square of the length, while in fibre optic cables, it varies inversely as the length.

8-2.3 Optical Fibres - Review

Optical fibres transmit light by the phenomenon of total internal reflection and can propagate for long distances because the absorption coefficient is extremely small for the wavelength used.

Although a ray of light is totally internally reflected, it does not penetrate into the outer layer cladding. This effect is important because it can lead to losses in the cladding. It also reduces the time required for a ray that is not parallel to the axis to reach the end of the fibre because the ray travels faster in the cladding.

In a planar dielectric only those rays whose components, normal to the core-cladding interface that form standing waves, are allowed to propagate. Thus, there are a finite number of transverse modes that propagate, and for a very thin dielectric (1 to 2 μ m width) only a single transverse mode can propagate. This dielectric is called *single mode* dielectric and the other dielectrics are called *multimode* dielectrics.

Because the allowed rays have different path lengths, they will arrive at the end at different times if they travel in a core with a uniform index of refraction. This causes a pulse to broaden and therefore limits the data rate that can be transmitted by the fibre. This effect, called modal dispersion, can be greatly reduced by using a graded index fibre. The index decreases towards the edge so that the longer path length rays, which spend more time near the edge of the core, will have a greater velocity. When the index profile is optimised, it can reduce the modal dispersion by more than two orders of magnitude.

The other type of dispersion is wavelength dispersion, and it is due to the variation of the index of refraction with the wavelength. Atoms in the fibre act as oscillating dipoles that interact with light and the interaction is stronger for blue light as it is for red. As a result, n for blue light is larger than n for red light. The wavelength dispersion is reduced by operating at lower wavelengths ($\cong 1.3$ μ m) and by using a laser source instead of a light-emitting diode LED source. The bandwidth of the laser emission is much less for a laser.

Only those rays that have a large angle of incidence($>i_c$) at the core cladding interface will be totally internally reflected. As a result, only a small amount of light from the light source will be transmitted down the fibre. More light can be put into the fibre by a laser diode that by an LED and more light can be put in by an edge-emitting LED than by a face-emitting LED. This is because an edge-emitting LED emits more highly collimated light.

Two electro-optic processes that produce loss in fibres are scattering and absorption. Scattering is caused by oscillating atomic dipoles being driven by the electric-field of the incident wave that emits electromagnetic energy in directions not parallel to the incident

beam. Electrons can absorb light and thereby be excited into a higher energy state. Electrons in the transition metals such as iron, copper and chromium are particularly effective in doing this in the wavelength region of interest, and therefore, must be kept below the parts per billion range if the fibre is to be of high quality. There are also losses due to mechanical effects.These include bending, separation, displacement and rotation at a joint. Loss due to bends is not great unless the radius of the curvature of the bend is of the order of 100 times the fibre core.

8-2.4 Planar Dielectric - Total Internal Reflection

Consider the light propagation in the planar dielectric shown in Fig. 8-5.

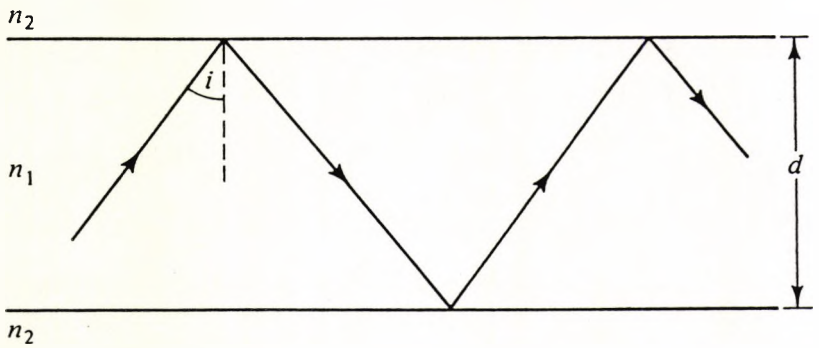


Fig. 8-5 A ray in a planar dielectric that is totally internally reflected.

The planar dielectric is two-dimensional and lies in the *x-z* plane. The inner core has an index of refraction that is larger than that of the outside cladding ($n_1 > n_2$), and a ray will be totally reflected back and forth if the angle of incidence is larger than the critical angle ($i > i_c$). It can be shown that all of the light is reflected when ($i > i_c$) by considering the Fresnel equations for reflection, which can be written:

$$r_{\perp} = \frac{n_1 \cos i - n_2 \cos t}{n_1 \cos i + n_2 \cos t} \tag{8-1}$$

and

$$r_{//} = \frac{n_1 \cos t - n_2 \cos i}{n_1 \cos t + n_2 \cos i} \tag{8-2}$$

when ($n_1 > n_2$).

Using Snell's law,

$$\cos t = (1-\sin^2 t)^{1/2} = \left[1-\left(\frac{n_1}{n_2}\right)^2 \sin^2 i\right]^{1/2} = -jB \tag{8-3}$$

when ($i > i_c$).

By choosing -j rather than +j (since this predicts the true physical behaviour as the beam attenuates into the cladding for $i > i_c$) eq. (8-1) can be written as:

$$r_\perp = \frac{n_1/n_2 \cos i + jB}{n_1/n_2 \cos i - jB} = \frac{A+jB}{A-jB} \tag{8-4}$$

Clearly $r_\perp$ is complex with a magnitude of one and thus all the light is reflected.

Equation (8-4) can be expressed in terms of the phasors shown in Fig. 8-6.

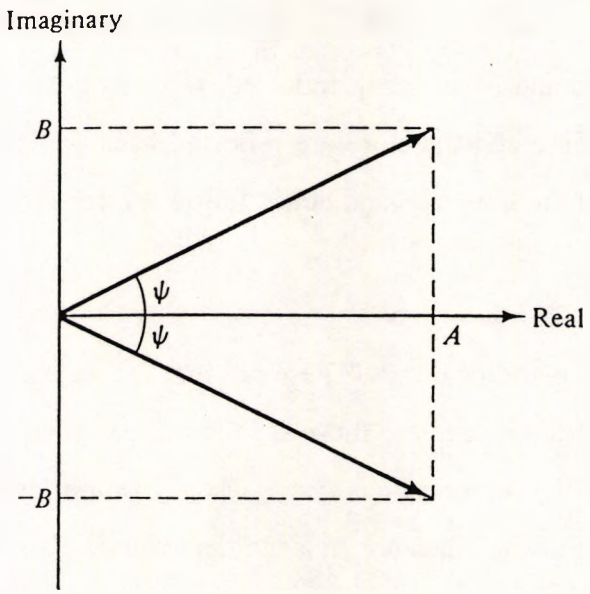


Fig. 8-6 Phasor representation of *A+jB and A-jB.*

That is:
$$r_\perp = \frac{\cos\psi_\perp + j\sin\psi_\perp}{\cos\psi_\perp - j\sin\psi_\perp} = \frac{e^{j\psi\perp}}{e^{-j\psi\perp}} = e^{2j\psi\perp} \tag{8-5}$$

Where,

$$\tan\psi_\perp = \frac{B}{A} \tag{8-6}$$

Physically, this equation means that all of the light is reflected and there is a phase change of 2ψ ; the reflected ray leads the incident ray by 2ψ .

Using a similar procedure, it can be shown that:

$$r_{//} = e^{2j\psi_{//}} \tag{8-7}$$

and,

$$\tan\psi_{//} = \left(\frac{n_1}{n_2}\right)^2 \tan\psi_{\perp} \tag{8-8}$$

Even though the beam is totally reflected, it does not penetrate through the cladding.

8-2.5 Propagation Modes

The rays that propagate in the fibre are often broken down into three sets namely, the *central* ray, *meridional* rays and *skew* rays. The central ray is parallel to the fibre axis which travel directly down the fibre and never being reflected, whereas the meridional rays pass across the centre of the fibre and therefore are reflected back and forth in a plane. The skew rays never intersect the fibre axis and hence follow a three-dimensional path.

Basic fibre theory is concerned with meridional rays. These fall into two categories, low order and high order modes. Low order modes are those rays launched at small angles within the acceptable angle, while high order modes occur when rays are launched at large angles. Single-Mode fibres result when the core area and the numerical aperture are so small that only one mode can propagate.

Other modes of propagation do exist, but these do not affect the basic theory. One important mode is the *transverse* mode.

8-2.5.1 Transverse Modes

A ray can be broken up into its z-component parallel to the dielectric axis and its x-component normal to the core-cladding interface. Only those rays whose x-components form standing waves can propagate, since only they constructively interface with each other. As a result, only a finite number of rays, or modes, are allowed to propagate.

The path length travelled by the ray reflected up and back is $2d$, where d is the core width of the planar dielectric shown in Fig. 8-7, and the ray is reflected twice during this interval. The incident angle is define as ϕ in this *Chapter*.

The phase difference δ, for this path length difference is given by:

$$\delta = (2\pi)2\frac{d}{\lambda_0 / (n_1 \cos\phi_m)} - 4\psi = 2m\pi \tag{8-9}$$

since the effective wavelength in the x-direction is $\lambda_0 / (n_1 \cos\phi_m)$, where λ_0 is the wavelength in a vacuum. The change must be an integral multiple of 2π for there to be constructive interference of the x-components, and 4ψ is subtracted because δ is a phase lag and 4ψ is a phase gain. Solving for the allowable value of ϕ, ϕ_m, it can be shown that:

$$\cos\phi_m = \frac{\lambda_0}{2\pi n_1 d}(m\pi + 2\psi) \tag{8-10}$$

since,

$$\cos\phi_m \le \left[1 - \left(\frac{n_2}{n_1}\right)^2\right]^{1/2} \tag{8-11}$$

$$m \le \frac{2n_1 d}{\lambda_0}\left[1 - \left(\frac{n_2}{n_1}\right)^2\right]^{1/2} - \frac{2\psi}{\pi} = \frac{V - 2\psi}{\pi} \tag{8-12}$$

The quantity V is often called the normalised film thickness. It can be shown that for a planar dielectric symmetric about the core axis, $m \ge 1$.

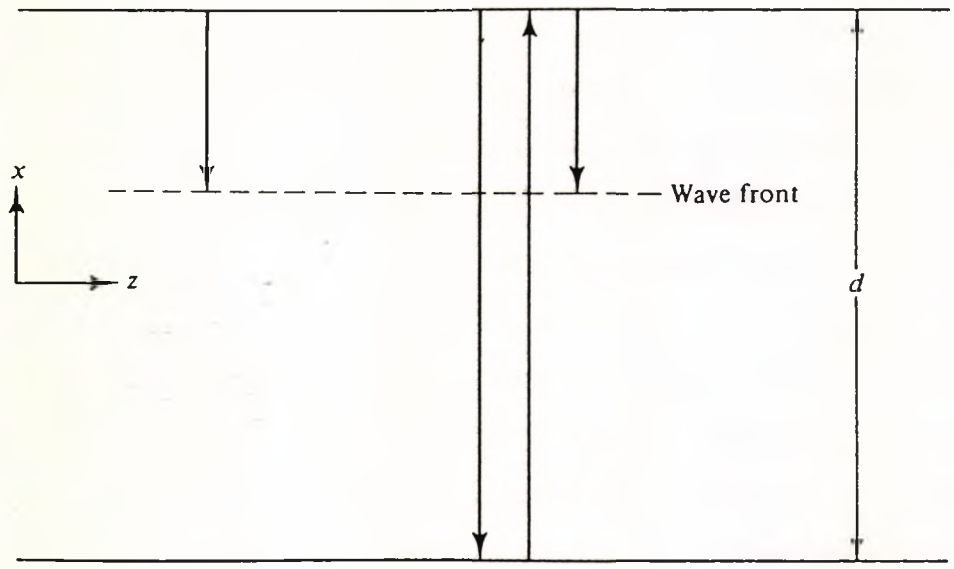


Fig. 8-7 The x-component of the doubly reflected wave must have a phase that is an integer multiple of 2π greater than that of the unreflected ray since the x-components form standing waves.

Note the x-component of the doubly reflected wave must have a phase that is an integer multiple of 2π greater than that of the unreflected ray, since the x-components form standing waves.

8-2.6 Dispersion

Two types of dispersion, namely *material* and *modal* are encountered in fibres which limit bandwidth. Material dispersion results from the fact that different wavelengths travel at different velocities in the same medium. Consequently, the various wavelengths launched simultaneously within the flux will not arrive at the receiver simultaneously, but will suffer time dispersion due to differences in travel time. This effect can be reduced by using an emitter with a narrow spectrum of emission, e.g. a laser.

Modal dispersion is caused by the difference in path length between low order modes and high order modes. In a true modal dispersion, wavelength dispersion causes the signal to broaden thereby limiting the data rate. The longer wavelength light travelling in the same path as the shorter wavelength light will travel faster and therefore will arrive sooner at

its destination. The difference between the time of arrival of the slowest and fastest moving waves is a representation of the pulse broadening.

Modal dispersion can be reduced in step-index fibres by decreasing the numerical aperture to allow only the lower modes to propagate. In graded-index fibre the effect is compensated for by the high order modes travelling faster in the lower-index regions, so that the time differential between high and low order modes is not as large in graded-index fibres as it is in step-index fibres.

Dispersion is generally only a problem in long distance communications and consequently graded-index fibres, although more costly than step-index fibres, are used in these applications in conjunction with lasers. For shorter distances (<500 m) and/or lower bandwidth, step-index fibres are favoured for lower costs and easier coupling methods.

Values for $n(\lambda)$ can be computed from the Cauchy's phenomenological equation:

$$n = A + \frac{B}{\lambda^2} + \frac{C}{\lambda^4} \tag{8-13}$$

where the values of A, B and C are found from the experimental values of n at different wavelengths as shown in Table 8-1.

Table 8-1 Index of refraction of solids for different wavelengths in the visible

Substance	Violet (410 nm)	Blue (470 nm)	Green (550 nm)	Yellow (580 nm)	Orange (610 nm)	Re (660
Crown glass	1.5380	1.5310	1.5260	1.5225	1.5216	1.52
Light flint	1.6040	1.5960	1.5910	1.5875	1.5867	1.58
Dense flint	1.6980	1.6836	1.6738	1.6670	1.6650	1.66
Quartz	1.5570	1.5510	1.5468	1.5438	1.5432	1.54
Diamond	2.4580	2.4439	2.4260	2.4172	2.4150	2.41
Ice	1.3170	1.3136	1.3110	1.3087	1.3080	1.30
Strontium titanate ($SrTiO_3$)	2.6310	2.5106	2.4360	2.4170	2.3977	2.37

8-2.7 Step Index Fibres

A step index fibre is one for which the index of the core n_1, is constant and is larger than the index of the cladding n_2, as shown in Fig. 8-8. Because $n_1 > n_2$, there is total internal reflection for $\phi > \phi_c$ just as there was for a planar dielectric. The step index fibre differs from the planar dielectric only in that it is two-dimensional with a circular cross section.

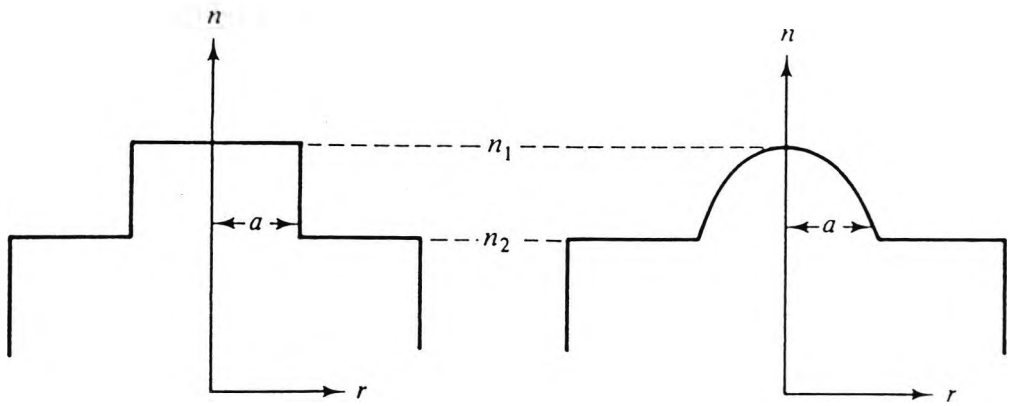


Fig. 8-8 The index profile: (a) step index, and (b) graded index fibres.

The meridional ray illustrated in Fig. 8-9(a) is one that passes through the centre of the fibre and as a result, follows the same saw-tooth planar path followed by the rays in the planar dielectric. The skew ray illustrated in Fig. 8-9(b) is one that does not pass through the centre and as a result, follows a three-dimensional path.

In terms of mode description of the electromagnetic radiation in the fibre, the meridional rays correspond to the TE_{1m} and TM_{1m} modes. The two subscripts are necessary since they are two dimensional. The skew rays correspond to what are called HE_{1m} and EH_{1m}. The first term describes which field dominates and the subscript 1, a measure of how tight is the helix.

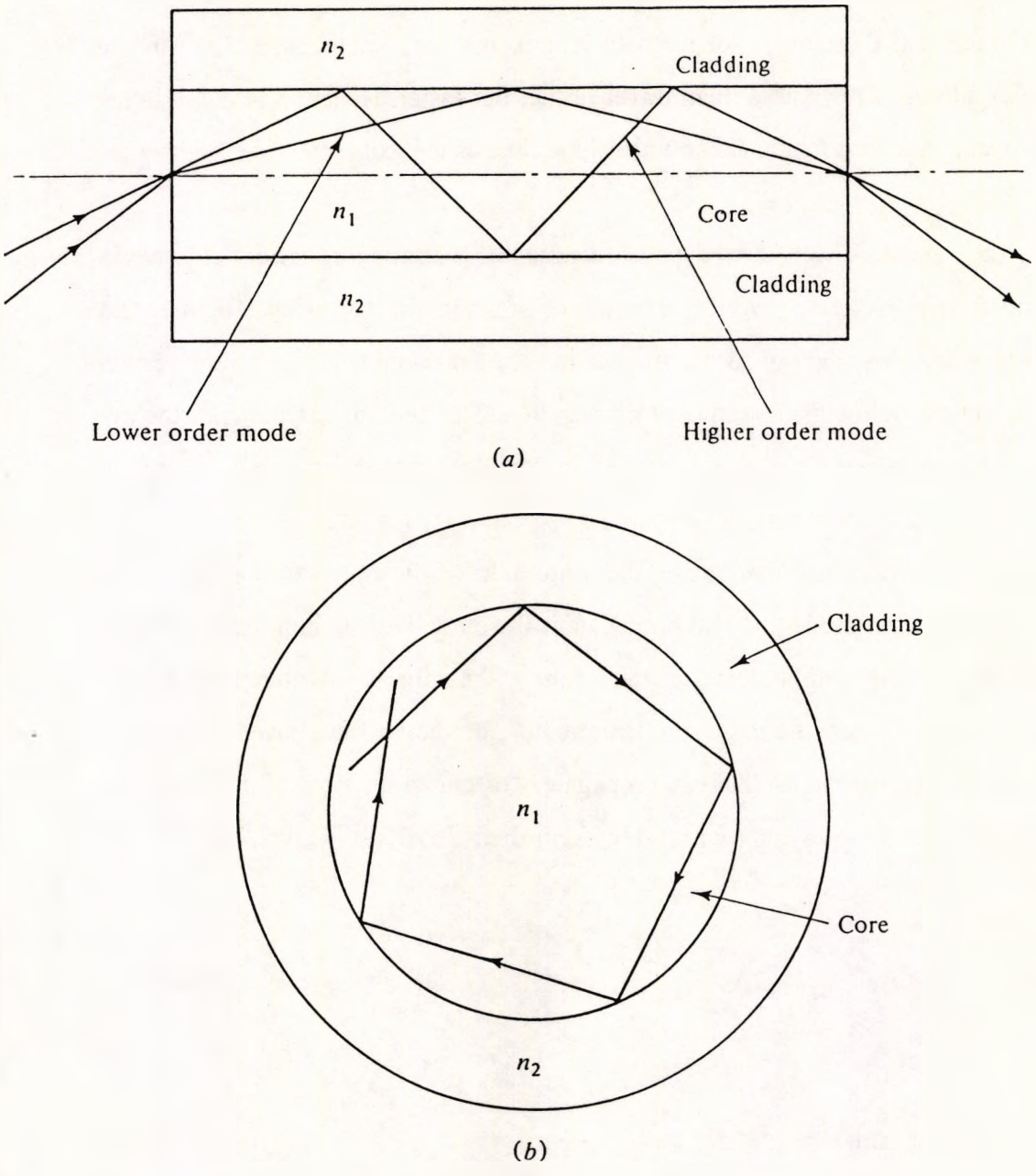


Fig. 8-9(a) The planar ray path of meridional rays, and **(b)** The three-dimensional path of a skew ray.

8-2.8 Graded Index Fibres

The index of the core in graded index fibre, illustrated in Fig. 8-8 has a maximum value at the centre and decreases towards the edges. The advantage of using this type of fibre is that the modal dispersion can be greatly reduced. The axial ray travels the shortest distance, but it moves the slowest since it sees the largest average index of refraction.

The off axis meridional rays move in sinusoidal paths. The higher order modes have a larger amplitude and therefore a longer path length, but they spend more time in the lower index material. This makes them travel farther but faster. Hence, it is possible for them to arrive at their destination at about the same time as the axial ray.

Physically, the rays follow a curved path because the vibrating electric field sees a different index of refraction above the direction of propagation than it does below and for a ray above the axis, the ray sees a smaller index of refraction. Thus it slows down when it is vibrating below the direction of propagation. This braking effect bends the ray down For propagation below the axis, the ray is continually bent upwards.

The input angle of incidence determines the amplitude of the ray path and the mode order. The highest order mode that will propagate is the mode with an amplitude equal to the fibre radius. If the amplitude is greater than *a*, then the ray will not be totally internally reflected. Clearly the larger the fibre radius, the larger the allowed amplitude and larger the number of modes that can propagate. To match the time of arrival of the different modes, the variation in $n(r)$ must be controlled closely. It is given by:

$$n(r) = n_1\left[1 - 2\Delta\left(\frac{r}{a}\right)^{\gamma}\right]^{1/2} \tag{8-14}$$

where

$$\Delta \cong \frac{n_1 - n_2}{n_1} \tag{8-15}$$

with n_2 being equal to $n(a)$.

8-2.9 Light Insertion

Only light that is totally internally reflected travels very far in an optical fibre. Thus, only the rays that make an angle of $\theta \leq \theta_c$, the critical fibre axis in Fig. 8-10, propagate down the fibre. From Snells law:

$$\sin\theta_c = \frac{n_1}{n_0}\sin(\pi/2 - \phi_c) = \frac{n_1}{n_0}\cos\phi_c \qquad (8\text{-}16)$$

when the index of the material adjacent to the fibre is n_0. From Eq. (8-11), using the equality sign:

$$\sin\theta_c = \frac{(n_1^2 - n_2^2)^{1/2}}{n_0} \qquad (8\text{-}17)$$

The numerator is often called the numerical aperture (NA) and it decreases as n_2 approaches n_1.

Semiconductor light emitters are used for fibre optic light source because they can be made as small as the cross section of the optical fibres. This is a particular stringent condition for single mode fibres, which have radii of only a few microns.

Not only should the diameter of the light source be smaller than the fibre diameter, it is preferable for it to emit collimated light.

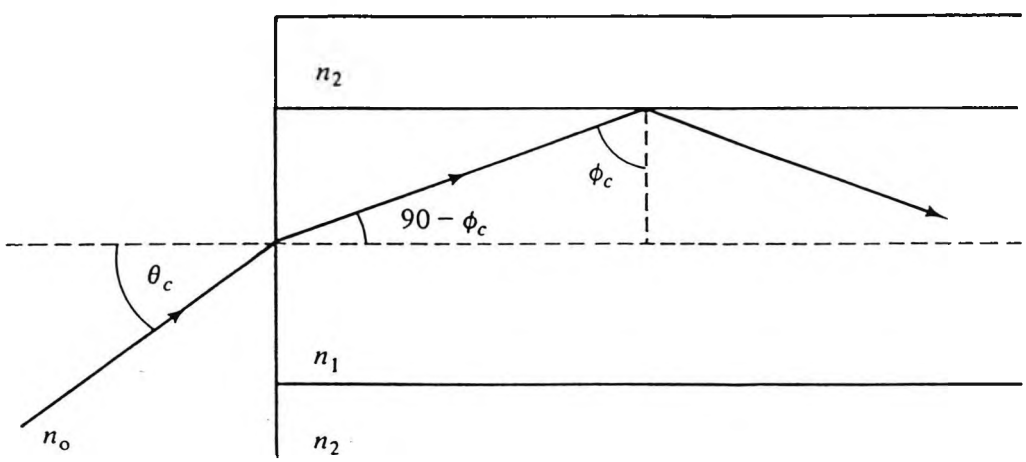


Fig. 8-10 Diagram used to determine the critical input angle and numerical aperture.

8-2.10 Transmission Losses

There are four main causes of transmission losses in optical fibres, namely:

1. Material absorption
2. Material scattering
3. Scattering due to irregularities at the core-cladding interface
4. Mechanical effects

8-2.10.1 Material Absorption

Material absorption is caused by molecular impurities within the core of the fibre which absorb certain wavelengths. High purification processes during manufacture limit the problem, but can be very costly. Alternatively, a suitable emitter is chosen whose peak wavelength corresponds approximately to the spectral region of maximum transmission of the fibre. Plastic fibres, for example, generally have minimum absorption between 630 and 670 nm and are therefore recommended to be used with visible red emitters.

8-2.10.2 Material Scattering

In discussing dispersion, the atoms can be described as harmonic oscillators that were driven by the oscillating electric field of the travelling wave. These oscillating dipoles behave as antennas, and therefore they emit radiation, but not in the direction of the primary beam. For the conservation of energy the beam energy is attenuated by the amount of energy not radiated in the direction of the primary beam. This loss is called scattering loss.

Material scattering is also caused by particle impurities and by fluctuations in temperature and composition (*Rayleigh scattering*) which interrupts the reflection path of the light rays. Further scattering is caused by irregularities at the core-cladding and subsequently loss of energy on reflection.

8-2.10.3 Mechanical Effects

Curvature of the fibre may also contribute to losses which is small if the radius of the curvature is much larger than the radius of the fibre, as is usually the case. When the fibre is bent, the input beam making an angle θ_c with the fibre interface, now makes an angle $\phi < \phi_c$ with normal to the cladding so it is no longer totally internally reflected. It is therefore necessary to find the angle ϕ'' for which the ray in the fibre makes an angle of θ_c with the normal to the cladding. The loss is then the energy of the beams making an angle with the fibre interface between ϕ_c and ϕ''. The fraction of the energy loss at the bend, using ray theory with the aid of Fig. 8-10, can be shown to be:

$$\frac{\Delta E_{loss}}{E} = \frac{2n_1 a}{R} \frac{\sin^2 \phi_c}{\sin\theta_c \cos\phi_c} \qquad (8\text{-}18)$$

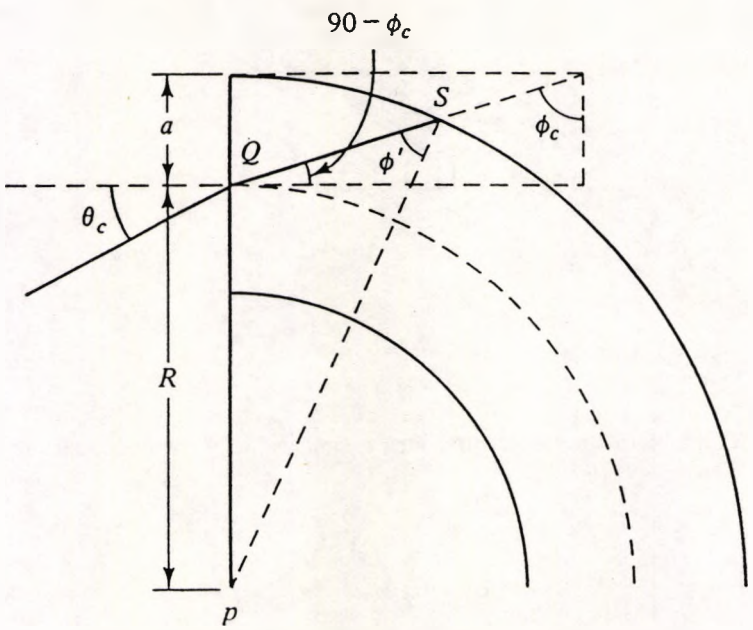


Fig. 8-11 Diagram used to calculate the loss at a bend ($\phi'' < \phi_c$)

Other sources of mechanical losses occur at a joint or termination. They are due to a displacement of the axes, a physical separation of the two ends, a rotation of the axes and surface roughness at the joint.

A common type of connector is the resilient ferrule shown in Fig. 8-12. The alignment is achieved by pressing the tapered ferrules into a tapered bushing. When the ferrule

contains an emitter or detector, the ferrule is held in place with a press plate. When two optical fibres are coupled, a threaded cap is used.

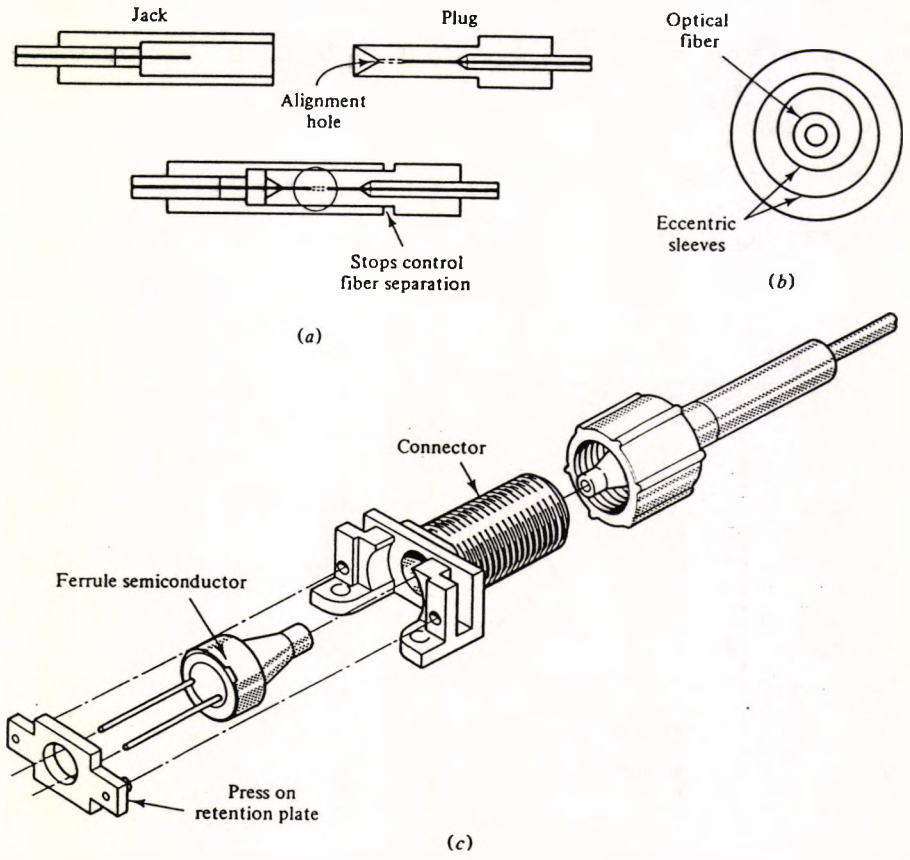


Figure 2-27 The (*a*) tube, (*b*) double eccentric, and (*c*) semiconductor ferrule connectors.

Fig. 8-12 A semiconductor ferrule connector.

8-3 Fibre Optics Communication - A Proposed Application

The vicinity surrounding high voltage (HV) equipment such as an impulse generator in an HV laboratory, may be regarded as a hostile electromagnetic environment. Although there are changes towards digital techniques in impulse voltage measurements, the traditional method is by use of a multistage capacitive or resistive dividers. The reduced

voltage at the lowest stage is usually a few hundred volts with respect to earth. This is fed directly to the deflecting plates of a specialised high voltage oscilloscope which is normally placed in an interlocking screened room within the laboratory. The operator is safe and can communicate with the controller who is at the viewing gallery in a virtually interference free environment.

However, it is far from a desirable position being in a screened room during testing, especially in the light of present concern to the exposure of the human body to high levels of electromagnetic radiation, (Baochu and Maohua 1991), (Garbe *et al.* 1992) . Hence, an optical coupling device was developed for this application in which case, a standard measuring oscilloscope could be used.

8-3.1 Optical Test Procedure

An analogue optical transmitter and receiver modules as opposed to a digital system were built with discret components using a suitable emitter and detector. These were mounted on separate printed circuit board (pcb). Although digital techniques are by far more superior (they do not have drift or noise problems) the analogue technique was less expensive and quite adequate for the intended bandwidth of operation. Moreover, the emphasis was on the optical transmission of the induced loop voltage and not in the measurement accuracy of the interface method.

Each unit was placed inside a small screened box with the appropriate *BNC* and *SMA* connectors. The transmitter module was battery powered as a precaution against the introduction of possible interference problem into the system, since it was used in a hostile electromagnetic environment. A high frequency (HF) amplifier was incorporated in the receiver, due to the low level input signal. The units were tested with regards bandwidth, noise and distortion, mainly a contributory factor due to the circuit components layout and tracks arrangement. The results were excellent, even well above the intended operating range.

The transmitter unit was easily connected to a directional coupler as these are fitted with *BNC* output connectors. This is shown in the photograph in Fig. 8-14. The two devices were interconnected with a 20 m 150 μ m fibre optics cable. (The 20 m corresponds to the distance between the coupling transducer in the hostile electromagnetic environment and the oscilloscope on a less hostile one).

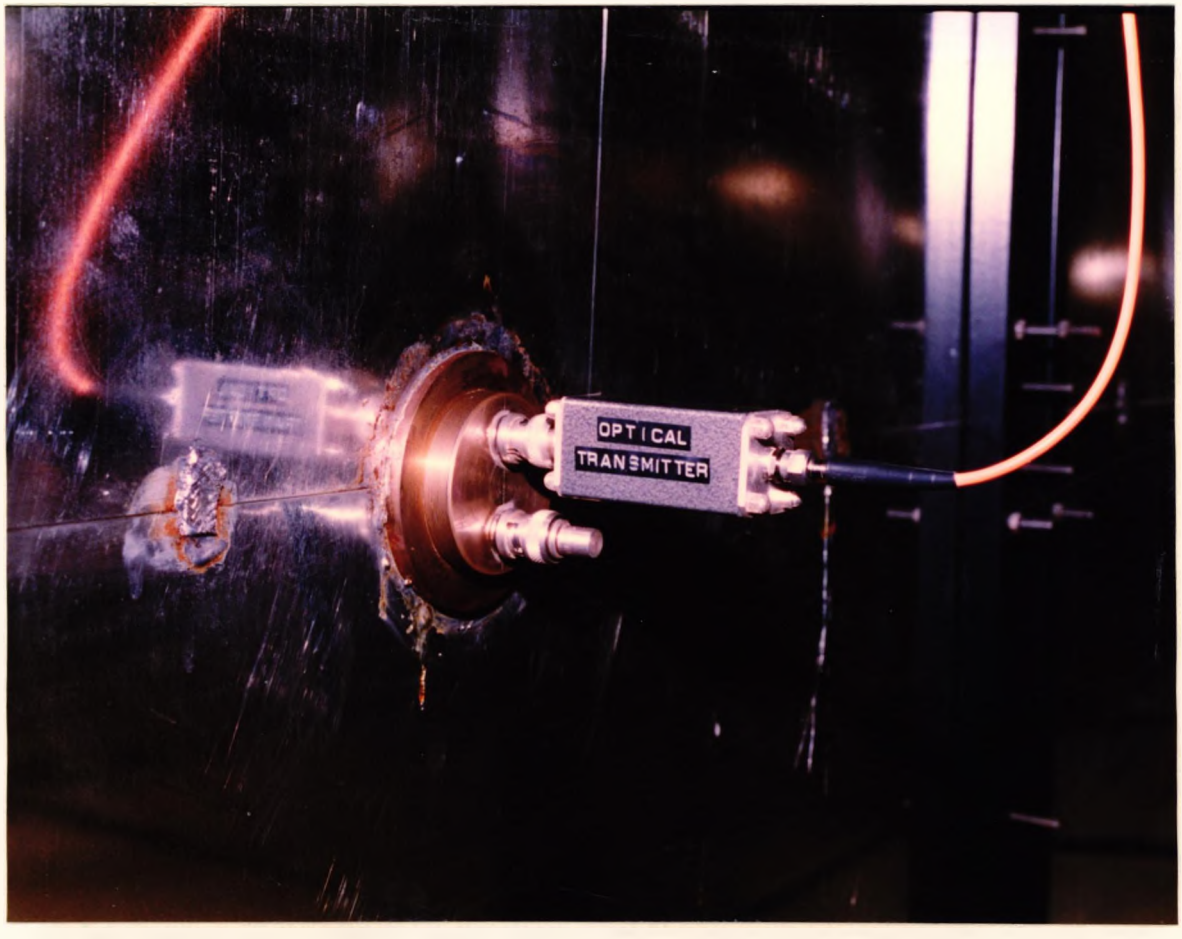


Fig. 8-14 Photograph of the transmitter unit connected to the directional coupler.

This test was identical to the investigation of pulse sharpening condition, (Chapter 6-9).

When the travelling pulse impinged on the loop, it caused a voltage to be induced in the loop. This induced voltage was then converted by the emitter module and optically transmitted to the detector unit placed adjacent to the oscilloscope. After reconversion

and amplification the output pulse, or impulse voltage as it were, was sent via coaxial cable to the oscilloscope.

Fig. 8-15 shows a photograph of the measurement set-up, the receiver module with optical and coaxial cable connections can be seen. A typical test result is shown in Fig. 8-16. Comparison with the result in Fig. 6-24, it can be seen that there is a small drop in the peak induced voltage. This was contributed mainly to losses in the fibre and in the conversion processes.

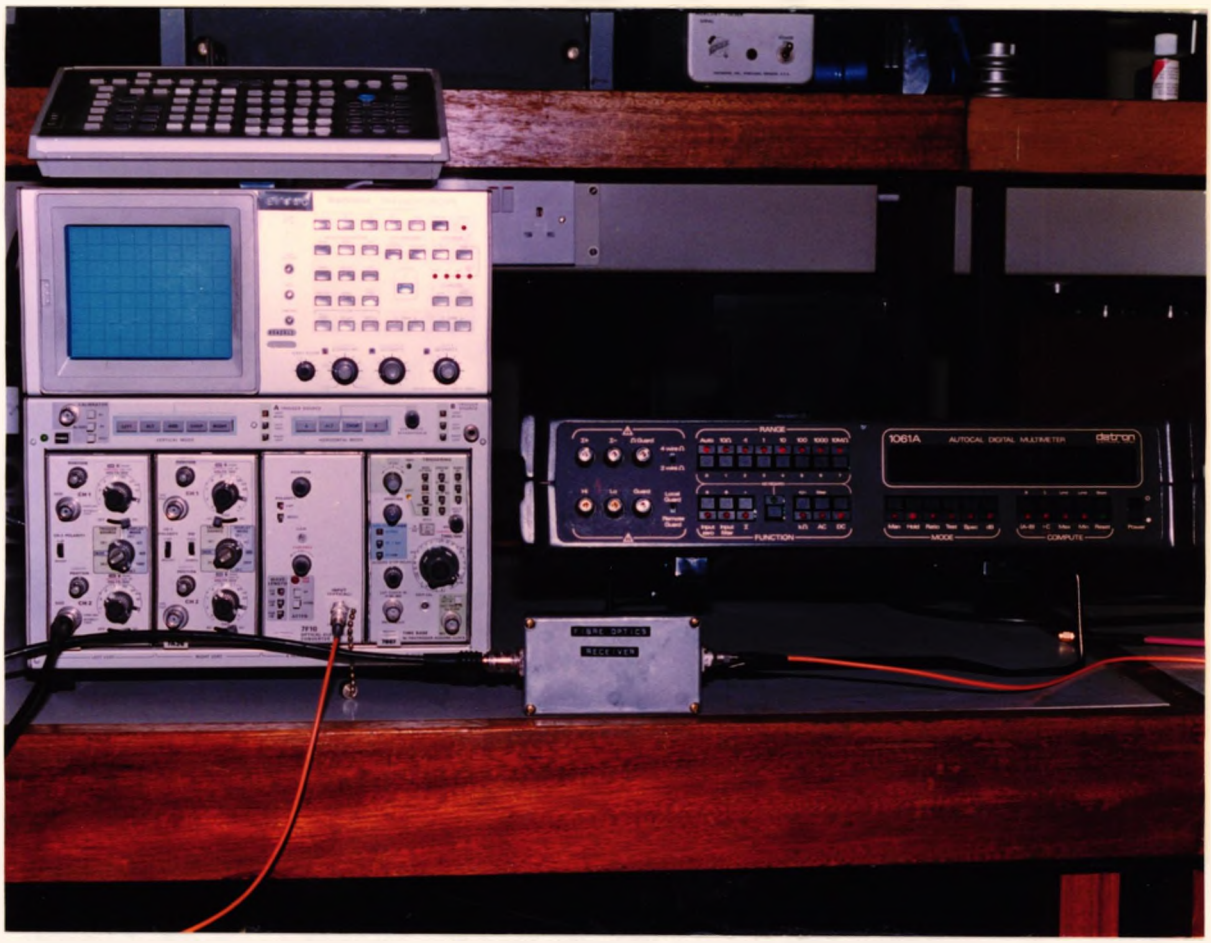


Fig. 8-15 A photograph of the measurement set-up.

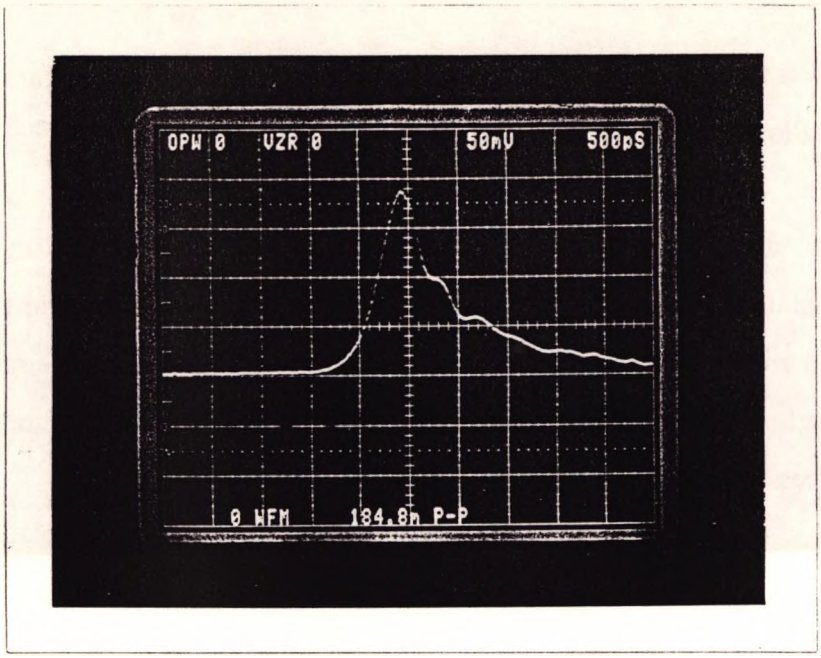


Fig. 8-16 Measurement of peak impulse voltage by optical transmission.

8-2.3 Summary

Successful operational functions of a system relies on a disturbance-free and accurate measurements. In high voltage measurements, when an object under test has a failure, high frequency oscillating currents flow to earth and can cause a high potential of several kilo-volts above earth. The resulting problems of earthing and power supply connections are less with galvanic isolation from the test area is achieved by means of fibre-optic links.

In principle the optical measurement system functioned well as was intended and illustrated that it is possible for an impulse voltage waveform in a hostile EM environment to be optically transmitted and measured using general purpose oscilloscopes. The primary concern was the integrity of the waveform and no attempts were made to distinguish amplitude levels as this was beyond the scope of the intended programme of investigation. Moreover, the tests were not carried out in a high voltage laboratory as intended and the maximum impulse that could be generated was 80 kV.

No further testing was necessary at this stage since the integrity of fibre cable with regards EM interference and noise are well established. The screening tests carried out on the device enclosure were satisfactory.

Regarding the facilities of the Tektronic 7854 (described in *Chapter 3*), it was proposed by Ryder and Holbrook (1982), that an optically coupled sampling system (*OCSS*) for pulse measurements can be made by using an appropriate sampling head remotely from the mainframe oscilloscope. Specially made extender cables are provided for this purpose. In this way the signal from the probe is first optically sampled and then digitally transmitted to the oscilloscope's optical input amplifier module. Since the sampling heads are static sensitive, extensively shielding, such as placing the sampling head in a copper cylinder, had to be carried out.

This section gives an introduction of optical transmission of a signal, such as an impulse voltage. For these tests the output of up to 1 kV was derived from the mercury pulser. Further work on impulse voltage measuring technique is reported in *Chapters* 5 *and* 6.

The polymer cables described can also be used to illuminate inaccessible areas. Using only one filament lamp or other light source many independent items can be illuminated, thereby improving reliability. Such applications include illumination in mimic displays, teaching aids, e.g. maps, plans etc., panel illuminations, e.g. meters, switches, dials, etc.

Other applications include illumination of microscopes, tool tips, proximity sensing and remote sensing of light sources.

Chapter 9

Discussions and Conclusions

9-1 DISCUSSIONS

Simultaneous measurements of the electric and magnetic field-components are of considerable practical importance. The measurement of the sum or difference of the currents (or voltages) gives a direct relationship between these two components. Whilst these can be determined at any angular position of the loop, the set-up is not very simple. The other method described in this thesis, enables these components to be measured and distinguished at the angle for maximum coupling. The component of the electric-field coupling can be measured at the 0/180 degree position where the influence of the magnetic coupling is negligible. The component of the magnetic-field coupling can be then found by deduction.

Although the results show very close values in the equality conditions ($\dot{B} = \dot{D}$), it should be pointed out that there could be some small discreptancies in the measurements. This is particularly so when the induced voltage, due to the electric-field coupling was measured. An angular error of a degree can give rise to a few millivolt change. The arrangement is such that it is difficult to obtain an accuracy better than half of a degree in angular adjustment. Moreover, the results were taken under near ideal conditions due to the experimental set-up and measuring technique.

Mathematical functions are performed by a software incorporated within the main-frame oscilloscope. The risetime is computed with respect to the specifications of the program. The value of 443 ps for the induced voltage response of the loop is shown in the result in Fig. 7-8. From the waveform (which initially rises and tails off relatively slowly) a more meaningful measurement of the risetime is high lighted by the cursors, i.e. the fastest rate of change. This is computed to be 398 ps, also shown in the result. Hence the loop sensor can successfully couple to signals of frequencies close to 1 GHz. The frequency response of the loop was calculated to be >2 GHz. Although the risetime of the wavefront leaving the pulser was measured to be < 300 ps, this sharp front was degraded at the junction of the coaxial line and the open line conductor, matched by a resistive network. The 10% - 90% risetime of an exponential (RC) system to a step function is 0.35 of the period of the sine wave signal at its 3 dB point applied to the same system. Using this criterion, the measured value shown in Fig. 7-8 does not agree with the calculated value due to the limitation of the pulse risetime as it coupled with the loop.

With the implimentation of the developed loop probe in the configuration as an **E**-field sensor, the traditionally used high voltage resistive and capitive divider (with their inherent technical problems) may become a thing of the past.

9-2 CONCLUSIONS

Although computer interfacing is indespensible in industrial, medical and related technologies for measurement applications and process control, before starting a computer it is sometimes desirable or essential to look at other measurement technique and an analytic approach. Although accuracy is paramount, consideration must always be given to the economic point of view. Sometimes it is not necessary to incorporate a sophisticated and expensive measurement system in a simple application. Moreover, such systems are not always practical in a field site where only an approximation of the result would suffice. The devices developed and embodied in the measurement technique in this experimental study, although novel in certain applications, outlined a simple and cost effective alternative.

The work reported in the thesis clearly demonstrated that the goal was accomplished, with an extension of the feasibility that the new developed measurement system in some unique practical applications. A complete characterisation of the transmission line model in terms of losses could not have been accomplished. This was due to the behaviour of the material used for the earthplane, under fast pulse operating condition, that exhibited a phenomena whereby the pulse sharpens (i.e. shorter front times) as it propagated along the line. This property was verified and the results given.

This method used in the experimentation of making the electric- and magnetic-field response equal, is much preferred since the loop is match on one side to the oscilloscope impedance, thereby preventing the setting-up of small reflective pulse patterns. Also a higher signal output is obtained since there is no voltage drop in the loop resistor. This is very useful in low signal strength areas. Since the $50\,\Omega$ *BNC* loading of the loop matched the $50\,\Omega$ input impedance of the oscilloscope and both their return conductors are connected through the earthplane, the loop may be regarded as double sided terminated with identical loads. The calculations shown are valid for this configuration.

The coupler is small as was originally designed. Only the loop conductor diameter was made larger to obtain the equality condition. The technique is simplicity in itself. It is cheap, easy to set up and use and is very accurate. Owing to its small physical size, the loop readily lends itself to be integrated within a measurement system.

Dr Kanda's (1984) theory was verified experimentally, but it is felt that in some practical applications, e.g. Frequency Swept Measurements, it may not be possible to match the load termination of the loop accurately enough. Hence, the new equations developed for this purpose and to fulfil the general condition. For equal electric- and magnetic-field response the geometrical alteration of the loop, described in the thesis would seem to be a better proposition compared with adding resistors in the loop circuit.

In diagnostics purposes and the setting-up of fast equipment, it is desirable to have pulses with very fast risetimes. The fast front or leading edge can be used to investigate the response of measuring equipment, performance tests and fault detection on transmission

systems. The 1 kV coaxial pulser with sub-nanosecond risetime which was designed and used in the investigations, is capable in meeting of these requirements.

It is envisaged that this kind of loop sensor thus described maybe used to measure the polarization ellipses of the electric and magnetic field vectors in the near-field region. It may also be used to measure the time-dependent Poynting vector from which it should be possible to describe the energy flow. Preliminary tests showed that sensitivity characteristic of the measurement technique in detecting small changes in impedances, such as in curvatures, can be readily adapted in EMC measurements.

9-3 SUGGESTIONS FOR FURTHER WORK

1. It was shown that the directional coupler incorporating suitable loop probes, can readily be adapted to measure the peak values and waveshapes of fast transient voltages. Proper calibrating with a known reference is necessary so that it can be used as an accurate, yet simple high voltage divider for impulse voltage measurements, by coupling directly into the electromagnetic field. This method should be free from some of the associated technical problems inherent in high voltage capacitive and resistive dividers. Work is continuing in this area.

2. It is possible that two similar coupling loops placed close and perpendicular to each other, may be used to detect a pulse, such as a Nuclear Electromagnetic Pulse (NEMP), travelling in any arbitrary direction. Also the two-loop method can be used in further Electromagnetic Compatibility (EMC) measurements in detecting unintentional EM interference emission.

3. High voltage testing of the line where a fast high amplitude pulse such as a lightning EMP is injected into the line. By placing loop sensors in various sections in the earthplane of the transmission system, studies of the corona distortion on the waveshape as the pulse travels along the line, can be made.

4. Preliminary tests showed that the tinned-steel earthplane exhibited some kind of pulse sharpening phenomena when a fast pulse propagated along the line. It was

observed that the pulse risetime decreased slightly, i.e. steeper front, resulting in a small increase in the induced voltage. This was measured at the directional coupler mounted near the termination of the line, and comparative studies made with the same directional coupler mounted near the source. Research into this phnomena is in progress.

5. In the application of a loop probe as an **E**-field sensor for the reduction of an impulse high voltage for measurement, effective shielding from the magnetic field is necessary. The field should be confined to a given area in which case a pair of local parallel hemispherical rod-rod electrodes is suggested. However, calculations show that by utilisting a pair of toroidal tube electrodes in the form of stress distributors, will confine the electric field around the circumference of the toroids, thus preventing corona. This work is planned for future study. It is envisaged that a study of the measured field using numerical analysis, will be performed by the Finite Element Method (FEM).

6. Although the response of the designed loop is good, the response can be made to improve quite significantly by replacing the *BNC* connectors (with matching load) with that of equivanent *SMA* connectors and load. This work is in progress.

References:

1. Agrawal, A.K., Price, H.J. and Gurbaxani, S.H. (1980). "Transient response of multiconductor transmission lines excited by a nonuniform electromagnetic field," *IEEE Trans. on Electromagnetic Compatibility*, Vol. EMC-22, No. 2, pp. 119-129.

2. Aksun, M.I. and Mittra, R. (1993). "Spurious Radiation from Microscript Inter-connects," *IEEE Transactions on Electromagnetic Compatibility*, Vol. 35, No. 2, pp. 148 - 158.

3. Allan, H.R and Curling, C.D. (1949). "The Reflectometer," Proc. IEE. Pt. 3, pp. 25-30.

4. Allen, O.E. and Hill, D.A. (1993). "Time-Domain Antenna Characterisations," *IEEE. Trans. on Electromagnetic Compatibility*, Vol. 35, No. 3, pp. 339-346.

5. Allibone, T.E., Hawley, W.G., and Perry, F.R. (1934). *J. IEE.*, 75, 670.

6. Allibone, T.E. and Saunderson, J.C. (1989). "Corona at very high direct voltages. VI. Corona in rod/plane gaps," Sixth Int. Symp. High Voltage Eng., New Orleans, Paper No. 22.02.

7. Allibone,T.E., Jones, J.E., Saunderson, J.C., Taplamacioglu, M.C. and Waters, R.T. (1993). "Spacial characteristics of electric current and field in large direct-current coronas," Proc. Royal Society, No. 441, pp. 125-146.

8. Allibone, T.E. (1989-1994). *Personal Communications.*

9. Aucoin, M. and Russell, B.D. (1987). "Detection of distribution high-impedance faults using burst noise signals near 60-Hz," *IEEE Trans. PWRD-2*, pp. 342-348.

10. Baochu, Y and Maohua, Z. (1991). "Analyzation of observed results to index of blood serum immunoglobulin of high voltage workers," 7th ISH, Dresden, Paper No. 94.04, Vol. 9, pp. 101-102.

11. Bahder, G., Garcia, F.G., Barnes, H.C., and McElroy, A.J. (1974). *IEEE Trans.* Pas-93, 960.

12. Bannister, P.R. (1968). "New theoretical expressions for predicting shielding effectiveness for the plane shield case," *IEEE Trans. Electromagn. Compat.*, Vol. EMC-10, No. 1, pp. 02-07.

13. Bem, J.D. and Wieckowski, T.W. (1992). "Probes for electromagnetic pulse measurements," Proc. of the International Symposium on EMC, Beijing, China.

14. Boff, A. F. (1951). "Power Meter and Mismatch Indicator," Wireless Engineer, Sept.., 1951, pp. 278-281.

15. Bortnick, I.M. and Cooke, C.M. (1972). *IEEE Trans. Pwr. Appar. Sys.*, PAS-91, 2196.

16. Bronaugh, E. L . and Lambdin, W. S. (1988). "Electromagnetic Interference Test Methodology and Procedures," Vol. 6, Gainesville, VA: Interference Control Technologies, Inc.

17. Bucci, O.M., D'Elia, G. Leone, G. and Pierri, R. (1990). "Far-field pattern determination from the near-field amplitude measurements on two surfaces," *IEEE Trans. Antenna Propagat.*, Vol. 38, No. 11.

18. Burbridge, R.F., Edwards, D.J. and Kanso, A. (1987). "A comparison of the open plate transmission line and closed TEM cell for EMC measurements," British Electromagnetic Measurements Conference, NPL, UK, pp. 29/1 - 29/3.

19. Burke, J. and Poddio, A. J. (1980). "Numerical Electromagnetics Code (NEC) - method of moments part 1, 2 and 3," Naval Ocean System Certer, San Diego, C.A. in Report NOSC TD 116, Jan. 1980.

20. Casey, K.F. (1981) "Low-frequency electromagnetic penetration of loaded apertures" *IEEE Trans. on Electromagn. Compat.*, Vol. 23, No. 4, pp.367-377.

21. Casey, K. F. (1885). "Quasi-static electric and magnetic field penetration of a spherical shield through a circular aperture," *IEEE Trans on Electromagn. Compat.*, Vol. EMC-27, No. 1, pp. 13-17.

22. Cerri, G., De Leo, R. and Mariani Primiani, V. (1993). " A Rigorous Model for Radiated Emission Prediction," *IEEE Trans on Electromagn. Compat.*, Vol. 35, No. 1, pp. 102-109.

23. Chen, C.C. (1970). "Transmission through a conducting screen perforated periodically with apertures," *IEEE Trans. Microwave Theory Tech.*, Vol. MIT-18, No. 5, pp. 627-632.

24. Christopoulos, C. and Herring, J.L. (1993). "The Application of Transmission Line Modeling (TLM) to Electromagnetic Compatibility Problems," *IEEE Trans. on EMC* Vol. 35, No. 2, pp. 185-191.

25. Clare, C.P. Corporation, 220. (1990) Reference Manuals.

26. Clade, J.J., Gary, C.H. and Lefevre, C.A. (1969). "Calculation of corona losses beyond the critical gradient in alternating voltage," *IEEE PAS*, Vol. 88, No. 4, pp. 695-703.

27. Clifford, P. (1989-1993). *Personal Communications.*

28. Crawford, M.L. and Workman, J.L. (1979). "Using a TEM cell for EMC Measurements of Electronic Equipment," NBS Technical Note, 1013, April, 1979.

29. Criel, S., Martens, S. and De Zutter, D. (1994). "Theroetical and Experimental Near-Field Characterisation of Perforated Shields," *IEEE Trans. Electromagm. Compat.*, Vol. 36, No. 3, pp. 161-168.

30. Cwik, T and Mittra, R. (1985). "Scattering from periodic screens," *IEEE Trans. Electromagn. Compat.*, Vol. 5, No. 4, pp. 263-283.

31. Cwik, S., Martins, L. and De Zutter, D. (1994). "Theoretical and Experimental Near-Field Characterization of Perforated Shields," *IEEE Trans. Electromagn. Compat.*, Vol. 36, No. 3, pp. 161-168.

32. Daum, W. (1989-1994). *Personal Communications.*

33. de Jong and Groenveld, P (1987) "A Simple RF Immunity Test Set-up," The Second Symposium on EMC, Montreux, June, 1977.

34. de Jesus, C. and Correia de Barros, M.T. (1994). "Modelling of corona dynamics for surge propagations studies," *IEEE PES*, Winter Meeting, Paper No. 94, WM043-0, PWRD.

35. Djordevic, A. R. and Sarkar, T. K. (1993). "An Investigation of Delta-*I* Noise on Integrated Circuits," *IEEE Trans. on EMC*, Vol. 35, No. 2, pp. 134-147.

36. Dyer, S.A. and Holbrook, R.L. (1986). "An Optically Coupled Sampling System for Transient Electromagnetic Measurements," *IEEE Trans. on Instrumentation and Measurement*, Vol.1M-35, No.4, pp. 456-462.

37. Edwards, M. (1987). "Internal Calibration for Precision DMM's," British Electromagnetic Measurements Conference, NPL, UK, pp. 33/1 - 33/4.

38. Elliot, R.S. (1881). In: Antenna Theory and Design. (Englewood Cliffs, NJ: Pretence-Hall).

39. Garbe, H., Behrmann, G. and Baumann, J. (1992). "A long-term investigation of the electromagnetic environment with respect to radiation exposure limits," IEE Eighth International Conference on Electromagnetic Compatibility, No. 362, pp. 54-57.

40. Ibe, A.O. and Cory, B.J. (1985). "A travelling wave-based fault locator for two and three- terminal network," *IEEE Trans*, pp. 228-233.

41. Johnk, C.T.A. (1988). In: Engineering Electromagnetic Fields and Waves. (New York: Wiley).

42. Johns, A.T. and Agarwal, P. (1990). "A new approach to power line protection based upon the detection of fault induced high frequency signals," Proc. IEE, 137 307-313.

43. Johns, A.T., Lai, L.L., El-Hami, M., and Daruvala, D.J. (1991). "New approach to directional fault location for overhead power distribution feeders," Proc. IEE, 138, pp. 351-357.

44. Harmouth, H.F. (1984). In: Antennas and Waveguides for Nonsinusoidal Waves. (New York: Academic Press).

45. Howard, P.R. (1957). *Proc. IEE*, 104, Part A, 123.

46. Kanda, M. (1977). "The characteristics of broadband, isotropic electric field and magnetic field probes," National Bureau of Standards, (U.S.), NBSIR 77-868.

47. Kanda, M. (1984). "An electromagnetic near-field sensor for simultaneous electric and magnetic field measurements," *IEEE Transactions on EMC*, Vol EMC-26, No. 3, pp. 102-110.

48. Kanda, M. (1986). "Time-domain sensors and radiators," In: *Time-Domain Measurements in Electromagnetics*, ed. by E.K. Miller, New York: Van Rostrand Reinhold.

49. Kanda, M. and Hill, D.A. (1992). "A Three-Loop Method for Determining the Radiation Characteristics of an Electrically Small Source," *IEEE Trans. on Electromagnetic Compatibility*, Vol. 34, No.1, pp. 01-03.

50. Kanda, M. (1994) "Standard Antennas for Electromagnetic Interference Measurements and Methods to Calibrate Them," *IEEE. Trans. on Electromagnetic Compatibility*, Vol. 36, No. 4, pp. 261-273.

51. Kawaguchi, Y., Sakata, K. and Menju, S. (1971a,b). *IEEE Trans. Pwr. Appar. Sys.*, PAS-90, 1072 and 1079.

52. Lai, L.L., Ndeh-Che, F., Chari, T., Rajroop, P.J. and Chandrasekharaiah, H.S. (1993) "HVDC Systems Fault Diagnosis with Neural Networks," Proc. 5th European Con- ference on Power Electronics and Applications, The European Power Electronics Association, Vol. 8, pp. 145-150.

53. Lai, L.L., Ndeh-Che, F., Chu, K.H., Rajroop, P.J., and Wang, X.F. (1993). "Design Neural Networks with Genetic Algorithms for Fault Section Estimination," 29th UPEC.

54. Lai, L.L., and Daruvala, D.J. "A new approach to arcing fault detection on overhead distribution feeders," Proc. IEE, 12th CIRED.

55. Lai, L.L., Ndeh-Che, F. and Chu, K.H. (1994). "Application of ferrites and high frequency signals to protection of power systems," CEPSI, The Association of Electricity Supply Industry of East Asia and Western Pacific, New Zealand.

56. Laroussi, R. and Costache, G.I. (1994). "Far-Field predictions from Near-Field Measurements using an Exact Integral Equation Solution," *IEEE Trans on EMC*, Vol. 36, No. 3, pp. 189-195.

57. Li, K., Lee, C.F., Poh, S.Y., Shin, R.T. and Kong, J.A.(1993) "Application of FDTD Method to Analysis of Electromagnetic Radiation from Heatsink Configuration,"

IEEE Trans. on EMC, Vol. 35, No. 2, pp. 204-213.

58. Logan, J.T., and Richardson, O. (1937). "Arc frequency component relaying," Summary of experience on the Georgia power Company System, Internal report, Atlanta, Georgia.

59. Lynch, A.C. (1989-1992). *Personal Communications*

60. Mansour, M.M., and Swift, G.W. (1985) "A mult-microprocessor based travelling wave relay - theory and realization," *IEEE PICA*, pp. 212-219.

61. Menju, S. and Tsuchikawa, Y. and Kobayashi, N. (1972). *IEEE Trans. Pwr. Appar. Sys.*, PAS-93, 390.

62. Middlekoop, R. (1991). "Time-Domain Calibration of Field Sensors for EMP Measurements," *IEEE Trans. on Instrumentation & Measurement*," Vol. 40, No.2, pp. 455-459.

63. Moser, J.R. (1988). "Low-frequency low impedance electromagnetic shielding," *IEEE Trans. Electromagn. Compat.*, Vol. 30, No. 3, pp. 202-210.

64. Nishikata, A. and Sugiura, A. (1992). "Analysis for electromagnetic leakage through a plane shield with an arbitrary-oriented dipole source," *IEEE Trans. Electromagn. Compat.*, Vol. 34, No. 1, pp. 284-291.

65. Nitta, T. and Shibuya, Y. (1971). *IEEE Trans. Pwr. Appar. Syst.*, PAS-90, 1065.

66. Omick, S.R. and Castillo, S.P. (1993). "A New Finite-Difference Time-Domain Algorithm for the Accurate Modeling of Wide-Band Electromagnetic Phenomena," *IEEE Trans. on EMC*, Vol. 35, No. 2, pp. 215-222.

67. Parkes, D.M. and Smith, P.D. (1987). "A practical method of predicting fields and monopole current waveforms," British Electromagnetic Measurements Conference,

NPL, UK, pp. 7/1 - 7/3.

68. Paris, L., and Cortina, R. (1968). *IEEE Trans.*, PAS-87, 947.

69. Paul, C.R.(1976) "Frequency response of multiconductor transmission lines illuminated by an electromagnetic field," *IEEE Trans. on Electromagn.* Compat., Vol. EMC-18, No.4, pp. 183-190.

70. PCL - 848A/B IEEE - 488, Reference Manual.

71. Pedersen, A. (1970). *IEEE Trans. Pwr. Appar. Syst.*, PAS-89, 2043.

72. Peng, J., Balanis, C.A. and Barber, G.C. (1993). "NEC and ESP Codes: Guidelines, Limitations, and EMC applications", *IEEE Trans. on EMC*, Vol. 35, No. 2, pp. 124-

73. Pocklington, H.C. (1897) "Excitation of a thin loop antenna by a plane wave," Proc. Cambridge Phil. Soc. 9, 324.

74. Podgorshi, A.S. (1986). "Measurements of transients in High-Voltage Systems," *Proc. IEEE*, Vol. 74, No. 1, pp. 108-110.

75. Porti, J.A. and Morente, J.A. (1994). "A Numerical Analysis of Wire Antenna Loaded with Varistor-Composite Materials," *IEEE Trans. on EMC*, Vol. 36, No. 1, pp. 23-31.

76. Rajroop, P.J. (1990). "An EMP coupling and measuring techique in testing the performance of a transmission system," *Internal Report*, City University, London.

77. Rajroop, P.J. and House, H. (1991). "EMP coupling and measuring techniques in testing the performance of transmission lines," Proceedings of the 7th International Symposium on High Voltage Engineering, Dresden, Paper No. 83.02, pp. 103-106.

78. Rajroop, P.J., House, H. and Lai, L.L. (1992). "A novel EMP and measuring technique illustrated by testing the performance of fast pulse on transmission lines," Proceedings of the 8th International Conference on Electromagnetic Compatibility, IEE, UK, pp. 80-84.

79. Rajroop, P.J. and Lai, L.L. (1993a). "Application of the directional coupler as an accurate fault locator on a transmission line," Proceedings of the 8th International Symposium on High Voltage Engineering, Yokohama, Paper No.56.05, pp. 475-478.

80. Rajroop, P.J. and Lai, L.L. (1993b) "EMC using loop probes," Proceedings of the 8th International Symposium on High Voltage Engineering, Yokohama, Japan, Paper No. 79.02, pp.449-452.

81. Rajroop, P.J. and Lai, L.L. (1995) "Equal response measurements of a modified B/D near field probe sensor," Proceedings of the 9th International Symposium on High Voltage Engineering, Graz, Austria, Paper No. 8385.

82. Russell, B.D., Chinchali, R.P., and Kim, C.J., (1988). "Behaviour of low frequency spectra during arcing faults and switching events," *IEEE Trans. PWRD-3*, pp. 1485-1492.

83. Russell, B.D., Mehta, K. and Chinchali, R.P., (1988). "An arcing fault detection technique using low-frequency current components - performance evaluation using recorded field data," *IEEE Trans. PWRD-3*, pp. 1493-1500.

84. Sarkar, T.K., Ponnapolli, S. and Arvas, E. (1990). "An accurate method of computing far-field antenna pattern from near-field measurements," In: Antenna and Propagation Symp. Dig., Vol. 1, (Dallas, TX).

85. Schmitt, H.J. (1960). "Transients in cylindrical antenna," IEE Monograph No. 337E.

86. Scott, C. (1989). In: The Spectral Domain Method in Electromagnetic, Norwood, MA: Artech House, pp. 01-23.

87. Seddon, N. and Thornton, E. (1988). "A high voltage short risetime pulse generator based on a ferrite pulse sharpener," *Review. Scientific Instruments*., 59, 11, 2497.

88. Sengupta, D.L. and Tai, C.T. (1976). "Radiation and reception of transients by linear antennas," In: Transient Electromagnetic Fields (New York: Springer-Verlag, ch. 4).

89. Struss, W. (1995). "Calibration of digital recorders and impulse calibrators with traceability to national stsndards," Proc. 9th ISH, Graz, Europe, Vol. S4, pp. 4495-1 to 4495-4.

90. Swarup, K.S., Chandrasekharraiah, H.S., Lai, L.L. and Ndeh-Che, F. (1993). "Application of neural networks to fault diagnosis for HVDC systems," Neural Networks and Genetic Algorithms, Springer-Verlag, Wien, New York, pp. 227-234.

91. Takuma, T. and Watanabe, T. (1970). "English translation in Electrical Engineering in Japan," 90, No. 3, 166

92. Taylor, C.D., Satterwhite, R.S. and Harrison, W.Jr. (1965) "The response of terminated two-wire transmission line excited by a nonuniform electromagnetic field," *IEEE Trans. on Antenna Propagation*, Vol. AP-13, pp. 987-989.

93. Tirkas, P.A., Balanis, C.A., Purchine, M.P. and Barber, G.C. (1993). "Finite-Difference Time-Domain Method for Elecrtromagnetic Radiation, Interfereence, and Interaction with Complex Structures," *IEEE Trans. on EMC*, Vol. 35, No. 2, pp. 192-203.

94. Thornton, E. (1987). "High current shunt with sub-nanosecond risetime," British Electromagnetic Measurements Conference, NPL, UK, pp. 5/1 - 5/4.

95. Thornton, E. (1990-1994). *Personal Communications*.

96. Upton, M.E.G. and Marvin, A.C. (1994). "The Fields due to a Small Loaded Loop in Free Space," *IEEE Trans. on EMC*, Vol. 36, No.1, pp. 07-13.

97. Waters, R.T., and Jones, R.E. (1964a). Phil. Trans. Roy. Soc., 256A, 185.

98. Wedepohl, L.M. 1963). "Application Matrix Methods to the solution of Travelling-Wave Phenomena in Polyphase Systems". Proc. IEE, 110, pp. 2200-2212.

99. Wei-Gang, H. and Semlyem, A. (1987). "Computation of electromagnetic transients on three-phase transmission lines with corona and frequency dependent parameters," *IEEE Trans. Power Delivery*, Vol. 3, No. 2, pp. 887-898.

100. Wu, T.T. (1962). "Theory of the Thin Circular Loop Antenna," *Journal of Mathematicl Physics*, Vol. 3, No. 6, pp.1301-1304.

101. Yang, R. and Mittra, R. (1985). "Coupling between two arbitrarily oriented dipoles through multilayered shields," *IEEE Trans. Electromagn. Compat.*, Vol. EMC-27, No. 3, pp. 131-136.

Appendix :

APPENDIX 1:

1-0 Stress Calculations

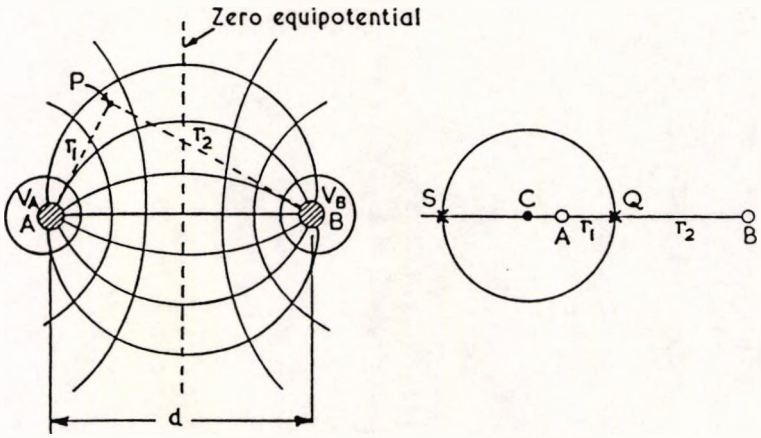


Fig. A1-1 Electric field between parallel conductors.

It can be shown that the potential difference (P.D.) between cylinders A and B of radius r is $2V$,

and,
$$2V = \frac{q}{\pi\varepsilon}\ln(k) \tag{A1-1}$$

where,

$$k = \frac{h}{r} + \sqrt{\frac{h^2}{r^2} - 1} \tag{A1-2}$$

Also,

$$k = \frac{r_1}{r_2} = \frac{s + (h - r)}{s - (h - r)} \tag{A1-3}$$

where r = 2 mm (radius of the 4 mm diameter conductor) and

h = 121 mm (critical height of the conductor above the plane + conductor radius)

From (A1-2),

$$k = \frac{121 * 10^{-3}}{2 * 10^{-3}} + \sqrt{\left(\frac{121 * 10^{-3}}{2 * 10^{-3}}\right)^2 - 1}$$

$$= 120.99$$

From (A1-3)

$$k(s-x) = s+x$$

where,

$$x = (h-r),$$

$$ks - s = kx - x$$

$$s(k-1) = x(k+1)$$

$$s = \frac{x(k+1)}{k-1} \qquad \text{(A1-4)}$$

Substituting in (A1-4),

$$s = \ 120.98$$

From (A1-1),

$$q = \frac{2V\pi\varepsilon}{\ln(k)} \qquad \text{(A1-5)}$$

$$= 0.579 \ \mu C/m$$

$$r_1 = s + 119 = 239.98$$

$$r_2 = s - 119 = 1.98$$

From,

$$E = \frac{q}{2\pi\varepsilon}\left(\frac{1}{r_1} + \frac{1}{r_2}\right) \qquad \text{(A1-6)}$$

Substituting,

$$E = 52.96 \text{ kV/m or } 53 \text{ kV/m}$$

Stress voltage for the breakdown of air is 30 kV/m

Therefore, corona voltage = (30/53). 50 kV

= 28.3 kV.

NOTE: The 4 mm diameter conductor chosen is thus adequate for the line and without the occurance of corona at voltages of up to 28 kV. Operation of voltages greater than this and up to 53 kV will allow an experimental study of the effects of corona on the measured waveforms, due to the fast wave fronts.

APPENDIX 2:

2-1 Line Matching Network Calculations

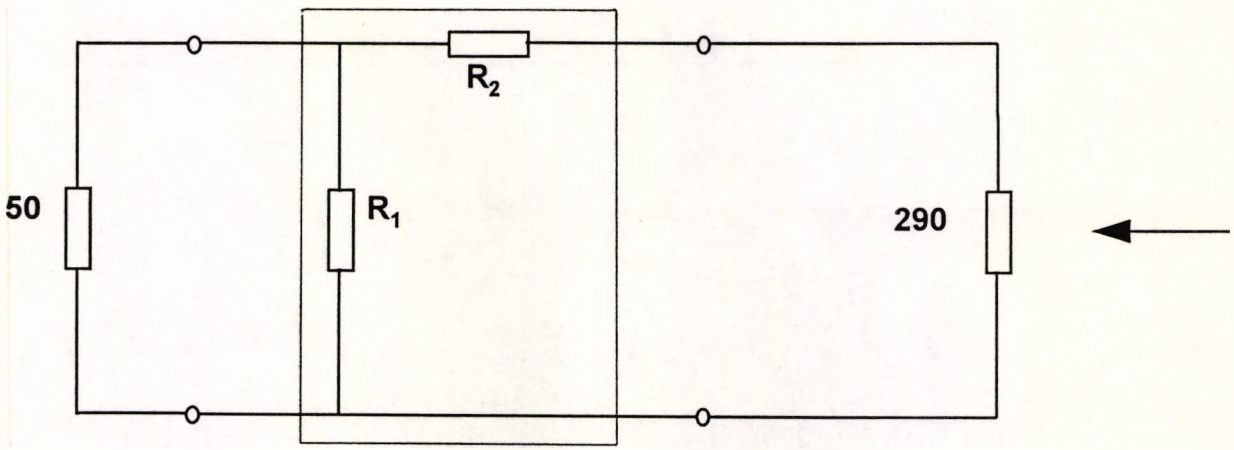


Fig. A2-1 Circuit diagram for calculation of the line matching resistors.

The computer calculations (shown in Appendix 2-3:) for the characteristic impedance of the transmission line is 290 ohms. The 50 ohm is the impedance of the coaxial and measurement system.

From Fig. A2-1,

$$290 = (50 \,//\, R_1) + R_2 \qquad \text{(A2-1)}$$

$$R_2 = 290 - \frac{50R_1}{50 + R_1} \qquad \text{(A2-2)}$$

$$= \frac{290(50 + R_1) - 50R_1}{50 + R_1}$$

$$R_2(50 + R_1) = 14500 + 240R_1$$

$$R_1R_2 = 14500 - 50R_2 + 240R_1 \qquad \text{(A2-3)}$$

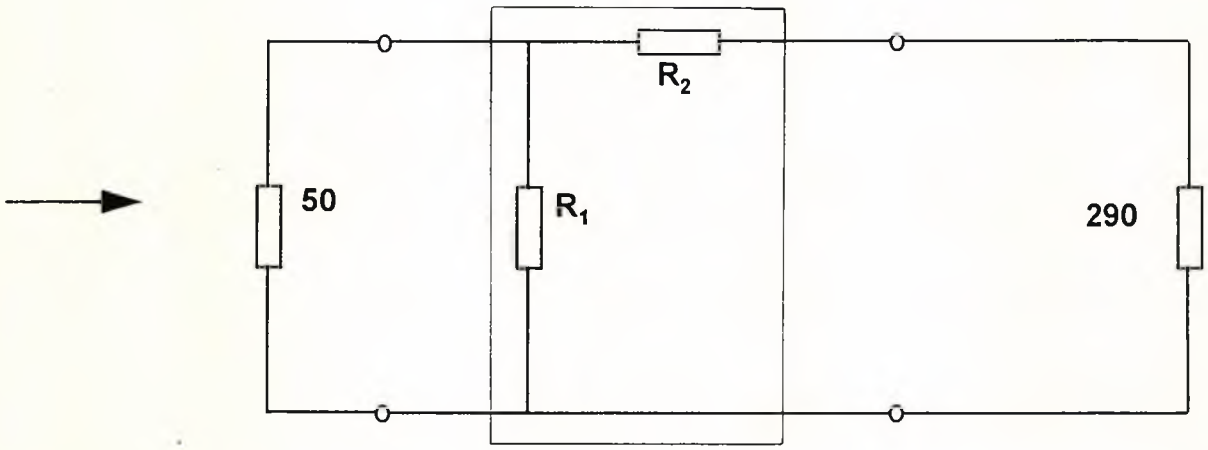


Fig. A2-2 Circuit diagram for calculation of the line matching resistors.

From Fig. A2-2,

$$50 = R_1 // (R_2 + 290) \qquad \text{(A2-4)}$$

$$50 = \frac{R_1(R_2 + 290)}{R_1 + R_2 + 290}$$

$$50R_1 + 50R_2 + 14500 = R_1R_2 + 290R_1$$

$$14500 + 50R_2 = R_1(R_2 + 240) \qquad \text{(A2-5)}$$

$$R_1R_2 = 14500 + 50R_2 - 240R_1 \qquad \text{(A2-6)}$$

From (A2-3),

$$R_1R_2 = 14500 - 50R_2 + 240R_1$$

From (A2-6), $R_1R_2 = 14500 + 50R_2 - 240R_1$

Substracting (A2-3) from (A2-6),

$$R_2 = 4.8R_1 \qquad \text{(A2-7)}$$

From (A2-5),

$$14500 + 50R_2 = R_1(R_2 + 240)$$

$$R_1 = \frac{14500 + 50R_2}{R_2 + 240} \qquad \text{(A2-8)}$$

Substituting for R_2,

$$R_1 = \frac{14500 + 240R_1}{240 + 4.8R_1}$$

$$R_1^2 = \frac{14500}{4.8}$$

$$R_1 = 55$$

From (A2-7),

$$R_2 = 4.8 \times 55 = 264$$

All values in ohms.

These values of resistors were used to construct a network so that the characteristic impedance of the line matched the impedance of the measuring system.

APPENDIX 2:

2-2 Calculation of the Characteristic Impedance of the Line

2-2.1 Capacitance between Parallel Conductors

The capacitance between parallel circular conductors may be readily evaluated, provided that the wire radius, a, is small compared with the spacing, d, between them. The potential at the surface of each conductor due to its own charge and to the charge on the other conductor can be calculated. The relationship between the line charge and the potential difference (p.d.) between the lines then gives the capacitance. Thus for the system shown in Fig. A1-1, let the line charge be :

$+q$ and $-q$ coulombs/m

Potential at the surface of A due to its own charge is:

$$-\int_{z}^{a}\frac{q}{2\pi\varepsilon r}dr \qquad \text{(A2-9)}$$

Potential at the surface of A due to charge on B is:

$$-\int_{z}^{d}\frac{-q}{2\pi\varepsilon r}dr \qquad \text{(A2-9)}$$

where z is the distance to a zero -potential point and $a << d$.

Hence,

$$V_A = \frac{q}{2\pi\varepsilon}\log_e\frac{z}{a} + \frac{q}{2\pi\varepsilon}\log_e\frac{d}{z}$$

$$= \frac{q}{2\pi\varepsilon} \log_e \frac{d}{a} \qquad \text{(A2-10)}$$

Similarly,

$$V_B = \frac{-q}{2\pi\varepsilon} \log_e \frac{d}{a} \qquad \text{(A2-11)}$$

so that

$$V_{AB} = V_A - V_B$$

$$= \frac{q}{\pi\varepsilon} \log_e \frac{d}{a} \qquad \text{(A2-12)}$$

and,

$$C = \frac{q}{V_{AB}} = \frac{\pi\varepsilon}{\log_e (d/a)} \quad \text{F/m} \qquad \text{(A2-13)}$$

If $d = 2h$ and $a = r = 2$,

$$C = \frac{2\pi\varepsilon}{\log_e \frac{2h}{a}} \qquad \text{(A2-14)}$$

Substituting,

$$C = \frac{2\pi 10^{-9}}{36\pi \log_e \left(\frac{2x121}{2}\right) 10^{-3}}$$

$$= 11.584 \text{ x } 10^{-9} \text{ F/m}$$

Where,

$$\varepsilon = \varepsilon_0 \varepsilon_r = \frac{1}{36\pi 10^{-9}}, \quad \varepsilon_r = 1 \text{ for air.}$$

Also,

$$C = \frac{2\pi\varepsilon}{\log_e (k)} \qquad \text{(A2-15)}$$

where,

$$k = \frac{h}{r} \pm \sqrt{\frac{h^2}{r^2} - 1} \qquad \text{(A2-16)}$$

$= 120.99$ [calculated from (A2-3)]

$$C = \frac{2\pi 10^{-9}}{36\pi \log_e(120.99174).10^{-3}}$$

Hardly any change because a (or r) $<< h$.

It can be shown that:

$$L = \frac{\mu}{2\pi} \log_e(k) \qquad \text{(A2-17)}$$

$= 11.584 \times 10^{-12}$ F/m

where,

$$\mu = \mu_0 \mu_r = \mu_0 = 4\pi 10^{-7} H/m \quad \text{(for air)}$$

$$L = \frac{4\pi 10^{-7}}{2\pi} \times 4.7957 \times 10^{-3}$$

$= 9.59 \times 10^{-7}$ H/m

The *characteristic impedance* (Z_0) of the line can be calculated from:

$$Z_0 = \sqrt{\frac{L}{C}} \qquad \text{(A2-18)}$$

Substituting,

$$Z_0 = \sqrt{\frac{9.59 \times 10^{-7}}{11.5844 \times 10^{-12}}}$$

$= 287.7$ ohms

2-3 Computer Calculation of *C* and *L* for the Line

The computer program cannot easily deal with the line conductor in its circular form, therefore its dimensions had to be resolved into an octagon. The eight x,y coordinates of the vertex with reference to the earthplane were calculated for a conductor of 4 mm diameter at a distance of 119 mm from the plane. The values of the x,y coordinates are shown Fig A2-3.

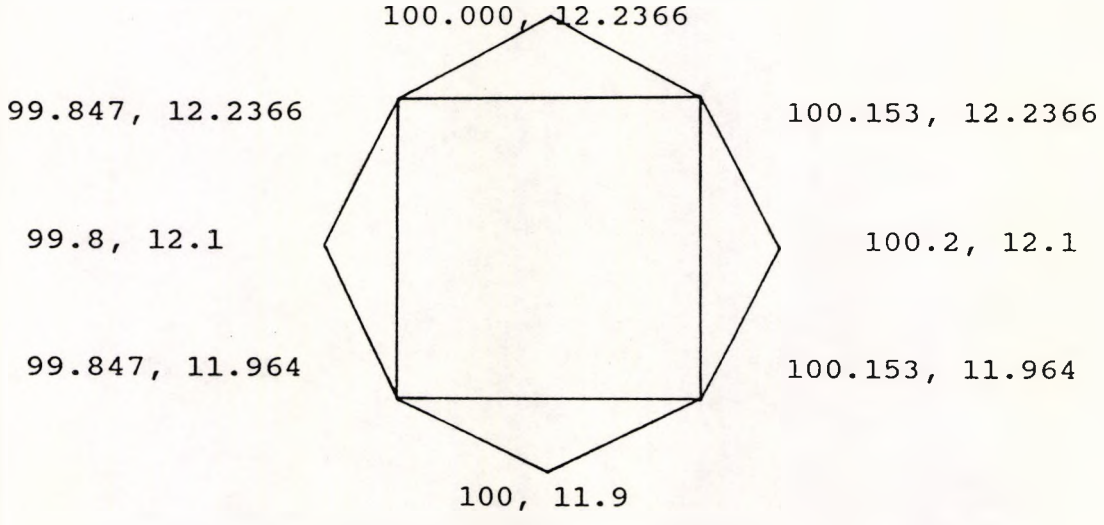


Fig. A2-3 The x-y coordinates of the 4 mm line conductor.

A print-out of the computer analysis shows the following values:

Capacitance C = 0.11513 pF/cm

Inductance L = 9.651 nH/cm.

$$Z_0 = \sqrt{\frac{L}{C}}$$

$$= \sqrt{\frac{9.651 \times 10^{-7}}{11.513 \times 10^{-12}}}$$

$$= 289.6 \text{ ohms.}$$

This is in good agreement with the values calculated from the line constants.

APPENDIX 2-4:

Computer Analysis for the Capacitance and Inductance of the Line

```
                                MOM1.0
                  METHOD OF MOMENTS PARAMETER CALCULATOR
                        OUTPUT FILE 4m8s7s.out

GEOMETRY OPTION                          :  GROUND PLANE AT Y=0

NUMBER OF ACTIVE CONDUCTORS              :  1

NUMBER OF GROUNDED CONDUCTORS            :  0

NUMBER OF DIELECTRIC INTERFACES          :  0

NUMBER OF SUBINTERVALS/SIDE              :  7

MAX. EXTENT OF DIEL. DISCRETIZATION :  500.000

DIELECTRIC DATA:
REGION #  1 REAL EPSILON =    1.0000    LOSS TANGENT =    0.0000

CONDUCTOR DATA:
ACTIVE CONDUCTOR #    VERTEX #      (X,Y) COORDINATES
            1             1       100.000     11.900
            1             2       100.153     11.984
            1             3       100.200     12.100
            1             4       100.153     12.237
            1             5       100.000     12.300
            1             6        99.847     12.237
            1             7        99.800     12.100
            1             8        99.847     11.963


PARAMETER CALCULATOR RESULTS:

CAPACITANCE MATRIX (pf/cm)

                1
    1        0.11513

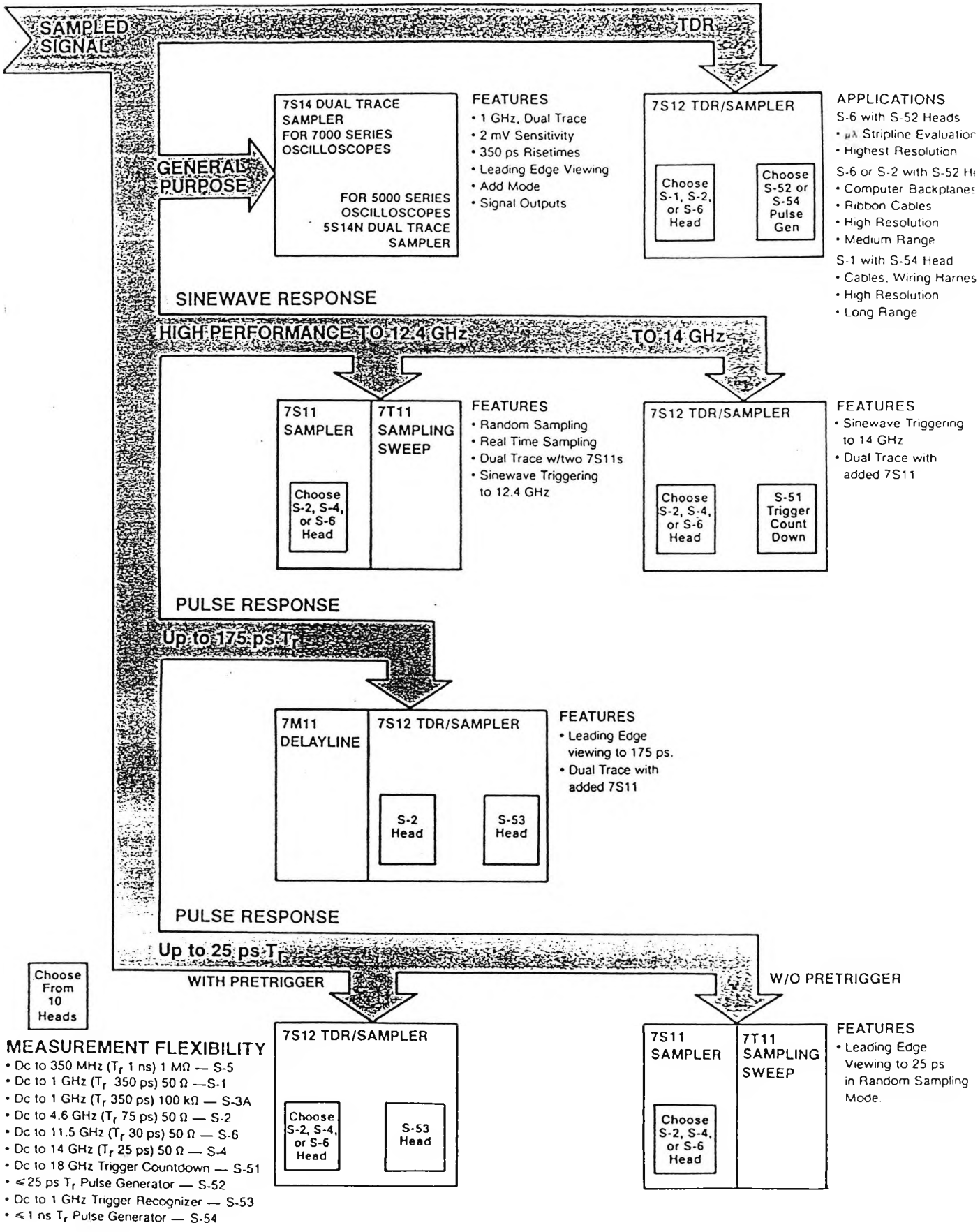
CAPACITANCE MATRIX (pf/cm) NO DIELECTRIC

                1
    1        0.11513

INDUCTANCE MATRIX (nh/cm)

                1
    1        9.691
```

Sampling Decision Tree for Repetitive Signals



E - and H - Field Sensors

Free-space sensors with fibre optic link for near-field and far-field measurement in the HF range

Manufacturer	field	use for	signal	frequency range	measuring range	size
EMCO	E E	CW CW	$\sqrt{\lvert E_x\rvert^2+\lvert E_y\rvert^2+\lvert E_z\rvert^2}$	10 kHz ... 1 GHz 100 MHz ... 18 GHz	1 ... 250 V/m 2 ... 500 V/m	8 cm$^{\phi}$ x 7.5 cm 3.5 cm$^{\phi}$ x 8.5 cm
Holaday	E	CW	$\lvert E_x\rvert, \lvert E_y\rvert, \lvert E_z\rvert$	10 kHz ... 1 GHz	0.1 ... 300 V/m	<12 x 12 x12 cm
Nanofast	E	CW/pulse	$E_x(t)$	2 kHz ... 500 MHz	0.1 V/m ... 200 kV/m	2 sensors: 6.3 cm$^{\phi}$ x 15 cm, 11.75 cm$^{\phi}$
MEB (Berlin)	E + H	CW	$\sqrt{\lvert E_x\rvert^2+\lvert E_y\rvert^2+\lvert E_z\rvert^2}$ $\sqrt{\lvert H_x\rvert^2+\lvert H_y\rvert^2+\lvert H_z\rvert^2}$	75 kHz ... 30 MHz	10 ... 1200 V/m 0.03 ... 3 A/m	sphere 15.5 cm$^{\phi}$ (+ wires)
Thomson-CSF	E H	CW/pulse CW/pulse	$E_x(t)$ $H_x(t)$	10 kHz ... 1 GHz 150 kHz ... 1.2 GHz 100 kHz ... 1.3 GHz	13 mV/m ... 31.6 V/m 7 V/m ... 1 MV/m 0.02 A/m ... 2.65 kA/m	8.2 cm$^{\phi}$ 1 cm$^{\phi}$ x 4 cm (+ socket) 2.2 cm$^{\phi}$ x 2 cm
Univ. Stuttgart	E H	CW/pulse CW/pulse	$E_x(t), E_y(t), E_z(t)$ $H_x(t), H_y(t), H_z(t)$	50 Hz ... 100 MHz 1 kHz ... 100 MHz	500 V/m ... 200 kV/m 0.5 A/m ... 500 A/m	spheres 9 cm$^{\phi}$ (+ wires)

E - Field Sensors in the LF Range

Manufacturer	use for	frequeny range	measuring principle	signal	measuring range	size
Gevotron	AC	$16^2/_3$ ... 400 Hz	cap. sensor	E_x	0.1 kV/m ... 100 kV/m	5 cm$^{\phi}$ sphere + fiber optic link
Radians Innova	AC	5 ... 2000 Hz	cap. sensor	E_x	0.4 V/m ... 2000 V/m	30 cm$^{\phi}$ disc
		2 ... 400 kHz			0.06 V/m ... 200 V/m	30 cm$^{\phi}$ disc
Holaday	AC	5 ... 2000 Hz	cap. sensor	E_x	1 V/m ... 40 kV/m	30 cm$^{\phi}$ x 10 cm
		2 ... 400 kHz			1 V/m ... 40 kV/m	

Combined E/H - field sensors for the LF range

Manufacturer	use for	frequeny range E	measuring range E	frequeny range H/B	measuring range H/B	signal
Holaday	AC	50 ... 1000 Hz	1 V/m ... 200 kV/m	50 ... 1000 Hz	0.01 µT ... 2 mT	E_x, B_z
		2 kHz ... 300 kHz	1 V/m ... 2 kV/m	8 kHz ... 300 kHz	1 ... 2000 mA/m (≈ 1nT ... 2µT)	E_x, B_z

H - Field Sensors in the LF Range

Manufacturer	use for	frequency range	meas.principle	signal	measuring range	size
Field star (Dexsil)	AC	16⅔ ... 150 Hz	ind.coils (?)	$\sqrt{B_x^2+B_y^2+B_z^2}$	0.004 µT... 1 mT	16 x 10 x 3.5 cm
Gevotron	AC	16⅔ ... 400 Hz	ind. coil	B_x	0.1 µT... 1 mT	5 cm$^{\phi}$ sphere + fiber optic link
Holaday	AC	5 ... 2000 Hz	ind. coil	B_x	0.02 µT... 2 mT	11.6 cm$^{\phi}$ (disc)
Holaday	AC	2 kHz ... 400 kHz	ind. coils	$\sqrt{B_x^2+B_y^2+B_z^2}$	0.006 µT ... 40 mT	12.7 cm$^{\phi}$ (sphere)
Programma	AC	5 ... 2000 Hz	ind. coils	B_x, B_y, B_z, B	10 nT ...10 mT	38 x 11 x 2.5 cm
Projekt Elektronik	DC, AC	DC, 20 Hz ... 4 kHz	Hall probe	B_x	0.01 µT... 200 µT	1.5 cm$^{\phi}$ x 30 cm
Radians Innova	AC	5 ... 2000 Hz	ind. coils	$\sqrt{B_x^2+B_y^2+B_z^2}$	0.01 µT(?)... 2 mT	43 cm long, coil
Radians Innova	AC	2 kHz ... 400 kHz	ind. coils	$\sqrt{B_x^2+B_y^2+B_z^2}$	0.01 µT(?)... 2 µT	43 cm long, coil
Holaday	DC, AC	DC ... 1 kHz	Hall probes	$\sqrt{B_x^2+B_y^2+B_z^2}$	0.1 ... 300 mT	13 x 7 x 2 cm
Projekt Elektronik	DC, AC	DC, 20 Hz ... 35 kHz	Hall probe	B_x	0.01 mT ... 2 T	≈ 1 cm$^{\phi}$ x 7 cm
Walker	DC, AC	DC, 10 Hz ... 10 kHz	Hall probe	B_x	0.01 mT ... 15 T	16 x 9 x 5 cm